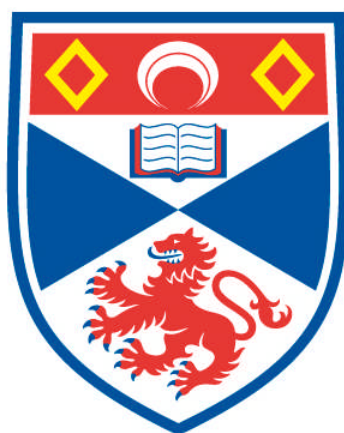


SCANDIUM-BEARING OPEN FRAMEWORK MATERIALS

Stuart Raymond Miller

**A Thesis Submitted for the Degree of PhD
at the
University of St Andrews**



2008

**Full metadata for this item is available in
Research@StAndrews:FullText
at:**

<http://research-repository.st-andrews.ac.uk/>

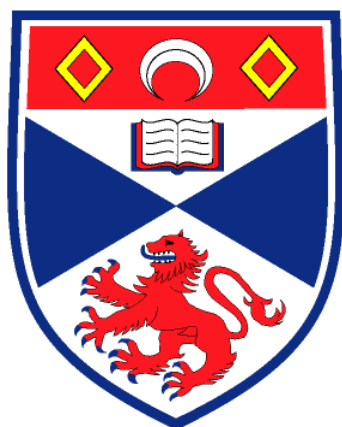
Please use this identifier to cite or link to this item:

<http://hdl.handle.net/10023/570>

This item is protected by original copyright

**This item is licensed under a
Creative Commons License**

Scandium-bearing Open Framework Materials



University
of
St Andrews

A thesis presented for the degree of

Doctor of Philosophy

in the Faculty of Science of the University of St. Andrews

by Stuart Raymond Miller, BSc (Hons)

October 2007

Declaration

1. I, Stuart Miller, hereby certify that this thesis, which is approximately 55,000 words in length, has been written by me, that it is the record of work carried out by me and that it has not been submitted in any previous application for a higher degree.

Date..... Signature of candidate.....

2. I was admitted as a research student in October, 2003 and as a candidate for the degree of PhD in October, 2004; the higher study for which this is a record was carried out in the University of St Andrews between 2003 and 2007.

Date..... Signature of candidate.....

3. I hereby certify that the candidate has fulfilled the conditions of the Resolution and Regulations appropriate for the degree of PhD in the University of St Andrews and that the candidate is qualified to submit this thesis in application for that degree.

Date..... Signature of supervisor.....

4. In submitting this thesis to the University of St Andrews I wish access to it to be subject to the following conditions: for a period of 1 year from the date of submission, the thesis shall be withheld from use. I understand, however, that the title and abstract of the thesis will be published during this period of restricted access; and that after the expiry of this period the thesis will be made available for use in accordance with the regulations of the University Library for the time being in force, subject to any copyright in the work not being affected thereby, and a copy of the work may be made and supplied to any bona fide library or research worker, that my thesis will be electronically accessible for personal or research use, and that the library has the right to migrate my thesis into new electronic forms as required to ensure continued access to the thesis. I have obtained any third-party copyright permissions that may be required in order to allow such access and migration.

Date..... Signature of candidate.....

Abstract

Here I report the hydrothermal chemistry of scandium, examining the behavior of the Sc^{3+} cation in various systems, including phosphates, phosphites, phosphonates and carboxylates. In total, 27 different materials, 23 of which are novel, have been synthesised and their structures solved.

Seven different scandium phosphate-based materials have been successfully synthesised using amines and alkali hydroxides as structure directing agents, producing chain, layer and framework materials. Thermal analysis of these materials indicated that they were not stable upon removal of the template, because there are hydrogen bonding networks between the template and free OH groups on the phosphate groups. Certain conditions lead to the crystallization of either kolbeckite, $\text{Sc}(\text{PO}_4)\cdot 2\text{H}_2\text{O}$, or a langbeinite-type structure, $(\text{NH}_4)_2\text{Sc}_2(\text{HPO}_4)(\text{PO}_4)_2$, which are dense frameworks.

Investigation of scandium phosphites leads to the formation of more thermally stable frameworks. Investigation of scandium phosphite-based materials using different structure directing agents yielded three framework phosphite materials and one layered phosphite / phosphate. The use of lithium hydroxide and ethylenediamine within scandium phosphite systems resulted in the crystallization of a gainesite type framework, $(\text{LiSc}(\text{HPO}_3)_2)$ and $(\text{H}_3\text{N}(\text{CH}_2)_2\text{NH}_3)_2\text{Sc}_4(\text{HPO}_3)_8$, which distorts in order to accommodate the amine, but not the lithium cation. Decreasing the potential for the formation of hydrogen bonding networks in the phosphite systems led to the formation of framework structures, however these structures did not retain their crystalline integrity upon removal of the template.

In order to impart structure directing properties upon scandium-based materials but avoid the formation of hydrogen bonding networks upon which the crystalline integrity is dependent, scandium phosphonates were investigated. Seven different scandium phosphonate materials have been synthesised, two of which have been solved from powder diffraction data, and one from a combination of powder diffraction data, molecular modeling and single crystal data. Synthesis of scandium phosphonate materials yielded two thermally stable, porous materials with reversible water adsorption properties, $\text{NaSc}(\text{CH}_3\text{PO}_3)_2\cdot\text{H}_2\text{O}$ and $\text{Sc}_2(\text{O}_3\text{PCH}_2(\text{NHC}_5\text{H}_{10}\text{NH})-\text{CH}_2\text{PO}_3)_3\cdot 4\text{H}_2\text{O}$.

The success of this approach led to the examination of scandium carboxylate metal organic framework materials. The incorporation of Sc^{3+} into microporous carboxylate frameworks yielded three aliphatic scandium carboxylates and six aromatic scandium carboxylates. The scandium analogue of MIL-53 shows potential for gas adsorption studies, as well as illustrating that scandium carboxylates can be isostructural to metal carboxylate materials

already published. The scandium terephthalate, $\text{Sc}_2(\text{O}_2\text{C}_6\text{H}_4\text{CO}_2)_3$, is a small pore framework material with an unprecedented structure type, the adsorption properties of which have been examined using a variety of different small gas molecules and hydrocarbons, including X-ray analysis of the structures whilst adsorbing different molecules. ^{45}Sc MAS NMR has been performed on the materials prepared pure and characterized in this thesis, in order to establish a library of chemical shifts for scandium in different framework environments.

Acknowledgements

To begin, I would like to thank my supervisor Dr. Paul Wright for giving me the opportunity to complete this research. His supervision, guidance, expert advice and enthusiasm towards research have been a significant contributing factor towards the success of this work. I will always be indebted to him.

I am also grateful to have worked alongside such gifted and dedicated scientists, without whom some of the work presented in this thesis would not have been possible. Professor Alex Slawin is thanked for the collection of single crystal data and for her advice and guidance in regards to crystallography. Dr. Philip Wormald and Dr. Sharon Ashbrook are thanked for their help and guidance involving NMR and the collection of NMR spectra and Dr. David Apperley (EPSRC Solid State NMR Service) is also thanked for the collection of NMR data. Dr. Simon Teat, Dr. John Warren and Dr. Tim Prior are thanked for their help and guidance towards data collection at Daresbury.

Mrs Sylvia Williamson is thanked for providing training and help towards the collection of adsorption isotherms. Dr. Caroline Mellot-Draznieks is thanked for help with molecular modelling. Dr. Christian Serre, Dr. Philip Llewellyn, Dr. Sandrine Bourelly, Miss Lucia Gaberova, Dr. Thomas Devic and Dr. Yaroslav Filinchuk are thanked for their work involving gas adsorption and single crystal experiments performed in Marseilles and Grenoble. Drs. Nandini Radhamonyamma, Jorge Gonzalez, Robert Hodgkins, Stewart Warrender and Calum Dickinson are thanked for their support, friendship and counsel.

For all the happy moments both outwith and within the Chemistry Department a special thanks is also given to Dr. Timothy Miller, Louise Brown, Jonathan Kearney, David Aldous, Gavin and Lydia Hill, Neal McLoughlin, Charlotte Jones, Lyndsey Ritchie, Lynn Power Drs Ben and Emily Parham and anyone whose name I may have left out.

Finally, but most importantly I would like to thank all my family for their continual support, belief and encouragement during these years. An unreserved thank you goes to my girlfriend, Lynzi Robb, who has been a rock for me during the most difficult points of this work. I am completely indebted to my parents, Elizabeth and Raymond, brothers and partners, John, Michael, Jacqui and Amy, and the dog, Shiell, for their unwavering belief in me and continual support and encouragement (and sitting at my feet) throughout my education.

Publications arising from this work

1. **Hydrothermal synthesis and structure of organically templated chain, layered and framework scandium phosphates**, S. R. Miller, A. M. Z. Slawin, P. Wormald, P. A. Wright, *J. Solid State Chem.*, 2005, **178**, 1737
2. **Synthesis and structure of the framework scandium methylphosphonates $\text{ScF}(\text{H}_2\text{O})\text{CH}_3\text{PO}_3$ and $\text{NaSc}(\text{CH}_3\text{PO}_3)_2 \cdot 0.5\text{H}_2\text{O}$** , S. R. Miller, E. Lear, J. Gonzalez, A. M. Z. Slawin, P. A. Wright, N. Guillou, G. Fèrey, *Dalton Trans.*, 2005 **20**, 3319
3. **A microporous scandium terephthalate, $\text{Sc}_2(\text{O}_2\text{CC}_6\text{H}_4\text{CO}_2)_3$, with high thermal stability**, S. R. Miller, P. A. Wright, C. Serre, T. Loiseau, J. Marrot, G. Fèrey, *Chem. Commun.*, 2005, **30**, 3850
4. **The first route to large pore metal phosphonates**, J. A. Groves, S. R. Miller, S. J. Warrender, C. Mellot-Draznieks, P. Lightfoot, P. A. Wright, *Chem. Commun.*, 2006, **31**, 3305

Dedication

This thesis is dedicated to both my Granny Jess (1927-1994) and my Grandad Geordie (1923-1997) and my parents, Raymond and Elizabeth, each of whom have shaped my life making me the person I am today.

Thank you

Table of Contents

Section		Page
<i>Chapter 1: Introduction</i>		
1.1	Microporous Solids	2
1.2	Hydrothermal Synthesis	5
1.3	Crystal Formation	9
1.4	Mixed Co-ordination Frameworks	9
1.5	Metal Organic Framework (MOF) Materials	11
1.6	The History and Chemistry of Scandium	13
1.7	Aims	15
<i>Chapter 2: Experimental Techniques</i>		
2.1	Introduction	17
2.2	The Basics of Crystallography	17
2.2.1	Crystals	17
2.2.2	Seven Crystal Systems	18
2.2.3	Miller Indices	20
2.2.4	X-Rays	20
2.2.5	Diffraction of X-rays by crystals	22
2.2.6	Direct Methods	26
2.2.7	The Patterson Function	27
2.3	Structure determination by x-ray diffraction methods	27
2.3.1	Single crystal diffraction	27
2.3.2	Powder Diffraction	28
2.3.3	Synchrotron Radiation	29
2.4	Structure determination combining powder XRD and molecular modelling techniques	31
2.4.1	Rietveld Refinement	40
2.5	Nuclear Magnetic Resonance in the solid state	41
2.5.1	The NMR Spectrometer	42
2.5.2	<i>Solution State versus Solid-State NMR</i>	42
2.5.3	The Vector Model	43
2.5.4	The Rotating Frame	44
2.5.5	Radiofrequency, RF, Pulses	45
2.5.6	Relaxation	47
2.5.7	Dipole-dipole interactions	47
2.5.8	Chemical Shift	49
2.5.9	Magic Angle Spinning (MAS)	51
2.5.10	High power decoupling	51
2.5.11	Cross Polarisation	52
2.5.12	Direct Polarisation	53
2.5.13	Quadrupolar Nuclei	53

2.6	Gas Adsorption	56
2.7	General Synthesis and Analysis	57
<i>Chapter 3: Scandium Phosphates</i>		
3.1	Aims	60
3.2	Introduction	60
3.3	Experimental	62
3.4	Results and Discussion	69
3.4.1	$[(\text{H}_3\text{NC}_2\text{H}_4\text{NH}_3)_3][\text{Sc}_3(\text{OH})_2(\text{PO}_4)_2(\text{HPO}_4)_3(\text{H}_2\text{PO}_4)]$ - Structure 1	73
3.4.2	Scandium phosphates templated with diaminobutane	81
3.4.3	$[(\text{H}_3\text{NC}_4\text{H}_8\text{NH}_3)_3][(\text{Sc}(\text{OH}_2))_6\text{Sc}_2(\text{HPO}_4)_{12}(\text{PO}_4)_2]$ – Structure 2	82
3.4.4	$[(\text{H}_3\text{NC}_4\text{H}_8\text{NH}_3)_2(\text{H}_3\text{O})][\text{Sc}_5\text{F}_4(\text{HPO}_4)_8]$ – Structure 3	88
3.4.5	$[\text{C}_6\text{H}_{11}\text{NH}_3][\text{ScF}(\text{HPO}_4)(\text{H}_2\text{PO}_4)]$ - Structure 4	93
3.4.6	$\text{Sc}(\text{PO}_4) \cdot 2\text{H}_2\text{O}$ – Structure 5	100
3.4.7	$(\text{NH}_4)_2\text{Sc}_2(\text{HPO}_4)(\text{PO}_4)_2$ – Structure 6	105
3.4.8	$\text{LiSc}(\text{PO}_4\text{H})$ – Structure 7	113
3.5	Conclusions	116
<i>Chapter 4: Scandium Phosphites</i>		
4.1	Introduction	121
4.2	Experimental	122
4.3	Results and Discussion	125
4.3.1	$\text{Sc}(\text{HPO}_3)_2\text{Li}$ - Structure 8	129
4.3.2	$[(\text{H}_3\text{N}(\text{CH}_2)_2\text{NH}_3)_2][\text{Sc}_4(\text{HPO}_3)_8]$ – Structure 9	136
4.3.3	$[(\text{H}_3\text{N}(\text{CH}_2)_4\text{NH}_3)_2][\text{Sc}_5\text{F}_4(\text{HPO}_3)_6(\text{H}_2\text{PO}_3)_2(\text{PO}_4)]$ – Structure 10	141
4.3.4	$\text{Sc}_2(\text{HPO}_3)_3$ – Structure 11	146
4.4	Conclusions	150
<i>Chapter 5: Scandium Phosphonates</i>		
5.1	Aims	154
5.2	Introduction	154
5.3	Experimental	156
5.4	Results	158
5.4.1	Mixed scandium / aluminium methyl phosphonates	161
5.4.2	$\text{Al}_{1-x}\text{Sc}_x\text{Al}_3(\text{CH}_3\text{PO}_3)_6$ – Structure 12	163
5.4.3	$\text{ScAl}_3(\text{PO}_3\text{CH}_3)_6$ - Structure 13	168
5.4.4	$\text{ScF}(\text{H}_2\text{O})\text{CH}_3\text{PO}_3$ – Structure 14	178
5.4.5	$\text{NaSc}(\text{CH}_3\text{PO}_3)_2 \cdot \text{H}_2\text{O}$ – Structure 15	180
5.4.6	$\text{ScOH}_2\text{Sc}(\text{OH}_2)_2(\text{CH}_3\text{PO}_3)_3$ – Structure 16	186
5.4.7	$\text{Sc}_3(\text{O}_3\text{PC}_2\text{H}_4\text{PO}_3)(\text{HO}_3\text{PC}_2\text{H}_4\text{PO}_3\text{H})_3 \cdot \text{H}_3\text{O}$ – Structure 17 <i>Scandium bisphosphonates templated with piperazine-based</i>	191
5.4.8	<i>bisphosphonate ligands</i>	196
5.4.9	$\text{Sc}_2(\text{O}_3\text{PCH}_2(\text{NHC}_5\text{H}_{10}\text{NH})\text{CH}_2\text{PO}_3)_3 \cdot 4\text{H}_2\text{O}$ – Structure 18	198

5.5	Discussion	206
Chapter 6: Scandium carboxylates		
6.1	Aims	210
6.2	Introduction	210
6.3	Experimental	213
6.4	PART 1: Scandium Carboxylates Synthesised using Aliphatic Carboxylic Acids	218
6.4.1	Scandium succinate $\text{Sc}_2(\text{O}_2\text{CC}_2\text{H}_4\text{CO}_2)_3$ – Structure 19	219
6.4.2	Scandium succinate hydroxide $\text{Sc}_2\text{OH}(\text{O}_2\text{CC}_2\text{H}_4\text{CO}_2)_{2.5}$ – Structure 20	222
6.4.3	Scandium glutarate $\text{Sc}_2(\text{O}_2\text{CC}_3\text{H}_6\text{CO}_2)_3$ - Structure 21	225
6.5	PART 2: Scandium Carboxylates Synthesised using Aromatic Carboxylic Acids	228
6.5.1	Scandium 4,4'-biphenyldicarboxylate $\text{Sc}(\text{O}_2\text{CC}_{12}\text{H}_8\text{CO}_2)_{1.5} \cdot (\text{H}_2\text{O})_{0.125}$ 22	230
6.5.2	Scandium isophthalate $\text{Sc}_2(\text{O}_2\text{CC}_6\text{H}_4\text{CO}_2)_3$ - Structure 23	235
6.5.3	Scandium terephthalates	239
6.5.4	Scandium terephthalate hydroxide (α) $\text{Sc}(\text{OH})[\text{O}_2\text{CC}_6\text{H}_4\text{CO}_2]$ – Structure 24	243
6.5.5	Scandium terephthalate hydroxide (β) $\text{Sc}(\text{OH})[\text{O}_2\text{CC}_6\text{H}_4\text{CO}_2]$ – Structure 25	245
6.5.6	Scandium terephthalate $\text{Sc}_2(\text{O}_2\text{CC}_6\text{H}_4\text{CO}_2)_3$ – Structure 26	248
6.5.7	Scandium terephthalate fluoride $\text{ScF}[\text{O}_2\text{CC}_6\text{H}_4\text{CO}_2]$ – Structure 27	254
6.6	Conclusions	256
6.7	Further Examination of Adsorption Properties of Scandium Terephthalates	257
Chapter 7: A note on the ^{45}Sc MAS NMR of scandium-bearing open framework solids		
7.1	A note on the ^{45}Sc MAS NMR of scandium-bearing open framework solids	267
Chapter 8: General Summary, Conclusions and Further Work		
8.1	General Conclusions	279
8.2	Further Work	281
Chapter 9: References		
		284

Chapter 1: Introduction

1.1 Microporous Solids

Over the past 25 years, there has been a considerable interest in the synthesis of novel microporous materials such as crystalline silicates, metal organic framework materials and amorphous carbons. Microporous solids are materials which contain channels and pores typically in the region of 2.5 to 20Å. These structurally diverse materials are capable of interaction with other chemical species, both through surface reactions and reactions within the pores of the material, leading to numerous potential applications.

In 1756 the Swedish mineralogist Axel Fredrick Cronstedt discovered that stilbite, a naturally occurring mineral, visibly lost water when heated, and consequently was responsible for naming this class of minerals, zeolites.² Zeolites, derived from the Greek words meaning 'boiling stones', are classically defined as crystalline, porous aluminosilicates with tetrahedral connectivity that, via ring formation, can create channels which may run in all three dimensions throughout the structure. Aluminosilicates consist of a tetrahedral silicate framework where the silicate units are partially substituted by AlO₄ tetrahedra. This imparts a negative charge to the framework, owing to the differences in formal charge between Si⁴⁺ and Al³⁺, so to attain electro neutrality additional cations must be incorporated. The number of cations depends on the number of aluminium cations substituted into the framework and the charge of the extra framework cations

The general formula and composition of a zeolite is:



where cations M of valence n neutralise the negative charges on the zeolite framework.

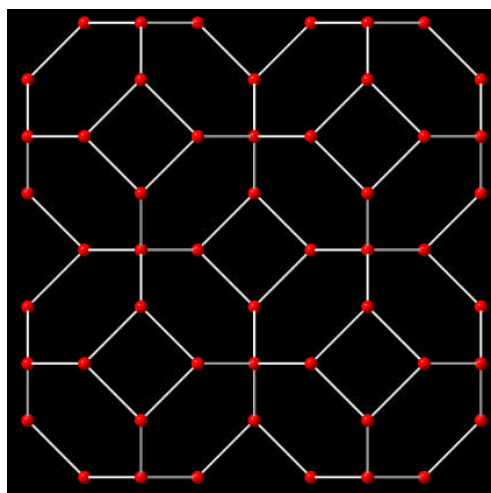


Figure 1.1: An example of a typical zeolite framework, sodalite. The red 'nodes' represent tetrahedral Al or Si whereas the line connecting the nodes represents the T-O-T bridge.

Additional cations which are found within zeolites do not form part of the framework. These cations occupy 'non-framework' positions normally situated within the pores or cavities of the zeolite and are often referred to as exchangeable cations, due to their ability to be replaced by other cationic species.

The first synthetic homologue of a natural zeolite, levynite, was reported in 1862 by de Sainte Claire Deville³ and marked the beginning of a whole new genre of inorganic chemistry. In 1932, McBain introduced the term 'molecular sieves' in order to describe microporous carbons and zeolites with selective adsorption properties.⁴ However it was not until the early 1940s that synthetic attempts at novel zeolites were reported by mineralogists interested in increasing the framework stability of naturally occurring minerals. In 1948 Union Carbide, an American chemical company, found the first industrial applications for zeolites, pioneering the synthetic molecular sieve/zeolite business.⁵ Also around this time, Barrer⁶ and Milton⁷ were responsible for the synthesis of the first *novel* aluminosilicates and, in recognition of their efforts, modern day literature now refers to Barrer and Milton as the 'founding fathers' of zeolite chemistry.

The synthesis of a series of aluminophosphates (AlPOs) during the early 1980s by Flanigen and co-workers⁸ marked the beginning of a revolution in open framework chemistry. Unlike aluminosilicates, aluminophosphates do not need extra framework cations for charge balancing like the aluminosilicates, as the formal negative charge associated with each $[\text{AlO}_4/2]^-$ tetrahedron is balanced by the formal positive charge associated with each $[\text{PO}_4/2]^+$

tetrahedron. Not only did Flanigen show that it was possible to utilise the chemistry of phosphorus with the framework architecture instead of silicon, her work inspired the synthesis of hundreds of novel open framework solids. Consequently the classical definition of a zeolite has had to be altered to accommodate the rapidly increasing number of novel open frameworks being reported. These structures can have one of as many as 25 transition metal element replacing aluminium, which leads to a seemingly endless possibility of novel materials.⁹

A modern, and more accommodating, definition of a zeolite-like (zeotypic) material is a tetrahedrally connected solid oxide structure, which has a high degree of crystallinity and well defined pore structures.

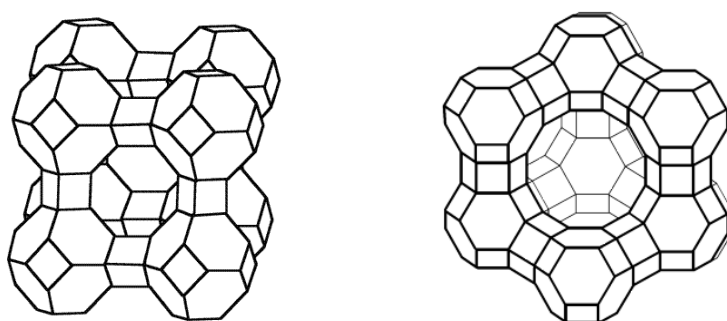


Figure 1.2: Schematic representations of zeolite A and zeolite X. Each line is representative of a T-O-T bond. Classically the 'T' atoms are aluminium or silicon, however Flanigen's work inspired iso- and aliovalent replacement of the cation, as well as replacing the oxo-anion component of the framework.

The widespread and varied topology allows widespread application of zeotypes in modern industry, with synthetic zeotype materials exhibiting a variety of desirable properties, from sorbents and catalysts to ion exchange materials and molecular sieves.⁹⁻¹³ An early and simple method for characterising microporous materials was by pore sizes and channel systems. Channel systems are defined by the shape and dimensions of the pores, whereas the pore size is defined by the number of T-atoms which produce the aperture. Currently there are over 165 framework architectures known¹⁴, and characterising microporous materials by channel systems and pore sizes is no longer straightforward. The concept of primary and secondary building units was therefore employed to simplify the characterisation of these frameworks.

Primary building units (PBUs), in the case of zeolites, are TO_4 tetrahedra. These are the smallest subunits from which zeolite frameworks are constructed. TO_4 tetrahedra are

arranged into geometric configurations known as secondary building units (SBUs), which are the building blocks from which all known open frameworks can be theoretically assembled. Figure 1.3 illustrates the simplest units in zeolite frameworks¹⁵, showing how they can be connected, and some of the secondary building units which can be constructed.

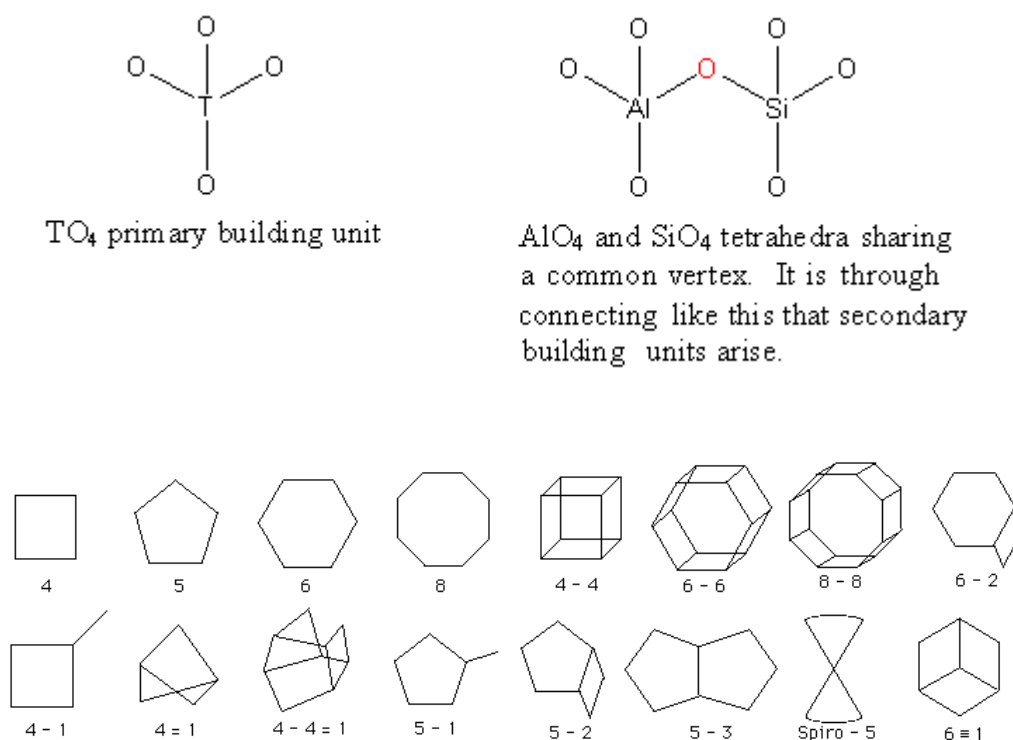


Figure 1.3: Secondary building units and their symbols. Each vertex represents the central atom of a tetrahedra (T) and each line is representative of a T-O-T bond, shown at the top of figure 1.2

1.2 Hydrothermal Synthesis

Zeolites are naturally formed in the presence of the high temperatures and pressures found in the Earth's crust. Consequently early attempts to produce synthetic homologues of zeolites were unsuccessful. It was not until the 1950s that Barrer and Milton redirected zeolite chemistry towards an alternative and milder preparation, the hydrothermal route.^{6, 7, 16}

Hydrothermal synthesis is based on the principle that many of the precursors used in microporous framework formation are insoluble under 'normal' conditions, and are found to be more soluble at non-standard temperatures and pressures.

Currently most microporous materials are synthesised via the hydrothermal route, commonly carried out in polytetrafluoroethylene (PTFE) lined acid digestion bombs under autogeneous pressure, usually between 60° and 250°C.

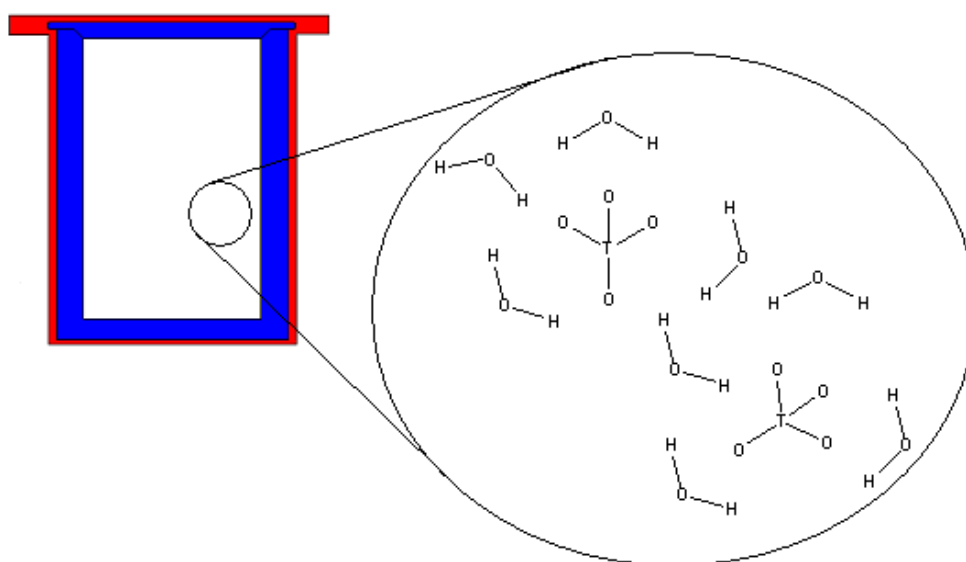


Figure 1.4: Cross section of an autoclave (PTFE lined acid digestion bomb) showing the Teflon liner (blue) and the steel outer casing (red). The schematic shown within the circle is a simple representation of what is happening in the autoclave.

Chemical behaviour inside the autoclave is an area of open framework synthesis which is only starting to be understood. A complete understanding of crystal growth within the autoclave would be required for the rational design of novel open frameworks leading to potential industrial application. It is known that the composition of reaction variables, including time, temperature, template, concentration of reactants, pH and preparation method, have considerable effect on the framework topology. Although temperature and time can be increased or decreased in order to maximise the efficiency of the reaction, the composition of the reaction gel is a more complicated issue. Due to the ‘closed system’ nature of the autoclave, most of the reaction variables directly affect each other, increasing the complexity of the reaction.

The addition of, or variation in, the organic template molecule is regarded as one of the most important factors that should be considered in the synthesis of novel microporous materials. The addition of an organic molecule, such as an amine or ammonium salt, to a reaction gel influences the properties of the pores and architecture of the framework. It has been shown that the framework, of some materials, grow around an organic molecule such as that of sodalite,¹⁷ shown in figure 1.5.1 and figure 1.5.2.

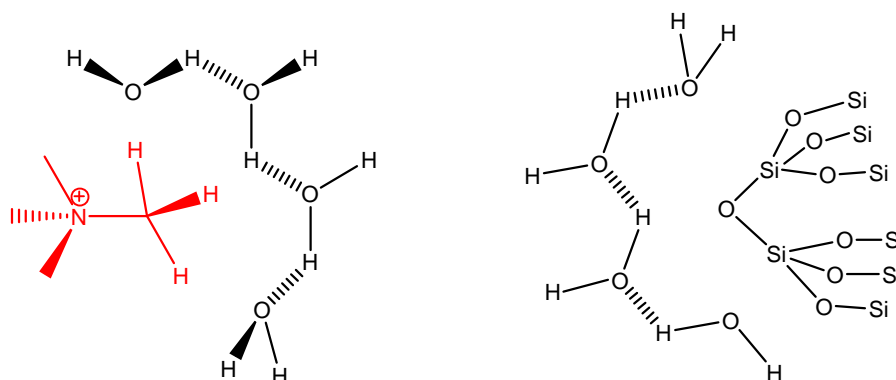
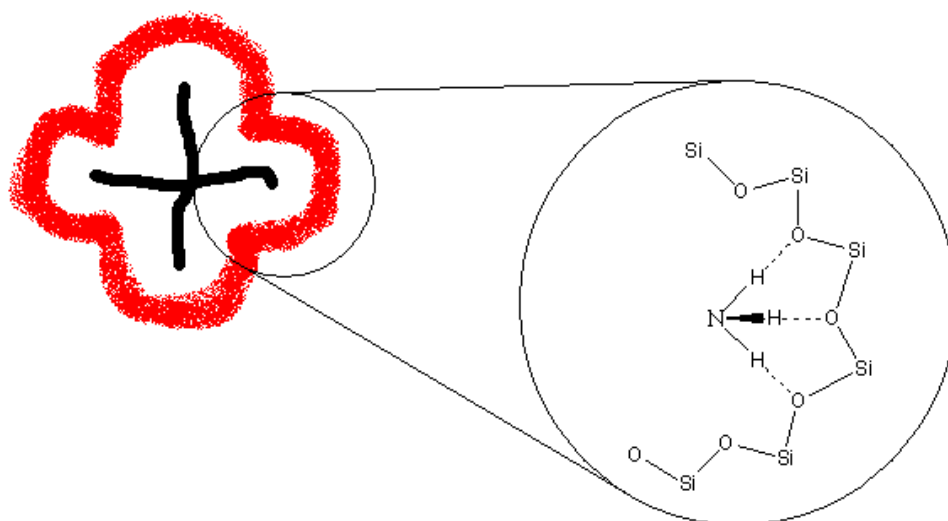


Figure 1.5.1: Amine group and TO₄ units, shown here as linked SiO₄ tetrahedra are surrounded 'hydration spheres'. Assuming that the kinetics are acceptable these will overlap, forming composite species, shown below.



The formation of the composite species, shown above, is followed by nucleation and then crystal growth to give a regular array of pores and channels.

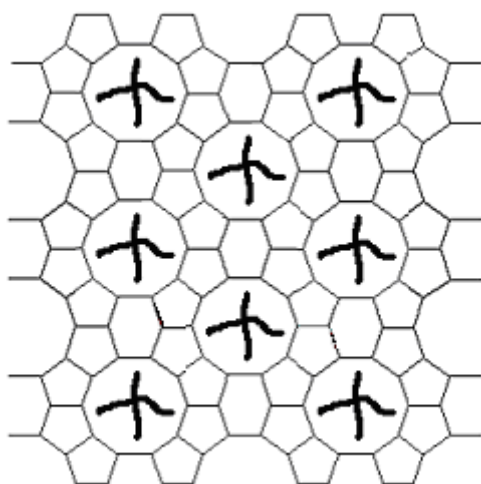


Figure 1.5.2: Schematic diagram illustrating the potential formation of siliceous zeolite ZSM-5.¹⁷ The tetramethyl-ammonium hydroxide, shown here in red, creates a sphere of water molecules around itself, as does the SiO_2 . These spheres can then overlap to form a composite species. The composite species come together to form an open framework, known as ZSM-5.

Synthesising novel microporous materials in this manner relies heavily upon serendipity, as there is no set rule which indicates whether the molecule will act as a template, structural directing agent or take no part in the reaction at all. The issue of templating and structure directing is a complex matter, with some molecules acting as a template for specific microporous systems, but not for others. The same material can also be synthesised using different organic molecules, with pore sizes and dimensions bearing no real resemblance to the organic molecule responsible for them. Consequently organic molecules within microporous materials are classified in three ways¹⁸:

1. Templates: This leads to the formation of a unique structure, which relates to the geometry of the template
2. Structural direction agents: This refers to organic molecules which lead to the preferential synthesis of a particular structure, e.g. two different organic molecules being used for the synthesis of the same framework.

3. Space fillers: These occupy pores in molecular sieves and act to exclude water in order to stabilise the framework.

1.3 Crystal Formation

There have been many hypotheses about mechanisms by which crystal may form. It is thought that the two main routes are either the transformation of the solid gel phase, or by solution phase nucleation and then crystallisation.¹⁹

Transformation of the solid gel phase

This mechanism is based on the principle that the composition of the reactants matches that of the final product. When treated under hydrothermal conditions, or even dried slowly, crystallisation occurs. Evidence for this mechanism has been provided using various techniques, including in-situ X-ray diffraction.²⁰

Solution phase crystallisation

Zeolites crystallising from a clear solution²¹ cannot be explained in terms of chemical reactions at the solid/solution phase boundary. Instead it has been hypothesised that a nucleation occurs in the solution state, allowing complete freedom of motion of the crystallising units.²² Many believe that in a standard hydrothermal reaction, an equilibrium exists between the solid gel and the corresponding solution. This equilibrium shifts toward the solution when nucleation occurs, thus the gel is always dissolving in the solution, providing the continuous supply of building units for crystal formation. This mechanism of formation could also support the hypothesis that secondary building units are formed from the combination of primary building units, which can then randomly move in suspension until they find a suitable place to crystallise.

1.4 Mixed Co-ordination Frameworks

In the years that followed the initial breakthrough by Barrer and Milton, many novel zeolite structures were reported. All of these structures consisted entirely of corner-sharing SiO₄ or AlO₄ tetrahedra. Bonding within zeolite frameworks is largely covalent, however it can be

useful to imagine these framework solids as comprising of a network of cations and anions bonded together through ionic interactions. This allows a greater understanding of framework formation and can be used in conjunction with the application of 5 rules, postulated by Pauling in 1929.²³

1. The Coordination Principle – *“a coordination polyhedron of anions surrounds each cation. The cation-anion distance is determined by the sum of the cation and anion radii and the number of anions coordinating with the cation is determined by the relative size of the cation and anion.”*
2. Electrostatic Valency Principle – *“in a stable ionic structure, the total strength of the valency bonds that reach an anion from all neighboring cations is equal to the charge of the anion.”*
3. Sharing of Polyhedral Elements (I) – *“the existence of edges (and particularly faces) common to coordination polyhedra decreases the stability of ionic structures”*
4. Sharing of Polyhedral Elements (II) – *“in a crystal containing different cations, those with large valence and small coordination number tend not to share polyhedral elements with each other.”*
5. Principle of Parsimony – *“the number of essentially different kinds of constituents in a crystal tends to be small.”*

In 1954, Loewenstein applied Pauling’s third rule to zeolitic materials.²⁴ Loewenstein explained why the maximum substitution of silicon by aluminium in a zeolite system is 50%. This implies that the Si/Al ratio should always be equal to, or greater than one, there are very few known exceptions to this rule.²⁵ Loewenstein reported that the formation of Al-O-Al connectivity, when both aluminium cations were at the centre of AlO_4 tetrahedra, is strictly prohibited. Loewenstein remarked that for Al-O-Al bonds to be allowed; at least one of the aluminium cations must be coordinated to five or six anionic species, i.e. oxygen atoms. There are some exceptions to this hypothesis, in that there has been zeolite frameworks constructed entirely of aluminium, however these materials have been prepared via non-hydrothermal conditions.^{26, 27}

The work carried out by Flanigen and co-workers⁸ on synthesising and characterising the first aluminophosphates framework, led onto the replacement of both the metal and non-metal species. A consequence of this is that some metallic species, including aluminium, are capable of coordination to more than 4 anionic species, such as oxygen. The implications

that the inclusion of coordination polyhedra which are not solely tetrahedra, together with incorporation of metallic species other than aluminium has been very significant. Over 25 chemical elements of the main block and the transition elements have been incorporated into open framework solids as major components.⁹ This has enabled many new framework architectures to be synthesised, which involve different polyhedra, such as $[XO_6]$, $[XO_5]$, $[XO_4]$ pyramidal, or $[XO_3]$ as well as tetrahedra. Owing to the larger coordination environments, Loewenstein's rules are no longer effective, allowing polymeric units, infinite chains or layers of MO_6 octahedra.

In addition to this, the classical convention that polyhedra only corner share has been altered since the characterisation of edge sharing and face sharing polyhedra. Possible dimer units for different polyhedral units are shown in figure 1.6.

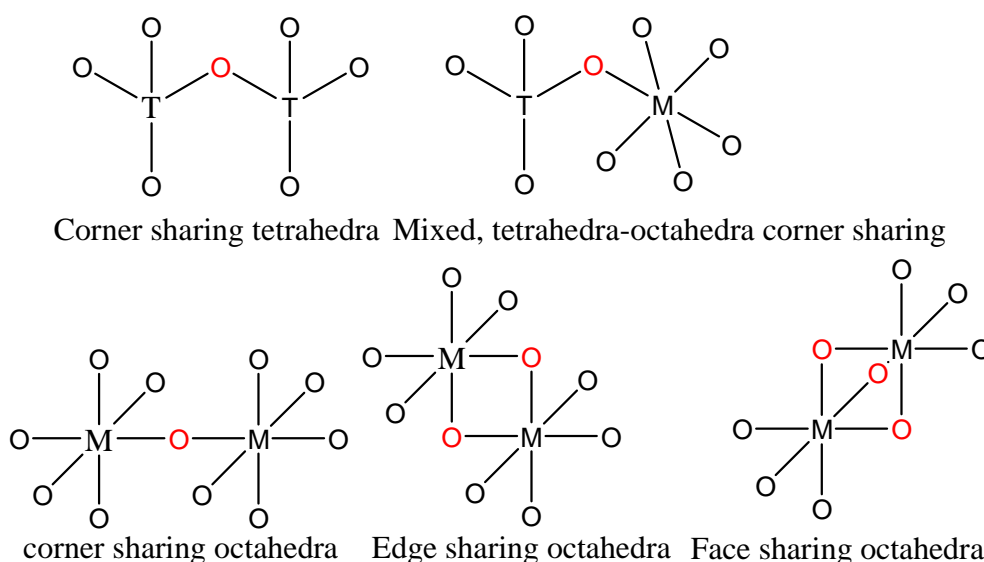


Figure 1.6: Schematic representation showing some of the possible conformations that tetrahedral and octahedral primary building units may assume when connecting.

1.5 Metal Organic Framework (MOF) Materials

Metal organic framework (MOF) materials are materials in which metal centres are joined to each other through organic 'linker' molecules. Research into this area of materials has become increasingly common over the last 15 years as such materials have several potential applications ranging from adsorption, storage and separation of molecules;²⁸ for example, there is currently intense interest in the use of porous solids for hydrogen storage^{29, 30} and

purification,³¹ to aid fuel cell technologies in the increasing and constant demand to provide a higher quantity and quality of clean energy

MOF materials can be thought of simply as the addition of linker molecules to metal cations sites, which assume a regular array and can result in the formation of porous framework materials which extremely low framework densities. This is represented in its simplest form in figure 1.7.

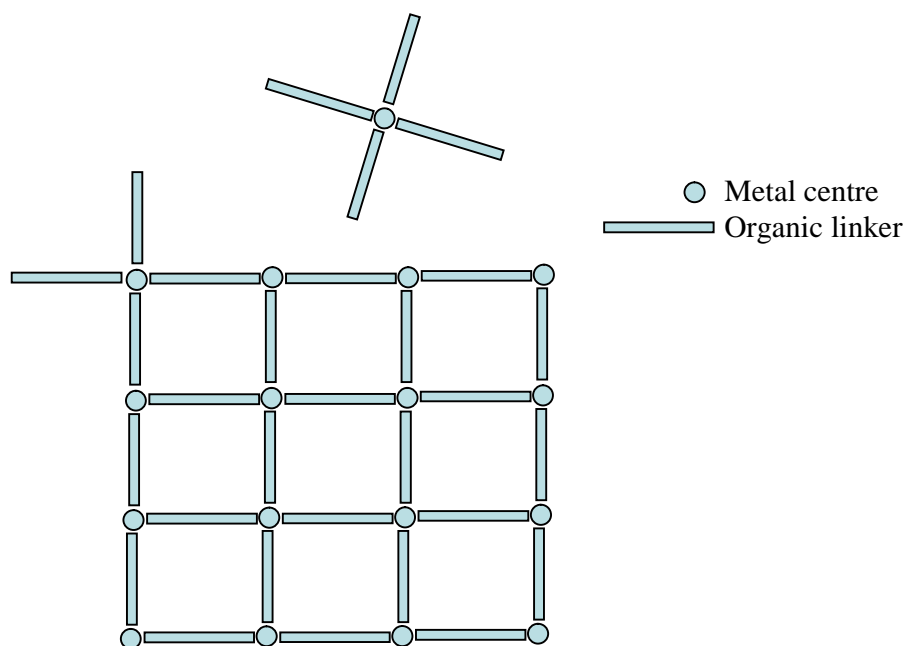


Figure 1.7: Schematic representation of a MOF material showing metal centres linking together via organic linker units to form a 'porous', material

Over the past 15 years there has been continual and increasing research into the formation of novel MOF materials. In particular metal carboxylate systems have received attention, using di- and trivalent metals with di- and tri-carboxylic acids. Within the metal carboxylate materials, various metal environments have been reported, such as four zinc atoms coordinating to the same oxygen atom, i.e. MOF-5, or three chromium atoms coordinating to the the same μ_3 oxygen atom, such as in the case of MIL-100 or MIL-101.^{32, 33}

Bipyridyl ligands have also been used successfully within MOF materials, which rely on bonding between the metal centre and the nitrogen atom of the bipyridyl ligand. These ligands have also been reported in mixed systems, in which both carboxylic acids and bipyridyl molecules have been used to produce porous MOF materials.³⁴

More recently, metal phosphonate systems have been reported in the literature. As many templated phosphate and phosphite materials lack structural stability upon removal of the template, the use of phosphonic and bisphosphonic acids within microporous materials provides a route for the functionality and structural directing effects of organic moieties to be included without compromising the structural integrity of the material.

1.6 The History and Chemistry of Scandium

Dmitri Mendeleev is credited as being the primary creator of the first version of the Periodic Table of elements. Unlike tables proposed by others, he noted gaps in the table, and predicted that as of yet unknown elements existed with properties appropriate to fill those gaps. Mendeleev predicted the existence of the element 'ekaboron', and in 1871 predicted an atomic weight of 44 g mol^{-1} . The prefix 'eka' is derived from Sanskrit (the classical language of India), meaning one. The name 'ekaboron' is given as the then unknown element was predicted to be one element away from boron in the Periodic Table.

Scandium was discovered by Lars Fredrik Nilson³⁵ in the minerals euxenite and gadolinite, which had not yet been found anywhere except in Scandinavia. Nilson processed about 10g of euxenite and other rare earths, and isolated about 2g of high purity scandium oxide.

The relative abundance of scandium is apparently far higher in the sun and certain stars than it is here on earth. It is about the 23rd most abundant element in the Sun, compared to the 50th most abundant on Earth; however, there are no reports of it occurring in concentrated deposits, but rather in very minute quantities in over 800 mineral species.³⁶

The metallic form of scandium was first reported in 1937 by Fischer, Brunger, and Grienerlaus who electrolyzed a eutectic melt of potassium, lithium, and scandium chlorides at 700 to 800 °C. Pure scandium is now produced by reducing scandium fluoride with calcium metal. The production of the first pound of 99% pure scandium metal was announced in 1960.

Scandium is mainly observed naturally in a trivalent cationic state, and although reduction can occur, there are few examples of Sc^{2+} .³⁷ The ionic radius of Sc^{3+} indicates that isoivalent and alioivalent substitution into open framework solids should be possible. Figure 1.8 gives a comparison of the ionic parameters for scandium and other metal cations which have been incorporated into open framework solids.

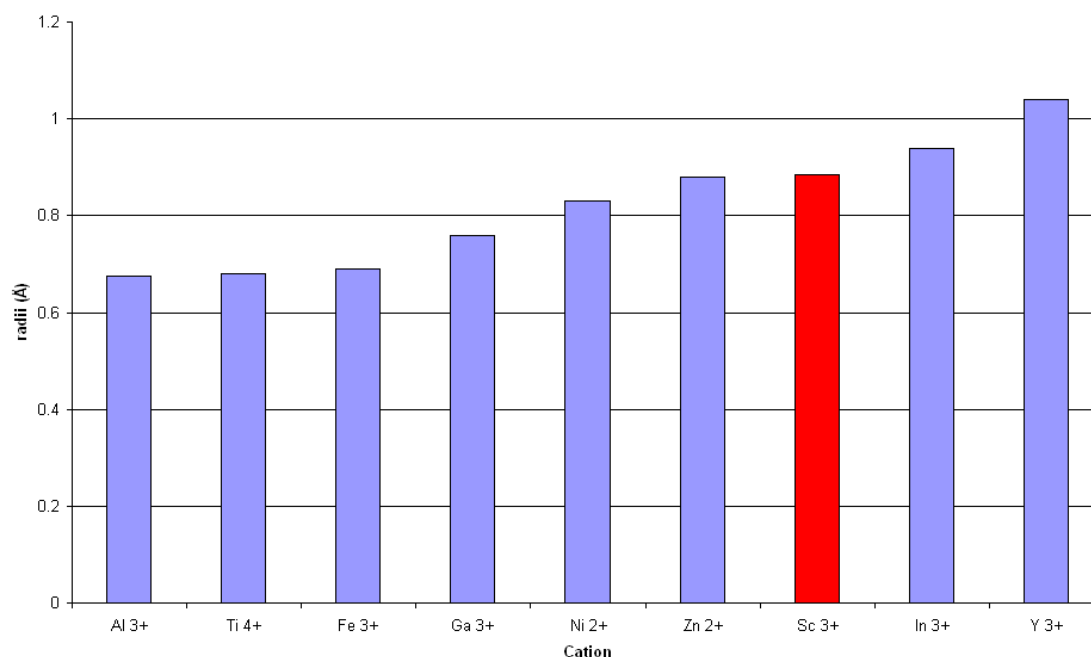


Figure 1.8: Ionic Radii of 6 Co-ordinate metal cations

Owing to the cationic radii of the Sc^{3+} cation, it is envisaged that scandium will coordinate to six anionic species, i.e. oxygen anions, resulting in an octahedral coordination environment, similar to that noted for other trivalent transition metals, e.g., chromium, yttrium and aluminium.

As scandium does not occur in concentrated deposits, obtaining enough scandium for research purposes has previously been too expensive. Within the past 10 years, scandium oxide is becoming increasingly available, at an affordable price, being obtained as a by-product from uranium mill tailings.³⁷

Scandium is a silver-white metal which develops a slightly yellowish cast upon exposure to air. It is a relatively soft metal, and can be associated with yttrium and the rare-earth metals more than it can be with aluminum or titanium. It is a very light metal and has a much higher melting point than aluminium, 1541°C as opposed to 660°C , making it of interest to spacecraft designers.³⁸

Scandium oxide, Sc_2O_3 is a relatively inert solid, although it is soluble in strongly acidic or alkaline solutions. It is an insulator and thus unlikely to impart any electronic or magnetic properties to solids, however these are similar attributes to Al_2O_3 , which has been extensively used in open framework synthesis since the middle of the 20th century.

The crystalline integrity of scandium oxide remains after it has been thermally treated to temperatures in excess of 1000°C, a desirable attribute which could potentially be imparted upon scandium-containing solids.

Scandium is also ideal for structural characterisation. It is a good X-ray scatterer, allowing characterisation by single crystal diffraction and powder diffraction and has a 100% abundant quadrupolar ($I = 7/2$) nucleus, ^{45}Sc , and therefore is amenable to characterisation by solid state NMR.

Due to the increased availability of scandium at a more affordable levy, research into its properties as a structure directing component of open framework solids has only just begun. It has only been in the past 5 years that scandium has been hydrothermally incorporated into silicates, phosphates³⁹⁻⁴⁶, phosphites, phosphonates⁴⁷, sulphates⁴⁸, carboxylates⁴⁹⁻⁵³ and fluorides.⁵⁴⁻⁵⁶ There are few examples describing investigations into the hydrothermal incorporation of scandium into microporous materials within the literature, those of which there are, will be described in the relevant chapters of this work.

1.6 Aims

The principle aim of the work contained within this thesis is to examine the hydrothermal chemistry of scandium during the crystallisation of open framework and microporous materials.

This will include investigation of the chemistry of the Sc^{3+} cation in phosphates, phosphites, phosphonates, silicates and carboxylates, with the goal of synthesising both novel materials and porous, thermal stable materials with potential applications in catalysis, sorption and separation.

It will be necessary to characterise novel materials as fully as possible. There is relatively little literature on the incorporation of scandium into open framework materials, and so there is little ^{45}Sc NMR data. One aim of this work is to characterise phase pure materials using ^{45}Sc MAS NMR techniques and therefore begin to map the chemical shift range of the ^{45}Sc nuclei within different local environments.

Chapter 2: Experimental Techniques

2.1 Introduction

As discussed in chapter 1, the main aim of this work is to investigate the hydrothermal chemistry of scandium. To accomplish this, scandium-based, crystalline open framework and microporous materials will be synthesised via hydrothermal routes, and characterised using various techniques. The aim of this chapter is to discuss the theory behind the different experimental techniques applied in this work

2.2 The Basics of Crystallography

2.2.1 Crystals

Crystal structures are arrangements of atoms that possess translational symmetry. They are conveniently described in terms of a lattice, an infinite periodic array of points in identical environments. The identical points are called lattice points and associating an arrangement of atoms (structural motif) with each lattice point gives rise to the crystal structure. The unit cell is the simplest repeating unit of a crystal. It defines the parameters and co-ordinates that, when repeated in all three dimensions, describe a crystalline solid. The unit cell requires six parameters to be defined properly; three lengths (a , b , c) and three angles (α , β , γ). When lattice points are applied to unit cells, they may be positioned differently to allow the description of different crystal systems.

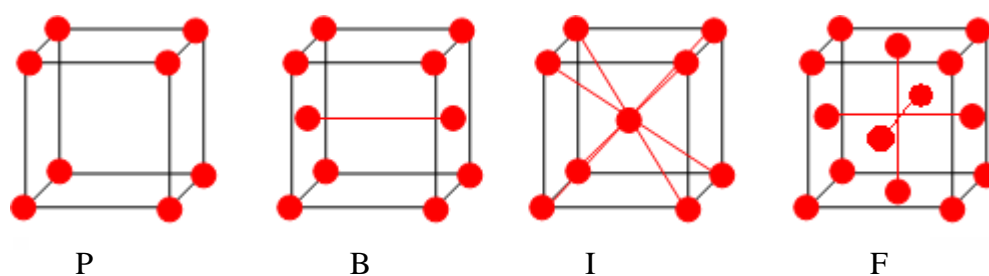


Figure 2.1: Possible lattice point positions. ‘P’ is representative of a primitive unit cell, ‘B’ is showing a lattice point centred on the (010) plane, or B-plane, ‘I’ is a body centred unit cell and ‘F’ shows a lattice point centred on all faces.

2.2.2 Seven Crystal Systems

All crystals may be described in terms of subunits that exhibit the same essential symmetry elements as the crystal itself. There are seven distinct types of subunits associated with the seven crystal systems, described in table 2.1.

Crystal system	Lengths	Angles	Defining symmetry
Triclinic	$a \neq b \neq c$	$\alpha \neq \beta \neq \gamma$	None
Monoclinic	$a \neq b \neq c$	$\alpha = \beta = 90^\circ \gamma \geq 90^\circ$	Twofold axis or mirror plane or inverse twofold axes
Orthorhombic	$a \neq b \neq c$	$\alpha = \beta = \gamma = 90^\circ$	Three orthogonal twofold or inverse twofold axes
Tetragonal	$a = b \neq c$	$\alpha = \beta = \gamma = 90^\circ$	One fourfold or inverse fourfold axes
Trigonal	$a = b = c$	$\alpha = \beta = \gamma \leq 120^\circ$	One threefold or inverse threefold axes
Hexagonal	$a = b \neq c$	$\alpha = \beta = 90^\circ \gamma = 120^\circ$	One sixfold or inverse sixfold axes
Cubic	$a = b = c$	$\alpha = \beta = \gamma = 90^\circ$	Four threefold axes

Table 2.1: Seven crystal systems

The seven crystal systems described in table 2.1 can be classified further depending upon the symmetry elements present in the system. There are 32 different ways in which rotation axes, mirror planes, centres of symmetry and rotary inversion axes can be used to describe the 7 crystal systems.

There are fourteen distinctive space lattices known as Bravais lattices which are formed by combination of the lattice type and crystal system. Table 2.2 shows the simplest combinations which make up Bravais lattices.

System	Bravais Lattice
Triclinic	P
Monoclinic	P, C
Orthorhombic	P, C, I, F
Tetragonal	P, I
Trigonal	P
Hexagonal	P
Cubic	P, I, F

Table 2.2: 14 Bravais Lattice, seven primitive and seven non-primitive.

Combination of the 32 point groups and the 14 Bravais lattices produces 230 unique three dimensional arrangements, known as space groups. These 230 combinations are the only ways in which identical objects can be arranged in a three dimensional space.

The 32 point groups were derived without using translation elements of symmetry. Combinations of rotations plus parallel translations produce screw axes. Screw axes are designated by integers n and m where $n = 1, 2, 3, 4$ or 6 and $m < n$, e.g. 3_1 indicates a threefold screw axis with a translation between equivalent points $1/3$ of a unit translation.

Combining mirror planes and translations produces a glide plane. Glide planes can be described by referring to vectors a , b and c which define the unit cell edges. An a -glide, perpendicular to the b axis, for example, results in reflection through the plane and translation by $1/2a$.

A space group is described by a capital letter to identify the lattice type (P, C, F, etc) followed by the point group symbols in which rotation and reflection symmetry is followed by the screw axes and glide planes. The effects that symmetry has on a unit cell is usually referenced to an arbitrary point x, y, z . The elements of symmetry for a specific point group act on the point and produce a list of equivalent positions.

2.2.3 Miller Indices

Miller indices (hkl) are integer values which define a set of parallel, equally spaced lattice planes within a particular unit cell. hkl intercept the x, y and z axes of a unit cell at lengths of a/h, b/k and c/l respectively.

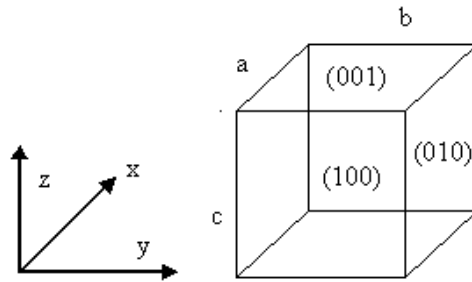


Figure 2.2: Indexing the three faces of a crystal or a unit cell. If an index is 0 the planes are parallel to the associated axes.

2.2.4 X-Rays

X-rays are short-wavelength electromagnetic radiation with a wavelength, λ , in the range of 0.1 to 100Å. X-rays are generated by bombarding a metal target with electrons accelerated through approximately 10000 to 30000 electron volts. Two types of x-rays result from this interaction.

1. As the electrons hit the target they slow down, or potentially stop, and in doing so, lose energy. Most of this energy is converted to heat, but some is exhibited as a broad spectrum of wavelengths, including x-rays
2. The electrons from the electron source have enough energy to ionise electrons from the target atoms and so create vacancies in the lower electron orbital. These vacancies are filled by electrons from the outer shell dropping down, Aufbau principle, and in doing so energy is released in the form of x-rays. These transitions are quantised, therefore have a specific energy values associated with each transition. They are also subject to the condition that $\Delta l = \pm 1$, e.g. $p \rightarrow s$ or d .

Consider Copper where a vacancy in the 1s orbital can be filled by electrons from the 2p and 3p orbitals.

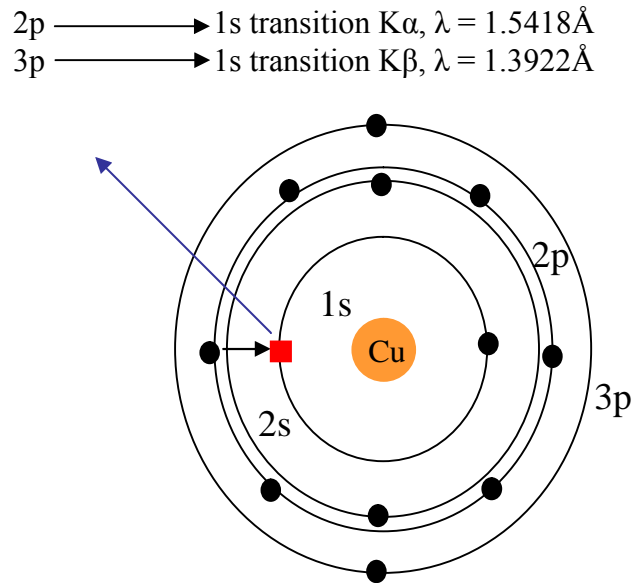


Figure 2.3: Vacant 1s orbital position, red square, in copper being filled by a 2p electron, black circle. The blue arrow represents the emitted x-ray.

The $K\alpha$ wavelength is more intense than the $K\beta$ as the 2p to 1s transition occurs more frequently than the 3p to 1s transition. The $K\alpha$ transition occurs as a doublet of $K\alpha_1$ and $K\alpha_2$, with a small difference in energy and hence λ , as there are two possible spin states for the 2p electrons.

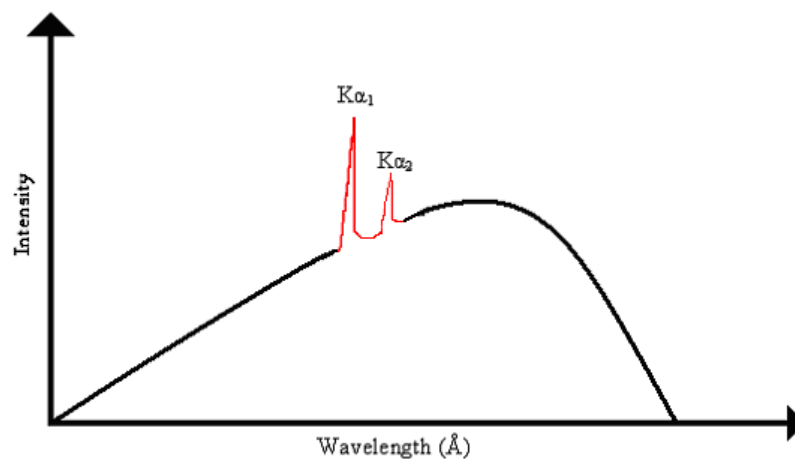


Figure 2.4: Spectrum of white radiation produced when electrons bombard copper. Only the $K\alpha_1$ and $K\alpha_2$ peaks are shown, with a wavelength of 1.5405 and 1.54433 \AA respectively.

2.2.5 Diffraction of X-rays by crystals

In order to successfully determine the composition of crystal, and ultimately the unit cell, structural analysis by x-ray diffraction is one of the most powerful analytical techniques available.

When x-rays are passed through a crystal they are scattered by every atom within the lattice. The 'scattered' x-ray beam does not alter in wavelength, however depending upon the distance it has had to travel, it may alter in phase from that of the original x-ray. If the phase of the x-ray has been altered, destructive interference occurs, and if the phase of the x-ray is the same, constructive interference occurs, figure 2.7.

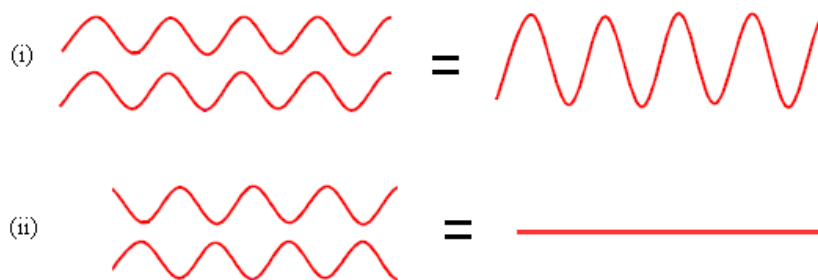


Figure 2.5: Illustration of Constructive and Destructive interference, using the two possible extremes as example, waves which are (i) exactly in phase and (ii) waves which are exactly out of phase

Bragg's law describes the interference pattern generated by x-rays which interfere constructively with each other after they have been scattered by the crystal. When an x-ray beam enters a crystal, the angle between the incident beam, I , and the lattice planes of the crystal is designated theta, θ . Beams which reach lower lattice levels of a crystal structure, travel a greater distance (shown as $AB + BC$ on figure 2.6) this is known as the path difference. The path difference can also be written as $2 d \sin \theta$. For total constructive interference to occur, the path difference must equal an integer of the wavelength of the x-ray beam.

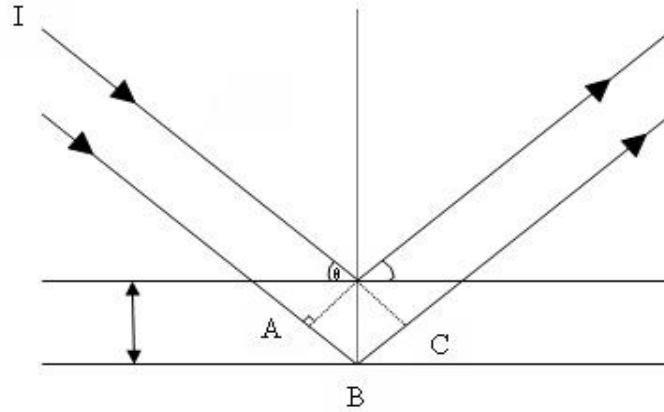


Figure 2.6: Mathematical analogy proposed by Bragg to explain the diffraction of x-rays by two planes of a crystal.

Therefore:

$$n\lambda = 2d \sin \theta$$

Equation 2.1: The Bragg Equation

Diffraction may be observed when $n\lambda = 2d \sin \theta$, where n is an integer. The intensity of reflections varies, and get weaker at higher scattering angles. When x-rays interact with an electron, they induce an oscillation in the same direction of the electric vector for the incident beam. The oscillation electron then acts as an x-ray source itself, as it radiates the x-ray beam with the same or lower frequency as the incident beam. If the electron which is struck is completely free then the scattered radiation is proportional to the displacement of the electron as it oscillates. A phase difference between the incident and scattered beams is induced such that the secondary scattered x-ray wave differs in phase by 180° .

The diffraction pattern is obtained by the Fourier transformation of the electron density within the unit cell.

The amplitude $|F|$ and phase ϕ of a diffracted wave are integral to each reflection in a crystal diffraction pattern.

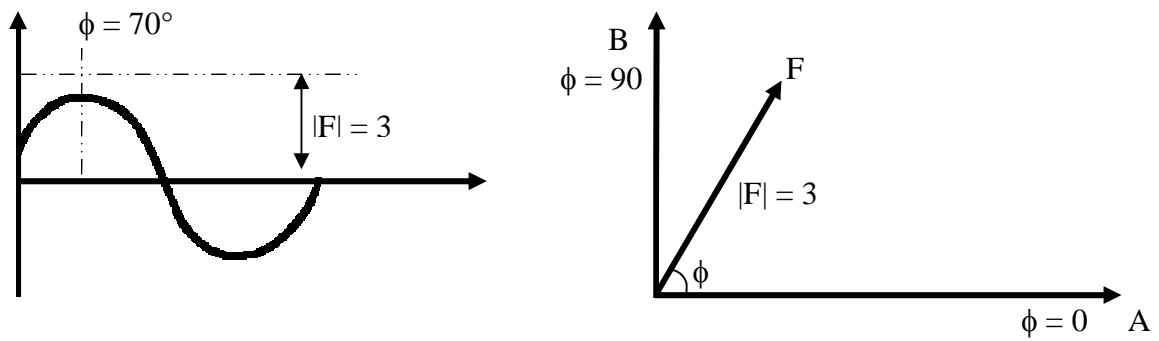


Figure 2.7: The figure shown on the left shows a wave with an amplitude and phase, which is represented as a vector in the diagram on the right. Vector 'F', has both a magnitude $|F|$ and a direction ϕ .

The position of the arrow head in the vector diagram in figure 2.7 can therefore be given as co-ordinates along the A and B axes. This can be illustrated by the equations shown below in equation 2.2.

$$|F|^2 = A^2 + B^2 ; \tan \phi = B/A$$

$$\therefore A = |F| \cos \phi \text{ and } B = |F| \sin \phi$$

Equation 2.2: The position of the intensity can be calculated by using Pythagoras theorem and trigonometry

Intensities can be added together in order to form an image of the electron density in the diffraction pattern.

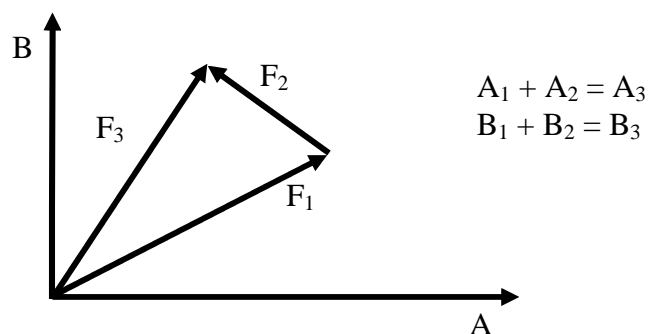


Figure 2.8: Vector addition diagram which shows the how different waves represented by vectors, F_1 and F_2 , can be combined to give an overall representation, shown by F_3

This is applicable to any number of waves, and due to the different trigonometric relationships given in equation 2.2, the A and B terms must be dealt with independent of each other. Indeed calculations performed by modern computational programs treat the A and B components individually, however in order to avoid writing each equation twice, both can be represented in the same equation by the introduction of a single complex number, i .

$$F = A + iB$$

In complex numbers: $e^{i\phi} = \cos\phi + i\sin\phi$

$$\begin{aligned} \therefore F &= |F| \cos\phi + i|F|\sin\phi \\ &= |F| (\cos\phi + i\sin\phi) \\ \therefore F &= |F| \cdot e^{i\phi} \end{aligned}$$

Each reflection can be represented by its three indices (hkl)

$$\therefore F(\text{hkl}) = |F(\text{hkl})| \cdot \exp [i\phi(\text{hkl})]$$

Where $F(\text{hkl})$ is known as the structure factor of the reflection with indices h, k and l

The structure factor, F , is the amplitude (including relative phase) of x-rays scattered by one unit cell in the direction of the hkl reflection. The measured intensity of the reflection is proportional to the square of the magnitude of F .

$$I \propto |F|^2$$

If the structure is known, i.e. the positions of all the atoms in the unit cell, the above equations can be used to calculate the structure factors. However, the opposing Fourier transform of the diffraction pattern is the crystal structure expressed in terms of electron density. This implies that the crystal structure can be resolved using the structure factors obtained, and the equation for calculating this is shown below, equation 2.3.

$$\rho_{(xyz)} = \frac{1}{V_c} \sum F_{(hkl)} \exp[-2\pi i(hx + ky + lz)]$$

Equation 2.3: *The electron density equation. V_c is the volume of the unit cell and is required to give the correct units for electron density*

The required phase information about the reflections, necessary to obtain the electron density from the diffraction pattern, is unknown. This is the phase problem. In order for equation 2.3 to yield accurate information, both the phase and amplitude values are required.

In order to calculate crystal structures, several methods have been introduced which combat the phase problem.

2.2.6 Direct Methods⁵⁷

Direct Methods are techniques that find the correct phases for diffraction peak intensities by statistical means. In order to implement direct methods, two generalisations must be made:

1. Electron density ≥ 0 . There cannot be any negative values
2. Only discrete atoms make up the structure.

The positive electron density must be obtained from the combination of the structure factor amplitudes with the correct phase components. Applying these constraints means that the phase component value is limited and thus the probable phase for a given group of reflections can be determined.

Atomic co-ordinates may then be obtained by using the calculated phase information and the normalised structural factors. Modern applications of this technique involve computer programs such as SIR⁵⁸, which calculates all the atomic co-ordinates in a fraction of the time.

2.2.7 The Patterson Function

The Patterson function relates the electron density to the squared sum of the structure factor.

$$\rho \propto |F_{(hkl)}|^2$$

This overcomes the phase problem as the measured intensities, I_{hkl} are proportional to $|F_{(hkl)}|^2$. Using the calculated electron density, a Patterson map can be generated with each of the atomic positions being defined as a set of vectors. This method is not usually used in structural determination of zeolites or zeotypes as many of the atoms in such frameworks have similar scattering abilities, consequently producing a Patterson map with a large number of very similar peaks. This makes it difficult to determine the atomic co-ordinates for the framework atoms.

2.3 Structure determination by x-ray diffraction methods

2.3.1 Single Crystal Diffraction

Single crystal diffraction is the most powerful analytical techniques available for structure characterisation. The application of this technique to structure resolution is now considered routine, due to the accuracy of laboratory equipment and the time taken for a computer to complete the many calculations which are needed in order to solve a structure. Since the early 1990s area detectors have been used for the collection of diffraction data, before this four-circle diffractometers were used. The most commonly used type of area detector is the charge-coupled device (CCD).

Single crystal diffraction requires a single crystal of material, which is mounted onto a glass fibre, aligned on a goniometer head and then placed into the x-ray beam. There is a detector situated behind the crystal in order to collect the x-ray reflections. When possible, single crystal x-ray diffraction data was collected on a Rigaku MM007/Mercury-CCD diffractometer or a MM007/Saturn equipped with XStream low temperature device working with monochromatic Mo $K\alpha$ radiation ($\lambda = 0.71073\text{\AA}$).

Single crystal diffraction is limited by the size of the crystal, with $10\mu\text{m}$ generally being at the lower limit for conventional single crystal techniques.



Figure 2.9: Goniometer head, upon which a glass fibre and single crystals can be mounted and aligned using the precision screws for translation and pitch to ensure that the crystal never leaves the x-ray beam

2.3.2 Powder Diffraction

Hydrothermal synthesis often produces crystals which are too small for single crystal diffraction. These samples are characterised by containing a small quantity of crystals, in either a disc or capillary tube, and rotating them around one axis in the x-ray beam. The orientations of the particles in these samples are random, which causes the observed diffraction pattern to be an average of many different orientations.



Figure 2.10: In-house powder X-ray analysis facility

Powder diffraction patterns result in the loss of structural information as peak overlap causes three dimensional information to be displayed in one dimension. This leads to ambiguities in space group determination, indexing and intensity assignment.

Throughout the course of this report, powder diffraction information has only been used for both the identification of phases, and the solution of structures (sometimes combined with molecular modelling techniques). All crystalline products were examined by X-ray powder diffraction on a STOE diffractometer with Ge monochromated Cu $K_{\alpha 1}$ radiation ($\lambda = 1.54056\text{\AA}$). The microcrystalline powders were examined in transmission geometry, where samples were mounted between two Mylar discs. Theoretical powder patterns were simulated using STOE WinXPow.⁵⁹

2.3.3 Synchrotron Radiation

Synchrotron radiation is many orders of magnitude more intense than the output from conventional laboratory x-ray tubes. Electrons are accelerated by a linear accelerator to speeds close to the speed of light, and their speed and trajectory are maintained by booster accelerators and magnets. When the electrons are travelling in a continual ring, they produce radiation, which is emitted at the point where the magnets ‘bend’ the electrons around the ring. Radiation continues at a tangent to the ring, and thus can be utilised at every magnetic bending point, this is shown diagrammatically in figure 2.11.

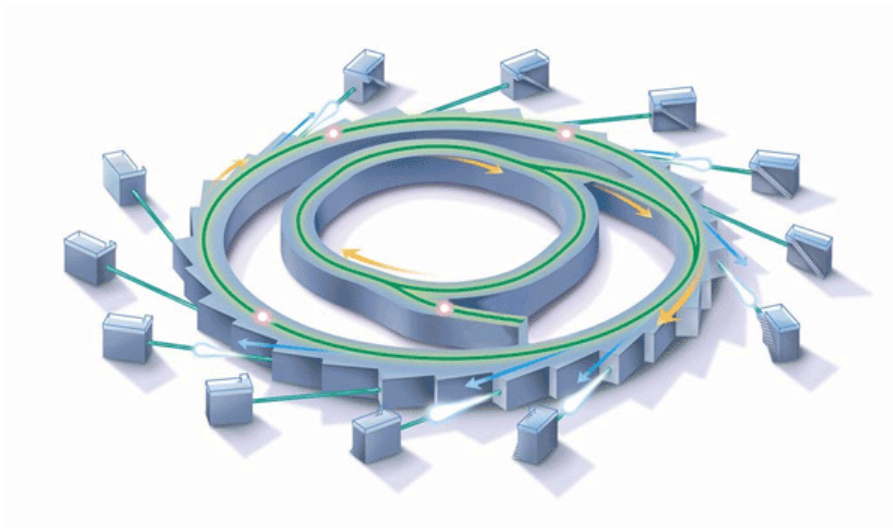


Figure 2.11: *Production of synchrotron radiation in a synchrotron storage ring. The orange arrows represent the direction of the electron beam, being redirected by the magnet situated around the ring. The synchrotron radiation is represented leaving the ring at a tangent, directed to experimental stations situated on the periphery of the ring*

The radiation which leaves the synchrotron storage ring at a tangent is known as a beam-line. This radiation has a full spectrum, ranging from infrared to x-rays. For most diffraction experiments, the desired wavelength is selected using a monochromator crystal. Station 9.8 at the Daresbury laboratories operates at an x-ray wavelength between 1.45\AA and 0.30\AA . There is greater intensity available using synchrotron radiation than using conventional laboratory diffractometers, enabling smaller crystals (i.e. $10 \times 0.8\mu\text{m}$) to be examined. Synchrotron single crystal x-ray diffraction was carried out on Station 9.8 or 16.2smx at the CCLRC synchrotron radiation sources, Daresbury Laboratories, using a Bruker SMART 1K CCD diffractometer.

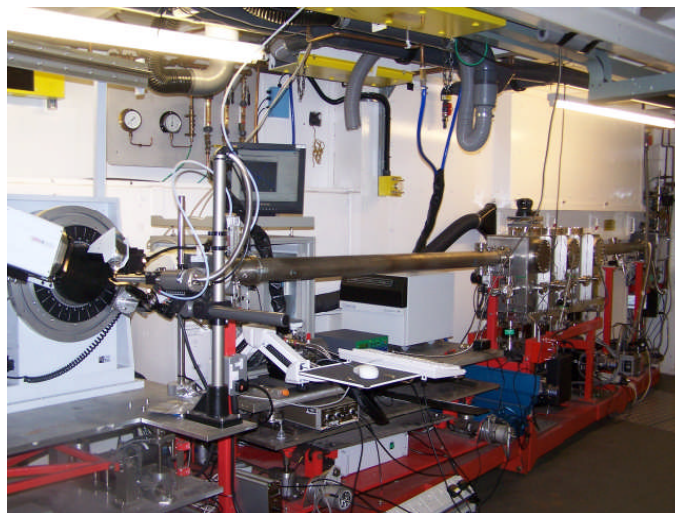


Figure 2.12: Station 9.8 at the synchrotron radiation facility, Daresbury, showing the single crystal station used for data collection on small single crystals.

2.4 Structure determination combining powder XRD and molecular modelling techniques

The hydrothermal synthesis of microporous materials does not always yield crystals large enough for their structures to be determined by single crystal methods. In such cases, it is possible to attempt structure solution using powder XRD data. This is a more difficult approach to use for structure determination, consequently far fewer structures are solved in this manner.

Once a crystalline product has been obtained, and crystal size or quality are insufficient for structure determination via single crystal techniques, powder diffraction methods can be utilised in order to determine the structure. Often when using powder diffraction methods for structure determination, only the heavier atoms can be found, as their scattering factors generally tend to dominate the experimentally obtained powder patterns. In these cases, a combination of powder diffraction structure solution packages and molecular modelling packages has proven to be helpful in the determination of structure of which powder analysis alone can not yield.⁶⁰

Structures which are determined using a combination of powder diffraction methods and molecular modelling must first be synthesised as a pure phase. An illustrative example is given here of the structural determination of $[\text{Ni}_2(\text{H}_2\text{O})_2 \text{N,N}'\text{-2-methylpiperazinebis-}$

(methylenephosphonic acid)].5.4H₂O, [Ni₂(H₂O)₂L].5.4H₂O. The powder diffraction data of the sample must be of high quality, preferably collected at a synchrotron source, however the pattern shown for this example, figure 2.13, was collected overnight on an in-house diffractometer. From the powder pattern, approximately 20 peaks should be selected and processed in order to determine the unit cell, using a program such as DICVOL04⁶¹.

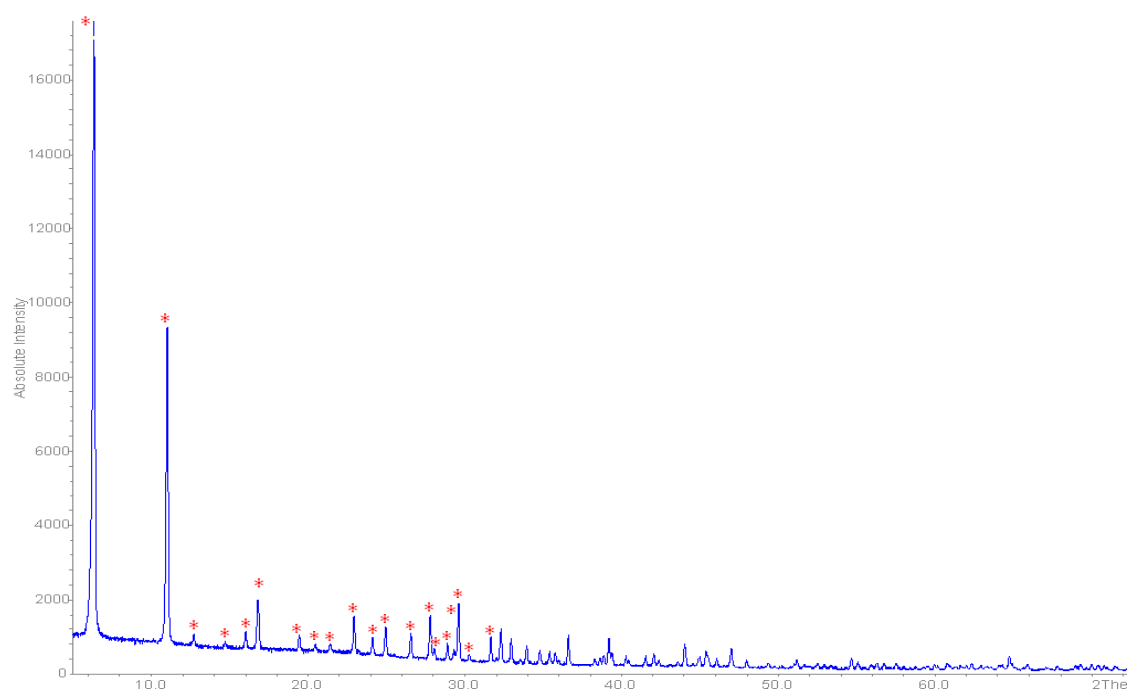


Figure 2.13: Powder diffraction pattern for [Ni₂(H₂O)₂L].5.4H₂O. The red marks indicate the peaks which were selected to determine the unit cell of the structure.

Following the successful determination of a unit cell, a space group should be decided upon. This is done by the examination of any systematic absence in the experimental data, and comparing these results to tables which can be found in the international journal of crystallography. At such an early stage of the structure determination, it is often more advisable to assign space groups which have lower symmetry operations imposed upon them, in order to increase the prospects of successful structure determination. If the structure is successfully solved but in the wrong space group, programs such as PLATON,⁶² are able to suggest any additional symmetry elements present.

The unit cell determined for the nickel bisphosphonate structure is given below in table 2.3, as well as possible space groups which would be permitted, given the systematic absences.

Unit Cell	Possible space groups
a = 27.93 Å $\alpha = 90.00$	R3 $\bar{R}3$
b = 27.93 Å $\beta = 90.00$	
c = 6.23 Å $\gamma = 120.00$	R3m $\bar{R}3m$

Table 2.3: The unit cell parameters and possible space groups, determined by examination of the systematic absences, for $[Ni_2(H_2O)_2L].5.4H_2O$

The unit cell was used in EXPO2004⁶³, a combination of the programs SIRPOW⁶⁴ and EXTRA⁶⁵. EXTRA uses Le Bail⁶⁶ algorithms to extract intensity from the experimental data, in the form of F_{hkl} 's, so that SIRPOW can use direct methods to calculate positions which are potentially electron dense. Figure 2.14 shows the input screen of EXPO2004 used in the determination of the nickel bisphosphonate structure. .

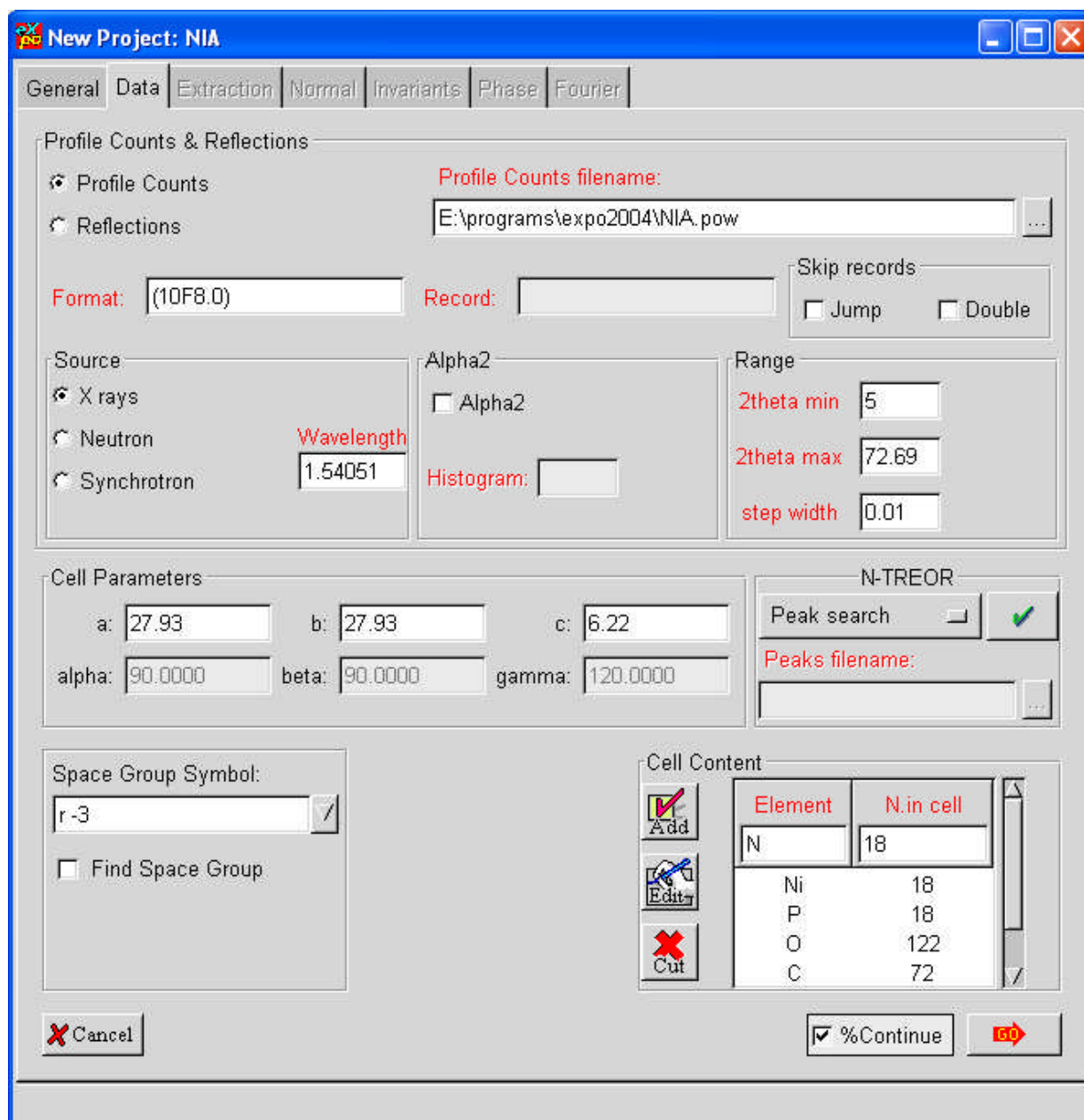


Figure 2.14: EXPO2004 input screen, showing the unit cell, wavelength and collection range for the experimental data and cell contents for $[\text{Ni}_2(\text{H}_2\text{O})_2\text{L}]\cdot 5.4\text{H}_2\text{O}$

Initial refinements using powder structure solution programs may only yield information about the positions of heavier atoms, however it may be possible to locate other atoms by Fourier maps. In the specific case of this example, the atomic positions which were originally suggested by direct methods were ignored, with the exception of the position given for the nickel atom. The atomic positions of some of the other atoms in the unit cell were identified through Fourier maps. Figure 2.15 shows the atoms which were located using EXPO2004.

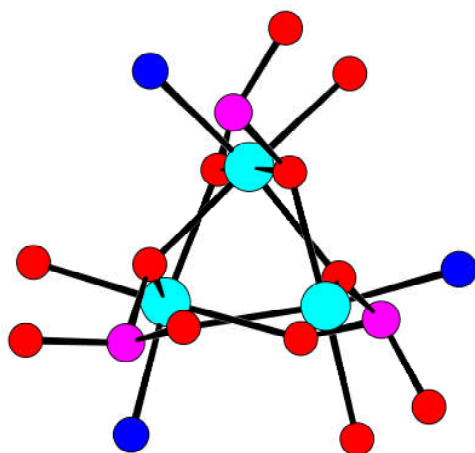


Figure 2.15: Nickel phosphonate chain identified from direct methods and Fourier maps. Cyan, purple and red represent nickel, phosphorus and oxygen respectively.

The atomic co-ordinates which were obtained from EXPO2004 were examined in Diamond, a molecular graphics program, and phosphorus to phosphorus distances were examined and compared to similar systems.⁶⁷⁻⁶⁹ From other structures, the piperazine ligand has only been found in the chair conformation, giving an average P-P distance of around 8Å.

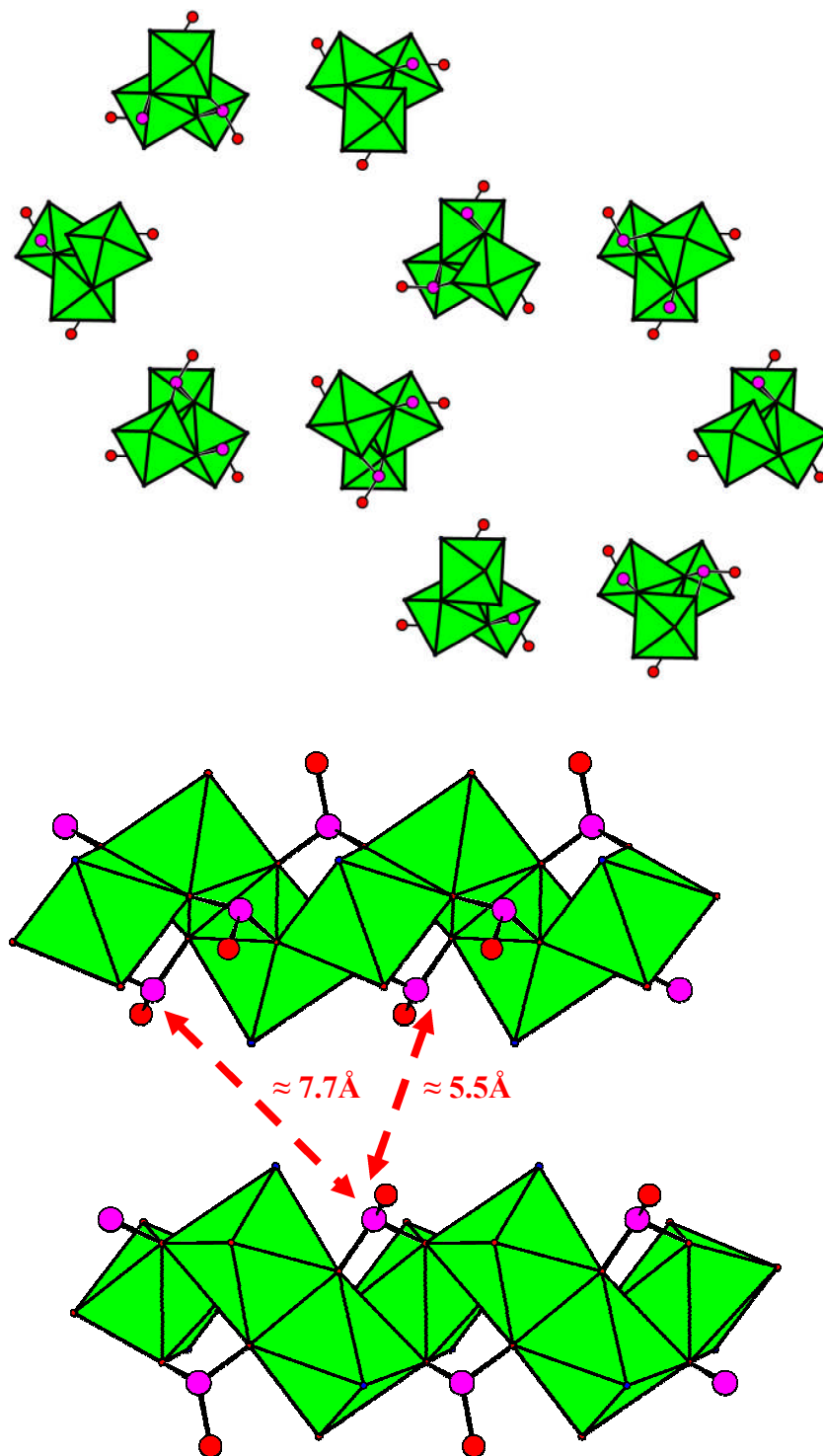


Figure 2.16: (Top): Unit cell of $[\text{Ni}_2(\text{H}_2\text{O})_2\text{L}]\cdot 5.4\text{H}_2\text{O}$ showing atoms which were found from direct methods and Fourier mapping. (Bottom) Relevant distances between the nearest phosphorus neighbours in the structure. Examination of the P-P distances in similar structures suggests an average distance of 8\AA

The atomic co-ordinates for the inorganic framework were input to Cerius² ⁷⁰, a molecular modelling package, figure 2.17. Using this software, it was possible to introduce the organic ligand to the structure, figure 2.18. This enabled the ligand to be placed in a variety of positions with the symmetry of the space group imposed at all times, allowing a visual check on the validity of the symmetry generated positions. One of the possible solutions for the position of the piperazine ring suggested that the nitrogens of the ring were situated within 2.5Å of the nickel atom. This meant that the nickel octahedron would have only one water molecule bonded to it, and a nickel – nitrogen bond as well. This solution agreed with the different bond lengths in the nickel octahedra and with thermal analysis of the material.

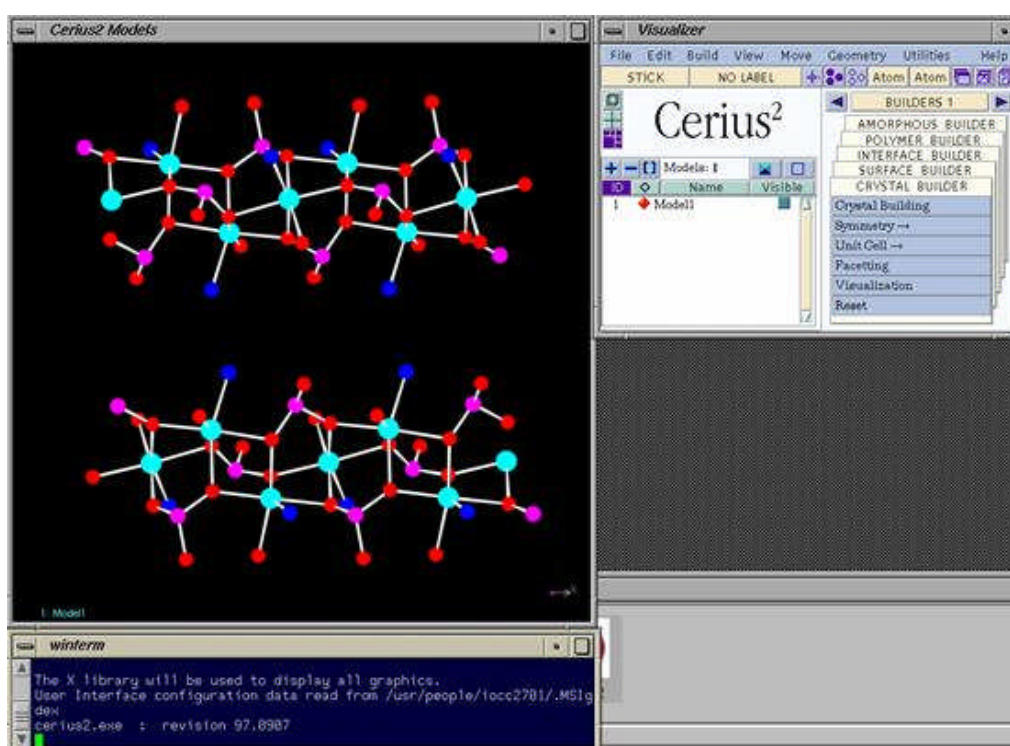


Figure 2.17: Screenshot from Cerius², showing the inorganic chains of the nickel phosphonate structure

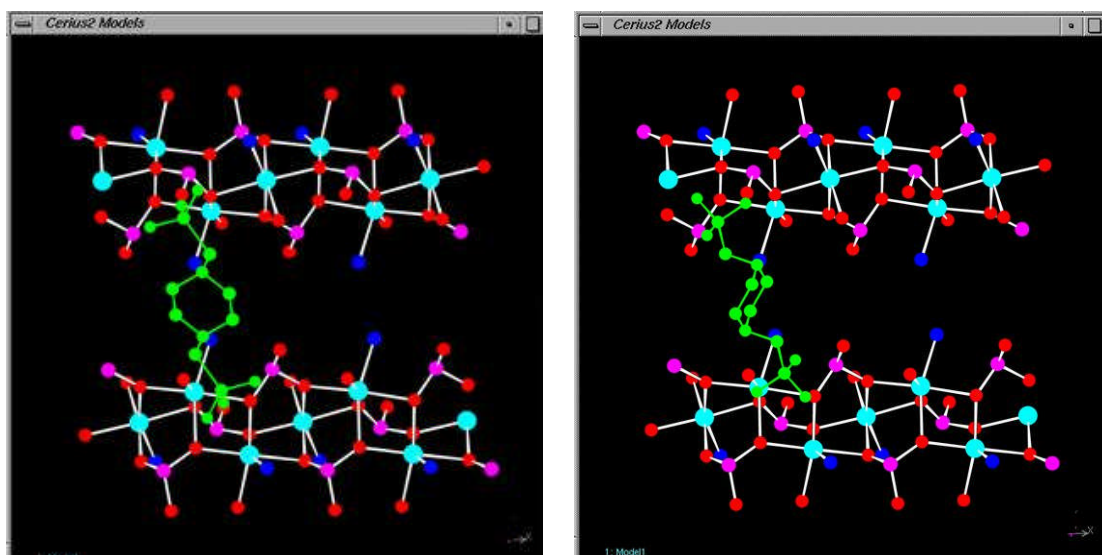


Figure 2.18 (left): Screenshot from Cerius², showing the introduction of the organic ligand, shown in green, between the inorganic chains. **(right):** rough positioning of the piperazine ring aligning phosphorus, oxygen and nitrogen atoms as close as possible.

Once the organic ligand was introduced between and joining the inorganic chains of the material, the energy of the structure was minimised by allowing the atoms to move. Two different types of force field were applied during the minimisation, with the organic and inorganic parts of the framework being minimised separately. The organic part was minimised using the CVFF force field, whereas the inorganic chains were minimised using a universal force field, figure 2.19.⁷¹

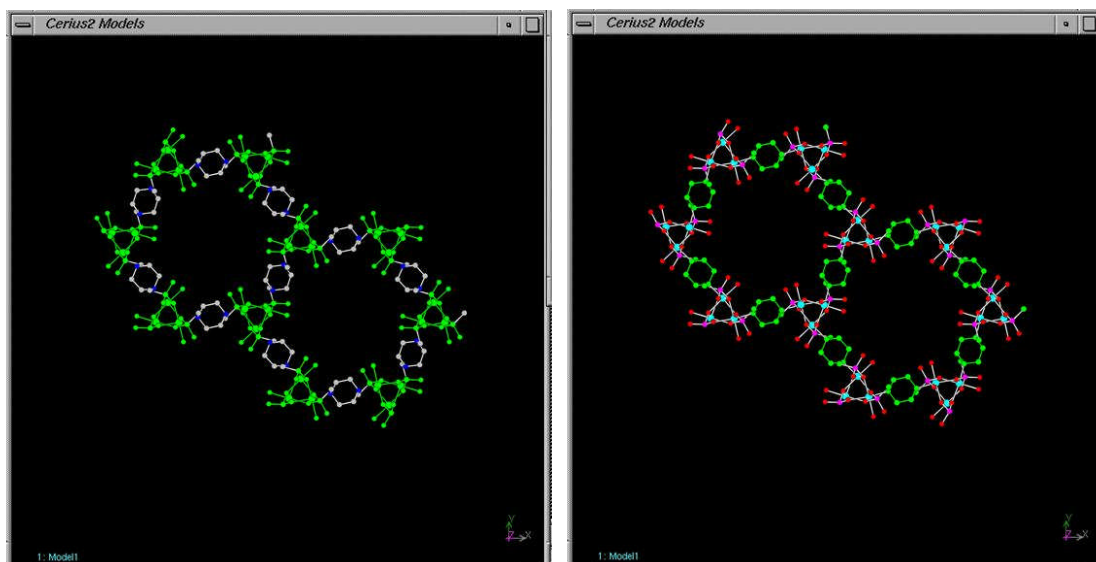


Figure 2.19 (left): View down [001] of $\text{Ni}_2(\text{H}_2\text{O})_2\text{L}5.4\text{H}_2\text{O}$ showing the organic moieties being minimised using the CVFF force field whilst the atomic positions of the inorganic chains remain unchanged. **(right):** View down [001] of $\text{Ni}_2(\text{H}_2\text{O})_2\text{L}5.4\text{H}_2\text{O}$ showing the inorganic chains being minimised using a universal force field whilst the atomic positions of the organic moieties remain unchanged.

Once an energy minimised framework was obtained, the atomic co-ordinates were input in GSAS, in order to refine the structure against the powder x-ray diffraction pattern using the method of Rietveld refinement, described later. The positions and quantity of the water molecules present within the pores were taken from a combination of positions suggested by the direct methods using EXPO2004, and thermal analysis of the material.

The final refinement cycles performed in GSAS were done without any constraints placed upon the framework or water molecules. The atomic positions and thermal parameters for every atom were refined without any damping placed upon them, giving a final residual value of 4.62%, figure 2.20.

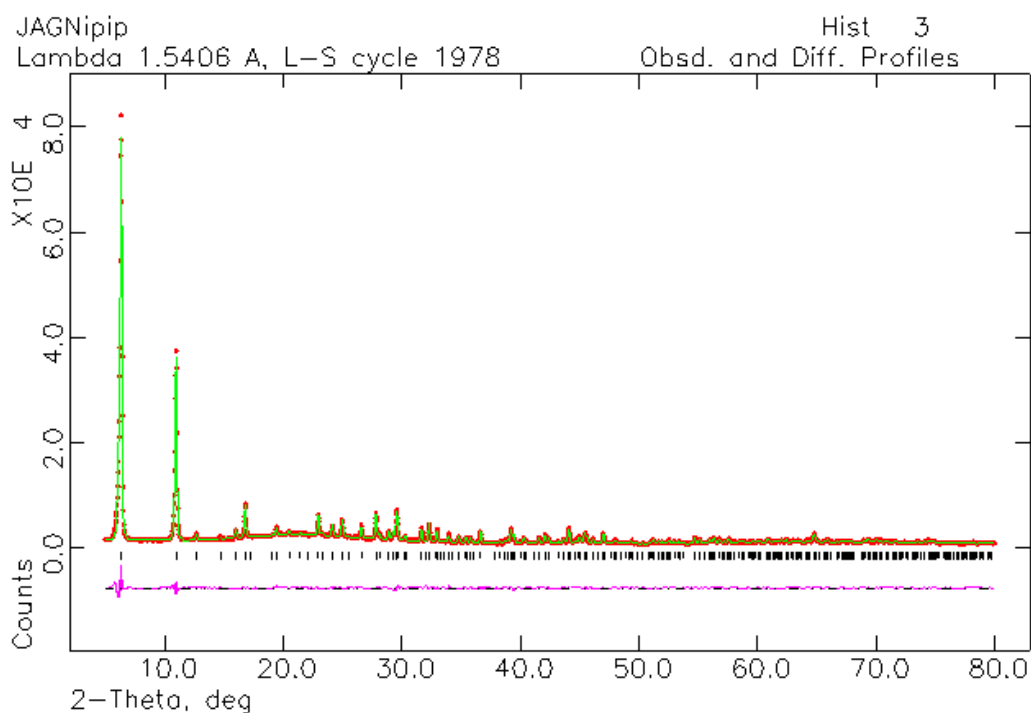


Figure 2.20: Final Rietveld refinement of $Ni_2(H_2O)_2LJ.5.4H_2O$.

If sufficient information is known about the structure, processes such as simulated annealing or energy minimisations may be performed using programs such as FOX⁷² and Cerius2.⁷⁰

2.4.1 Rietveld Refinement⁷³

As mentioned in section 2.3.2, there are inherent difficulties in structure solution from powder x-ray diffraction data due to the peak overlap and consequent loss of information. The Rietveld method is used to compare and refine proposed structural models, (obtained, for example, using programs such as EXPO)⁷⁴ against experimental data, (neutron or powder x-ray diffraction).

In the refinement, typically done using GSAS⁷⁵ a least squares method is applied in order to minimise any residual between the experimental data and that simulated from the proposed model. The least squares analysis defines the ‘best fit’ of the two data sets. The structure is refined with respect to the whole of the experimental powder profile. The weighted difference between the data sets can be calculated using equation 2.4.

Equation 2.4: Weighted difference between experimental and simulated data sets.

$$S_y = \sum w_i (y_i - y_{ci})^2$$

where y_i is the observed intensity at an arbitrary point and y_{ci} is the calculated intensity at the corresponding point. The term w_i is a suitable weight, based on the uncertainty of each reflection.

The goodness of fit between the calculated pattern and the observed data can be represented in the form of a residual percentage, or R value. The weighted profile R value R_{wp} , is calculated as:

$$R_{wp} = \sqrt{\frac{\sum w_i (y_i(obs) - y(calc))^2}{\sum w_i (y_i(obs))^2}}$$

Ideally, the final R_{wp} should be close to that of the statistically expected R value, R_{exp} ,

$$R_{exp} = \sqrt{\frac{(N - P)}{\sum_i w_i y_i(obs)^2}}$$

where N is the total number of observed data points and P is the number of parameters used to fit these points. The value R_{exp} indicates the quality of the data.

2.5 Nuclear Magnetic Resonance in the solid state

Nuclear magnetic resonance (NMR) spectroscopy is a relatively modern technique, with the first detection of signals being reported, in solids and liquids, in 1945 by Purcell and Bloch respectively. However it was not possible to find a useful chemical application for NMR until 1949, after the discovery of chemical shift effects. Since then it has become the most powerful spectroscopic technique for structural characterisation.

Details of NMR spectroscopy common to solution and solid state will not be discussed here as they have been discussed by many authors over the past fifty years. This chapter will focus on describing effects which dominate solid state NMR.

2.5.1 The NMR Spectrometer

There are three essential components required to complete an NMR experiment; a strong magnetic field, a radiofrequency source in order to excite nuclei and a method for detecting the excited nuclei. Figure 2.21 shows a picture of a NMR spectrometer and a schematic representation of a cross section of a spectrometer, a detailed description of how a solid state NMR spectrometer works is explained in ‘Spin Dynamics, Basics of Nuclear Magnetic Resonance’ by M. H. Levitt.⁷⁶

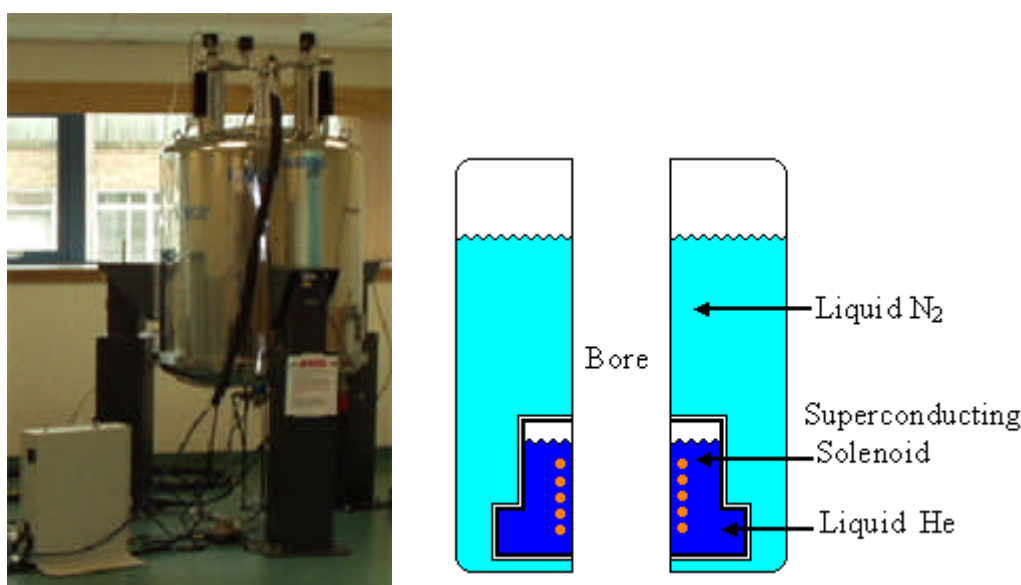


Figure 2.21: (left): Varian Infinityplus 500MHz spectrometer. (Right): schematic representation of a simplified cross-section of the magnet (right)

2.5.2 Solution State versus Solid-State NMR

In solutions, molecules are constantly experiencing Brownian motion, i.e. diffusing and tumbling randomly so that the nuclear magnetic moments in the system are continually moving relative to each other. This produces a fluctuating magnetic field at all points in the sample, which in the long term averages to zero but at any instant will have a component of random intensity and phase at the nuclear resonant frequency. This provides mechanisms for energy to be dispersed from the system and enable the nuclei to return to a thermal equilibrium.

In solids there is no random diffusion or tumbling of molecules. Consequently relaxation is achieved by paramagnetic impurities in the solid lattice. Neighbouring spins directly influence each other's magnetic field in two ways:

1. Static influences, due to the magnetic moment along the magnetic field axis which is of a magnitude and direction determined by the spin state of the nucleus.
2. Rotating influences, due to μ_{xy} of the precessing spin, μ_{xy} is the magnetic moment in the xy plane, and discussed in the next section.

The lifetime of the individual spin states is greatly reduced by the occurrence of the direct interchange of energy between spins which is permitted by the rotating component. This means that the rate of relaxation mechanisms in the solid state is different to those in solution.

2.5.3 The Vector Model

Describing nuclear spin by using a simple vector model allows some of the more complex aspects of NMR to be explained in simpler terms. Figure 2.22 shows the vector model of a collection of spin $\frac{1}{2}$ nuclei at thermal equilibrium in an applied magnetic field.

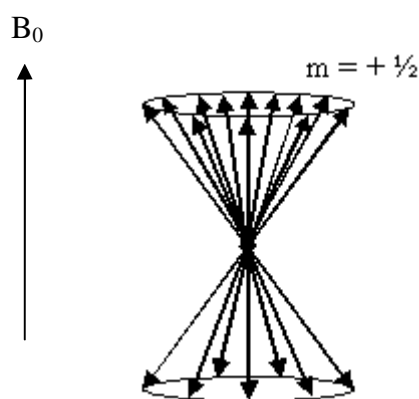


Figure 2.22: A vector model of a collection of spin $\frac{1}{2}$ nuclei at thermal equilibrium. There is slightly more magnetic moments in the $m = +\frac{1}{2}$ state, as discussed previously

When a sample is placed in a static magnetic field the nuclear spins either line up with the field or against it. At thermal equilibrium there is a population difference between the lower and the upper energy state of Δn_{eq} , described by the Boltzmann distribution. The net magnetisation for the sample is given by equation 2.10.

$$M_0 = \frac{1}{2} \gamma \hbar \Delta n_{\text{eq}}$$

Equation 2.10: Net magnetisation, given by M_0 , along the z -axis, i.e. the same direction as the magnetic field.

As the static magnetic field only has effect in one direction, along the z -axis, the magnetic moments in the perpendicular xy plane are randomly orientated. This means that for a large collection of spins, the total magnetisation in the xy plane is averaged to zero, and by implication the sample has magnitude M_0 aligned along the z axis, shown in figure 2.23.

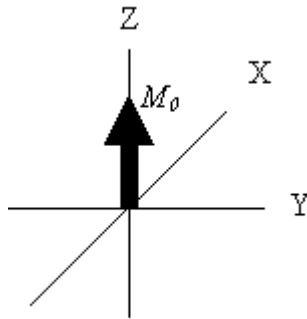
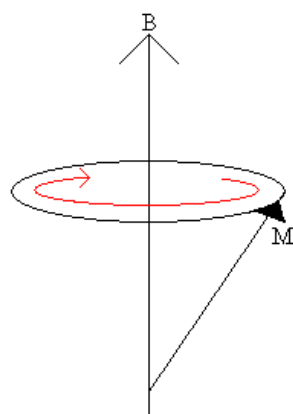


Figure 2.23: The net magnetic moment (M_0) for a large collection of spins. The z -axis is parallel to the static magnetic field.

2.5.4 The Rotating Frame

In a theoretical sample, which contains only ^1H nuclei which do not interact with each other, the motion of the total magnetisation of the spins ' \mathbf{M}_0 ' can be described as precessing around the magnetic field ' \mathbf{B}_0 ' at an angular frequency given by equation 2.11 and shown schematically in figure 2.24



$$\omega = \gamma B$$

Figure 2.24: Magnetisation ' M_0 ' precesses around the magnetic field ' B_0 ' at an angular frequency, ω .

Consequently, increasing either the magnetic field strength or the magnetogyric ratio or both will result in an increase in the precession frequency.

Nuclei within a sample experience two different magnetic fields; the static magnetic field, B_0 , which is parallel to the z-axis, and a weak radiofrequency field, B_1 . The radiofrequency field rotates in the xy plane at a frequency denoted by ω_{rf} , and due to the vector addition of B_0 and B_1 the total field experienced is tilted slightly away from the z-axis, rotating at a frequency of ω_{rf} .

This implies that the magnetisation ' M ' has a precession frequency around a field which itself is moving at a frequency of ω_{rf} and can be thought of as the laboratory frame of reference. In order to simplify the situation, vector analysis of NMR problems are solved assuming that one is already rotating around the z-axis at the same frequency as the radiofrequency pulse. This is known as the rotating frame of reference, conveniently making the radiofrequency field appear static.

2.5.5 Radiofrequency, RF, Pulses

When a short single pulse of intense monochromatic RF radiation (the frequency of which is close to that of the resonance frequency of the spins) is applied to a sample at thermal equilibrium, there is a small offset to the magnetic field, ΔB . The offset ΔB is negligible in comparison with the radiofrequency field, B_1 , so that the field experienced by the spins is simply given by B_1 .

The phase of the RF field is chosen to ensure that B_1 is situated along the x-axis, within the rotating frame. This allows the magnetisation to precess in the yz plane at a specific angular frequency. The position of the magnetisation within the yz plane, shown by figure 2.25, can be controlled by the duration of the RF pulse.

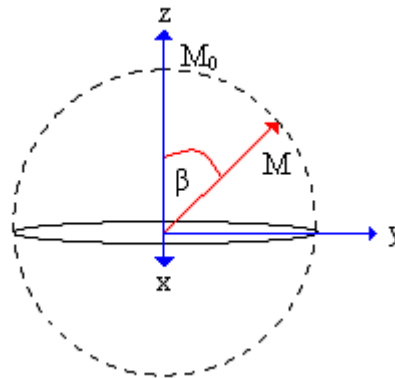


Figure 2.25: Vector representation of the effect of a RF pulse on a collection of nuclear spins. The magnetisation, M , is moved away from the z -axis into the yz plane through an angle β .

The angle through which the magnetisation is moved, β can be calculated using the following equation:

$$\beta = \gamma B_1 t_p$$

where t_p is the duration of the pulse in seconds

The most common pulses used are 90° and 180° . A 90° pulse rotates the net magnetisation, M_0 , from the z -axis to the y -axis, shown in figure 2.26



Figure 2.26: The red arrow represents the direction of the magnetisation before (left) and after a 90° pulse

2.5.6 Relaxation

Immediately after the application of a 90° pulse the only magnetic field which can exert any influence on the system is ΔB , in the rotating frame. The net magnetisation therefore precesses in the xy plane at a frequency given by:

$$\Omega = \gamma\Delta B = \gamma B_0(1 - \sigma) - \omega_{\text{rf}}$$

Where σ is the chemical shield constant and therefore by implication, when several nuclei with different chemical shifts are excited, they precess at different frequencies.

In the absence of an applied magnetic field, the spins begin to return to their thermal equilibrium and this is done via two main processes:

1. Longitudinal relaxation – which is the reformation of the Boltzmann population difference, (T_1)
2. Transverse relaxation – which is the re-establishment of random orientations for magnetisation in the xy plane.

2.5.7 Dipole-dipole Interactions

Dipole-dipole interactions are averaged to zero in solution state spectra due to the persistent Brownian motion of the molecules, however, there is no such motion in solids. Consequently, for spin $\frac{1}{2}$ nuclei, dipole-dipole usually have a greater effect on the line width of solid state spectra than any other interaction.

Dipole-dipole interactions are inter- or intramolecular interactions between molecules which have a permanent magnetic dipole moment, this is shown in figure 2.27. The strength of the interaction depends on the orientation and the distance of the relative dipoles and the magnetogyric ratios of the relative nuclei.

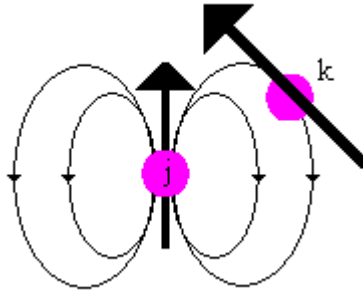


Figure 2.27: Magnetic field generated by spin 'j' at the site of spin 'k'. Spin interaction is mutual, i.e. the reverse would be true for k's influence on j.

The strength of the dipole-dipole interaction can be given by:

$$B_{jk} = \frac{\mu_0}{4\pi} \frac{\gamma_j \gamma_k \hbar}{r_{jk}^3}$$

For spins of the same isotopic species, i.e. homonuclear species, the dipole-dipole interaction is given by:

$$\hat{H}_{jk}^{DD}(\theta_{jk}) = b_{jk} \frac{1}{2} (3 \cos^2 \theta_{jk} - 1) (3 \hat{I}_{jx} \hat{I}_{kx} - \hat{I}_j \hat{I}_k)$$

Where θ_{jk} is the angle between the vector joining the spins and B_0 , which is shown in figure 2.30.

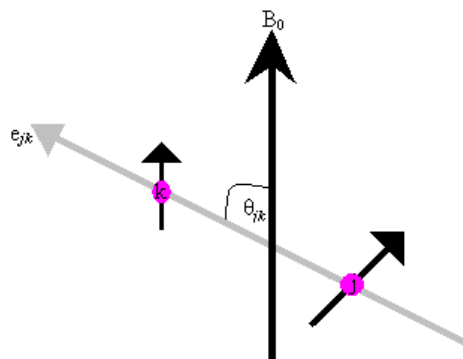


Figure 2.28: Illustration of how two spins k and j, may interact, showing the formation of θ_{jk} .

If the spins are of different isotopes, i.e. heteronuclear species, the dipole-dipole interaction is given by:

$$\hat{H}_{jk}^{DD}(\theta_{jk}) = b_{jk} \frac{1}{2} (3 \cos^2 \theta_{jk} - 1) \cdot 2 \hat{I}_{jx} \hat{I}_{kx}$$

Both the equation for homo- and heteronuclear dipole-dipole interactions includes dipole-dipole coupling which is given by:

$$d_{jk} = b_{jk} \frac{1}{2} (3 \cos^2 \theta_{jk} - 1)$$

which is equal to zero when θ_{jk} satisfies the following equation:

$$3 \cos^2 \theta_{jk} - 1 = 0$$

The solution to this equation is known as the magic angle, in which $\theta = 54.74^\circ$

2.5.8 Chemical Shift

In solution state NMR, rapid molecular tumbling averages an orientation-dependent quantity known as chemical shift. The rapid molecular tumbling produces a narrow line at a position known as the isotropic chemical shift, $\delta_{(iso)}$. The solid state spectra for a single crystal examining one type of crystallographically unique nucleus would show one resonance frequency. The chemical shift of the resonance frequency depends on the orientation of the crystal within the magnetic field, B_0 .

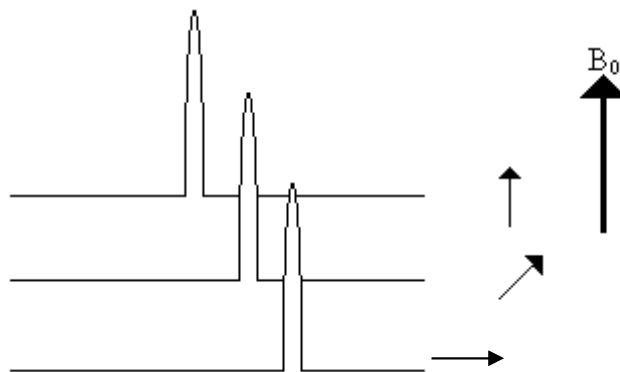


Figure 2.29: Illustration showing how chemical shift can change with the orientation of a single crystal, represented by the black arrows.

In spectra of powdered samples all orientations of a given site with respect to B_0 are present. This implies that most crystal systems, with the exception of cubic, have different chemical shift resonance frequencies, in relation to their orientation to B_0 , which therefore leads to broad line shapes known as powder patterns, figure 2.30.

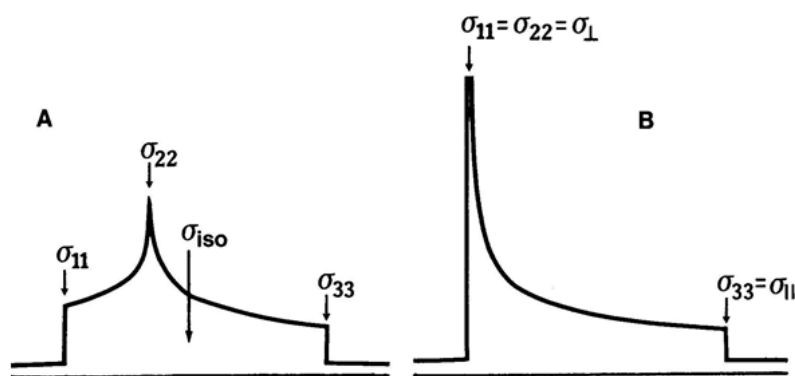


Figure 2.30: Simulated static powder patterns. (A) represents an asymmetric chemical-shielding powder pattern, whereas (B) represents an axially symmetrical chemical shielding powder pattern. The shielding element of the unique axis is described as σ_{\parallel} and the other two as σ_{\perp} .

The powder patterns shown in figure 2.30 have different values of ‘ σ ’ representing different points of the pattern. These are known as eigenvalues, which are the principle values of the chemical-shielding anisotropy.

2.5.9 Magic Angle Spinning (MAS)

The static spectra of powdered samples are poorly resolved (shown in figure 2.30) but considerable line narrowing can be achieved if samples are spun at the magic angle at a rate of rotation which is significantly faster than the width of the powder pattern. Spinning at the magic angle simulates Brownian motion being introduced to the sample which causes anisotropic effects of the chemical shift and the dipolar interactions to be averaged, consequently leaving a line centred at the isotropic chemical shift position.

In order to spin a sample at the magic angle, specially designed probes are used where the sample is rotated at 54.74° with respect to B_0 . The sample is held in a rotor which, once in the probe, is suspended on a bed of air and carefully spun at the desired speed. Figure 2.31 gives some examples of MAS probes, with an illustration of a cross-section of a probe showing the rotor spinning at the magic angle.

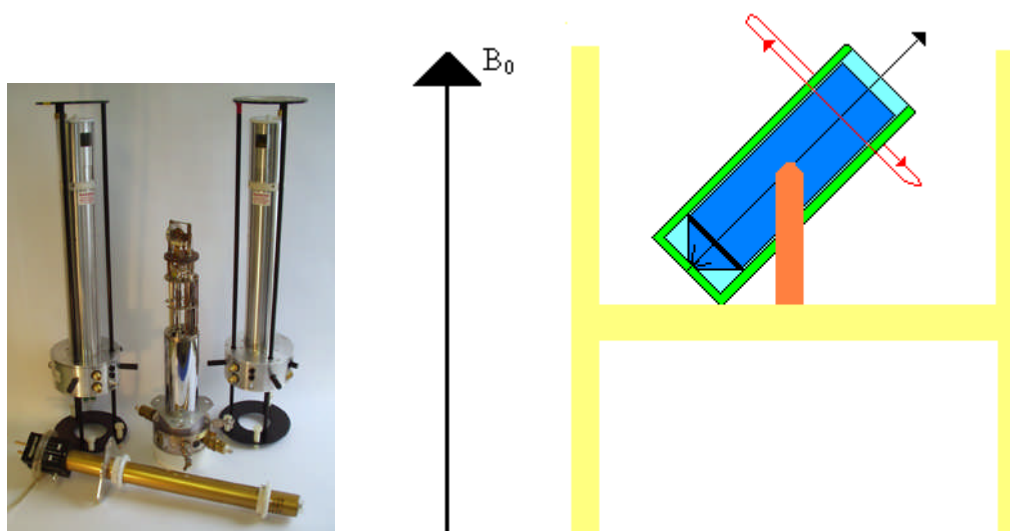


Figure 2.31: The photograph on the left shows the type of probes that can be used for magic angle spinning. The schematic on the right illustrates a rotor, blue, spinning at an angle of 54.7° to the applied magnetic field, B_0 .

2.5.10 High power decoupling

As previously mentioned, in order to eliminate the effects of direct dipolar anisotropy the sample would have to be spun at the magic angles at a rate which is greater than the width of the static powder spectra. This is not always possible as some nuclei, ^1H , ^{19}F and ^{31}P , have

high magnetogyric ratios and consequently larger dipolar coupling constants, which would require spinning speeds which are unattainable.

In instances where the dipolar coupling effects can not be eliminated through MAS, rf irradiation can be used. One of the most commonly used techniques which is used to eliminate heteronuclear dipolar coupling effects is known as continuous-wave decoupling, in which a long rf pulse of constant phase is applied to one of the isotopic species. Pulses of sufficiently high power have the effect of averaging out the heteronuclear dipolar interaction, and thus eliminating its contribution to the spectra of the other isotopic species.

More sophisticated techniques are used to eliminate the contribution of homonuclear dipolar interaction, the theory of which lies outside the scope of this report. Generally, dipolar interaction can be eliminated in inorganic systems through a combination of MAS and high power decoupling.

2.5.11 Cross Polarisation

Sensitivity and resolution of solid state spectra may be improved through magic angle spinning and high power decoupling however cross polarisation can be used to enhance the sensitivity of a nucleus with a low magnetogyric ratio.

Cross-polarisation relies on the transfer of energy from an abundant spin (^1H) to a dilute one (^{13}C). For cross polarisation to work there must be dipolar coupling between H and X. The technique requires a double channel probe as the both spin systems must be excited.

The pulse sequence, shown in figure 2.32, starts with a short 90° pulse on the H-channel, immediately followed by the application of a pulse on the y-channel, i.e. one which is phase shifted by 90° to the original pulse. This is known as a spin-lock pulse. During this a pulse is applied on the X-channel for a period of time known as the contact time. After the contact time, a FID is acquired on the X-channel during proton decoupling and this is known as the acquisition time.

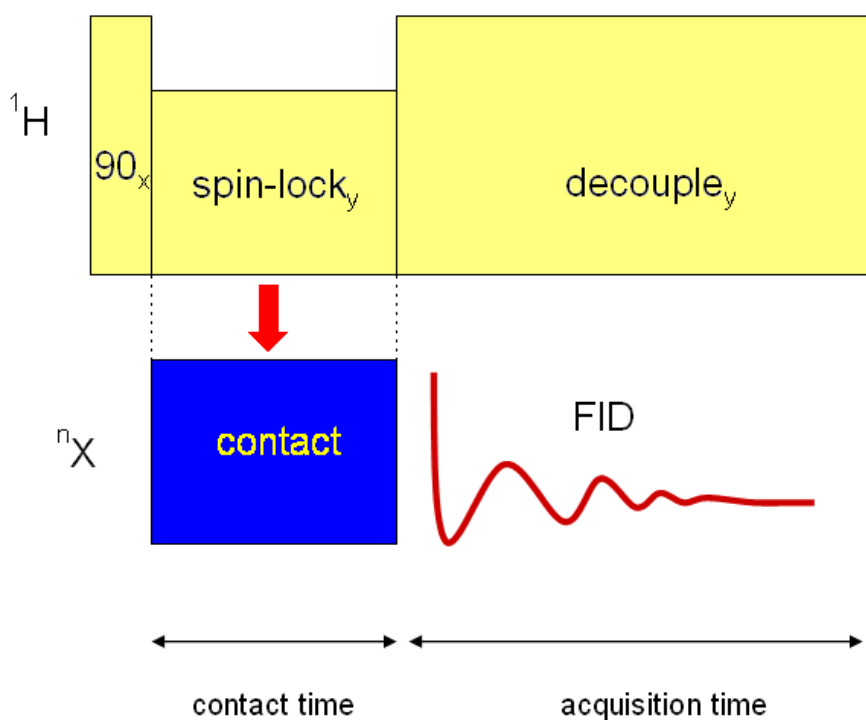


Figure 2.32: Cross Polarisation; The Pulse Sequence.

The Hartmann-Hahn match condition must be obtained to achieve efficient cross polarisation. The Hartmann-Hahn condition states that the H and X applied magnetic fields must precess at the same rate, i.e. $\gamma_H B_1^H = \gamma_X B_1^X$.

2.5.12 Direct Polarisation

Direct-polarisation is much simpler than cross polarisation. Only one short pulse on the X-channel is required then the signal is acquired with or without decoupling. Direct polarisation gives quantitative information which is lost in cross polarisation, providing the pulse recycle time is amenable. Direct polarisation experiments can, in principle, see all X nuclei in the sample which is can be a disadvantage if X nuclei are present within the probe.

2.5.12 Quadrupolar Nuclei

Over two thirds of the elements in the periodic table have a spin quantum number (I) greater than $\frac{1}{2}$, and such nuclei are known as quadrupolar nuclei. Those with an odd half integer spin quantum number, i.e. $I = 3/2, 5/2, 7/2$ etc, are abundant in inorganic materials.

Like spin $\frac{1}{2}$ nuclei, the nuclear spins of quadrupolar nuclei lose their degeneracy when placed in a magnetic field, and are further perturbed by chemical shift effects and direct dipole-dipole coupling etc. As quadrupolar nuclei have more than two energy levels, as opposed to spin $\frac{1}{2}$ nuclei, multiple transitions are possible as shown in figure 2.33.

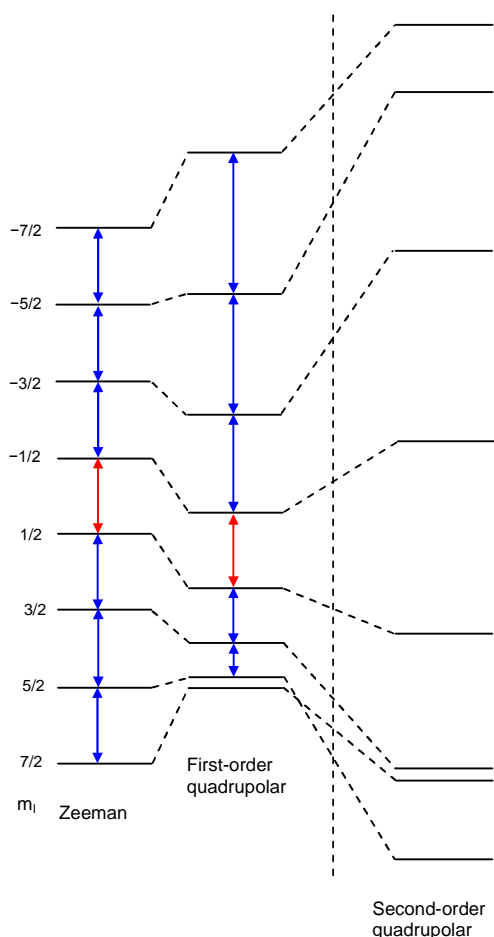


Figure 2.33: Energy level diagram for spin $7/2$ nuclei such as ^{45}Sc , showing the Zeeman interactions (red) the Zeeman interaction and the 1^{st} order quadrupolar perturbation (blue) and under the Zeeman interaction and both the 1^{st} and 2^{nd} order quadrupolar perturbations.

Quadrupolar nuclei have a non-spherical charge distribution and consequently a non-zero nuclear electric quadrupolar moment, eQ . The interaction of quadrupolar moments with an electric field gradient, which is known as quadrupolar interaction, strongly influences line widths and shapes. The line widths and shapes which are obtained from quadrupolar nuclei are influenced by two parameters:

1. The asymmetry parameter, η^Q , which reflects the deviation of the electric field gradient from cylindrical symmetry
2. The quadrupolar coupling constant, C_q .

The quadrupolar coupling constant is proportional to the product of the nuclear electric quadrupole moment, eQ and the magnitude of the electric field gradient along its principle axis, e_q , therefore;

$$C_q = e^2 qQ/h$$

When the value of C_q is very small relative to the Zeeman splitting, the quadrupolar interaction is known as first order interaction and when the value of C_q is high, the quadrupolar interaction is known as second order interaction. First order quadrupolar interaction can be usually be averaged in a sample by increasing the strength of the applied magnetic field, and a high spin rate for MAS, however second order interactions cannot be averaged. In order to examine the solid state spectra for nuclei which succumb to second order quadrupolar interactions special techniques must be used in order to minimise the quadrupolar effects. Such techniques include double rotation (DOR), which rotates the sample about two axes simultaneously, dynamic angle spinning (DAS), where the sample is spun around one axis and then a different one independently, or Multiple Quantum NMR.

Multiple Quantum Magic Angle Spinning NMR (MQMAS NMR) spectroscopy uses specific pulse sequences in order to excite multiple quantum coherences, such as the triple-quantum (3Q) coherence.

$$-\frac{3}{2} \longrightarrow \frac{3}{2}$$

These coherences cannot be directly detected, but are allowed to evolve over a period of time and then converted to an observable single quantum coherence by means of a specific pulse program.

The effectiveness of MQMAS NMR is illustrated in figure 2.34 which shows three spectra detected using a static sample, a sample spinning at the magic angle and using a multiple quantum pulse sequence whilst spinning at the magic angle.

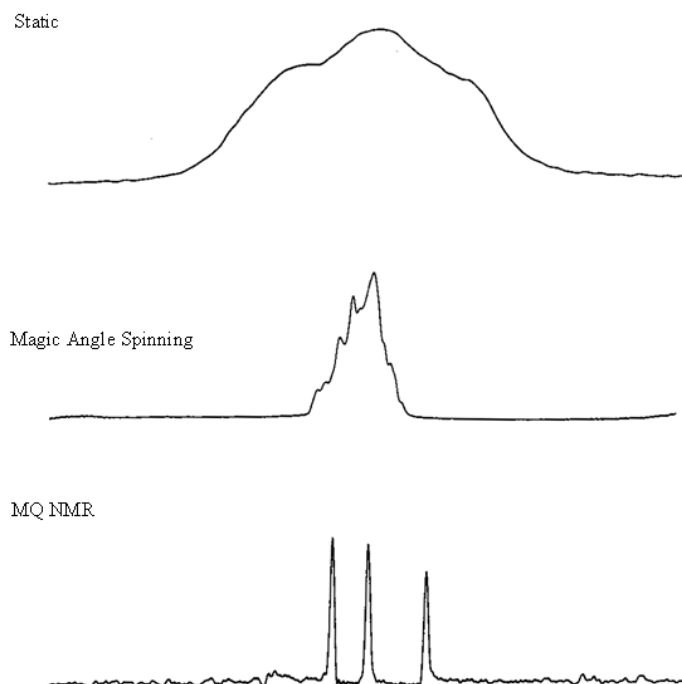


Figure 2.34: ^{23}Na spectra obtained for sodium citrate, illustrating the increasing resolutions from a static spectra, to MAS spectra, to a 3Q MAS spectra. The horizontal scale varies between spectra.⁷⁷

2.6 Gas Adsorption

The sorption of gases or vapours (sorbates) can be used in order to determine the surface area, pore volume and pore size distribution of porous solids, as well as the pore connectivity and surface chemistry. When the sorbate is within the porous solid, the phenomenon is known as adsorption, and typically the adsorption is measured at a constant temperature, as the pressure is varied.

There are two different ways in which gas adsorption can be measured;

- Volumetrically, where the amount of adsorption is inferred from pressure measurements that are made before and after adsorption.
- Gravimetrically, where the sample is weighed as the gas pressure is increased. The increase in weight in the sample can be correlated to the amount of uptake.

2.7 General Synthesis and Analysis

All reactions were carried out by hydrothermal crystallisation from aqueous gels in 25 ml Teflon-lined steel autoclaves (Parr type), unless specifically stated otherwise. Gels were prepared by thorough (1 h) mixing before heating. Once removed from the oven, products were filtered and washed with distilled water and dried at 100 °C. If necessary, the products were sonicated in water to remove residual Sc₂O₃. The coarse fraction usually gave crystalline powders. The resulting powders were routinely examined by X-Ray powder diffraction using a STOE Stadi/p diffractometer operating with monochromated Cu K_{α1} radiation ($\lambda = 1.54056\text{\AA}$). The content of carbon, hydrogen and nitrogen in the samples was measured by a Carlo Erba elemental analyser. The inorganic composition (Sc, Na, P, Si, O, F) was examined semi-quantitatively by EDX on a JEOL-5600 SEM with an Oxford INCA energy 200 EDX system. The EDX analysis reported in this work is calibrated using α -AlMePO and kolbeckite samples, when reporting aluminium, scandium and phosphorus compositions.

Thermogravimetric analysis was conducted on a TA Instruments SDT 2960 thermogravimetric analyser. Approximately 10 mg of sample was loaded in an alumina crucible and data collected from room temperature to 800°C at 5°Cmin⁻¹ in a flow of N₂, with calcined alumina as a reference sample.

Solid-state NMR spectroscopy experiments were carried out on the as-prepared materials at room temperature using either a triple channel Varian Infinityplus 500MHz spectrometer with a T3 Chemagnetics 4-mm probe at resonance frequencies of 121.480 and 202.466MHz for ⁴⁵Sc and ³¹P, respectively, or a Varian VNMRS 400MHz spectrometer with Chemagnetic Apex 4-mm probe at a resonance frequency of 97.138MHz for ⁴⁵Sc or a Varian Unityplus 300MHz spectrometer with a Chemagnetic apex 7-mm probe at a resonance frequency of 121.371MHz for ³¹P. A 1M aqueous solution of ScCl₃ and solid references of CaHPO₄·H₂O (Brushite) and adamantane were used as reference materials for ⁴⁵Sc, ³¹P and ¹³C, respectively. Samples were spun at the magic angle at a spinning speed of 13, 7.5 and 5 kHz with pulse durations of 1.5, 4 and 4 ms, and pulse delays of 0.2, 30 and 2 s for ⁴⁵Sc, ³¹P and ¹³C, respectively.

Details of the single crystal X-ray data collections for all structures are summarised throughout this thesis. Structures have been collected on one of the following in-house diffractometers; a Rigaku MM007RA (confocal optics, Cu radiation) and a Rigaku Mercury CCD detector or a Mo X-ray source and a Rigaku Saturn 70 CCD detector. Some of the

structures reported in this thesis have been determined from singles crystals which have either been too small, or too poorly scattering to be solved in the lab. The single crystal data for such samples has been collected on station 9.8 or 16.2SMX at the CCLRC synchrotron radiation source at Daresbury using a Bruker SMART 1K CCD diffractometer.

High-resolution X-ray powder diffraction data has been collected for selected samples on station ID-31 at the European Synchrotron Radiation Facility. In this case, data collection was carried out in Debye-Scherrer geometry, with the sample in a sealed quartz glass capillary using monochromated radiation with a wavelength of either 0.63248 or 0.800178Å . Details of the syntheses of each structure reported, along with crystallographic details, are given in the relevant chapters.

Chemicals used in the synthesis of solids reported in chapters 3 – 6 are listed below, along with the supplier from which they were purchased, and their purity.

The sources of the reagents were scandium oxide (Stanford Materials, 99.999%), scandium nitrate (Acros 99.9%), aluminium hydroxide (aldrich 99.999%) phosphorus acid (Porlabo, 85% aqueous solution), phosphorous acid (98%), phosphoric acid (Aldrich, 99.98%), methylphosphonic acid (Aldrich, 99.99%), ethylenebisphosphonic acid (Aldrich 99%), Piperazine (Aldrich 99%), formaldehyde (Aldrich 37%, in solution) and hydrochloric acid (Aldrich 18%, in solution) ethylenediamine (Avocado 99.99%), 1,4-diaminobutane (Aldrich 99.999%), cyclohexylamine (Acros) and HF (Aldrich, 48 wt% aqueous solution), lithium hydroxide (Acros 99%), sodium hydroxide (Aldrich 99%), succinic acid (Aldrich 99%), glutaric acid (Aldrich 98%), adipic acid (Aldrich 99%), pilmelic acid (Aldrich 99%), isothalic acid (Aldrich 99.9%), terephthalic acid (Aldrich 99.999%), 4,4'-biphenyldicarboxylic acid (99.9%)

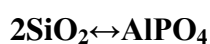
Chapter 3: Scandium Phosphates

3.1 Aims

The aim of the work described in this chapter is to investigate the suitability of the Sc³⁺ cation in forming novel scandium phosphate framework materials. This complements the limited amount of work on scandium phosphate structures already in the literature at the time of starting this project.

3.2 Introduction

Open framework phosphate systems have been extensively investigated since Flanigen and co-workers synthesised the first aluminophosphates in the early 1980s.⁸ Flanigen's work exploited the similarities between the two families of silica and aluminophosphate compounds.



This structural comparison also revealed a path towards microporous frameworks which were not purely tetrahedrally co-ordinated, therefore allowing different framework topologies. Further investigations into phosphate systems led to the first mixed co-ordination framework being reported in 1985, a gallium aluminium phosphate, which included a 5 coordinate Ga-centred trigonal-bipyramidal tetramer.⁷⁸ Throughout the 1990s and into the 21st century, new classes of open framework materials have been reported which incorporate cations in mixed octahedral and tetrahedral coordination within extended frameworks. Research into structures with mixed tetrahedral and octahedral coordination is of importance for the future design of structures with novel properties that derive from the octahedral coordinated cations, allowing a greater variety of applications.

Mixed co-ordination frameworks have allowed the incorporation of most of the elements in the transition block of the periodic table, consequently allowing frameworks to become 'tunable' for desired properties.⁹ One of the most recent elements to be incorporated into phosphate frameworks is scandium.⁴⁴⁻⁴⁶

There is little work which has been published which examines the hydrothermal behaviour of scandium, and indeed until recently scandium has been thought too expensive to obtain for

academic purpose. Over the past 4 years, and excluding publications arising from the work of this thesis, there have been a few publications which have indicated the potential usefulness of scandium as a main constituent within open framework solids. Of those publications which have explored the hydrothermal chemistry of scandium, many of them have examined the templating effect of ethylenediamine within a scandium phosphate system. To date, and excluding the work herein, there are four scandium phosphates, three of which are novel, which have been templated using ethylenediamine, out of a total of 6 scandium phosphate structures.

In 2002, Riou *et al*⁴⁵ reported the hydrothermal synthesis and characterisation of the first organically-templated scandium phosphate, $\text{Sc}(\text{HPO}_4)_2 \cdot 0.5(\text{N}_2\text{C}_2\text{H}_{10})$, Figure 3.1, isostructural with an indium and iron phosphate.^{79, 80}

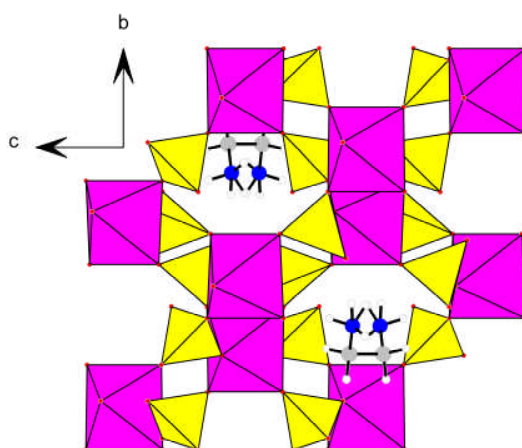


Figure 3.1: $\text{Sc}(\text{HPO}_4)_2 \cdot 0.5(\text{C}_2\text{N}_2\text{H}_{10})$ viewed along the $[100]$ axis. ScO_6 octahedra and PO_4 tetrahedra are shown as purple and yellow.

Riou postulated that this scandium phosphate ‘could appear as the first member of a new series of compounds with open frameworks’. At the same time, a separate publication by Bull *et al*⁴⁶ reported the synthesis and crystal structure of the first scandium-containing open framework solid; a scandium sulphate phosphate possessing large cages occupied by the template, azamacrocycle cyclen (1,4,7,10-tetraazacyclododecane). Both groups noted the suitability of scandium for incorporation into open frameworks and suggested that it had potential to give rise to new structures.

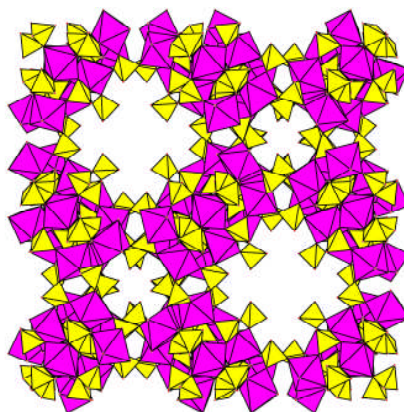


Figure 3.2: Representation of the framework structure of first scandium-containing open framework solid. The organic moiety is omitted for clarity.

A subsequent publication in 2003, by Bull *et al*²⁰, reported the synthesis and characterisation of a further four scandium phosphates and firmly established the ability of scandium to act as the main framework constituent in open framework solids.

3.3 Experimental

To investigate further the structural variety of templated scandium phosphates, scandium phosphate-based gels with a range of organic amines and inorganic starting compositions, given in tables throughout this chapter, were treated hydrothermally.

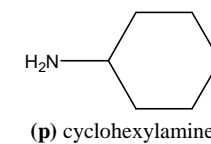
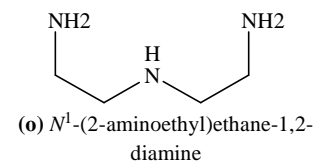
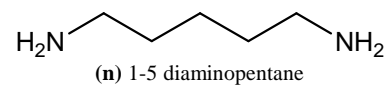
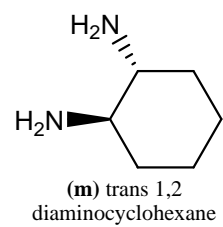
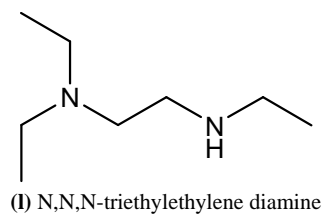
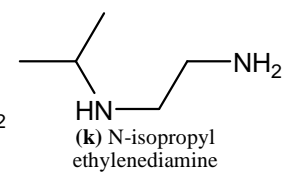
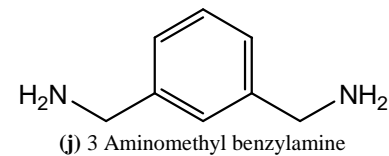
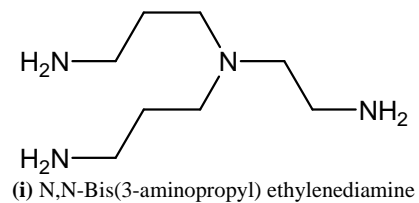
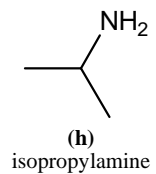
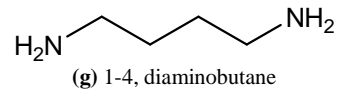
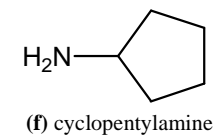
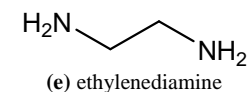
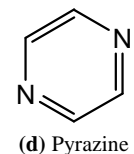
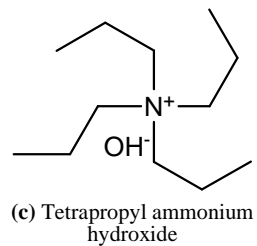
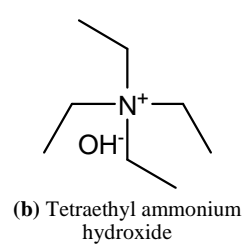
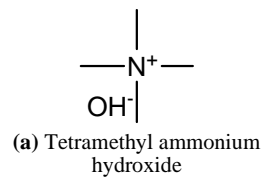
Ethylenediamine was the first templating agent investigated, with the initial reactant ratios chosen to be similar to those used successfully in other scandium phosphate preparations.

A second series of experiments was performed where 1,4-diaminobutane was added to the gel to act as the template instead of ethylenediamine. The reaction stoichiometries which were used are outlined throughout this chapter and are similar to the conditions used in the synthesis of scandium phosphates templated with ethylenediamine.

A third series of experiments was performed, in which a range of organic templates were used, including primary, secondary and tertiary amines and alkyl ammonium salts, in order to investigate the role different types of organic as SDAs. The inorganic compositions were similar to those of previous experiments which had yielded crystalline materials.

Organic molecules used in the search for novel scandium phosphate-based materials are shown in figure 3.3. These have been used under various conditions and at different ratios in order to investigate their effect on scandium phosphate-based systems. Table 3.1 lists the

reaction conditions used for a selection of templates, listing the product that was formed for each set of conditions. The products listed are described later in this chapter, within a discussion of why certain organic templates yield the same structure. It will also be informative to discuss the structures described in this chapter along with those already in the literature.



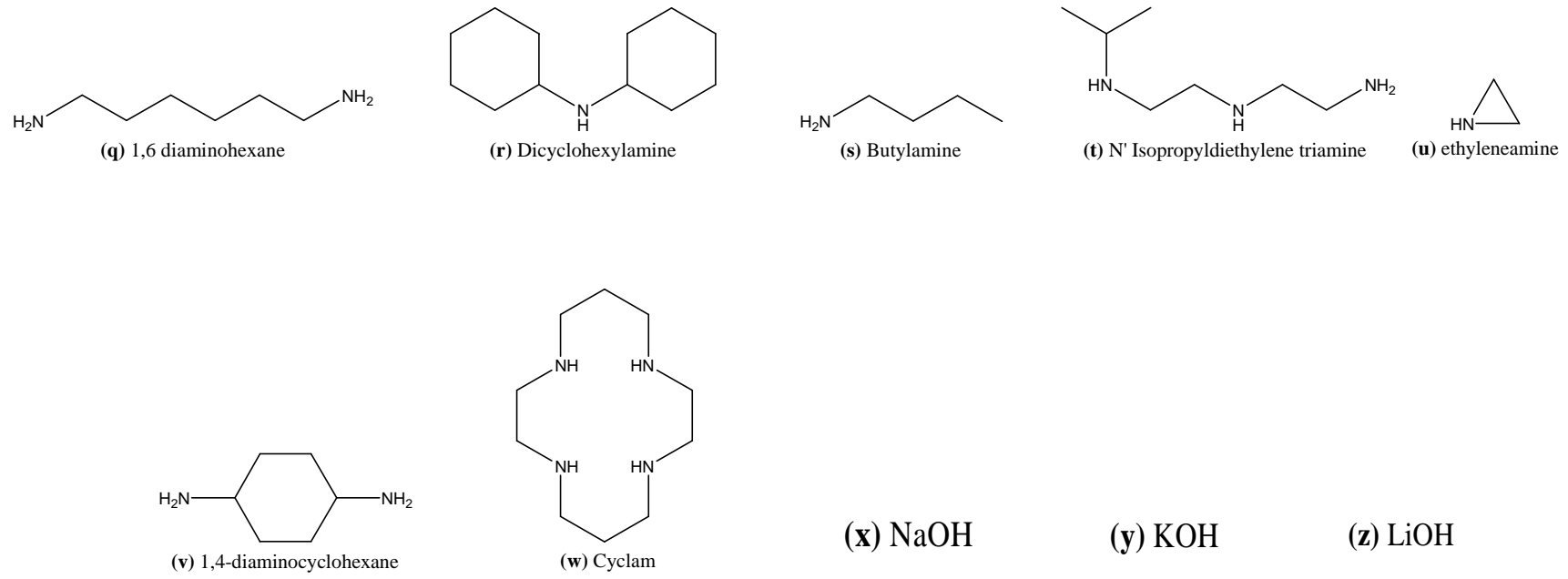


Figure 3.3: Structure directing agents used in the preparation of scandium phosphate-based materials

Table 3.1: Reaction conditions used for a selection of scandium phosphate based reactions. For comparative purposes, all reactions listed were carried out at 463K. The letters shown in the ‘template’ column correspond to templates shown in figure 3.3.

Reactants					Temp	Time	pH _i	pH _f	Product (structure number)
Sc ₂ O ₃	H ₃ PO ₄	HF	Template / eq	H ₂ O	°C	h			
1	1.7	0.5	E / 2.2	200	180	48	2	5	[(H ₃ NC ₂ H ₄ NH ₃) ₃][Sc ₃ (OH) ₂ (PO ₄) ₂ (HPO ₄) ₃ (H ₂ PO ₄)](1)
1	1	1	C / 1	200	190	48	2	6	Sc(PO ₄).2H ₂ O(5)
1	2	1	O / 1	200	190	48	3	7	Sc(PO ₄).2H ₂ O(5)
1	2	2	P / 1	200	190	72	1	7	[C ₆ H ₁₁ NH ₃][ScF(HPO ₄)(H ₂ PO ₄)](4) / Sc(PO ₄).2H ₂ O(5)
1	2	2	G / 1	200	190	72	1	7	[(H ₃ NC ₄ H ₈ NH ₃) ₃ Sc(OH ₂) ₆ Sc ₂ (HPO ₄) ₁₂ (PO ₄) ₂](2)/ [(H ₃ NC ₄ H ₈ NH ₃) ₂ (H ₃ O)][Sc ₅ F ₄ (HPO ₄) ₈](3)
1	2	2	Q / 1	200	190	48	1	3	Unknown
1	2	2	M / 1	200	190	48	1	4	Sc(PO ₄).2H ₂ O(5)
1	2	2	X / 1	200	190	48	1	3	Sc(PO ₄).2H ₂ O(5)
1	2	2	T / 1	200	190	48	1	4	Sc(PO ₄).2H ₂ O(5)
1	2	2	H / 1	200	190	48	1	4	Sc(PO ₄).2H ₂ O(5)
1	2	2	F / 1	200	190	72	1	4	Sc(PO ₄).2H ₂ O(5)
1	2	2	S / 1	200	190	48	1	4	Sc(PO ₄).2H ₂ O(5)
1	2	2	K / 1	200	190	48	1	3	Sc(PO ₄).2H ₂ O(5)
1	2	2	N / 1	200	190	48	1	5	Unknown phase
1	2	2	I / 1	200	190	72	1	5	Unknown phase
1	2	2	L / 1	200	190	48	1	4	Sc(PO ₄).2H ₂ O(5)

Reactants					Temp	Time	pH _i	pH _f	Product (structure number)
Sc ₂ O ₃	H ₃ PO ₄	HF	Template / eq	H ₂ O	°C	h			
1	2	2	J / 1	200	190	48	1	2	Unknown
1	2	1	Y / 1	200	190	48	1	2	Unknown
1	2	2	G / 2	200	190	48	1	3	[(H ₃ NC ₄ H ₈ NH ₃) ₃ Sc(OH ₂) ₆ Sc ₂ (HPO ₄) ₁₂ (PO ₄) ₂](2)/ [(H ₃ NC ₄ H ₈ NH ₃) ₂ (H ₃ O)][Sc ₅ F ₄ (HPO ₄) ₈](3)
1	2	1	G / 1	200	190	72	1	4	[(H ₃ NC ₄ H ₈ NH ₃) ₃ Sc(OH ₂) ₆ Sc ₂ (HPO ₄) ₁₂ (PO ₄) ₂](2)/ [(H ₃ NC ₄ H ₈ NH ₃) ₂ (H ₃ O)][Sc ₅ F ₄ (HPO ₄) ₈](3)
0.875	2	2	G / 2	200	190	48	1	3	[(H ₃ NC ₄ H ₈ NH ₃) ₃ Sc(OH ₂) ₆ Sc ₂ (HPO ₄) ₁₂ (PO ₄) ₂](2)/ [(H ₃ NC ₄ H ₈ NH ₃) ₂ (H ₃ O)][Sc ₅ F ₄ (HPO ₄) ₈](3)
0.875	2	1	G / 1	200	190	72	2	5	[(H ₃ NC ₄ H ₈ NH ₃) ₃ Sc(OH ₂) ₆ Sc ₂ (HPO ₄) ₁₂ (PO ₄) ₂](2)/ [(H ₃ NC ₄ H ₈ NH ₃) ₂ (H ₃ O)][Sc ₅ F ₄ (HPO ₄) ₈](3)
0.5	2	1	F / 1	200	190	48	2	5	Sc(PO ₄).2H ₂ O(5)
1	3.5	1	G / 1.5	200	190	48	1	4	[(H ₃ NC ₄ H ₈ NH ₃) ₃ Sc(OH ₂) ₆ Sc ₂ (HPO ₄) ₁₂ (PO ₄) ₂](2)/ [(H ₃ NC ₄ H ₈ NH ₃) ₂ (H ₃ O)][Sc ₅ F ₄ (HPO ₄) ₈](3)
0.5	3.5	1	G / 1.5	200	190	72	1	4	[(H ₃ NC ₄ H ₈ NH ₃) ₃ Sc(OH ₂) ₆ Sc ₂ (HPO ₄) ₁₂ (PO ₄) ₂](2)/ [(H ₃ NC ₄ H ₈ NH ₃) ₂ (H ₃ O)][Sc ₅ F ₄ (HPO ₄) ₈](3)
0.5	3.5	2	G / 1.5	200	190	72	1	4	[(H ₃ NC ₄ H ₈ NH ₃) ₂ (H ₃ O)][Sc ₅ F ₄ (HPO ₄) ₈](3)

Reactants					Temp	Time	pH _i	pH _f	Product (structure number)
Sc ₂ O ₃	H ₃ PO ₄	HF	Template / eq	H ₂ O	°C	h			
1	3.5	2	G / 1.5	200	190	48	1	2	[(H ₃ NC ₄ H ₈ NH ₃) ₃ Sc(OH ₂) ₆ Sc ₂ (HPO ₄) ₁₂ (PO ₄) ₂](2)/ [(H ₃ NC ₄ H ₈ NH ₃) ₂ (H ₃ O)][Sc ₅ F ₄ (HPO ₄) ₈](3)
1	3.5	1	G / 1	200	190	48	1	4	[(H ₃ NC ₄ H ₈ NH ₃) ₃ Sc(OH ₂) ₆ Sc ₂ (HPO ₄) ₁₂ (PO ₄) ₂](2)/ [(H ₃ NC ₄ H ₈ NH ₃) ₂ (H ₃ O)][Sc ₅ F ₄ (HPO ₄) ₈](3)
1	3.5	0	G / 1	200	190	48	2	5	[(H ₃ NC ₄ H ₈ NH ₃) ₃ Sc(OH ₂) ₆ Sc ₂ (HPO ₄) ₁₂ (PO ₄) ₂](2)/ Sc ₂ O ₃
0.5	3.5	0	G / 1	200	190	48	2	4	[(H ₃ NC ₄ H ₈ NH ₃) ₃ Sc(OH ₂) ₆ Sc ₂ (HPO ₄) ₁₂ (PO ₄) ₂](2)
1	3.5	3	G / 3	200	190	48	1	2	(NH ₄) ₂ Sc ₂ (HPO ₄)(PO ₄) ₂ (6)
0.5	3.5	3	G / 3	200	190	72	1	2	(NH ₄) ₂ Sc ₂ (HPO ₄)(PO ₄) ₂ (6)
0.5	4	0	G / 1	200	190	72	3	7	[(H ₃ NC ₄ H ₈ NH ₃) ₃ Sc(OH ₂) ₆ Sc ₂ (HPO ₄) ₁₂ (PO ₄) ₂](2)
0.5	3	0	G / 1	200	190	72	3	7	[(H ₃ NC ₄ H ₈ NH ₃) ₃ Sc(OH ₂) ₆ Sc ₂ (HPO ₄) ₁₂ (PO ₄) ₂](2)
0.5	3	0	Zi / 1	200	190	48	6	7	Unknown phase
0.5	3	0	Zii / 1	200	190	48	6	7	(Li) ₂ Sc ₂ (HPO ₄)(PO ₄) ₂ (6)
0.5	3	0	Ziii / 1	200	190	48	6	7	Unknown phase

3.4 Results and Discussion

The experimental program described gave rise to nine crystalline scandium phosphate-based materials, the powder x-ray diffraction patterns of which are given below in figure 3.4. The crystal structures of seven of these materials were solved and refined from single crystal diffraction data, with one being refined only from powder diffraction data as suitable crystals could not be obtained for single crystal analysis. The crystallographic information for each structure is listed in tables 3.2 and 3.3.

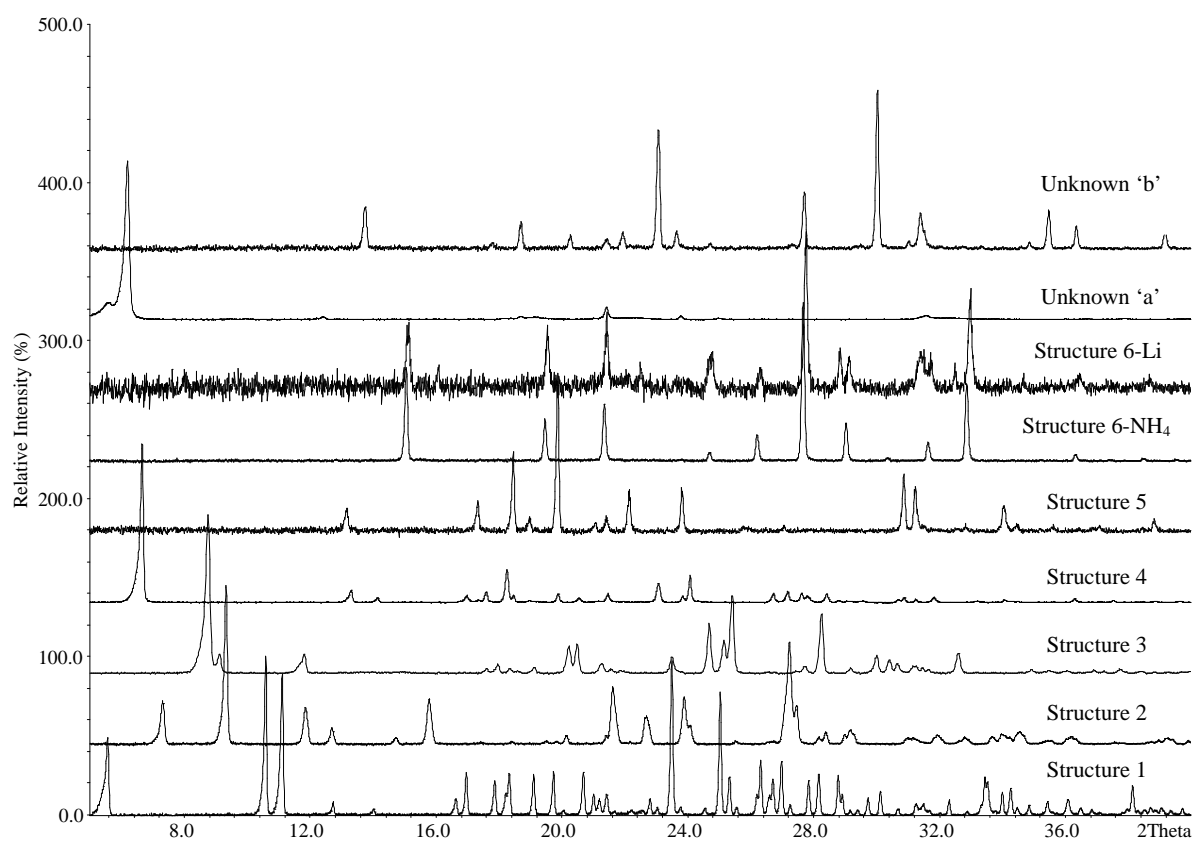


Figure 3.4: Powder X-ray diffraction patterns for the nine crystalline scandium phosphate-based materials synthesised during the course of this work

The positions of the hydrogen atoms in the reported in this chapter were located through a combination of valence bond sum calculations and Fourier mapping, with their positions being fixed to 0.98\AA for a C-H with $U_{\text{iso}}(\text{H})$ being 1.2 times the parent carbon atoms, 0.85\AA for a N-H bond with $U_{\text{iso}}(\text{H})$ being 1.5 times the parent nitrogen atom and 0.98\AA for a O-H bond with $U_{\text{iso}}(\text{H})$ being 1.5 equivalents of the parent oxygen atom.

Structures **1-4** and **6-7** were solved from single crystal data and structure **5** being refined from powder diffraction data. The crystallographic data are reported in Table 3.2 and 3.3.

Wherever possible, phase purity of bulk samples was confirmed by Rietveld refinement of structural (and instrumental) parameters against powder diffraction data. Rietveld refinement was performed with the GSAS program suite⁷⁵ using the atomic co-ordinates determined by the single crystal structure solution as a starting point. Instrumental parameters (background, zero-point, peak profile coefficients) and structural parameters (unit cell, atomic co-ordinates, thermal parameters) were refined, keeping constraints on the bond distances and angles. Close final fits to the observed data were achieved, with R_{wp} values between 5 and 10%, starting from structures determined from the single crystal experiments where ever possible. In order to characterise the materials further, TGA was performed and ^{45}Sc MAS NMR spectra measured for phase pure samples to determine the NMR properties of scandium in carboxylate frameworks. ^{45}Sc MAS NMR spectra are presented with the structures with the experimental conditions given in Chapter 2. Further analysis of ^{45}Sc NMR is given in chapter 7

Table 3.2: Crystallographic information for structures **1 – 3**

	Structure 1	Structure 2	Structure 3
Empirical Formula	$[(\text{H}_3\text{NC}_2\text{H}_4\text{NH}_3)_3][\text{Sc}_3(\text{OH})_2(\text{PO}_4)_2(\text{HPO}_4)_3(\text{H}_2\text{PO}_4)]$	$[(\text{H}_3\text{NC}_4\text{H}_8\text{NH}_3)_3][\text{Sc}(\text{OH})_6\text{Sc}_2(\text{HPO}_4)_{12}(\text{PO}_4)_2]$	$[(\text{H}_3\text{NC}_4\text{H}_8\text{NH}_3)_2(\text{H}_3\text{O})][\text{Sc}_5\text{F}_4(\text{HPO}_4)_8]$
Formula Weight	930.1	2080.0	1300.8
Temperature (K)	173	93	93
Wavelength (Å)/ Diffractometer	1.54178 (Copper) Cu K α	0.71073 (Mercury) Mo K α	0.71073 (Saturn) Mo K α
Crystal System / Space group	Triclinic / P $\bar{1}$	Trigonal / P $\bar{3}$	Monoclinic / C2/m
Unit Cell	a / Å	13.8724(3)	12.8538(4)
Dimensions	b / Å	-	14.9106(4)
	c / Å	9.435(11)	10.1906(3)
	α (°)	-	-
	β (°)	-	-
	γ (°)	-	-
Volume	755.0(14)	15725(7)	1916.14(10)
Z	2	1	2
Number of reflections	7973	8635	5862
Number of unique reflections	2033	1881	1756
2 θ range	8.26 – 67.76	1.70 – 25.34	2.71 – 25.35
Variables	218	154	93
R1 (I>2 σ I)	0.0701	0.0536	0.0518
R1 (all data)	0.0796	0.0686	0.0557
Max., Min. difference in electron density (eÅ ⁻³)	0.743, -0.565	0.656, -0.751	2.33, -1.10

Table 3.3: Crystallographic information for structures 4 - 7

	Structure 4	Structure 5	Structure 6	Structure 7
Empirical Formula	[C ₆ H ₁₁ NH ₃][ScF(HPO ₄)(H ₂ PO ₄)]	Sc(PO ₄).2H ₂ O	(NH ₄) ₂ Sc ₂ (HPO ₄)(PO ₄) ₂	Li ₂ Sc(PO ₄)(PO ₄ H)
Formula Weight	358.11	175.96	410.91	499.58
Temperature (K)	120	293	123	123
Wavelength (Å)/ Diffractometer	0.68920 / Station 9.8	1.54051 / STOE (powder XRD) Cu Kα	0.71073 / (Saturn) Mo Kα	0.7103 / (Saturn) Mo Kα
Crystal System / Space group	Orthorhombic / Pbca	Monoclinic / P2 ₁ /n	Cubic / P2 ₁ 3	Monoclinic P 2 ₁ /n
Unit Cell Dimensions	a / Å	10.1861(18)	5.4482(2)	4.8530(1)
	b / Å	-	10.2562(3)	8.1880(4)
	c / Å	-	8.94393(3)	7.6680(2)
	α (°)	-	-	-
	β (°)	-	90.654(4)	104.13()
	γ (°)	-	-	-
Volume	2592.6(14)	499.74(4)	1055.6(14)	295.48
Z	8	4	4	4
Number of reflections	19254	7973	10541	2827
Number of unique reflections	19481	2033	659	539
2θ range (°)	2.99 – 25.70	10.0 – 90.0	2.83 – 25.31	3.70 – 25.37
Variables / Restraints	169	10	66	61
R1 (I>2σI)	0.1552	0.0503	0.045	0.0541
R1 (all data)	0.2754	0.0696	0.120	0.0503
Max., Min. difference in electron density (eÅ ⁻³)	2.21, -1.35	-	0.99, -1.00	0.774, -1.057
Max., mean shift/su	-	0.03, 0.01	-	-

3.4.1 [(H₃NC₂H₄NH₃)₃][Sc₃(OH)₂(PO₄)₂(HPO₄)₃(H₂PO₄)] - Structure 1

Structure 1, [(H₃NC₂H₄NH₃)₃][Sc₃(OH)₂(PO₄)₂(HPO₄)₃(H₂PO₄)], was solved by direct methods and Fourier syntheses, using the SHELXS program⁸¹, from laboratory single crystal X-ray data collected on a small crystal, the crystallographic information is outlined in table 3.2. Atomic co-ordinates for structure 1 are given in table 3.4, below, and crystallographic information for all structures presented within this work are all included as crystallographic information files (CIFs) on a compact disc which accompanies this thesis.

Atom	x	y	z	Occ	U _{iso}	Multiplicity
Sc(1)	0.7134(2)	0.11432(14)	0.29234(7)	1	0.0125(4)	2
Sc(2)	0	0	0.5	1	0.0127(4)	1
P(1)	1.2539(3)	-0.13225(18)	0.31890(9)	1	0.0121(4)	2
P(2)	1.1562(3)	0.31468(18)	0.34742(9)	1	0.0120(4)	2
P(3)	0.5508(3)	0.2508(2)	0.09197(10)	1	0.0173(5)	2
O(1)	1.0150(8)	-0.0683(6)	0.2757(3)	1	0.0164(10)	2
O(2)	1.2044(8)	-0.1374(6)	0.4139(3)	1	0.0194(10)	2
O(3)	1.3469(8)	-0.3057(5)	0.3017(3)	1	0.0156(10)	2
O(4)	1.4618(8)	-0.0370(6)	0.2838(3)	1	0.017(1)	2
O(5)	0.9842(8)	0.2697(6)	0.2897(3)	1	0.0172(10)	2
O(6)	1.1320(8)	0.2085(6)	0.4342(3)	1	0.0188(10)	2
O(7)	1.0751(8)	0.4923(5)	0.3580(3)	1	0.0194(10)	2
O(8)	1.4262(8)	0.2982(5)	0.3104(3)	1	0.0156(10)	2
O(9)	0.7080(8)	0.1966(6)	0.1648(3)	1	0.0181(10)	2
O(10)	0.5148(9)	0.4362(6)	0.0732(3)	1	0.0254(11)	2
O(11)	0.2811(8)	0.1986(7)	0.1186(3)	1	0.0265(12)	2
O(12)	0.6517(9)	0.1763(6)	0.0174(3)	1	0.0251(11)	2
O(13)	0.7157(7)	0.0436(5)	0.4217(2)	1	0.0089(8)	2
N(1)	1.0029(11)	-0.0815(7)	0.1021(3)	1	0.0203(12)	2
N(2)	0.7288(10)	-0.4512(7)	0.1943(4)	1	0.0200(12)	2
N(3)	0.686(1)	0.6608(7)	0.4454(4)	1	0.0219(13)	2
C(1)	0.8136(13)	-0.1899(9)	0.1165(4)	1	0.0239(15)	2
C(2)	0.9219(13)	-0.3551(8)	0.1585(5)	1	0.0232(15)	2
C(3)	0.6163(11)	0.4967(8)	0.4693(4)	1	0.0188(14)	2

Table 3.4: Atomic co-ordinates for structure 1

A Rietveld refinement of high-resolution X-ray powder data collected at the ESRF was performed with the GSAS program suite⁷⁵ using the atomic co-ordinates determined by the single crystal structure solution as a starting point in order to confirm phase purity. Instrumental parameters (background, zero-point, peak profile coefficients) and structural parameters (unit cell, atomic co-ordinates, thermal parameters) were refined, keeping

constraints on the bond distances and angles. A close final fit to the observed data was achieved, with $R_{wp} = 10.0\%$, (figure 3.5) with the structure determined from the single crystal experiment, with atomic positions refining to positions very close to the values determined from single crystal diffraction.

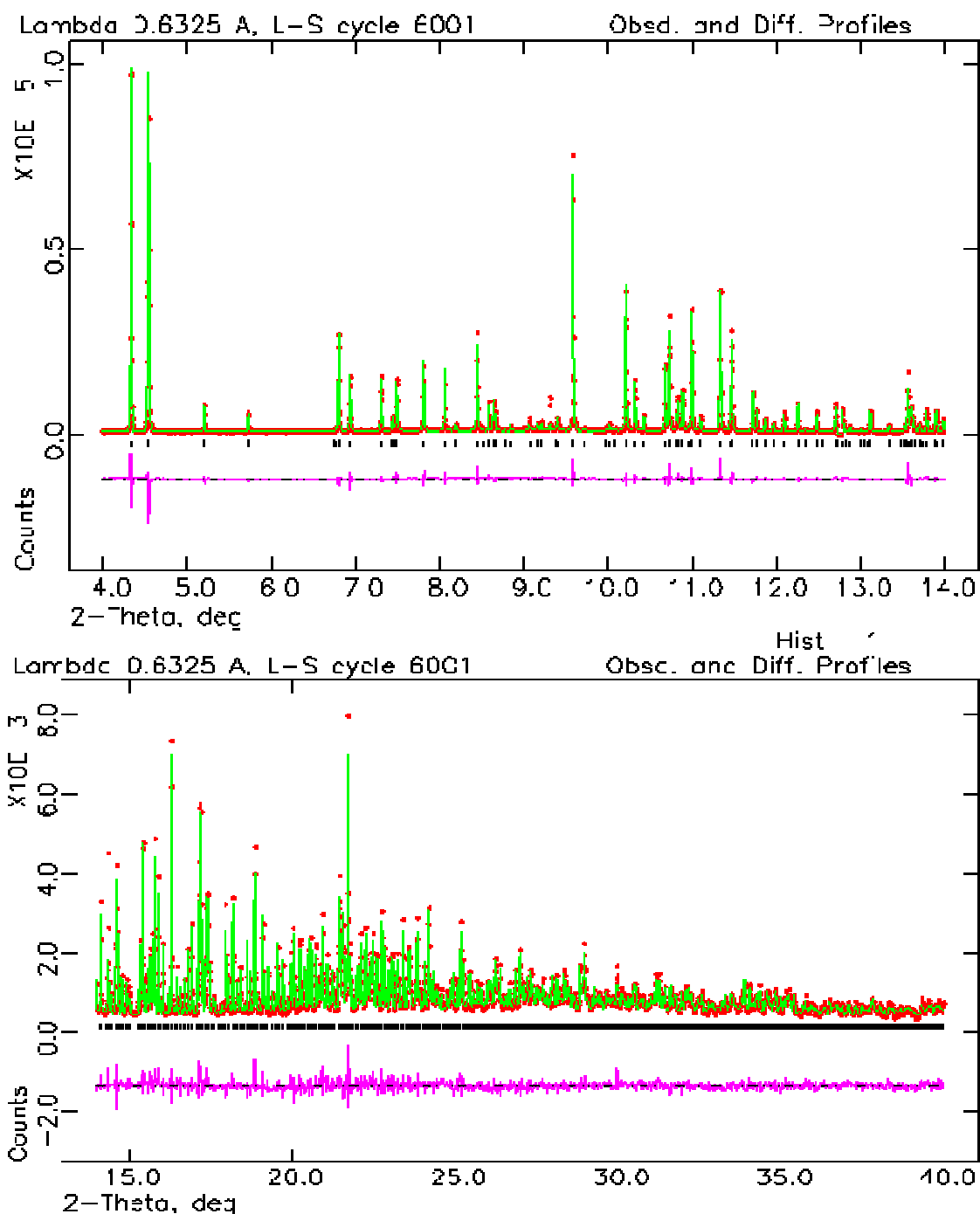


Figure 3.5: Rietveld refinement of powder x-ray diffraction data collected at the European Synchrotron Radiation Facility in Grenoble.

Structure **1** presents a novel two-dimensional mixed layered structure (1Sc:2P) containing ScO_6 corner-sharing to H_2PO_4 , HPO_4 , PO_4 tetrahedra and other ScO_6 octahedra. The main structural unit of structure **1** is a ribbon-like chain running parallel to the a -axis, figure 3.6. Each chain is made up of trimers of corner sharing ScO_6 octahedra, the two shared oxygen atoms of each trimer being part of a hydroxyl group.

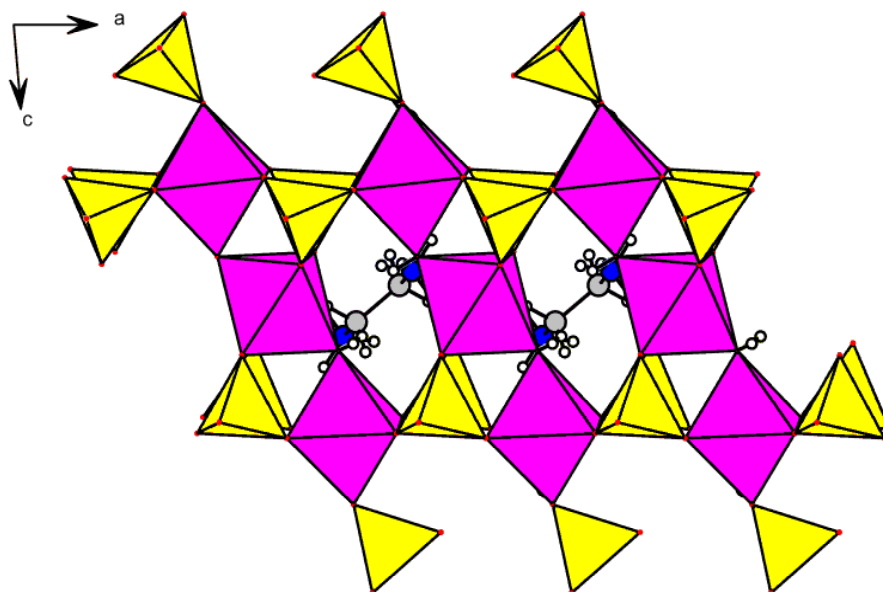


Figure 3.6: Projection down $[010]$ of structure **1**, showing ribbons extending parallel to the a -axis. (ScO_6 octahedra in purple, PO_4 tetrahedra in yellow, nitrogen in blue and carbon in grey. This colour scheme is adopted throughout this chapter)

Adjacent $\text{Sc}_3(\text{OH})_2$ trimers are linked along a by three apices of phosphate (PO_3OH) groups that share protons, the POH group of each of which points away from the ribbon. Two phosphate tetrahedra are attached by one corner to the $\text{Sc}_3(\text{OH})_2$ trimers at the edges of the ribbons to make up the structure. Adjacent ribbons are stacked along the b -axis and these stacks are arranged in a staggered way along c . The protonated ethylenediamine molecules occupy space between the ribbons and between stacks of ribbons, holding them together through hydrogen bonding with oxygens of the terminal phosphate groups. The interatomic distances and bond angles in the inorganic ribbons are as expected: Sc-O bond distances are between 2.084(7) and 2.190(8)Å and P-O distances are from 1.499(9) to 1.616(8)Å.

Ethylenediamine is surrounded by the $\text{Sc}_3\text{P}_6\text{O}_9$ columns, allowing hydrogen bonding between the framework and the template depicted graphically in figure 3.7.

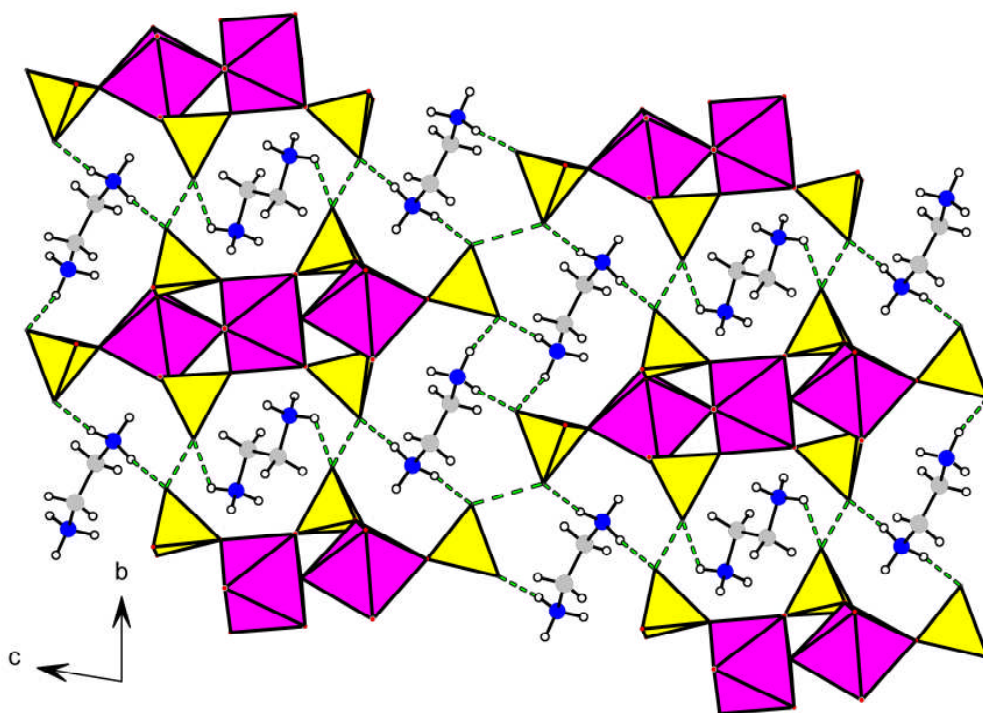


Figure 3.7: Projection down [100] of structure 1, showing the hydrogen bonding network present between the phosphate tetrahedra, HPO_4 and H_2PO_4 , and protonated ethylenediamine molecules

The positions of hydrogen atoms in the structure were interpreted from bond valence sum calculations⁸² and consideration of the distances of oxygens from nitrogens of the ethylene diamine molecules, which were taken to be protonated, and from other oxygens in a potential H-bonding network. The oxygen O(13) that bridges scandium atoms Sc(1) and Sc(2) (bond valence sum, b.v.s., = 0.97) is protonated. Oxygens O(3) and O(7) (b.v.s. 1.17 and 1.19, respectively) of phosphate groups that link the scandium trimers are part of POH groups that share protons $\text{O}(3)\text{-O}(7) = 2.52 \text{ \AA}$. The terminal (P(3)) phosphate tetrahedra possess three oxygens that have bond valence sums less than 2, O(10), O(11) and O(12) (b.v.s. values 1.14, 0.97 and 1.33). The O(10) - O(10) distance of 2.49 \AA suggests that these share a proton. O(11) is too far from other oxygens to be involved in hydrogen bonding and is taken to be protonated and O(12) is H-bonded to the organic nitrogen.

Table 3.5 lists results from valence studies of structure **1**, indicating which oxygens are likely to be protonated and those which are likely to be involved in hydrogen bonding, graphically depicted in figure 3.6.

Table 3.5: *Hydrogen Bonds for structure 1 supported with corresponding valence bond sum values and deviation from theoretical values. Data shown for O(3) and O(7) are provided in this order.*

Donor----Acceptor	d(D----A)Å	VBS for Acceptor	Deviation (%)
N(1)----O(12)	2.749(2)	1.3	31
N(1)----O(12)	3.009(4)	1.3	31
O(3)----O(7)	2.521(4)	1.2, 1.2	40, 39
O(10)----O(10)	2.499(3)	1.1	41

The final charge balanced structural formula is therefore $[(C_2N_2H_{10})_3]^- [Sc_3(OH)_2(PO_4)_2(PO_4H)_3(PO_4H_2)]$. CHN analysis, weight %, calculated, C, 7.75%, H, 4.01%, N, 9.08%; measured, C, 6.78%, H, 3.63%, N, 8.62%, suggesting some amorphous inorganic impurity is present.

Solid state ^{31}P MAS NMR (figure 3.8) gives a single broad peak at δ -9.7ppm, so that the different crystallographic sites are not resolved. ^{45}Sc MAS NMR (figure 3.9) shows two broad peaks at 35.4 and 8.8 ppm, consistent with two different scandium sites in the structure. ^{45}Sc is a quadrupolar nucleus, and quadrupolar interactions results in broad resonances. ^{13}C CP MAS NMR shows a broad peak at 37 ppm.

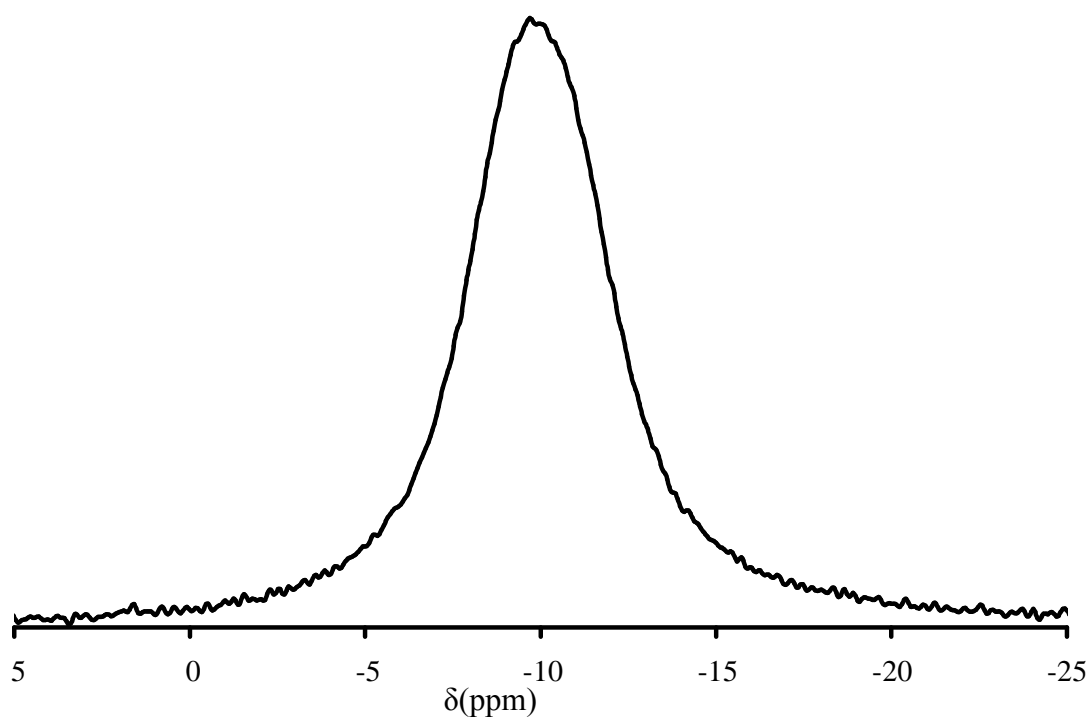


Figure 3.8: ^{31}P MAS NMR spectra for structure 1, showing a signal with a maximum at -9.7 ppm with a line-width of 960 Hz. The peak can be deconvoluted to give 2 peaks at -9.2 ppm and -10.7 ppm with an integral ratio of approximately 2:1 respectively.

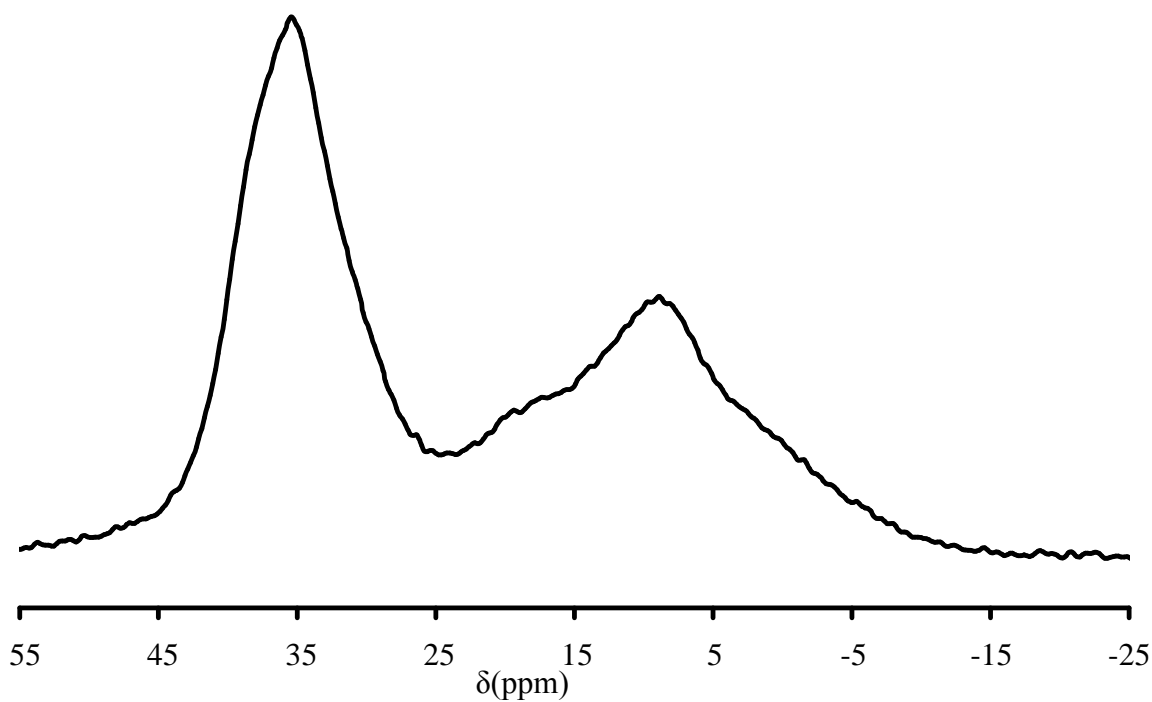


Figure 3.9: ^{45}Sc MAS NMR spectra of structure 1, showing two distinct peaks at 35.4 and 8.8 ppm with a line width of 1145 Hz and 2290 Hz, respectively.

Thermogravimetric analysis shows a significant weight loss (experimental, 18.82%; theoretical, 20.03%) occurring between 320 and 360 °C due to combustion of the organic.

The synthetic conditions for this phase were adapted from previous experiments that report the formation of scandium phosphates using ethylenediamine as the organic structure directing agent.^{45,46} It is instructive to compare the reaction conditions that yielded the chain structure, structure **1**, with the framework structures obtained previously with ethylenediamine. Table 3.6 outlines the reaction stoichiometries used for structure **1** with those for scandium phosphate materials prepared previously with ethylenediamine as the template. Considerable structural variety is possible in these systems owing to the ability of scandium to occur in different degrees of ‘condensation’. It is octahedral in all cases, however. Structure **1** is the first chain scandium phosphate structure observed with ethylenediamine.

Ref	Structure	Composition of Reactants						Temperature (h)	Time (°C)	Structure Type
		Sc ₂ O ₃	H ₃ PO ₄	HF	Template	H ₂ O	BO ₃ H ₃			
44	(C ₂ N ₂ H ₁₀) ₈ Sc ₈ (ScO ₂) ₄ (PO ₄) ₄ (HPO ₄) ₁₂ ·12H ₂ O	1	1.8	2	2	100	-	72	190	Framework
45	Sc(HPO ₄) ₂ ·0.5(N ₂ C ₂ H ₁₀)	1	2	1	1	200	-	48	190	Framework
42	(C ₂ N ₂ H ₁₀) ₂ Sc ₂ F ₆ (HPO ₄) ₂	1	4	40	2	230	2	336	170	Framework
40	[(H ₃ NC ₂ H ₄ NH ₃) ₃][Sc ₃ (OH) ₂ (PO ₄) ₂ (HPO ₄) ₃ (H ₂ PO ₄)]	1	1.7	0.5	2.2	200	-	48	190	Ribbons

Table 3.6: Reaction stoichiometries used in the preparation of scandium phosphates templated with ethylenediamine

3.4.2 Scandium phosphates templated with diaminobutane

Although, prior to this work, there have been no examples in the literature of scandium phosphates which have been templated using diaminobutane, there are numerous examples of diaminobutane being used as template within other metal phosphate systems.⁸³⁻⁸⁶

Diaminobutane was chosen as a primary diamine similar to ethylenediamine in basicity. Syntheses were attempted in the presence and absence of HF, because fluoride is known to act as a mineralising agent in similar preparations.⁴²⁻⁴⁵ Two scandium phosphates were synthesised as pure phases, one in the absence of HF and one in the presence of HF. Table 3.7 shows a direct comparison in the reaction conditions used to synthesise structure **2**, $[(H_3NC_4H_8NH_3)_3][Sc(OH_2)_6Sc_2(HPO_4)_{12}(PO_4)_2]$, and structure **3**, $[(H_3NC_4H_8NH_3)_2(H_3O)][Sc_5F_4(HPO_4)_8]$.

Table 3.7: Reaction conditions used in the synthesis of structure **2**, $[H_3NC_4H_8NH_3)_3][Sc(OH_2)_6Sc_2(HPO_4)_{12}(PO_4)_2]$, and structure **3**, $[(H_3NC_4H_8NH_3)_2(H_3O)][Sc_5F_4(HPO_4)_8]$

Name	Composition of Reactants					Time (h)	Temp (K)	pH (start)	pH (end)
	Sc ₂ O ₃	H ₃ PO ₄	HF	H ₃ N(CH ₂) ₄ NH ₃	H ₂ O				
<i>structure 2</i>	0.5	3	0	1	200	72	463	3	8
<i>structure 3</i>	0.5	3.5	2	1.5	200	72	463	2	7

3.4.3 [(H₃NC₄H₈NH₃)₃][(Sc(OH₂))₆Sc₂(HPO₄)₁₂(PO₄)₂] – Structure 2

Structure 2, [(H₃NC₄H₈NH₃)₃][(Sc(OH₂))₆Sc₂(HPO₄)₁₂(PO₄)₂], was solved from laboratory single crystal X-ray data, by direct methods and Fourier syntheses, using the SHELXS program.⁸¹ The crystallographic information is outlined in table 3.2. and the atomic coordinates are listed in table 3.8

Table 3.8: Atomic co-ordinates for structure 2

Atom	x	y	z	Occ	U _{iso}	Multiplicity
Sc1	-0.43850(9)	-0.14470(9)	1.40794(12)	1	0.0105(4)	6
Sc2	0	0	0	1	0.0084(6)	1
Sc3	0	0	0.5	1	0.0084(6)	1
P1	-0.18379(12)	-0.01516(12)	0.24528(16)	1	0.0113(4)	6
P2	-0.36825(12)	0.12651(12)	0.39669(16)	1	0.0109(4)	6
P3	-0.6667	-0.3333	0.2157(3)	1	0.0103(6)	2
O1	-0.2998(3)	-0.1091(3)	0.2862(4)	1	0.0143(9)	6
O2	-0.1389(3)	-0.0566(3)	0.1284(4)	1	0.0108(9)	6
O3	-0.1072(3)	0.0306(3)	0.3757(4)	1	0.0106(9)	6
O4	-0.1942(3)	0.0838(3)	0.1770(4)	1	0.0158(9)	6
O5	-0.4237(4)	0.0065(3)	0.3553(5)	1	0.0265(11)	6
O6	-0.3012(3)	0.1953(4)	0.2625(5)	1	0.0247(11)	6
O7	-0.4506(3)	0.1647(4)	0.4318(5)	1	0.0259(11)	6
O8	-0.2837(3)	0.1518(3)	0.5160(4)	1	0.0142(9)	6
O9	-0.5552(3)	-0.2345(3)	0.2605(4)	1	0.0136(9)	6
O10	-0.6667	-0.3333	0.0469(8)	1	0.0234(18)	2
O11	-0.3101(3)	-0.0513(3)	0.5765(4)	1	0.0143(9)	6
C1A	-0.3651(10)	0.059(1)	0.8956(13)	0.5	0.017(3)	6
C2A	-0.4622(10)	-0.0252(11)	0.9870(13)	0.5	0.010(3)	6
N1A	-0.2835(5)	0.0140(6)	0.8890(7)	0.5	0.0403(17)	6
N1B	-0.2835(5)	0.0140(6)	0.8890(7)	0.5	0.0403(17)	6

Structure 2 presents a 3 dimensional framework scandium phosphate structure, within which there are no Sc–O–Sc linkages, and therefore there is strict alternation between Sc and P in the framework. The structure can best be thought of as being made up of gently undulating sheets of ScO₆ octahedra and PO₄ tetrahedra, arranged in four-membered and six-membered rings, with the phosphate groups pointing away from the centre of the sheet and into the cavities between sheets.

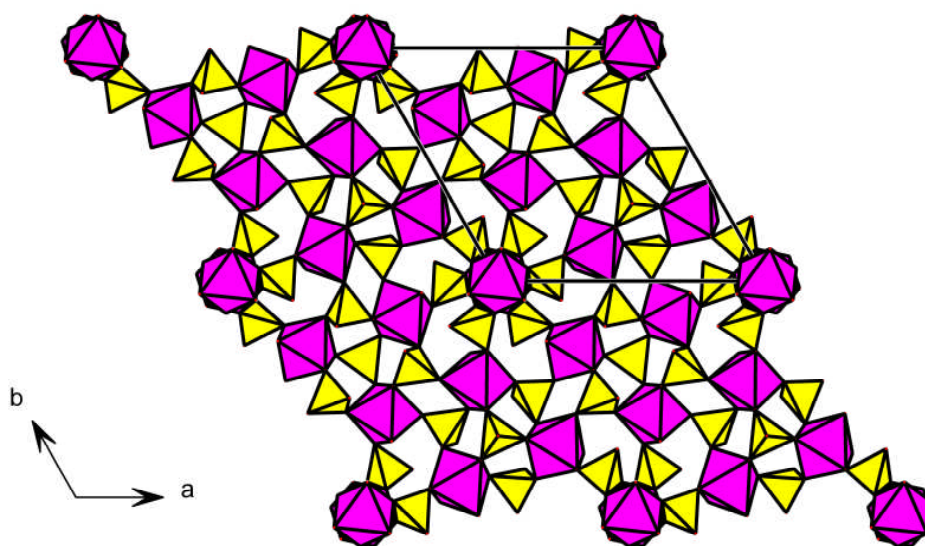


Figure 3.10: Structure 2 viewed down the $[001]$ axis, showing alternating Sc-O-P linkages with a layer. The organic 1,4-diaminobutane template molecules have been omitted for clarity. Unit cell edges are shown in black.

Adjacent sheets are then pillared by ScO_6 octahedra, the oxygen atoms of which are the vertices of phosphate groups directed away from the sheets. The gallery space between the layers is connected at its narrowest point through highly irregular, flattened windows comprising six ScO_6 octahedra (two of which are pillaring units) and six phosphate groups. The minimum and maximum O–O distances across the rings are 5.5 and 11.6 Å. The protonated template molecules occupy space between the layers, and interact with phosphate groups projecting into the interlayer space via hydrogen bonding. The interatomic distances are as expected. Sc–O bond distances are from 2.023(4) to 2.098(4) Å with the exception of Sc(1)–O(1), which corresponds to coordinated water, and displays a longer bond length (2.253(4) Å). P–O distances range from 1.495(4) to 1.593(8) Å.

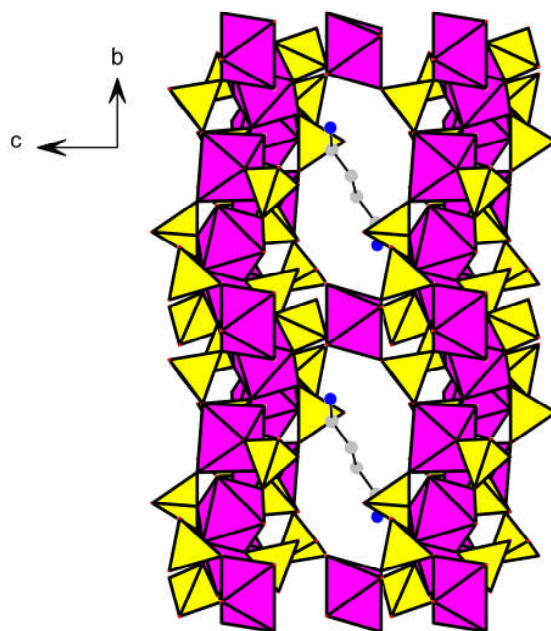


Figure 3.11: Projection onto the (100) plane of structure 2, showing the sheet-like structures which are interlinked by the ScO_6 octahedra. 1,4-diaminobutane can be seen occupying the channels through the crystal. Some of the 1,4-diaminobutane molecules have been omitted for clarity.

Hydrogen atoms were assigned to the framework by b.v.s. calculations. Accordingly, O(11) (b.v.s. 0.47) belongs to a water molecule coordinated to scandium. Also, the terminal oxygens of O(4), O(6) and O(10) (b.v.s. values of 1.22, 1.07 and 1.03) are expected to be protonated or involved in H-bonding. O(4), O(6) and O(10) are the only non-bridging oxygens on the three different phosphorus atoms, P(1), P(2) and P(3). Postulating a proton on each of these PO_4 tetrahedra, and considering the diaminobutane molecules to be fully protonated more than balances the negative charge on the framework. Of the oxygens with b.v.s. values close to 1, O(4) shows the closest approaches to the nitrogen of the organic template. It is therefore assumed that there is a disordered arrangement of protons between O(4) and the diaminobutane. For convenience the overall unit cell formula is written $[(\text{H}_3\text{NC}_4\text{H}_8\text{NH}_3)_3(\text{Sc}(\text{OH}_2))_6\text{Sc}_2(\text{HPO}_4)_{12}(\text{PO}_4)_2]$, where the amine is fully protonated. CHN analysis, wt%, calculated: C, 6.11%; H, 3.04%; N, 3.62%; measured: C, 6.98%; H, 2.54%; N, 4.09%.

Solid-state ^{31}P DP MAS NMR (Figure 3.12) gives four main peaks at δ -7.2, -9.9, -11.5 and -20.4 ppm, in the ratio 6:2:4:2, rather than 6:6:2. No evidence for lower symmetry was

observed from the x-ray diffraction, so the non-equivalence is attributed to the effects of proton disorder in the structure. It is known that 12 protons are distributed over 14 sites, so it is suggested that phosphorus P(2) and P(3) all belong to HPO_4 groups, whereas P(1) is present both as HPO_4 and PO_4 . The unprotonated groups could be those at -20.4 ppm (with a shift similar to that observed for PO_4 groups in $\text{ScPO}_4 \cdot 2\text{H}_2\text{O}$).⁴⁴ ^{45}Sc NMR (Figure 3.13) gives a single broad peak, which, based on the crystallography, must include three overlapping signals from the sample. ^{13}C MAS CP NMR gives two peaks at 39.3 and 25.7 ppm which correspond to the two crystallographically unique carbon atoms.

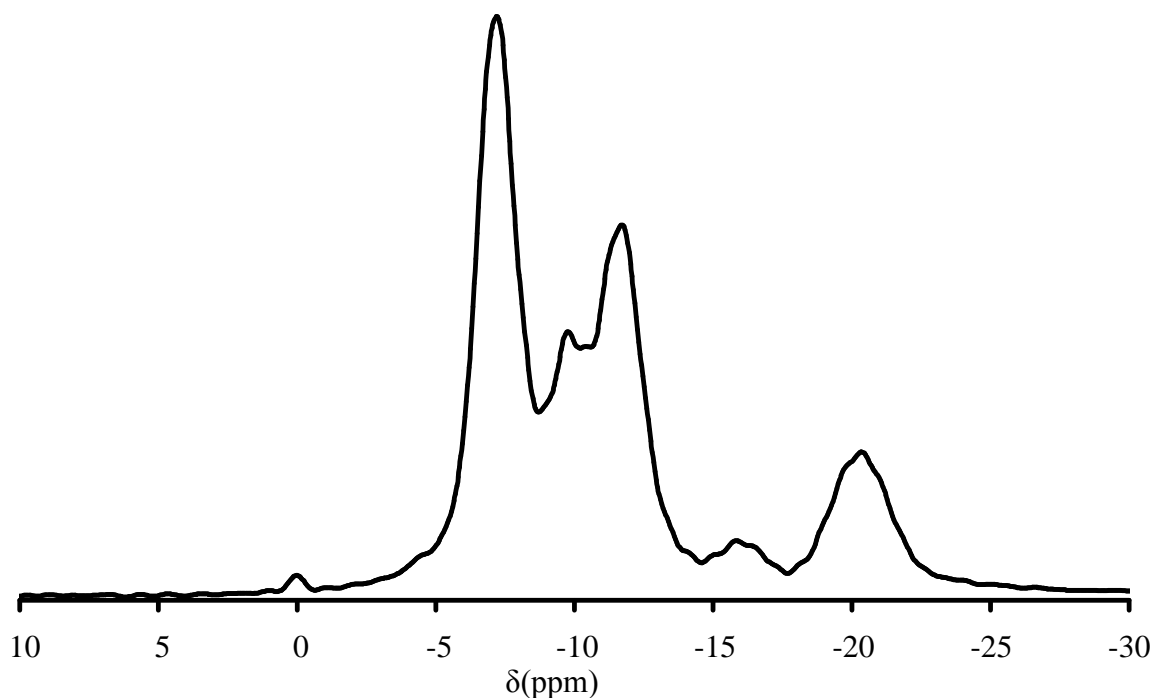


Figure 3.12: ^{31}P DP MAS NMR of structure 2. There are four main peaks at δ -7.2, -9.9, -11.5 and -20.4 ppm, in the ratio 6:2:4:2

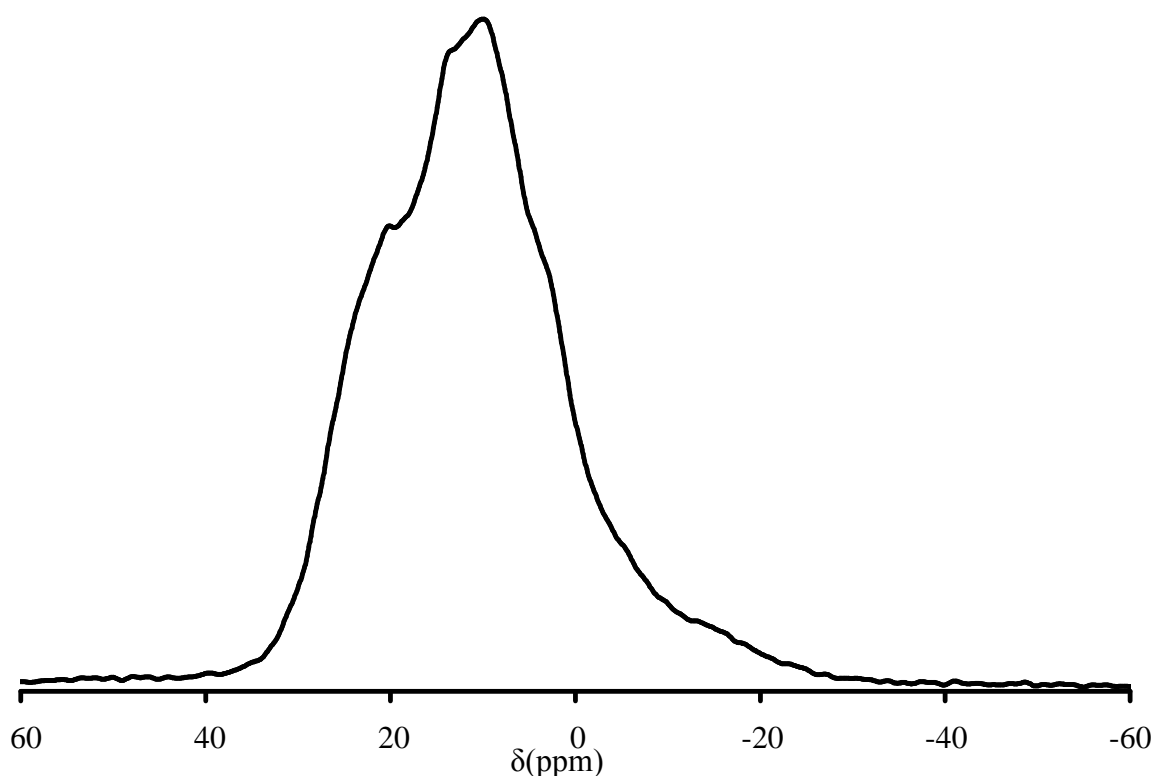


Figure 3.13: ^{45}Sc MAS NMR spectra of structure 2, showing one broad resonance at 10ppm with a line width of 3000Hz

Thermal analysis shows a weight loss in a single step of 18.9% between 250 and 600°C (theoretical loss from dehydration, 5.2%, from loss of organic, 13.0%). The product after heating is amorphous.

Structure 2 is closely related to indium^{87, 88} and iron(III)^{89, 90} phosphates prepared with imidazolium, diazabicyclooctane and sodium as structure directing agents, and isostructural with a ferric phosphate that, like structure 2, is templated by diaminobutane (table 3.9). The similarity in the ionic radii⁹¹ of these trivalent cations (Fe(III), 0.645Å ; Sc, 0.745Å ; In, 0.80Å) permit the same structure to crystallise. All of these structures are made up of similar layers, but whereas for structure 2 and the ferric phosphate prepared with diaminobutane⁸⁸ each layer has an identical orientation, in the other structures there is an alternation between layers in one orientation and layers related by a c glide. This results in a doubling of the c -axis repeat and a change in the space group symmetry from $\bar{P}3$ to $\bar{P}3c1$ in those structures. The cause of this change in stacking is due to the different organic amine used as a structure directing agent. The H-bonding arrangement with diaminobutane favours the stacking sequence in which each of the layers is crystallographically identical.

Compound	Template	Spacegroup	a / Å	c / Å	Reference
$[(\text{H}_3\text{NC}_4\text{H}_8\text{NH}_3)_3][(\text{Sc}(\text{OH}_2))_6\text{Sc}_2(\text{HPO}_4)_{12}(\text{PO}_4)_2]$	1,4-diaminobutane	$P\bar{3}$	13.8724	9.4351	structure 2
$\text{Na}_4[\text{In}_8(\text{HPO}_4)_{14}(\text{H}_2\text{O})_6] \cdot 12(\text{H}_2\text{O})$	Na^+	$P\bar{3}c1$	13.85	18.43	87
$[(\text{C}_3\text{N}_2\text{H}_5)_3][\text{In}_8(\text{HPO}_4)_{14}(\text{H}_2\text{O})_6](\text{H}_2\text{O})_5(\text{H}_3\text{O})$	imidazole	$P\bar{3}$	13.859	19.186	88
$[\text{H}_3\text{N}(\text{CH}_2)_4\text{NH}_3]_3[\text{Fe}_8(\text{HPO}_4)_{12}(\text{PO}_4)_2(\text{H}_2\text{O})_6]$	1,4-diaminobutane	$P\bar{3}$	13.495	9.396	90
$[\text{H}_3\text{N}(\text{C}_2\text{H}_4)_3\text{NH}_3]_3[\text{Fe}_8(\text{HPO}_4)_{12}(\text{PO}_4)_2(\text{H}_2\text{O})_6]$	Dabco	$P\bar{3}c1$	13.5274	19.2645	89

Table 3.9: Structures similar or isostructural to structure 2 including indium and iron(III) phosphates prepared with imidazolium, diazabicyclooctane, 1,4-diaminobutane and sodium as structure directing agents.

3.4.4 [(H₃NC₄H₈NH₃)₂(H₃O)][Sc₅F₄(HPO₄)₈] – Structure 3

Adding HF to the synthesis gel that contained diaminobutane resulted in the crystallisation of a different phase, structure 3.

Structure 3, [(H₃NC₄H₈NH₃)₂(H₃O)][Sc₅F₄(HPO₄)₈], was solved by direct methods and Fourier syntheses, using the SHELXS program⁸¹, from laboratory single crystal X-ray data, the crystallographic information is outlined in table 3.2. The atomic co-ordinates for structure 3 are listed in table 3.10.

Table 3.10: Crystallographic information for structure 3

Atom	x	y	z	Occ	U _{iso}	Multiplicity
Sc1	0.38292(10)	0.62566(9)	0.09594(12)	1	0.0097(4)	8
Sc2	0	0.5	0	1	0.0086(6)	2
P1	0.56194(19)	0.5	0.3025(2)	1	0.0078(5)	4
P2	0.2166(2)	0.5	0.2433(3)	1	0.0134(6)	8
P3A	0.1609(4)	0.6504(4)	-0.1510(6)	0.5	0.0058(18)	4
P3B	0.1514(5)	0.6526(4)	-0.1322(6)	0.5	0.0079(19)	4
F1	0.3886(4)	0.5	0.0196(5)	1	0.0106(11)	4
F2	0.5	0.6669(4)	0	1	0.0116(12)	4
O1	0.5070(4)	0.5853(3)	0.2460(5)	1	0.0133(10)	8
O2	0.6791(6)	0.5	0.2731(7)	1	0.0172(16)	4
O3	0.5814(5)	0.5	0.4561(6)	1	0.0099(14)	4
O4	0.2702(4)	0.5850(4)	0.2039(5)	1	0.0175(11)	8
O5	0.0984(6)	0.5	0.1885(7)	1	0.0184(16)	8
O6	0.2251(5)	0.5	0.4002(7)	1	0.0147(15)	8
O7	0.2729(5)	0.6492(4)	-0.0798(6)	1	0.0265(13)	8
O8	0.1162(5)	0.7448(4)	-0.1653(6)	1	0.0299(14)	8
O9A	0.0998(8)	0.5822(8)	-0.0827(11)	0.5	0.016(2)	4
O9B	0.0813(9)	0.6147(8)	-0.0472(11)	0.5	0.018(2)	4
O10A	0.1634(9)	0.6166(7)	-0.2942(10)	0.5	0.013(2)	4
O10B	0.1210(13)	0.6088(10)	-0.2783(15)	0.5	0.042(4)	4
O21	0.0013(19)	0.5	-0.432(2)	0.5	0.058(6)	4
C1	0.1103(7)	0.7272(6)	0.3906(9)	1	0.030(2)	8
C2	0.1978(8)	0.7758(7)	0.4895(10)	1	0.037(2)	8
N1	0.1241(5)	0.7258(5)	0.2442(7)	1	0.0258(16)	8

Statistical analysis of the diffraction data clearly indicates a centrosymmetric structure [mean $|E^*E - 1| = 0.966$; expected values are 0.968 for centrosymmetric and 0.736 for non-centrosymmetric] and the structure was thus solved and refined in C2/m.

Semi-quantitative energy dispersive x-ray analysis, figure 3.15, indicated the sample contained fluorine, and refinement of two sites which bridged Sc(1), originally identified as oxygen atoms gave a more satisfactory refinement, in terms of their thermal parameters,

when refined as fluorine atoms. The diaminobutane molecules are taken to be fully protonated, in order to balance the charge of the material.

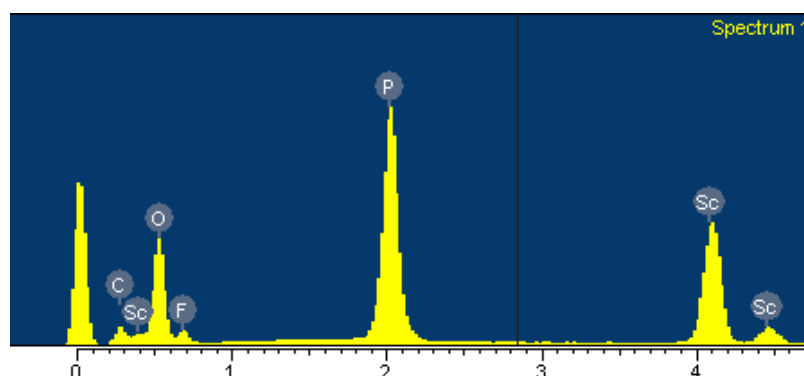


Figure 3.15: EDX chart for $[C_6H_{11}NH_3][ScF(HPO_4)(H_2PO_4)]$, showing a definite peak, contributed from the presence of fluorine in the material

Structure **3** presents a novel layered scandium phosphate material which is made up of scandium fluoride phosphate layers bridged by protonated diaminobutane molecules, as shown in figure 3.16. Each layer consists of isolated ScO_6 octahedra linked via phosphate groups to tetramers of corner-sharing ScO_4F_2 octahedra, which are linked through fluoride ions. The isolated ScO_6 octahedra are linked to the tetrameric squares through corner-sharing PO_4 tetrahedra which bond to scandiums by three apical oxygens, the remaining oxygens projecting into the interlayer space, shown in figure 3.17. In addition to this, one phosphate group is attached to the tetramer of ScO_4F_2 octahedra by two apical oxygens, the remaining two groups projecting into the interlayer space. The layers are bridged by protonated diaminobutane molecules, each $-NH_3^+$ group of which fits into recesses between four phosphate tetrahedra that project out from the layers. As a result, layers are stacked along the c -axis. Protonated water molecules also occupy this space.

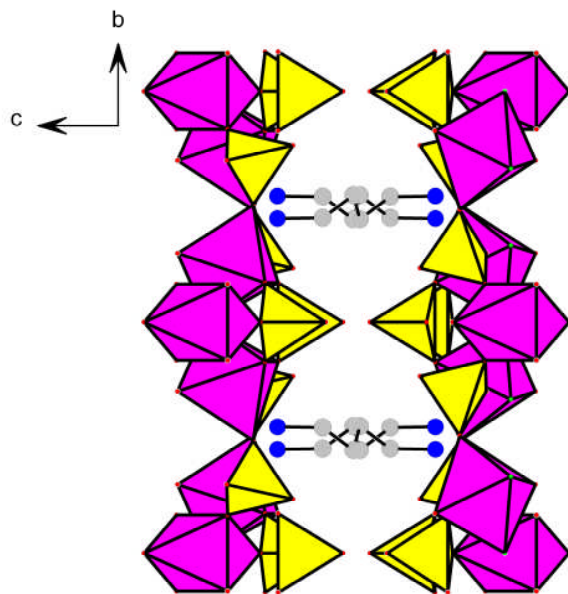


Figure 3.16: Projection onto the (100) plane of structure 3, showing the layers which are bridged by the organic moiety. 1,4-diaminobutane can be seen in inverted configurations occupying the channels through the crystal.

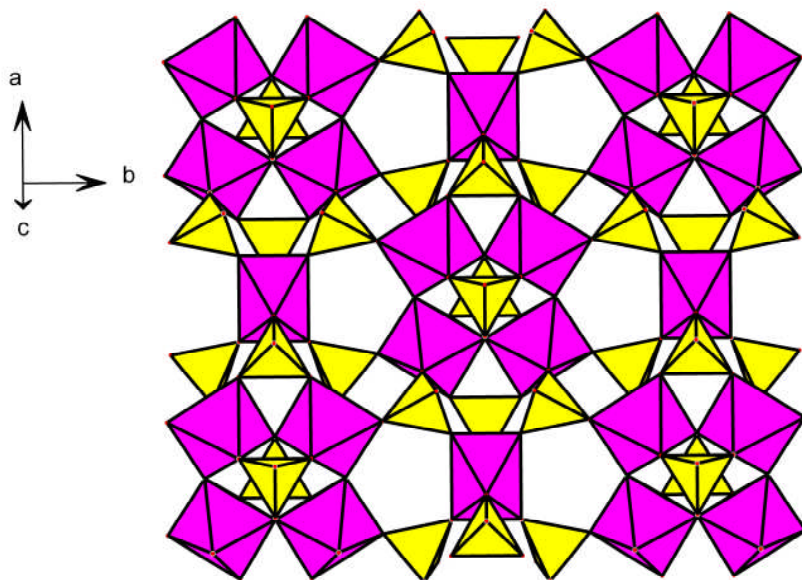


Figure 3.17: A view down the [001] axis, showing the 'average' framework architecture of structure 3.

Initially, structure solution gave layers, as shown in figures 3.16 and 3.17, with two crystallographically distinct scandium sites and three distinct phosphorus sites, the latter in

the ratio P(3):P(2):P(1) = 2:1:1. However, solid-state ^{31}P DP NMR shows four peaks in the ratio 1:1:1:1, shown in figure 3.18, below.

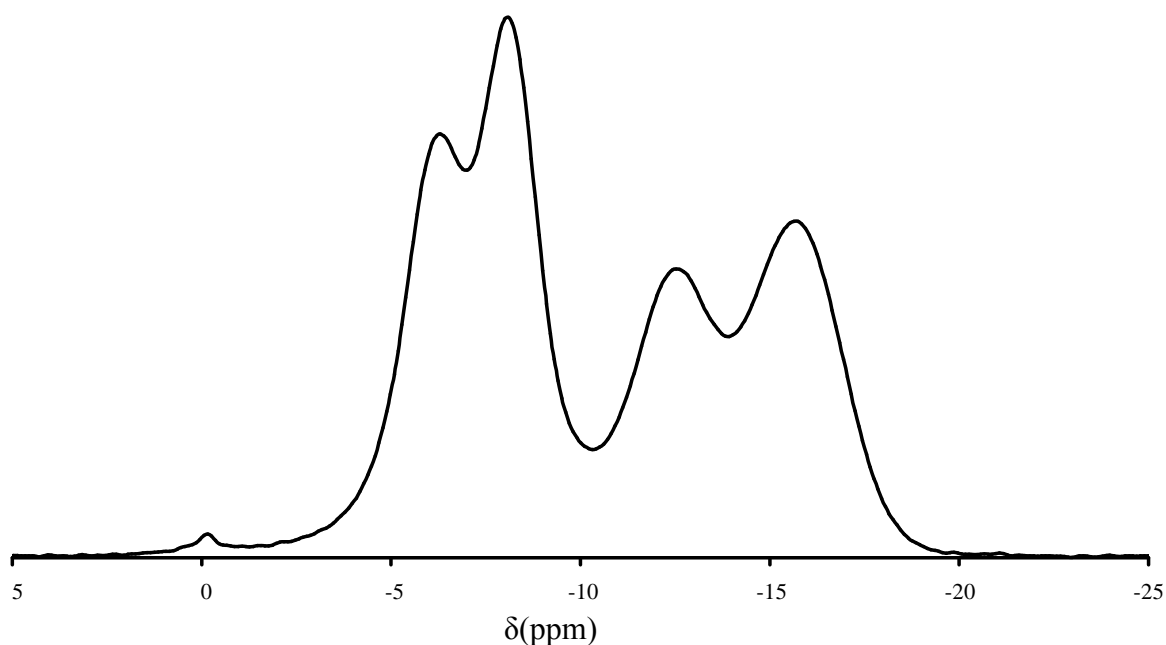


Figure 3.18: ^{31}P DP MAS NMR spectra for structure **3**, showing four peaks at -6.3, -8.2, -12.7 and -15.7 ppm.

Closer inspection of the structure indicated high thermal parameters associated with P(3) and O(9) and O(10), and improved refinement of the single crystal data was obtained by considering the structure to contain ScO_4F_2 octahedra with two different orientations, or tilts, as shown in figure 3.19. The differently tilted octahedra, which are associated with different positions of the attached phosphate tetrahedra, are thought to be disordered within domains of crystals of structure **3**, and result in crystallographic nonequivalence of some phosphorus and oxygen atoms in the structure.

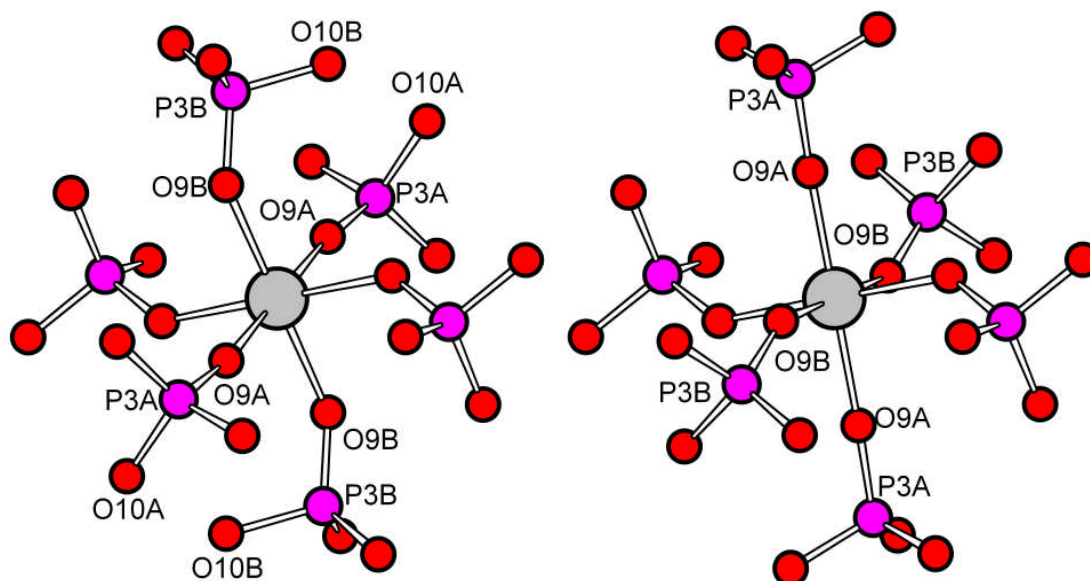


Figure 3.19: Projection down [001] of structure 3 showing both conformations which are possible due to tilts around P(3) and Sc(2).

^{45}Sc NMR shows a broad spectrum consistent with two broad overlapping peaks (most intense 8.3 ppm). ^{13}C MAS CP NMR shows two peaks at 42.19 and 25.7 ppm corresponding to the two chemically distinct carbon atoms in the template.

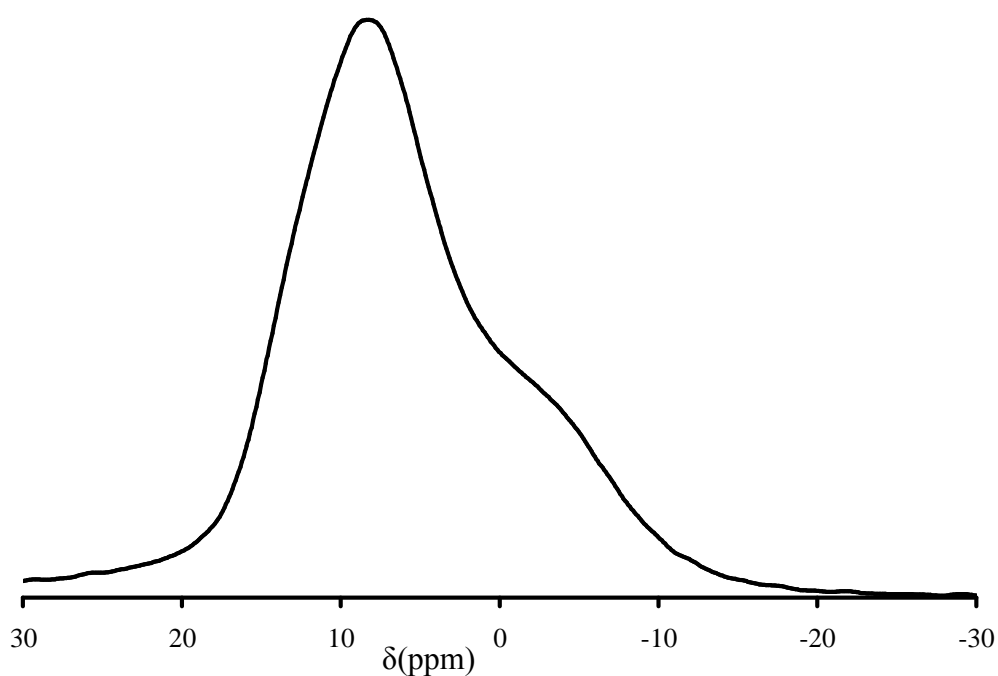


Figure 3.20: ^{45}Sc MAS NMR spectra for structure 3, showing a broad asymmetric peak with a maximum at 8.3 ppm.

The b.v.s. calculations were performed to locate protons on oxygen atoms of the framework. Oxygens O(2), O(3), O(6) and O(21), which do not bridge Sc and P, have b.v.s. values of 1.06, 1.24, 1.11 and 1.33, respectively. O(3) is close to O(6), 2.65 Å and is taken to hydrogen bond to it, sharing a proton. All the phosphate tetrahedra are therefore thought to be of the form PO₄H. In addition, O(21), which is 50% occupied, is taken to belong to protonated water molecules, giving the unit cell formula [(H₃NC₄H₈NH₃)₄(H₃O)₂][Sc₁₀F₈(HPO₄)₁₆]. CHN analysis, wt%, calculated: C, 7.57%; H, 3.10%; N, 4.42%; measured: C, 7.34%; H, 2.89%; N, 4.27%.

3.4.5 [C₆H₁₁NH₃][ScF(HPO₄)(H₂PO₄)] - Structure 4

Structure **4** was prepared using cyclohexylamine as the added primary amine from a synthesis gel including fluoride ions and illustrates how a primary amine can direct the scandium phosphate crystallisation. The crystals of structure **4**, [C₆H₁₁NH₃][ScF(HPO₄)(H₂PO₄)], were small and could not be analysed on a laboratory diffractometer, so data were collected on Station 9.8, at the Daresbury synchrotron radiation facility. Structure **4** was solved by direct methods and Fourier syntheses, using the SHELXS program⁸¹. The crystallographic information is outlined in table 3.3 and the atomic co-ordinates for structure **4** are listed in table 3.11.

Table 3.11: Atomic co-ordinates for structure **4**

Atom	x	y	z	Occ	U _{iso}	Multiplicity
Sc1	0.02949(7)	0.35299(5)	0.25069(3)	1	0.0103(2)	8
P1	-0.22303(11)	0.36279(7)	0.35344(3)	1	0.0103(2)	8
P2	-0.00873(11)	0.59963(7)	0.20448(3)	1	0.0129(2)	8
F1	-0.2199(2)	0.35460(15)	0.22389(6)	1	0.0123(4)	8
O1	-0.0723(3)	0.39583(19)	0.32052(9)	1	0.0137(6)	8
O2	-0.1646(3)	0.27816(18)	0.39219(8)	1	0.0135(6)	8
O3	-0.3761(3)	0.32020(18)	0.32270(8)	1	0.0121(6)	8
O4	-0.2838(3)	0.45325(19)	0.38850(8)	1	0.0164(6)	8
O5	0.0719(3)	0.5108(2)	0.23467(8)	1	0.0133(5)	8
O6	0.0035(3)	0.7001(2)	0.23492(9)	1	0.0177(7)	8
O7	0.0684(3)	0.60835(19)	0.15195(8)	1	0.0153(6)	8
O8	-0.2090(3)	0.57302(19)	0.19589(9)	1	0.0191(7)	8
N1	0.0018(4)	0.6280(2)	0.36069(11)	1	0.0173(8)	8
C1	0.0670(4)	0.6373(3)	0.41454(14)	1	0.0202(10)	8
C2	0.1591(5)	0.5360(3)	0.42913(14)	1	0.0278(11)	8
C3	0.2379(5)	0.5435(4)	0.48174(15)	1	0.0299(12)	8
C4	0.3633(5)	0.6339(3)	0.48513(14)	1	0.0271(11)	8
C5	0.2755(5)	0.7355(3)	0.47054(13)	1	0.0266(11)	8
C6	0.1924(5)	0.7307(3)	0.41740(14)	1	0.0235(10)	8

Elemental analyses indicate a C:N ratio of 6:1, confirming that the amine is included intact into the layered scandium phosphate. Fluoride was identified as a constituent of the structure from EDX analysis and atoms linking the chain of scandium atoms were attributed as fluorine on the basis of their temperature factors. The b.v.s. calculations suggest that protons are associated with oxygens O(2) and O(4) on P(1) phosphate tetrahedra (b.v.s. 1.17 and 1.18), and with O(8) on P(2) phosphate tetrahedra (b.v.s. 1.08), giving the formula $[\text{C}_6\text{H}_{11}\text{NH}_3][\text{ScF}(\text{HPO}_4)(\text{H}_2\text{PO}_4)]$.

In addition to structure **4**, the sample was also found to contain the known phase $\text{ScPO}_4 \cdot 2\text{H}_2\text{O}$, kolbeckite is the equivalent mineral, by analysis of the ^{45}Sc and ^{31}P MAS NMR, and X-ray powder diffraction pattern. $\text{ScPO}_4 \cdot 2\text{H}_2\text{O}$, is discussed later in this chapter. Attempts were made in order to synthesise a phase pure sample of structure **4**, but were unsuccessful. The stoichiometry reported in table 3.1 proved to be the most successful preparation in yielding the highest amount of structure **4** within the product. Rietveld refinement of powder x-ray diffraction data, for this sample, performed with the GSAS program suite and using the atomic co-ordinates determined by single crystal structure

solution from both structure **4** and the $\text{ScPO}_4 \cdot 2\text{H}_2\text{O}$ impurity⁴⁴ as a starting point in order to determine the amount of impurity present. Instrumental parameters (background, zero-point, peak profile coefficients) and structural parameters (unit cell, atomic co-ordinates, phase fractions, thermal parameters) were refined, keeping constraints on the bond distances and angles. A close final fit to the observed data was achieved, ($R_{\text{wp}} = 9.2\%$), with the structure determined from the single crystal experiment (figure 3.21). Structure **4** and $\text{ScPO}_4 \cdot 2\text{H}_2\text{O}$ were found to be present in a 2:1 ratio. The atomic co-ordinates obtained from the refined data have positions very close to the values determined from the single crystal experiment.

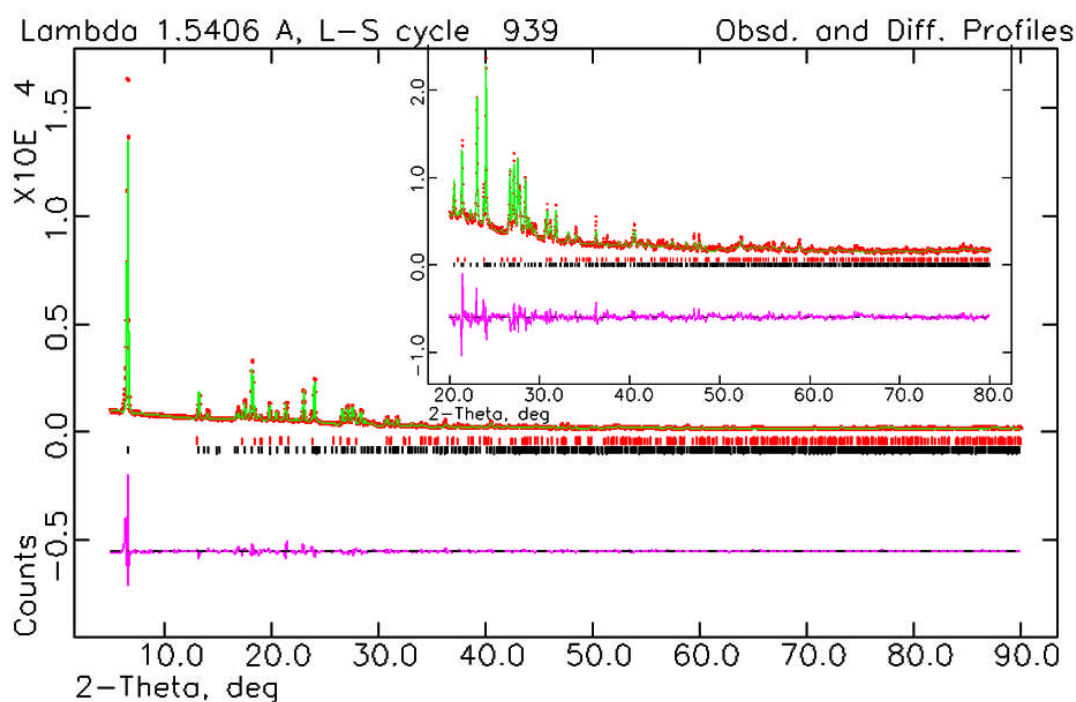


Figure 3.21: Rietveld refinement of structure **4**, $[\text{C}_6\text{H}_{11}\text{NH}_3][\text{ScF}(\text{HPO}_4)(\text{H}_2\text{PO}_4)]$, and kolbeckite, $\text{ScPO}_4 \cdot 2\text{H}_2\text{O}$. Final refinement gives an $R_{\text{wp}} = 9.2\%$, with structure **4** and kolbeckite found to be present in a 2: 1 ratio.

Structure **4** is a layered structure. Each layer is built from corner-sharing chains of ScO_4F_2 octahedra (the shared corners being the trans-fluoride ion) running parallel to the a -axis, shown in figure 3.22. Adjacent chains are linked along b by phosphate tetrahedra, the remaining 2 oxygens of the phosphate group projecting into the interlayer space.

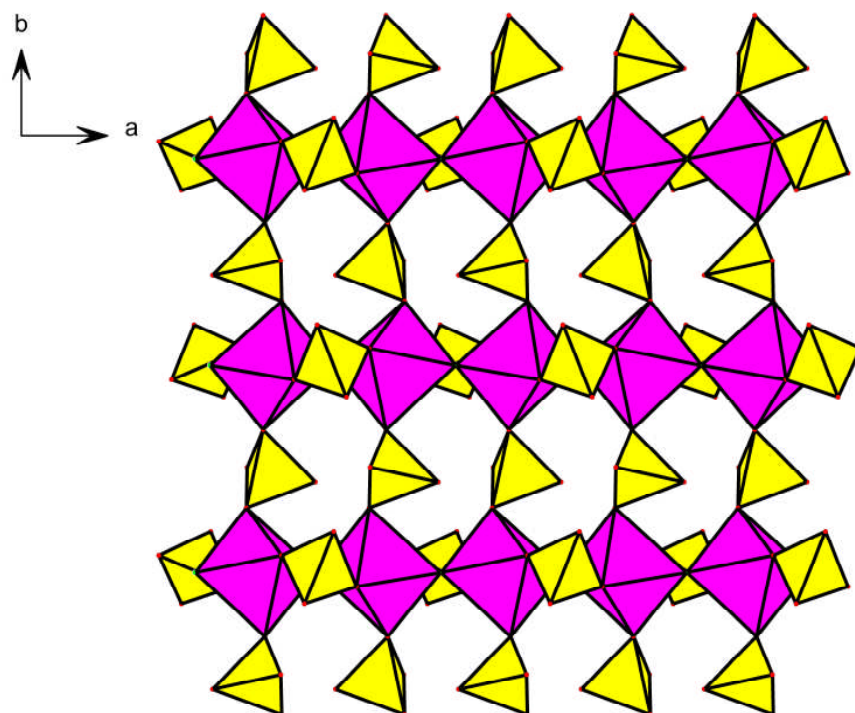


Figure 3.22: Projection down $[001]$ of structure 4, showing ScO_4F_2 octahedra forming chains, which are joined together by phosphate tetrahedra to form layers. Corner-sharing ScO_4F_2 octahedra are linked together via fluorine atoms.

In addition, adjacent ScO_4F_2 octahedra along the chain are bridged by phosphate tetrahedra by sharing fluorine atoms. This results in undulating chains of ScO_4F_2 octahedra. The remaining two unbound oxygens of these intrachain phosphate groups also project into the interlayer space.

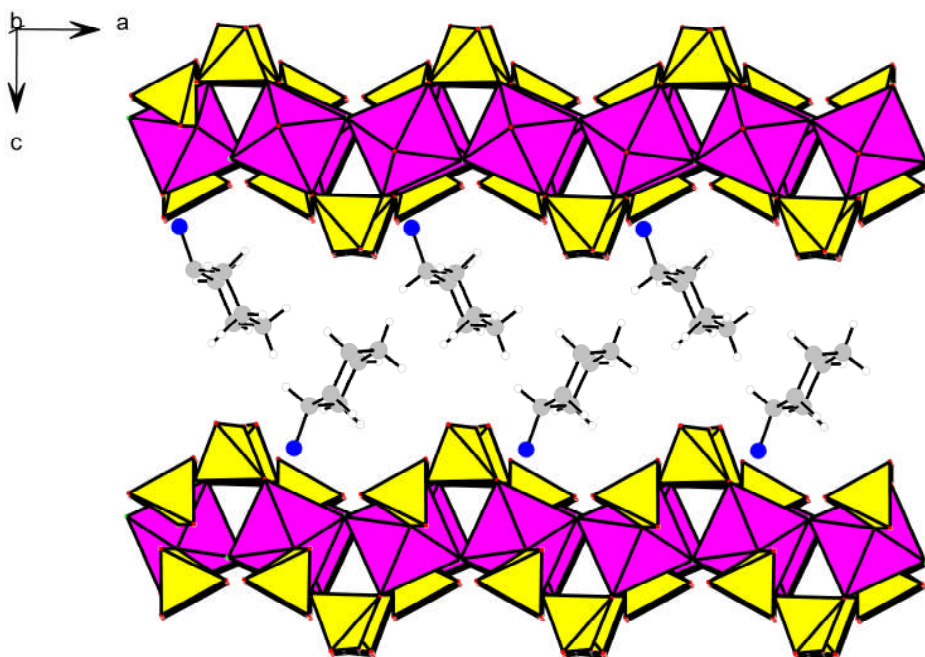


Figure 3.23: Projection down [010] of structure 4 showing undulating layers perpendicular to the *c*-axis separated by cyclohexylamine molecules. Symmetry related positions for statically disordered cyclohexylamine molecules have been omitted for clarity.

The cyclohexylamine molecules link via the protonated amine groups to the negatively charged layers. The cyclohexyl groups are in the chair configuration, with the amine groups in equatorial positions: amine groups from adjacent layers project into the interlayer space, figures 3.23 and 3.24. Hydrogen atoms were located and assigned through a combination of Fourier mapping and charge balancing.

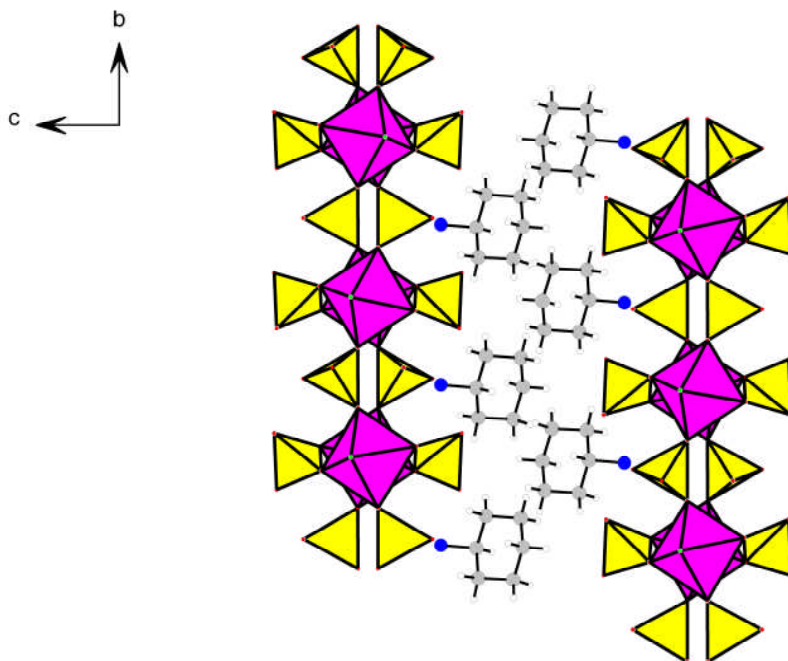


Figure 3.24: Projection down [100] of structure **4**, showing chains of ScO_4F_2 octahedra joined together by phosphate tetrahedral to form a sheet-like structure separated by cyclohexylamine molecules.

Solid-state ^{31}P NMR of the structure **4** and $\text{ScPO}_4 \cdot 2\text{H}_2\text{O}$ mixture, figure 3.26, shows three peaks, at -2.5, -15.4 and -18.6 ppm. The peak at -18.6 ppm can be attributed to the $\text{ScPO}_4 \cdot 2\text{H}_2\text{O}$ impurity so that those at -2.5 ppm and -15.4 ppm are attributed to the PO_4H_2 and PO_4H groups. ^{45}Sc NMR, figure 3.27, gives two peaks with characteristic quadrupolar line shapes, distributed around chemical shift values of 23.8 and -15.5 ppm. The first of these is from the $\text{ScPO}_4 \cdot 2\text{H}_2\text{O}$ impurity.

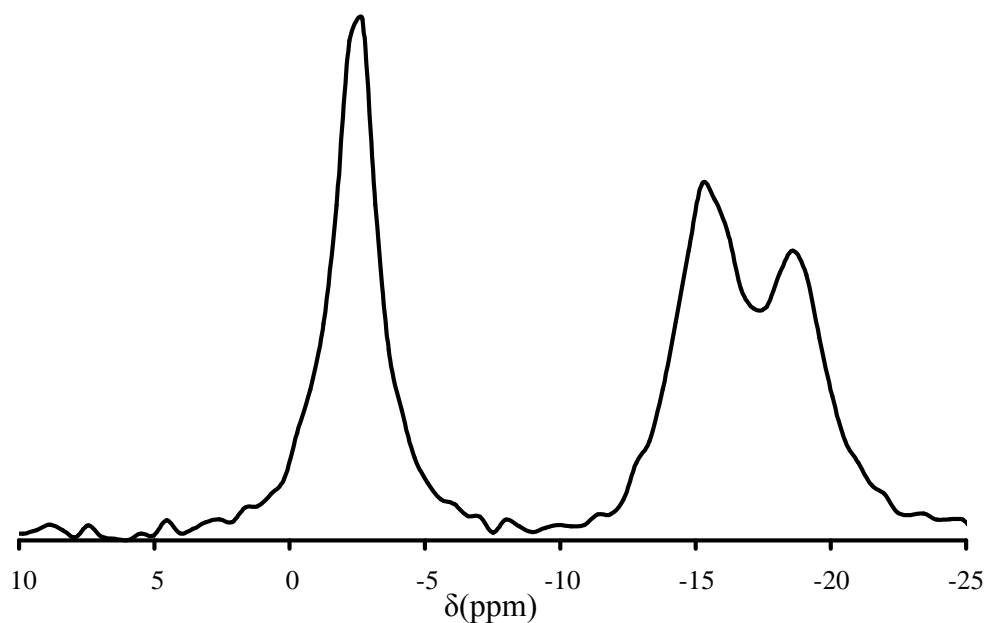


Figure 3.26: ^{31}P DP MAS NMR spectra for structure **4** showing peaks at 2.5 and -15.4 ppm which can be attributed to the two phosphorus environments found in structure **4**. The resonance observed at -18.6 ppm matches with that of the ^{31}P DP MAS NMR spectra for $\text{ScPO}_4 \cdot 2\text{H}_2\text{O}$ (figure 3.31) and is therefore attributed to the impurity phase present within the sample.

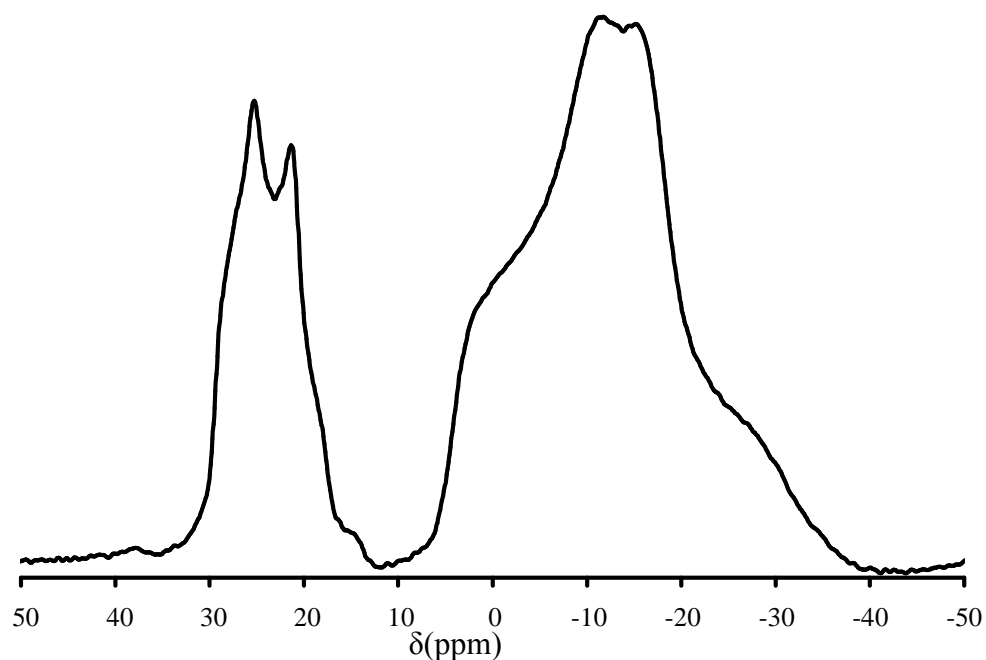


Figure 3.27: ^{45}Sc MAS NMR spectra for structure **4**, showing peaks at -15.5 and 23.8 ppm which can be attributed to scandium sites within structure **4** and the $\text{ScPO}_4 \cdot 2\text{H}_2\text{O}$ impurity respectively. Figure 3.32 shows the ^{45}Sc MAS NMR for $\text{ScPO}_4 \cdot 2\text{H}_2\text{O}$ for comparison.

In addition to the amines used in structures **1** – **4**, numerous experiments were carried out in order to investigate the structure directing effects of different known structure directing agents, SDAs, within scandium phosphate materials. When examining products obtained from using many of the SDAs shown in figure 3.3, two denser scandium phosphate phases were frequently observed (**5** and **6**). Many of the larger primary amines, all of the secondary and tertiary amines and alkali metal hydroxides yielded either structure **5** or structure **6**.

Structure **5** has been obtained during the synthesis and search for novel scandium phosphate materials. The addition to the reaction of secondary and tertiary amines or alkylammonium salts have resulted in the formation of structure **5**. This may be due to the lack of groups available in order to form strong hydrogen bonds and consequently stabilise the material. H-bond is prevalent in scandium phosphate materials.^{40-42, 44-46}

Some of the larger primary amines, in highly acidic conditions, as well as lithium hydroxide, yielded structure **6**. This is probably owing to the amine decomposing in the reaction solution, producing ammonium which readily directs crystallization.

3.4.6 Sc(PO₄).2H₂O – Structure **5** ‘Kolbeckite’

Single crystal x-ray diffraction data was not collected for structure **5**, as no suitable crystals were obtained. Powder x-ray diffraction data was collected on the in-house diffractometer, and this data was used in a Rietveld refinement, performed with the GSAS program suite using the atomic co-ordinates published by Bull *et al*,⁴⁴ which were determined from the single crystal structure solution from data collected at the synchrotron radiation source at Daresbury laboratories. Instrumental parameters (background, zero-point, peak profile coefficients) and structural parameters (unit cell, atomic co-ordinates, thermal parameters) were refined, with no constraints on the bond distances or angles. A close final fit to the observed data was achieved, ($R_{wp} = 4.3\%$, figure 3.28). The refined atomic co-ordinates generated by GSAS were found to be very close to the values published by Bull *et al*⁴⁴, determined from the single crystal experiment, suggesting that the sample has been synthesised as a pure phase. The atomic co-ordinates generated by GSAS are listed in table 3.12.

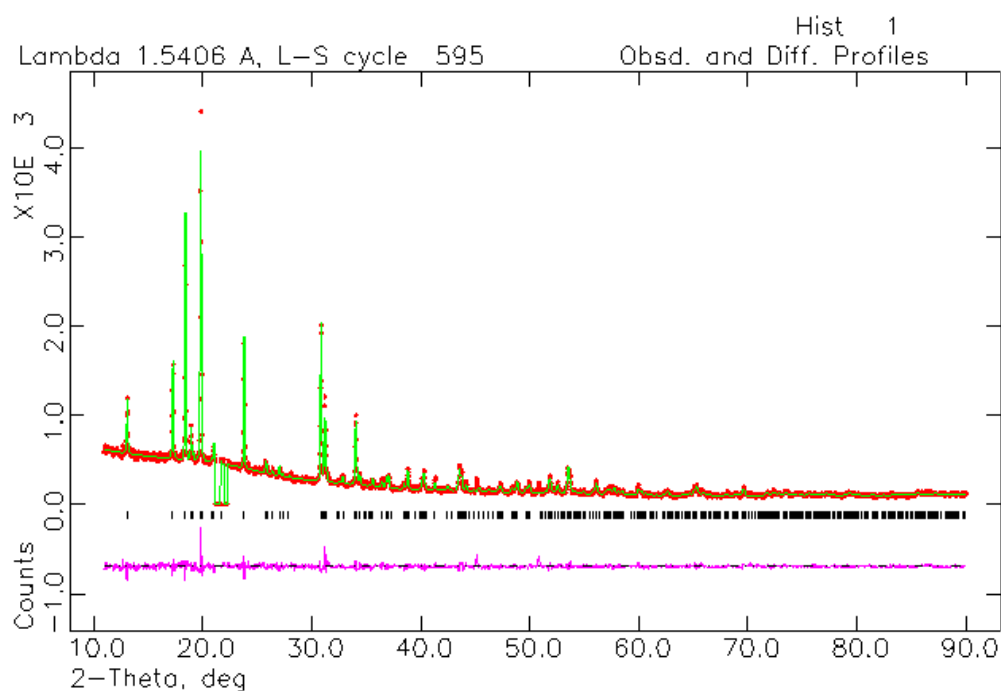


Figure 3.28: Powder diffraction pattern for structure **5**, $\text{Sc}(\text{PO}_4)\cdot 2\text{H}_2\text{O}$, refined against atomic co-ordinates reported by Bull *et al*⁴⁴.

Table 3.12: Atomic co-ordinates generated by GSAS for structure **5**.

Atom	x	y	z	U_{iso}	Occ	Multiplicity
Sc	0.0934(8)	0.3369(5)	0.2072(5)	0.0201	1	4
P	0.0831(11)	0.3421(7)	-0.1893(7)	0.0201	1	4
O1	0.4033(21)	0.4688(12)	0.2073(12)	0.0201	1	4
O2	0.1037(20)	0.4983(12)	-0.1876(12)	0.0201	1	4
O3	0.1035(19)	0.295(1)	-0.0313(13)	0.0201	1	4
O4	-0.1771(20)	0.3085(12)	-0.2478(13)	0.0201	1	4
O5	0.2931(21)	0.2868(11)	-0.2716(14)	0.0201	1	4
O6	0.0835(18)	0.3616(10)	0.4497(12)	0.0201	1	4

In structure **5**, $\text{Sc}(\text{PO}_4)\cdot 2\text{H}_2\text{O}$, the scandium-to-phosphorus ratio is 1:1, with a strict alternation between scandium octahedra and phosphate tetrahedra in the framework. Structure **5** is isostructural with a scandium phosphate mineral, kolbeckite, also known as eggonite or sterrettite⁹² and an indium phosphate material reported by Sugiyama *et al.*^{93, 94}

Structure **5** is a 3-dimensional framework structure with small channels present in all directions throughout the structure, figure 3.29 shows 8-membered ring channels along [100].

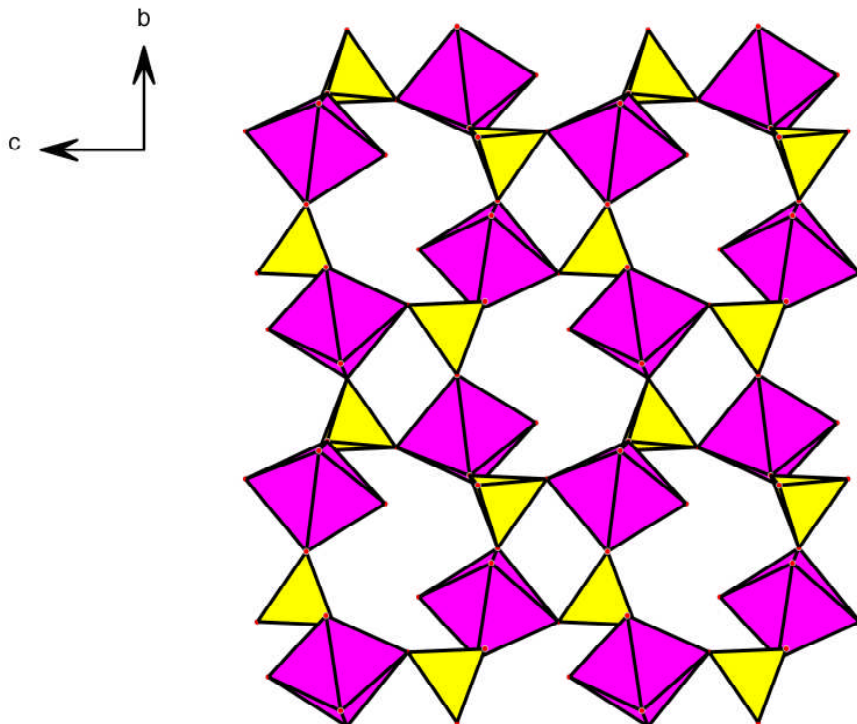


Figure 3.29: Projection along $[100]$ of structure **5**, showing oxygen atoms of the scandium octahedra within the 8 membered ring channel, which are assigned as water molecules.

The framework can be described as consisting of layers of ScO_6 octahedra joined together by three apices of a phosphate tetrahedra, with the fourth apex connecting to another layer, shown in figure 3.30. The phosphate tetrahedra point in alternative directions, so that every neighboring tetrahedra is connected to a different layer, enabling the layers to be fully connected.

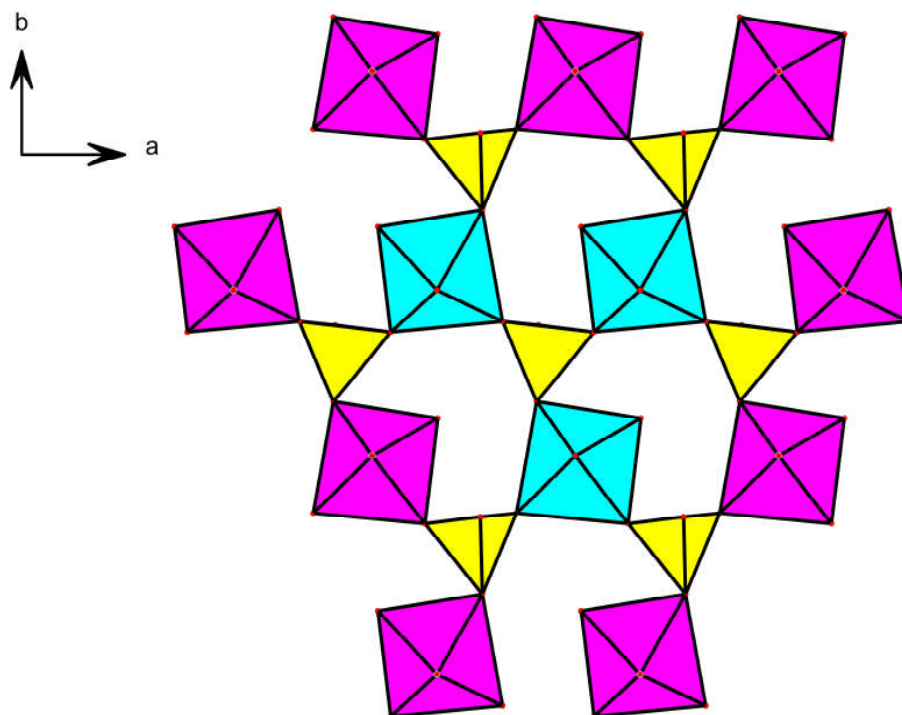


Figure 3.30: Projection along [001] showing part of a single layer of structure 5, illustrating how the phosphate tetrahedra connect to three scandium atoms within the same layer, and then alternate between the above and below layer, giving a fully connected framework.

Scandium is octahedrally coordinated to four framework oxygens and two water molecules. The inter-atomic distances are similar to those found in other scandium phosphate based materials, with Sc-OH₂ bond distances being longer in comparison at 2.163 – 2.185 Å.

Solid-state ³¹P DP MAS NMR (Figure 3.31) gives a single peak at -18.6 ppm, in concurrence with the impurity noted in the discussion of structure 4. ⁴⁵Sc NMR (Figure 3.32) gives a single peak at 23.8 ppm.

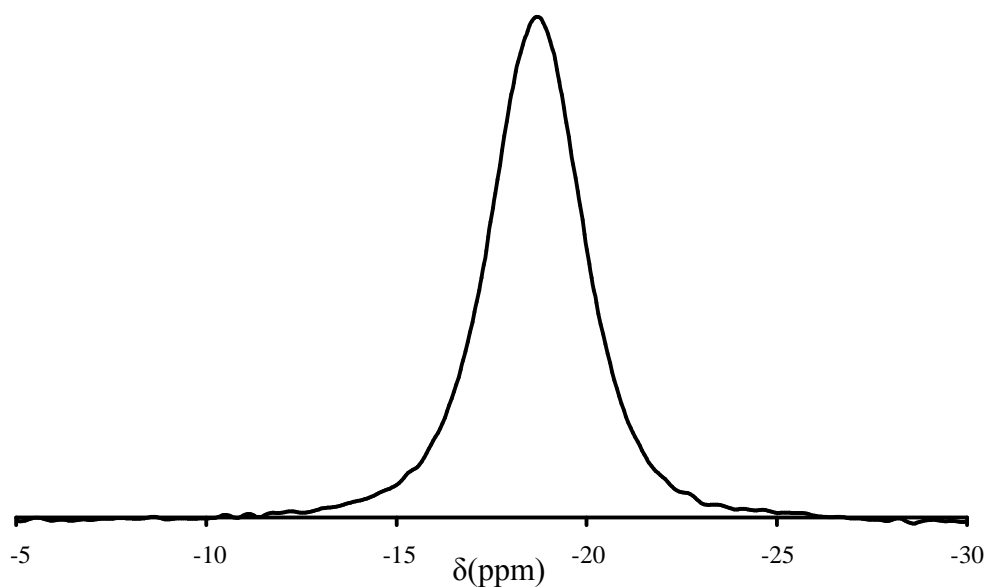


Figure 3.31: ^{31}P DP MAS NMR of structure 5 showing a single peak with a chemical shift of -18.6ppm.

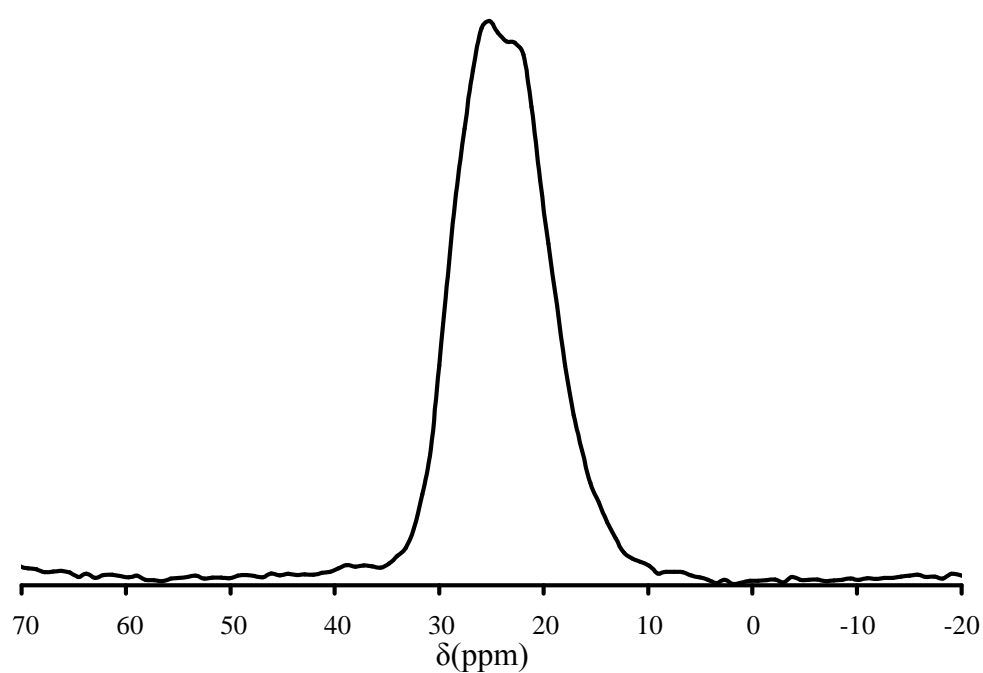


Figure 3.32: ^{45}Sc MAS NMR spectra of structure 5, showing one broad resonance at 23.8ppm

TGA shows a weight loss in a single step of 20% between 210 and 260°C (theoretical loss from dehydration, 20.6%) with associated loss of crystallinity.

3.4.7 (NH₄)₂Sc₂(HPO₄)(PO₄)₂ – Structure 6

Structure 6, (NH₄)₂Sc₂(HPO₄)(PO₄)₂, was solved from laboratory single crystal X-ray data by direct methods and Fourier syntheses, using the SHELXS program.⁸¹ The crystallographic information is outlined in table 3.3. The atomic co-ordinates for structure 6 are listed below in table 3.13.

Table 3.13: Atomic co-ordinates for structure 6.

Atom	x	y	z	Occ	U _{iso}	Multiplicity
Sc(1)	0.66322(11)	0.8367(1)	0.1632(1)	1	0.0104(6)	4
Sc(2)	0.10414(12)	0.8958(2)	0.3958(2)	1	0.0185(7)	4
P(1)	0.37566(17)	0.0167(5)	0.2102(5)	1	0.0129(6)	12
O(1)	0.4989(5)	0.9377(5)	0.2340(6)	1	0.0224(11)	12
O(2)	0.2703(5)	0.9556(6)	0.3012(6)	1	0.0303(14)	12
O(3)	0.4017(5)	0.1616(5)	0.2515(5)	1	0.0237(12)	12
O(4)	0.3299(5)	0.0089(5)	0.0670(5)	1	0.0236(12)	12
N(1)	0.3180(6)	0.682(6)	0.1820(3)	1	0.019(2)	4
N(2)	0.9568(8)	0.5432(8)	0.4568(8)	1	0.034(3)	4

Elemental analysis on the ‘as-prepared’ sample, wt%, calculated: H, 1.98%; N, 6.92%; measured: H, 2.43%; N, 6.70%.

Structure 6 is an ammonium scandium phosphate, which crystallises in the langbeinite structure type.^{95, 96} In typical langbeinite and langbeinite-type structures,⁹⁷⁻¹⁰³ the anionic framework (normally consisting of M²⁺) is charge-balanced with 2 singular cationic charges, e.g. an alkali metal or ammonium molecules or one 2+ charge (e.g. Be²⁺), giving the general formula A_xM_z(XO₄)₃. There are relatively few phosphate derivatives of the langbeinite type structure in the literature^{97, 98, 100-106} owing to the fact that most A_xM_z(XO₄)₃ compounds tend to crystallise in the closely related NASICON¹⁰⁷⁻¹¹⁹ structure type. The anionic structure can be described as being comprised of inter-connected ScO₆ octahedra and PO₄ tetrahedra, forming a three dimensional network.

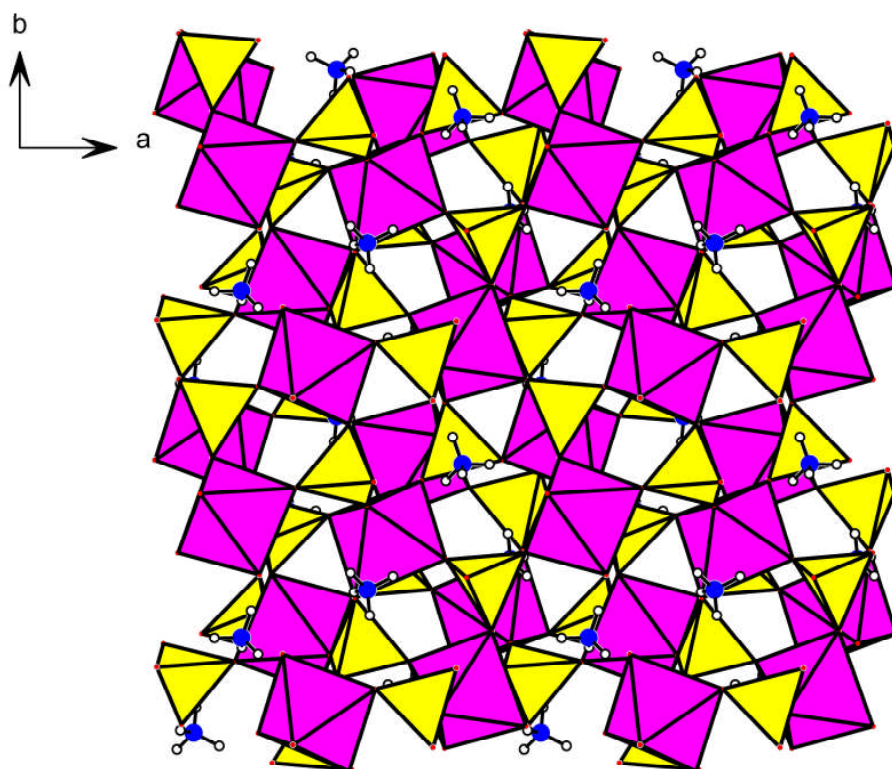


Figure 3.34: Structure 6 viewed along [001], showing a dense scandium phosphate material templated using ammonium molecules.

The framework of langbeinite-type structures can be described using different building units as visual aids. The first method used for describing the framework of this complex structure is based on $[M_2X_3O_{18}]$.

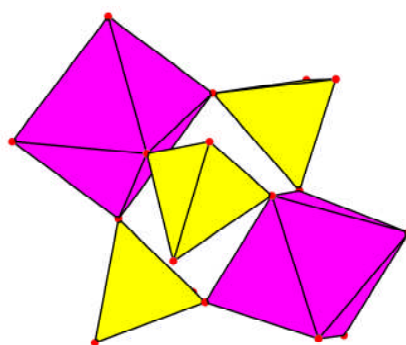


Figure 3.35: $[M_2X_3O_{18}]$ building units which are classically used in order to describe the langbeinite structure. Each building unit of this sort is surrounded by 12 neighbouring building units, making the complex cage system and structure.

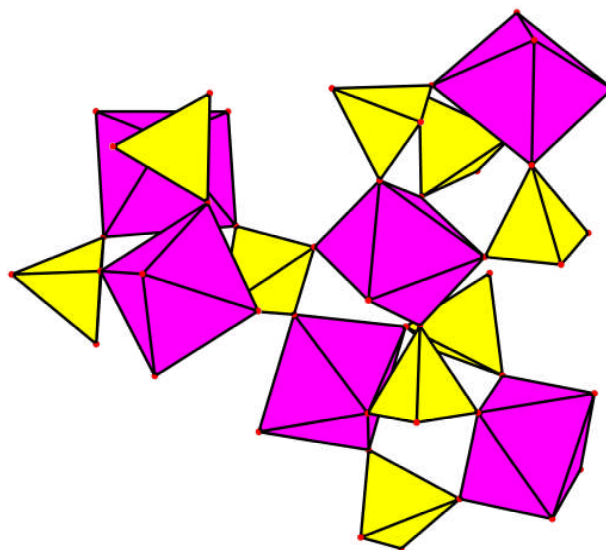


Figure 3.36: Representation of how three of the $[M_2X_3O_{18}]$ building units join together.

Norberg¹⁰⁴ proposed that the stacking of these $[M_2X_3O_{18}]$ building units was not the simplest way in which to describe the structures owing to the complexity of the framework and the stacking of the units. This led to postulation of an alternative, larger, building unit $[M_5X_6O_{39}]$, enabling the channels and cages formed with langbeinite frameworks to be more readily visualised.

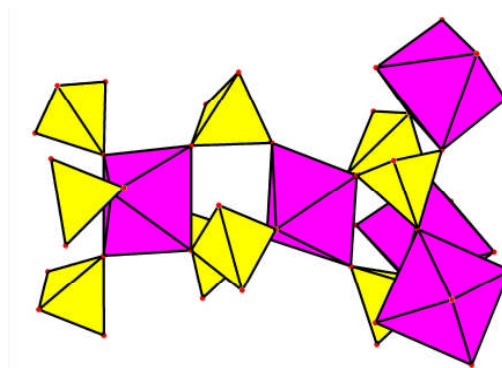


Figure 3.37: $[M_5X_6O_{39}]$ building units

Unlike other langbeinite type structures, the anionic framework of structure **6** imparts an overall negative charge on the crystal system which cannot be balanced by the ammonium cations. Like other langbeinite structures, structure **6** has two crystallographically unique sites which can accommodate charge balancing cations. Elemental analysis and EDX spectroscopy confirm the presence of nitrogen suggesting the presence of ammonium and the absence of any other potential charge balancing cations.

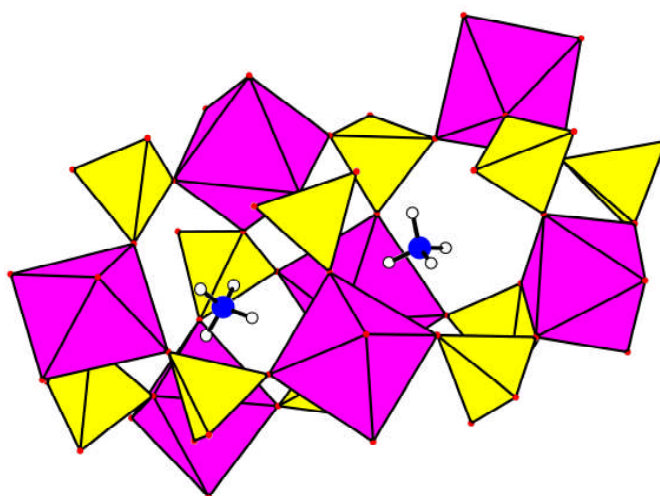


Figure 3.38: Cages within structure 5 which cause the ammonium cations to be isolated.

This is the first example of a langbeinite in which the framework metal element is completely trivalent. The normal composition of a langbeinite material is $A_2M_2(XO_4)_3$, where A is a charge balancing cation (i.e. NH_4^+ or K^+), M is a divalent metal, and (XO_4) is the anionic constituent of the framework (PO_4 or SO_4). Structures have been reported which contain a mixture of di- and trivalent metals in the framework sites. In these cases, the overall charge of the structure is normally balanced by the valence of the interstitial cation, e.g. Mg^{2+} with the charge associated with the anionic part of the framework, SO_4^{2-} or PO_4^{3-} .

As structure 6 consists of a singular trivalent metal, Sc^{3+} , and a single anionic constituent, PO_4^{3-} , the overall unbalanced charge, taking into account the ammonium molecules, is -1.

Examination of the residual electron density generated from the single crystal refinement suggests the possibility of a hydrogen atom present on any of the oxygens surrounding the phosphorus atom. Owing to the fact that all of the oxygen atoms present within the framework are bonded to both scandium and phosphorus, there is no possibility for a terminal P-OH group. It can therefore be envisaged that there are four hydrogen atoms disordered over all of the oxygen atoms present on three phosphate tetrahedra, i.e. four hydrogen atoms are disordered over twelve oxygen atoms. This information is supported by bond valence sum calculations, which shows little deviation from the appropriate bond valence sum values for each oxygen atom, table 3.13. Another crystallographic method used to determine whether it is likely for phosphate oxygens to be protonated is consideration of the P-O bond lengths. If the P-O bond length is close to 1.5 – 1.55 Å then the oxygen is normally considered not to be protonated, whereas if the bond length is closer to 1.6 Å, the phosphorus

has less of an electron-withdrawing effect on the oxygen, making the oxygen more susceptible to being protonated. The P-O bond lengths reported for structure **6**, listed in table 3.14, give no clear indication to the location of the proton.

Table 3.14: Bond valence sum values for structure **6**.

Atom	P-O bond length (Å)	BVS	Deviation (%)
O(1)	1.510	1.854	7
O(2)	1.548	1.724	14
O(3)	1.556	1.699	15
O(4)	1.533	1.752	12

In order to balance the charge of structure **6**, there must be one HPO₄ group present within the unit cell, giving a final structural formula of (NH₄)₂Sc₂(HPO₄)(PO₄)₂.

Whilst investigating structure **6**, its lithium scandium analogue was synthesised. The powder diffraction patterns of the lithium analogue, Li₂Sc₂(HPO₄)(PO₄)₂, and that of structure **6** are compared below in figure 3.39. Despite continual attempts, the lithium scandium langbeinite material has only been formed as a mixed phase, with the second phase being structure **7**.

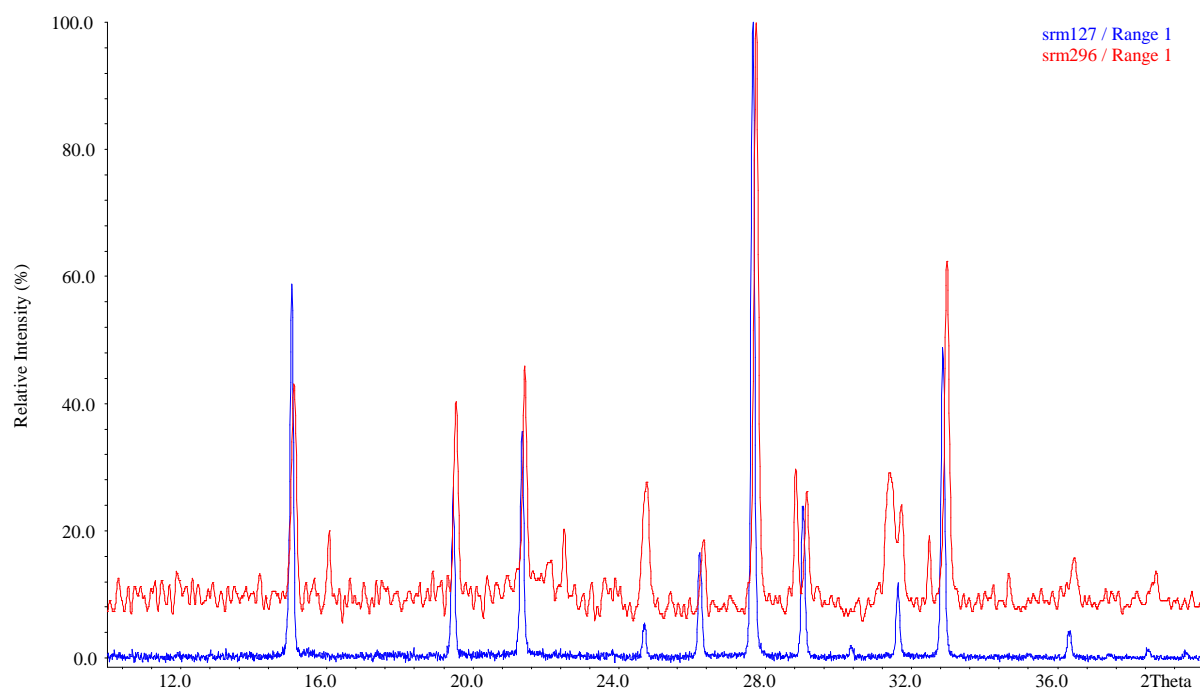


Figure 3.39: Powder diffraction patterns of structure **6** and its lithium scandium analogue.

Solid-state ^{31}P DP MAS NMR, figure 3.40, shows a single broad peak at -17.11ppm which can be attributed to the single phosphorus site located in the framework by crystallographic techniques. It is not possible to clearly resolve potential HPO_4 groups from PO_4 groups although there is a shoulder present on the peak. ^{45}Sc NMR, figure 3.41, shows 2 distinct peaks, at -1.67 and -20.94ppm, which might be attributed to the two crystallographically unique scandium present with the structure.

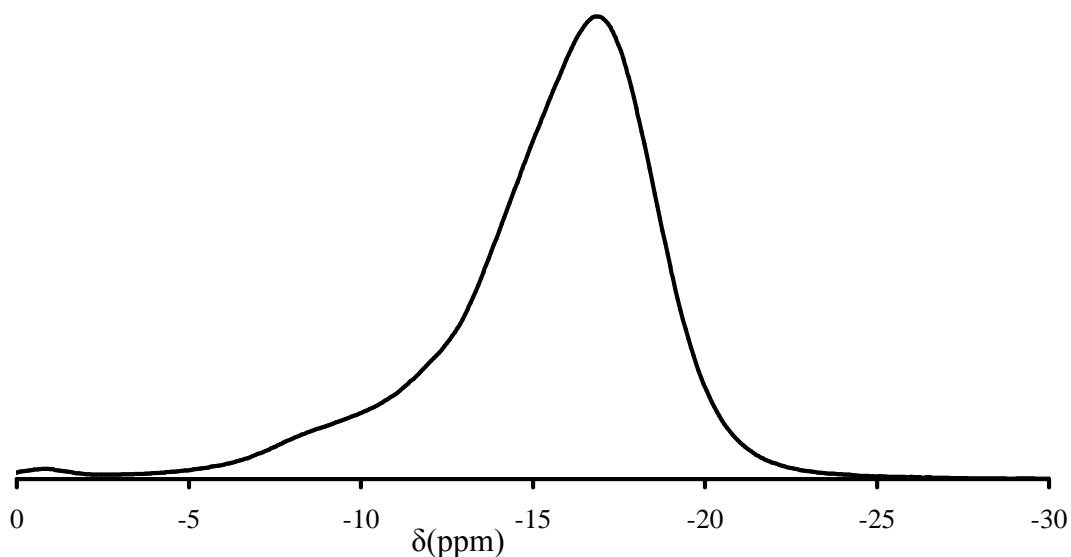


Figure 3.40: ^{31}P MAS NMR spectra of structure **6** showing a single broad resonance at -17.11ppm

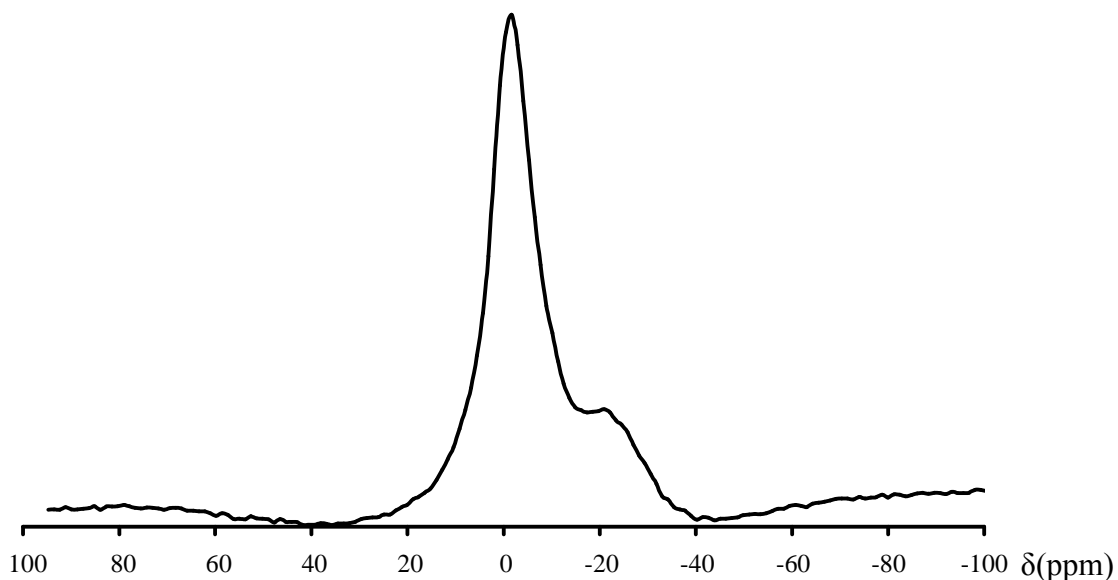


Figure 3.41: ^{45}Sc MAS NMR spectra for structure **6**, showing two independent resonances at -1.67 and -20.94ppm, which can be attributed to the two crystallographically unique scandium sites present within the structure.

Thermal analysis of structure **6** shows a weight loss occurring in a series of steps between 400°C and 900°C (figure 3.42). This is thought to be owing to the loss of ammonia from the cavities within the material (theoretical loss = 8.76%), followed by dehydration / dehydroxylation

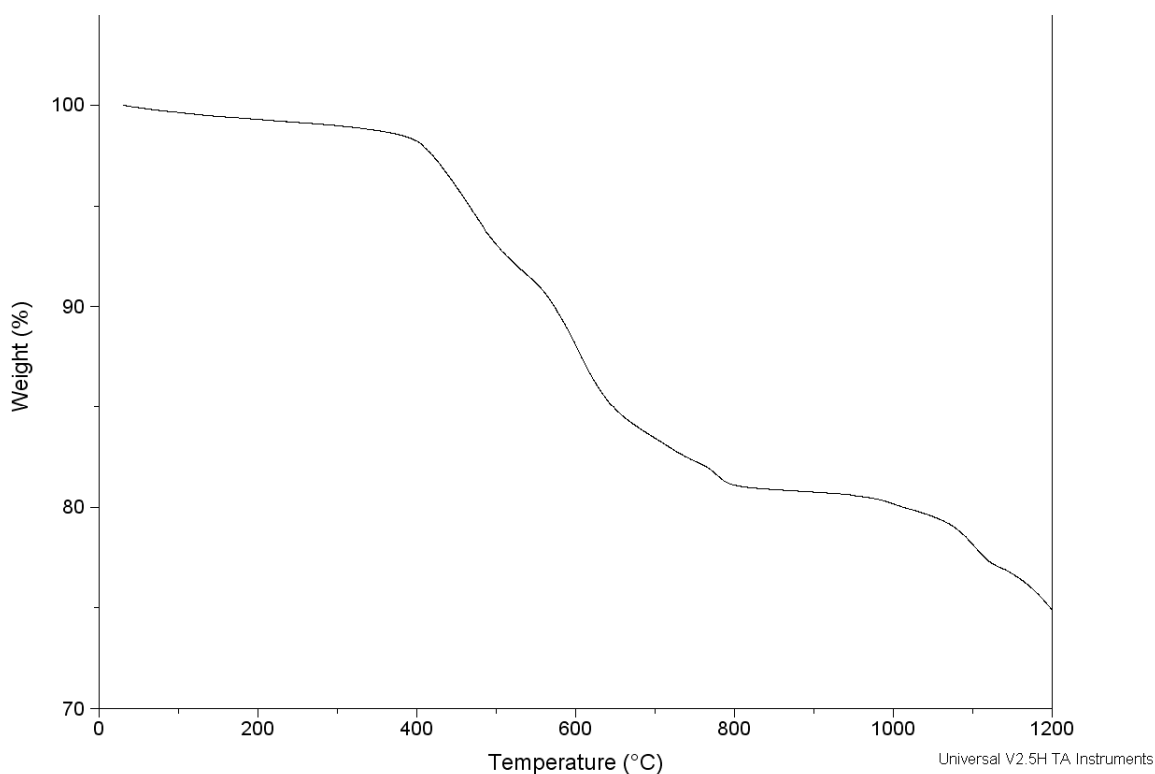


Figure 3.42: Thermogravimetric analysis of structure **6**, showing a multi stage weight loss between 400 and 900 °C, with additional weight loss at temperatures exceeding 1000°C.

Samples of ‘phase pure’ structure **6** have been heated at various temperatures under flowing nitrogen in order to investigate the materials thermal stability, and ultimately to find whether it is possible to remove the ammonium cations from within the cavities whilst maintaining the structural integrity of the material. Figure 3.43 shows the powder x-ray diffraction patterns of structure **6** heated at range of temperatures varying from 300 to 800°C. These correspond to the elemental analyses listed in table 3.15.

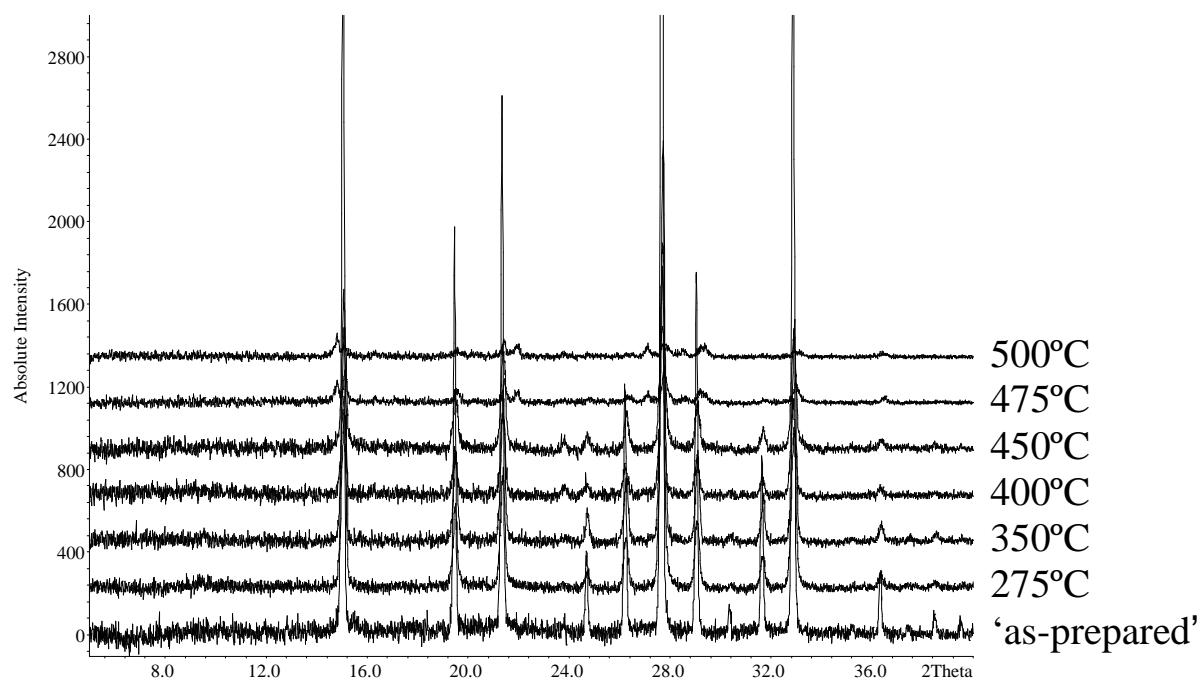


Figure 3.43: XRD patterns of structure **6** heated at a range of temperatures for 4 hours under flowing nitrogen.

Table 3.15: Nitrogen and hydrogen content of structure **6** after being heated under flowing nitrogen for 4 hours at temperatures from 275°C – 550°C.

Temperature	H%	N%
'as-prepared'	2.43	6.7
275	2.04	6.75
300	2.16	6.57
325	2.44	6.67
350	2.00	6.03
375	2.10	6.23
400	1.87	5.41
425	1.59	4.74
450	1.68	4.77
475	1.47	4.21
500	1.24	3.87
525	0.94	3.04
550	0.74	2.56

Although elemental analysis of structure **6** indicates that approximately 30% of the ammonium is removed after being heated at 450°C, XRD analysis indicates that some crystalline integrity remains. The integrity of the crystal structure remains until 475°C, at which point the structure begins to lose its crystallinity.

3.4.8 $\text{Li}_2\text{Sc}(\text{PO}_4)(\text{PO}_4\text{H})$ – Structure 7

Structure 7, $\text{Li}_2\text{Sc}(\text{PO}_4)(\text{PO}_4\text{H})$, was solved from laboratory single crystal X-ray data, by direct methods and Fourier syntheses, using the SHELXS program.⁸¹ The crystallographic information is outlined in table 3.2. and the atomic co-ordinates are listed in table 3.16.

Table 3.16: Atomic co-ordinates for structure 7

Atom	x	y	z	U_{iso}	Occ	Multiplicity
Sc(1)	0.5	0	0.5	0.0091(5)	1	2
P(1)	0.8622(2)	-0.15267(13)	0.22828(13)	0.0100(5)	1	4
O(1)	0.6391(6)	-0.1763(4)	0.3366(4)	0.0106(8)	1	4
O(2)	0.7361(6)	-0.0635(4)	0.0466(4)	0.0130(8)	1	4
O(3)	1.1006(6)	-0.0433(4)	0.3344(4)	0.0114(8)	1	4
O(4)	0.9837(7)	-0.3163(4)	0.1839(4)	0.0113(8)	1	4
Li(1)	0.3913(16)	-0.3656(10)	0.3426(10)	0.0192(18)	1	4

In structure 7, the scandium, phosphorus and oxygen atoms of the inorganic framework and the lithium atoms were readily located from direct methods using single crystal diffraction data. Structure 7 was obtained as a by-product whilst investigating the lithium analogue of structure 6. Structure 7 has not been obtained as a pure phase.

Structure 7 presents a 3 dimensional framework scandium phosphate structure, within which there are no Sc–O–Sc linkages, and therefore there is strict alternation between Sc and P in framework cation positions (figure 3.44).

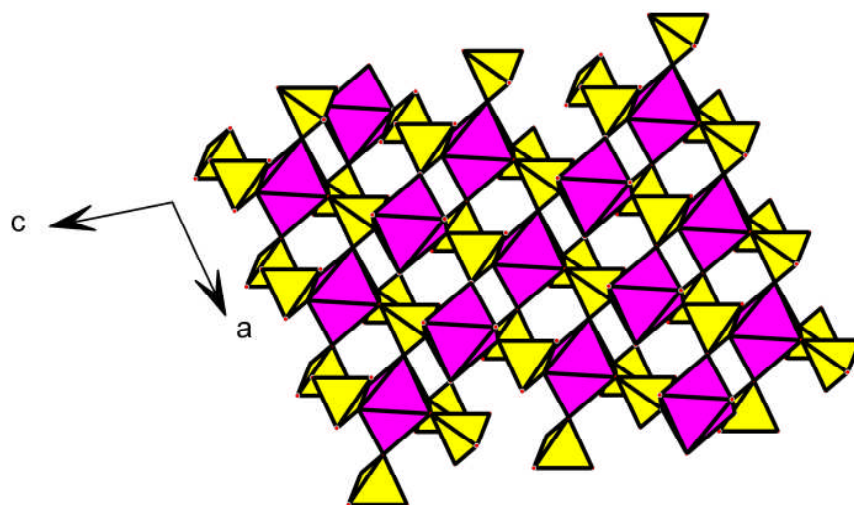


Figure 3.44: Projection down $[010]$ of structure 7 showing the scandium octahedra connected via phosphate tetrahedra

The phosphate tetrahedra share three common vertices with three ScO_6 octahedra, with the fourth P – O projecting into small channels which running parallel to the a -axis, figure 3.45.

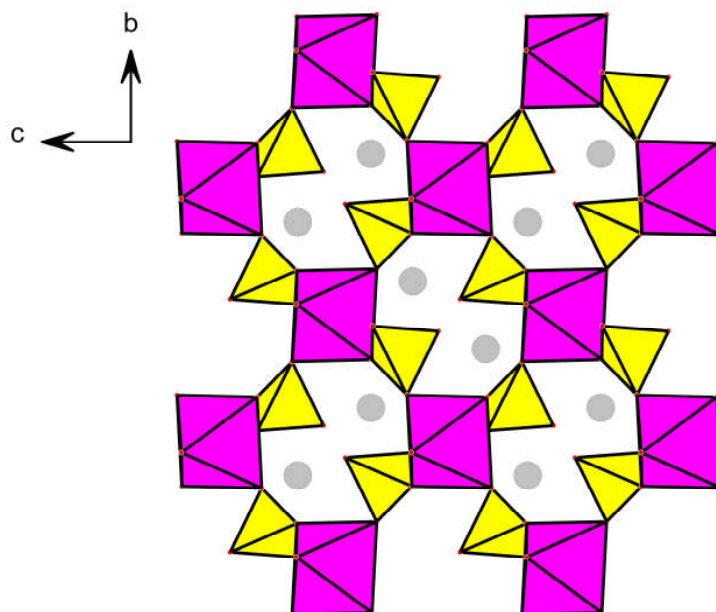


Figure 3.45: Structure 7 viewed down the $[100]$ axis, showing small channels which are occupied by lithium cations.

The lithium cations are located within the channels formed by the scandium and phosphate polyhedra. The lithium coordination is characterised by four short Li – O contacts, ranging from 1.974\AA to 2.081\AA , and one longer Li – O contact, 2.427\AA . The framework distances are as expected. Sc–O bond distances are from $2.071(3)$ to $2.129(4)\text{\AA}$ and P–O distances range from $1.527(3)$ to $1.533(3)\text{\AA}$, with one exception, P – O(4) being $1.557(2)\text{\AA}$ due to protonation of the oxygen. The distance between O(4) - O(4) is 3\AA . The only hydrogen atom assigned to structure 7, H(1), is partially occupied and shared between two oxygen atoms within the structure.

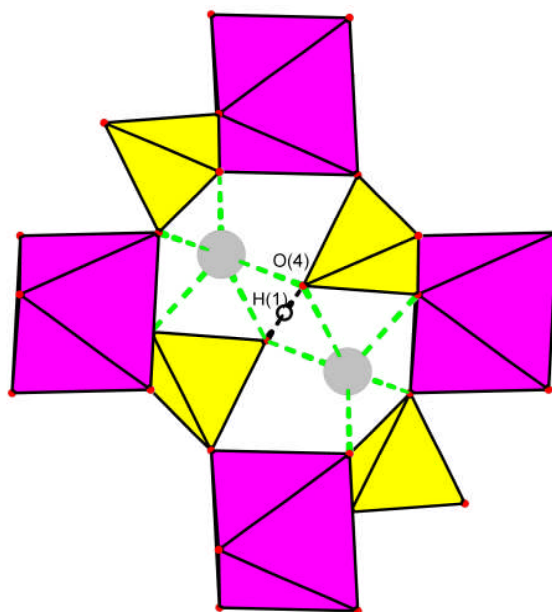


Figure 3.46: representation of the lithium environment within the channels of structure 7, also showing H(1), 50% occupied, being shared between two O(4) atoms.

Structure 7 is isostructural to an indium^{87, 88} and an iron(III) phosphate.^[80] The similarity in the ionic radii⁹¹ of these trivalent cations (Fe(III), 0.645Å ; Sc, 0.745Å ; In, 0.80Å) permit the same structure to crystallise.

3.5 Conclusions

The structure directing effects of various organic templates has been investigated whilst examining the hydrothermal chemistry of Sc^{3+} within phosphate materials. Products have been characterised by a multitude of techniques, including x-ray diffraction, thermal analysis and solid state NMR (^{45}Sc , ^{31}P and ^{13}C)

The stoichiometry of the gel is pivotal to the outcome of the reaction which is demonstrated by the formation of three different structures with the inclusion of ethylenediamine.^{41, 44, 45}

Since the publication of the first scandium phosphate-based materials in 2002 by Riou *et al*⁴⁵ and Bull *et al*⁴⁶, a further 10 novel scandium phosphate materials have been reported, four of these being from work described within this thesis.³⁹⁻⁴⁴ Table 3.17 lists the scandium phosphate based structures which can be found in the literature to date, as well as work discussed within this chapter which is yet to be published.

Table 3.16: List of scandium phosphate structures which have been published, highlighting the template within the structures

Structure	Organic Additive	Ref
$\text{Sc}(\text{HPO}_4)_2 \cdot 0.5(\text{N}_2\text{C}_2\text{H}_{10})$	ethylenediamine	45
$\text{Sc}_{56}(\text{SO}_4)_{98}(\text{PO}_4)_{22}[(\text{C}_8\text{N}_4\text{H}_{24})^{4+}]_{15} \cdot 34\text{H}^+ \cdot 57\text{H}_2\text{O}$	1,4,7,10 tetra-azacyclododecane	46
$(\text{C}_6\text{H}_{14}\text{N}_2)\text{Sc}_4\text{F}_2(\text{PO}_4)_4 \cdot 4\text{H}_2\text{O}$	1,4 diazabicyclo [2.2.2] octane	42
$(\text{C}_2\text{N}_2\text{H}_{10})_2\text{ScF}_6(\text{HPO}_4)_2$	ethylenediamine	39
$(\text{C}_2\text{N}_2\text{H}_{10})_8\text{Sc}_8(\text{ScO}_2)_4(\text{PO}_4)_4(\text{HPO}_4)_{12} \cdot 12\text{H}_2\text{O}$	ethylenediamine	44
$(\text{C}_2\text{N}_2\text{H}_{10})_2\text{Sc}_4(\text{HPO}_4)_8$	cyclam	44
$\text{Sc}_4(\text{HPO}_4)_8 \cdot 4(\text{H}_3\text{O})$	1,3-diaminopropane	44
$\text{Sc}(\text{PO}_4) \cdot 2\text{H}_2\text{O}$	pyridine	44
$\text{NaSc}(\text{HPO}_4)_2$	sodium borate	43
$[(\text{H}_3\text{NC}_2\text{H}_4\text{NH}_3)_3][\text{Sc}_3(\text{OH})_2(\text{PO}_4)_2(\text{HPO}_4)_3(\text{H}_2\text{PO}_4)]$	ethylenediamine	Structure 1, ⁴⁰
$[(\text{H}_3\text{NC}_4\text{H}_8\text{NH}_3)_3\text{Sc}(\text{OH}_2)]_6\text{Sc}_2(\text{HPO}_4)_{12}(\text{PO}_4)_2]$	1,4-diaminobutane	Structure 2, ⁴⁰
$[(\text{H}_3\text{NC}_4\text{H}_8\text{NH}_3)_2(\text{H}_3\text{O})][\text{Sc}_5\text{F}_4(\text{HPO}_4)_8]$	1,4-diaminobutane	Structure 3, ⁴⁰
$[\text{C}_6\text{H}_{11}\text{NH}_3][\text{ScF}(\text{HPO}_4)(\text{H}_2\text{PO}_4)]$	Cyclohexylamine	Structure 4, ⁴⁰
$(\text{NH}_4)_2\text{Sc}_2(\text{HPO}_4)(\text{PO}_4)_2$	1,4-diaminobutane	Structure 6

Within the structures reported in this chapter, scandium has been observed in a variety of environments, including isolated octaheda, $\text{Sc}_3(\text{OH})_2$ trimeric units, ScO_4F_2 chains and $\text{Sc}_4\text{O}_{16}\text{F}_4$ tetramers. Such geometries, or combinations of them, can be connected by one, two, three or four phosphate groups, forming chains, layers and framework materials. The solid state NMR of scandium for these samples show a range of typical quadrupolar peak shapes, and is discussed in more detail in chapter 7. Overlap between the resonances from crystallographically different sites make full line shape analysis difficult and would require further two-dimensional studies in order to assign the peaks to the different scandium environments (ScO_6 , ScO_5OH , ScO_4F_2 , $\text{Sc}(\text{OH})_2\text{O}_4$, etc.). The ScO_6 or ScO_4F_2 octaheda can be thought of as being linked via phosphate groups to give secondary building units, (SBUs) within the structures. Key SBUs within the phosphate structures reported in this chapter are shown in figure 3.47.

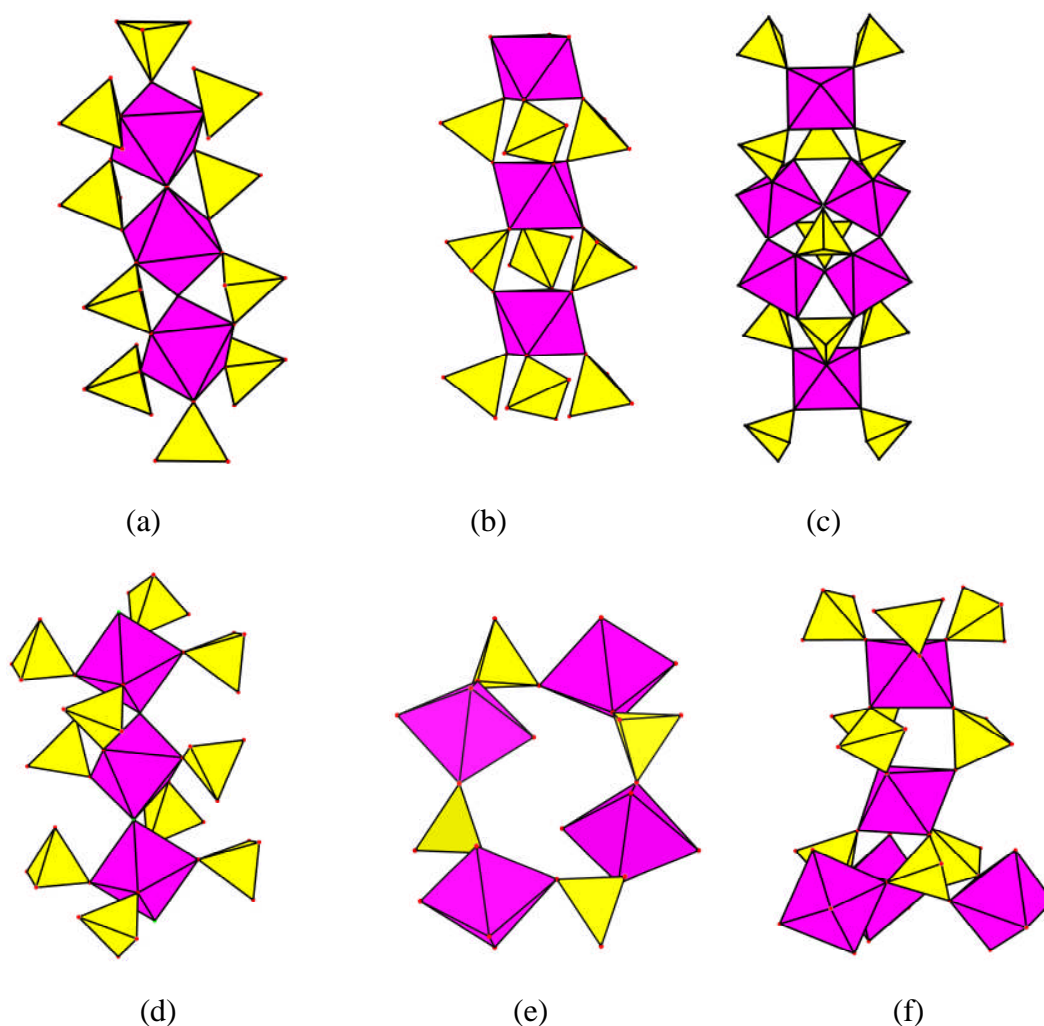


Figure 3.47: Secondary building units present within the scandium phosphate materials reported within this chapter. SBU's a – f are found within structures 1 – 6 respectively

In structure **1**, the scandium trimers are linked in ribbons; in structure **2** layers are attached through pillars to give central columns of octahedra, strictly alternating with phosphate groups; tetramers and isolated scandium octahedra are linked by phosphate groups into strips in structure **3**, (these connect to give layers); structure **4** is built of chains of scandium octahedra cross-linked by phosphate groups; the framework of structure **5** is built from the stacking of $\text{ScO}_4(\text{OH})_2$ units connected by one common PO_4 tetrahedral unit; in structure **6**, $\text{Sc}_5\text{P}_6\text{O}_{39}$ building units create cages, within which cationic species are located.

Primary amines have been shown to be particularly effective in templating scandium phosphate structures. Most reported scandium phosphates have been prepared using primary amines. There are now five reported structures prepared using ethylenediamine, with and without additional fluoride, which further increases the complexity of the structures that can form. Under the conditions employed for synthesis, secondary and tertiary amines and alkyl ammonium hydroxides did not yield novel templated scandium phosphate materials. It is likely that the additional hydrogen bonding that is possible, through the use of primary mono- and diamines, favours the interaction between protonated amines and P-OH groups of the phosphate materials. The smaller primary amines will have more protons available for hydrogen bonding per nitrogen and are also sterically favoured to achieve a close approach to the phosphate groups. For other amines, the dense phases kolbeckite, **5**, and langbeinite, **6**, are observed to crystallise. The new langbeinite phase $(\text{NH}_4)_2\text{Sc}_2(\text{PO}_4)_2(\text{HPO}_4)$, which forms around NH_4^+ (a breakdown product of the starting amines), is a rare example of a langbeinite structure where both framework cations sites are trivalent. Charge balancing in this sample requires protons to be distributed throughout the framework.

While it is therefore possible to prepare scandium phosphate-based frameworks, a main aim of this project, the presence of species such as fluoride, hydroxyl and water that make up additional scandium coordination sites on such solids renders the materials that have been prepared so far unstable to thermal treatment, probably owing to scandium becoming unstable with less than six-fold co-ordination and the loss of hydrogen bonding networks with the removal of the template.

All materials reported within this chapter have been treated thermally in order to analyse the crystallinity of the materials. The amine-templated materials (structures 1-4) decompose when the amine is removed from the structure.

Chapter 4: Scandium Phosphites

4.1 Introduction

Chapter 3 examined the synthesis and characterisation of novel scandium phosphates. A disadvantage of these organically-templated scandium phosphate materials in general is that their structures lose integrity upon heating. The loss of crystallinity can be related to the removal of the organic species, and consequent destruction of the hydrogen bonding system between the ($-\text{NH}_3^+$) group of the protonated amine and the oxygen atoms of (HPO_4) or (H_2PO_4) groups.⁴⁰ This chapter describes attempts to synthesise novel materials in which the potential for hydrogen bonding is reduced by changing the oxo-anion part of the inorganic network from the tetrahedral phosphate group to the pyramidal phosphite group.

Since the discovery of microporous aluminophosphates by Flanigen *et al*⁸, there has been intense interest in the synthesis and characterisation of transition metal phosphates templated by organic amines. By comparison, there have been relatively few examples describing the synthesis and structures of transition metal phosphites. Replacing the tetrahedral phosphate group, (PO_4)³⁻, by a pyramidal phosphite unit, (HPO_3)²⁻, as demonstrated by Clearfield *et al*¹²⁰, has resulted in a new class of structurally diverse materials. Figure 4.1 shows a comparison between a phosphate tetrahedral unit and a pyramidal phosphite unit, highlighting the reduced bonding abilities of the phosphite unit.

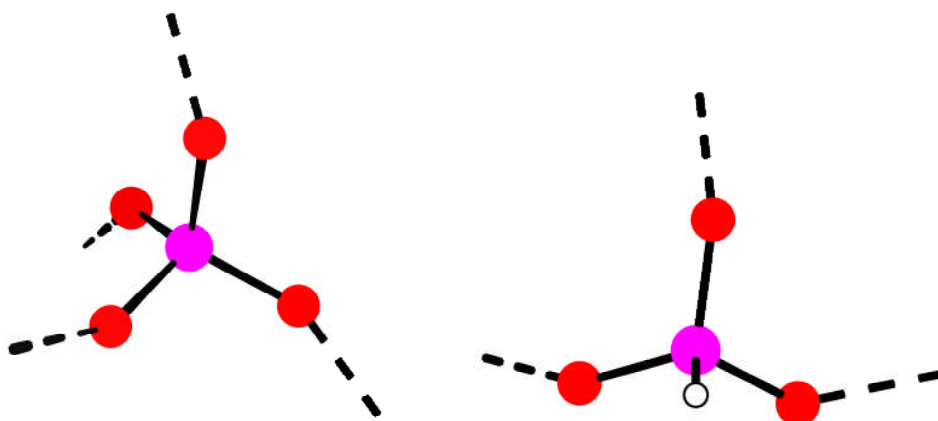


Figure 4.1: Left: Phosphate tetrahedral unit shown with dotted lines attached to the oxygens indicating the bonding potential of the unit. Right: Phosphite pyramidal unit, shown with a reduced bonding ability in comparison with the phosphate unit.

Metal phosphite materials are of interest because the phosphite ion, $(\text{HPO}_3)^{2-}$, is chemically similar to that of the phosphate $(\text{PO}_4)^{3-}$, so that it might be anticipated that metal phosphites would exhibit a structural chemistry of similar diversity to that of their phosphate analogues, although novel structural features would be expected due to the difference in formal charge between P(III) and P(V) in the phosphite and phosphate units. Similarly to zeotypic materials, metal phosphites have been reported which contain channels, cavities and layers^{121, 122}, in which the free space within the material is lined by terminal hydrogens of the phosphite pyramid, in place of oxygens of the phosphate tetrahedra.

Over the past decade, many transition metal elements have been incorporated into phosphite materials yielding a variety of chain, layered and framework materials.¹²³⁻¹²⁹ Here we explore the feasibility of including scandium within phosphite frameworks, and examine its potential to create porous framework materials.

There is only one example in the literature of a scandium phosphite material. This is isostructural to iron, aluminium and gallium phosphites,^{130, 131} and was prepared as a by-product in the hydrothermal investigation of a sodium scandium borophosphite / phosphate system.¹³² This material has also been prepared in the exploratory studies reported here, but as a pure phase

4.2 Experimental

Scandium phosphite-based gels were prepared, initially with similar stoichiometric ratios to those reported in chapter 3 for the scandium phosphates, and then altered to allow a greater and more appropriate variety of starting compositions. A selection of the reaction stoichiometries can be found in table 4.1.

Ethylenediamine was the first templating agent investigated, owing to the observed variety of scandium phosphate materials prepared using this diamine. Further experiments were performed using a variety of different templating agents, including primary, secondary and tertiary amines, alkyl ammonium salts, and even alkali metals as additives to the reaction gels. These gels were heated at a variety of temperatures and times, both in the presence and absence of HF, which was used as mineralising agent.

Table 4.1: Reaction stoichiometries and conditions used for the synthesis of scandium phosphite materials. The template corresponds to those listed in figure 3.3

Sample Number	Reactants				Temp (C)	Time (hrs)	pH _i	pH _f	Product (structure number)	
	Sc ₂ O ₃	H ₃ PO ₃	HF	Template / eq	H ₂ O					
26	1	3	2	1(a)	200	190	48	2	6	Sc(HPO ₃) ₃ (11) + unknown a
116	0.5	3.5	1	1(g)	200	190	48	3	7	[(H ₃ N(CH ₂) ₄ NH ₃) ₂][Sc ₅ F ₄ (HPO ₃) ₇ (HPO ₄)] (10)
117	0.5	7	1	1(g)	200	190	48	2	3	Unknown phase b
145	0.5	3.5	1	1(p)	200	190	48	3	7	Sc(HPO ₃) ₃ (11) + unknown phase c
146	0.5	3.5	1	1(f)	200	190	48	3	6	Sc(HPO ₃) ₃ (11)
147	0.5	3.5	1	1(e)	200	190	48	3	6	[(H ₃ N(CH ₂) ₂ NH ₃) ₂][Sc ₄ (HPO ₃) ₈] (9)
151	0.5	2	1	2(p)	200	190	48	3	7	Unknown phase c
152	0.5	2	1	1(p)	200	190	48	3	7	Unknown phase c
164	0.5	2.5	1	1(g)	200	190	48	3	7	[(H ₃ N(CH ₂) ₄ NH ₃) ₂][Sc ₅ F ₄ (HPO ₃) ₇ (HPO ₄)] (10)
167	0.5	3	2	1(g)	200	190	48	3	6	[(H ₃ N(CH ₂) ₄ NH ₃) ₂][Sc ₅ F ₄ (HPO ₃) ₇ (HPO ₄)] (10) + Unknown phase d
168	0.5	3	1	2(g)	200	190	48	2	7	[(H ₃ N(CH ₂) ₄ NH ₃) ₂][Sc ₅ F ₄ (HPO ₃) ₇ (HPO ₄)] (10)
176	0.5	2	1	1(e)	200	190	48	2	7	[(H ₃ N(CH ₂) ₂ NH ₃) ₂][Sc ₄ (HPO ₃) ₈] (10) + unknown phase e
177	0.5	2.5	1	1(e)	200	190	48	3	6	[(H ₃ N(CH ₂) ₂ NH ₃) ₂][Sc ₄ (HPO ₃) ₈] (9)
178	0.5	3	1	1(e)	200	190	48	3	7	[(H ₃ N(CH ₂) ₂ NH ₃) ₂][Sc ₄ (HPO ₃) ₈] (9)

Sample Number	Reactants					Temp (C)	Time (hrs)	pH _i	pH _f	Product (structure number)
	Sc ₂ O ₃	H ₃ PO ₃	HF	Template / eq	H ₂ O					
179	0.5	4	1	1(e)	200	190	48	4	7	[(H ₃ N(CH ₂) ₂ NH ₃) ₂][Sc ₄ (HPO ₃) ₈] (9)
180	0.5	2	2	2(e)	200	190	48	1	6	[(H ₃ N(CH ₂) ₂ NH ₃) ₂][Sc ₄ (HPO ₃) ₈] (9) + unknown phase e
182	0.5	3	2	2(e)	200	190	48	2	7	[(H ₃ N(CH ₂) ₂ NH ₃) ₂][Sc ₄ (HPO ₃) ₈] (9)
183	0.5	3.5	2	2(e)	200	190	48	3	7	[(H ₃ N(CH ₂) ₂ NH ₃) ₂][Sc ₄ (HPO ₃) ₈] (9)
185	0.5	3	3	3(e)	200	190	48	1	6	[(H ₃ N(CH ₂) ₂ NH ₃) ₂][Sc ₄ (HPO ₃) ₈] (9)
298	0.5	3	-	*	200	190	48	4	7	Unknown phase f
299	0.5	3	-	*	200	190	48	4	7	Sc(HPO ₃) ₂ Li (8)
300	0.5	3	-	*	200	190	48	4	7	Unknown phase g

Table 4.1 (continued): Reaction stoichiometries and conditions used for the synthesis of scandium phosphite materials. The template corresponds to those listed in figure 3.3

4.3 Results and Discussion

Amine templated scandium phosphites

As discussed in the introduction to this chapter, there are no reported studies into the hydrothermal synthesis of scandium phosphites. Three novel scandium phosphite-based materials were prepared and their structures solved during the exploratory studies of this thesis, in addition, a mixed phosphite-phosphate solid was prepared, owing to the partial oxidation of the phosphorous acid under the synthetic conditions. The synthetic conditions for the materials discussed in this chapter are listed in table 4.1.

Figure 4.2 illustrates the X-ray diffraction patterns of the crystalline scandium phosphite or phosphite / phosphate phases which have been observed in this work.

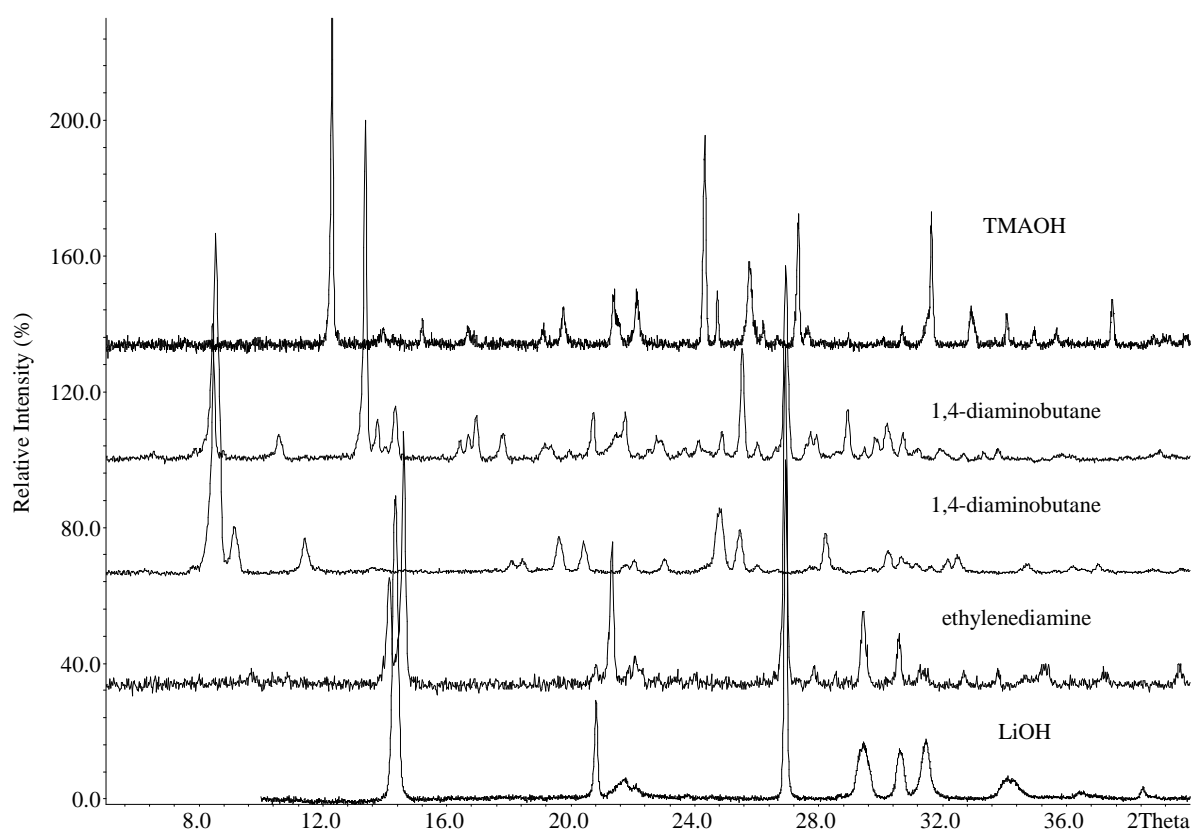


Figure 4.2: XRD patterns for a selection of scandium phosphite-based materials synthesised during the course of this work. The templating agent used in the reactions are listed above their respective diffraction patterns

The positions of the hydrogen atoms in the reported in this chapter were located through a combination of valence bond sum calculations and Fourier mapping, with their positions being fixed to 0.98(1)Å for a C-H with $U_{\text{iso}}(\text{H})$ being 1.2 times the parent carbon atoms, 0.85(1)Å for a N-H bond with $U_{\text{iso}}(\text{H})$ being 1.5 times the parent nitrogen atom and 0.98(1)Å for a O-H bond with $U_{\text{iso}}(\text{H})$ being 1.5 equivalents of the parent oxygen atom.

All structures were solved from single crystal data with the crystallographic data are reported in Table 4.2 and 4.3. Wherever possible, phase purity of bulk samples was confirmed by Rietveld refinement of structural (and instrumental) parameters against powder diffraction data. Rietveld refinement was performed with the GSAS program suite⁷⁵ using the atomic co-ordinates determined by the single crystal structure solution as a starting point. Instrumental parameters (background, zero-point, peak profile coefficients) and structural parameters (unit cell, atomic co-ordinates, thermal parameters) were refined, keeping constraints on the bond distances and angles. Close final fits to the observed data were achieved, with R_{wp} values between 5 and 11%, starting from structures determined from the single crystal experiments where ever possible. In order to characterise the materials further, TGA was performed and ^{45}Sc MAS NMR spectra measured for phase pure samples to determine the NMR properties of scandium in carboxylate frameworks. ^{45}Sc MAS NMR spectra are presented with the structures with the experimental conditions given in Chapter 2. Further analysis of ^{45}Sc NMR is given in chapter 7

Table 4.2: Crystallographic information for structures **8** and **9**

	Structure 8	Structure 9
Empirical Formula	LiSc(HPO ₃) ₂	[(H ₃ N(CH ₂) ₂ NH ₃) ₂][Sc ₄ (HPO ₃) ₈]
Formula Weight	889.07	943.92
Temperature (K)	93	173
Wavelength (Å)/ Diffractometer	0.71073 (Saturn) Mo Kα	0.71073 (Saturn) Mo Kα
Crystal System / Space group	Tetragonal / I 41 / a m d	Monoclinic / P2/n
Unit Cell Dimensions	a / Å b / Å c / Å β (°)	9.3479(34)Å 9.0351(33)Å 9.7181(36)Å 117.425(0)
Volume	742.57(51)	728.544(486)
Z	8	4
Number of reflections	1597	4222
Number of unique reflections	93	1429
2θ range (°)	3.13 – 18.83	4.52 – 28.06
Variables	20	101
R1 (I>2σI)	0.1168	0.0360
R1 (all data)	0.1217	0.0411
Max., Min. difference in electron density (eÅ ⁻³)	1.282, -0.640	0.674, -0.537

Table 4.3: Crystallographic information for structures **10** and **11**

	Structure 10	Structure 11
Empirical Formula	$[(\text{H}_3\text{N}(\text{CH}_2)_4\text{NH}_3)_2][\text{Sc}_5\text{F}_4(\text{HPO}_3)_7(\text{HPO}_4)]$	$\text{Sc}_2(\text{HPO}_3)_3$
Formula Weight	1300.8	329.85
Temperature (K)	93	123
Wavelength (Å)/ Diffractometer	0.6911 / (Station 9.8)	0.6910 / (Station 9.8)
Crystal System / Space group	Monoclinic / C2/m	Hexagonal / P63/m
Unit Cell Dimensions		
a / Å	12.8880(16)	8.289(5)
b / Å	14.8351(11)	-
c / Å	10.5309(20)	7.697(4)
β (°)	103.093(1)	-
Volume	1961.192(50)	458.0(5)
Z	2	2
Number of reflections	10563	4034
Number of unique reflections	2997	460
2 θ range (°)	1.93 – 29.94	3.77 – 24.90
Variables	143	28
R1 (I>2 σ I)	0.0681	0.0247
R1 (all data)	0.0932	0.0252
Max., Min. difference in electron density (eÅ ⁻³)	1.122, -1.145	0.408, -0.418

4.3.1 LiSc(HPO₃)₂- Structure 8

Structure **8**, LiSc(HPO₃)₂, was solved by direct methods and Fourier syntheses from laboratory single crystal X-ray data, using the SHELXS program⁸¹. The crystallographic information is outlined in table 4.2. The atomic co-ordinates for structure **8** are listed below in table 4.4. The position of the hydrogen atom was located in the difference Fourier map. The P-H bond distance was restrained to be 1.25(1)Å with U_{iso}(H) set to 1.2 times that of the parent phosphorus atom.

Table 4.4: Atomic coordinates for structure **8**

Atom	x	y	z	U _{iso}	Occ	Multiplicity
Sc(1)	0	0.25	0.375	0.026(3)	1	4
P(1)	0	0.30668(18)	0.17147(8)	0.037(5)	0.5	16
H(1)	0	0.46952	0.16795	-1.2	0.5	16
O(1)	0	0.25	0.25267(17)	0.064(6)	1	8
O(2)	0	0.56465(3)	0.37254(10)	0.058(3)	1	16
Li(1)	0.25	0.75	0.25(9)	0.03(4)	0.25	16
Li(2)	0.218(9)	0.75	0.223(3)	0.03(4)	0.5	16

Structure **8**, LiSc(HPO₃)₂, is a three dimensional framework scandium phosphite structure, within which there are no Sc–O–Sc linkages, and therefore there is strict alternation between Sc and P in the framework. Structure **8** is isomorphous with the sodium zirconium beryllophosphate mineral, Gainesite, reported by Moore *et al*¹³³ and contains a two dimensional pore network, with each channel being bound by non-planar 8MRs, which run parallel to [100] and [010], figure 4.3. Lithium ions occupy the cavities, statistically disordered over positions in the channels, illustrated in figure 4.3 as grey spheres.

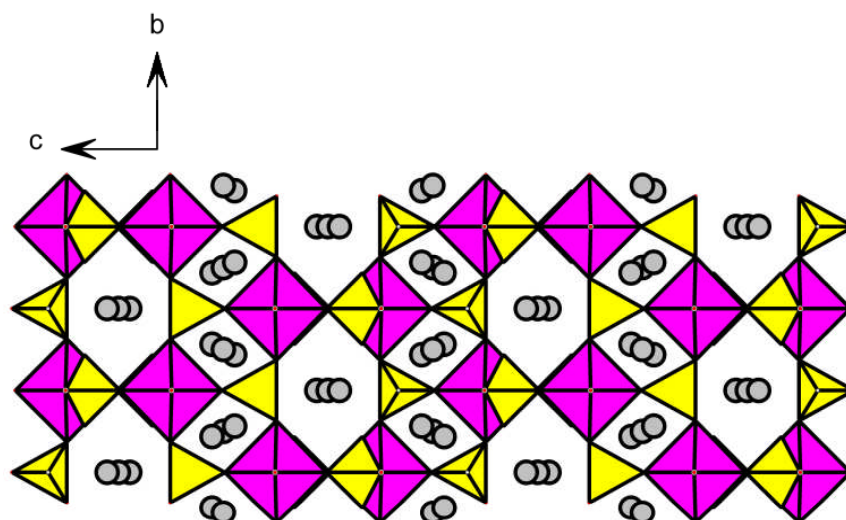


Figure 4.3: Projection down [100] and structure **8** showing disordered lithium cations (grey spheres) within the pore network.

There is disorder of the phosphite pseudo pyramid, which can point in one of two directions consequently to allow for this, P(1) and H(1) are half occupied. This is also observed in the mineral Gainesite, reported by Moore *et al*, where phosphate groups are 50% occupied.

Structure **8** can be described using $M_9(HPO_3)_{18}$ building blocks, figure 4.4, as visual aids in order to understand the connectivity of the framework. The manner by which these $M_9(HPO_3)_{18}$ building units stack within the framework is shown schematically in figure 4.5.

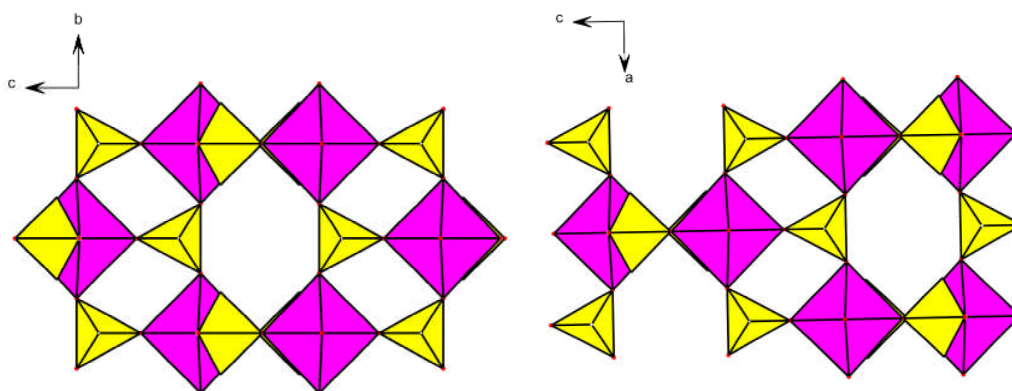


Figure 4.4: Projection down [100] and [010] (left and right images respectively) of the $M_9(HPO_3)_{18}$ building units which make up the framework of structure **8**.

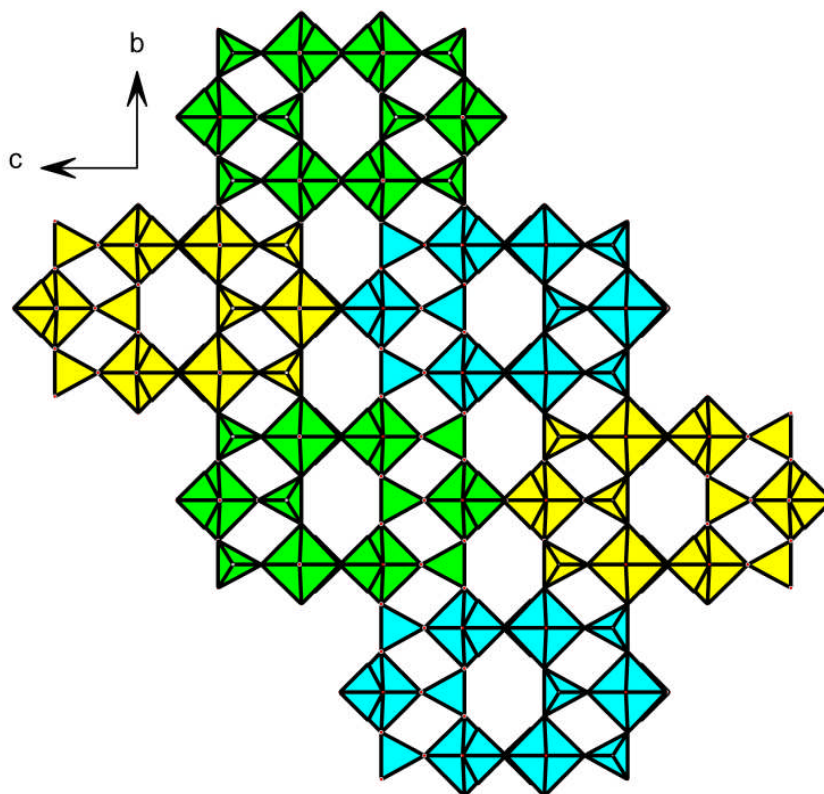


Figure 4.5: Projection down $[100]$ of structure **8** highlighting different $M_9(HPO_3)_{18}$ building units, illustrating how they stack in respect to each other along the b -axis.

Initial structure solution for structure **8** indicated the presence of one crystallographically unique phosphorus site, which is half occupied owing to disorder. It was thought that this would result in one distinct phosphorus peak in the ^{31}P NMR spectra, with the structure being composed of domains consisting entirely of phosphite groups pointing in one direction. However solid state ^{31}P DP NMR clearly shows 3 peaks in the ratio of 1:2:1, shown below in figure 4.6.

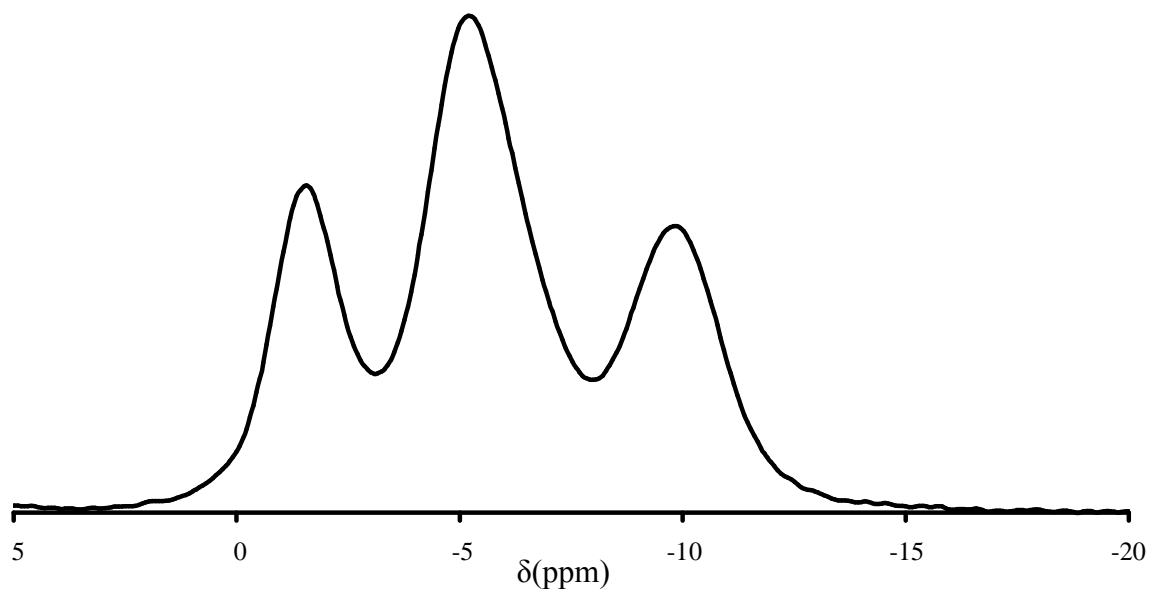


Figure 4.6: ^{31}P DP MAS NMR spectra for structure **8**, showing 3 peaks at -1.6, -5.3 and -9.9ppm in a ratio of 1:2:1 respectively.

Examination of the disordered phosphite groups and how they can arrange in respect to each other provides an explanation for the three distinct phosphorus sites observed in the ^{31}P MAS NMR spectra. The disorder arrangement of the phosphite pseudo pyramids are shown below figure 4.7, which can be simplified to figure 4.8.

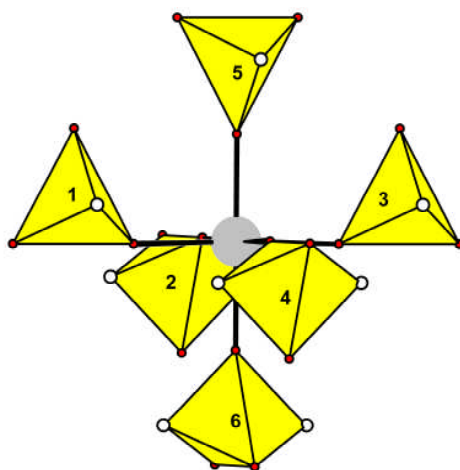


Figure 4.7: Disordered arrangement of phosphite pseudo pyramids located around one scandium octahedral unit. The numbers of the polyhedra relate to the text below

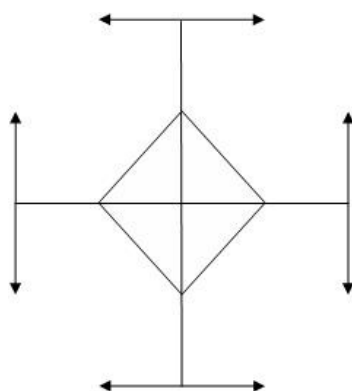


Figure 4.8: Simplification of figure 4.7, showing the scandium octahedron connected to eight phosphite pseudo pyramids, which are represented by doubled headed arrows in order to attribute for the disorder. The polyhedral units labeled '5' and '6' in figure 4.7 have not been shown in this figure for clarity.

There are several different ways in which the disordered phosphite units can be arranged around a single scandium octahedra which can help to explain the absence of a single peak in the ^{31}P MAS NMR spectra. Figure 4.9, below, shows some of the ways in which the phosphite pseudo pyramids can be arranged in respect to each other.

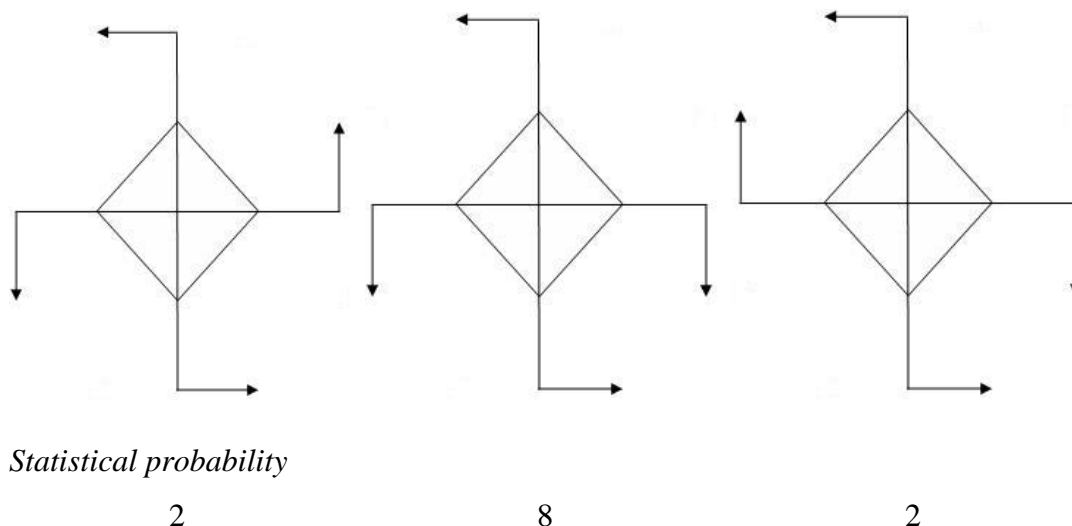


Figure 4.9: Schematic representation of possible orientations of the phosphite pseudo pyramids (represented by arrows). Some of the phosphite polyhedra (labelled '5' and '6' in figure 4.7) have been omitted for clarity.

^{45}Sc NMR, figure 4.10, gives an intense signal in the 0 to 20 ppm region and also a very broad signal ranging from 20 ppm to 120 ppm with a quadrupolar bandshape. The intense signal, with peaks at 3.3 and 10.9 ppm, cannot be separated in an MQMAS experiment, figure 4.11, so it appears that the structure relates to a quadrupolar bandshape with broadening and consequently suggests the presence of only a single scandium site within structure **8**. The very broad signal is not detected in the multiple quantum experiment, suggesting that it must have a very high quadrupolar coupling constant in order to give such a broad line. This signal is believed to be a contribution from residual scandium oxide present within the sample.

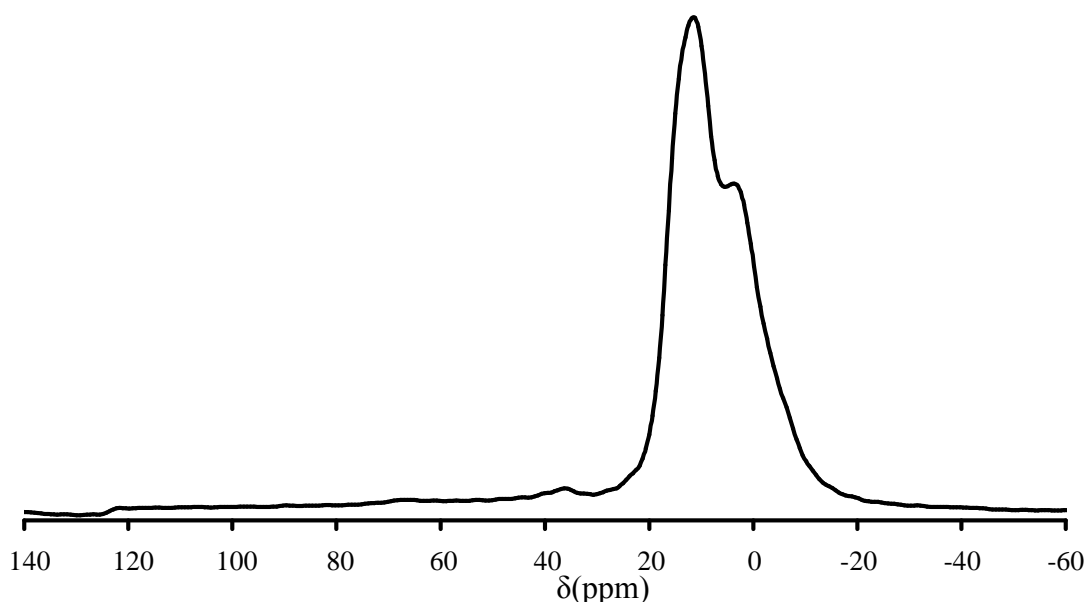


Figure 4.10: ^{45}Sc MAS NMR spectra for structure **8**, showing an intense signal with peaks at 3.3 and 10.9 ppm, and a broad signal from about 20 to 120 ppm, believed to be from residual scandium oxide present within the sample.

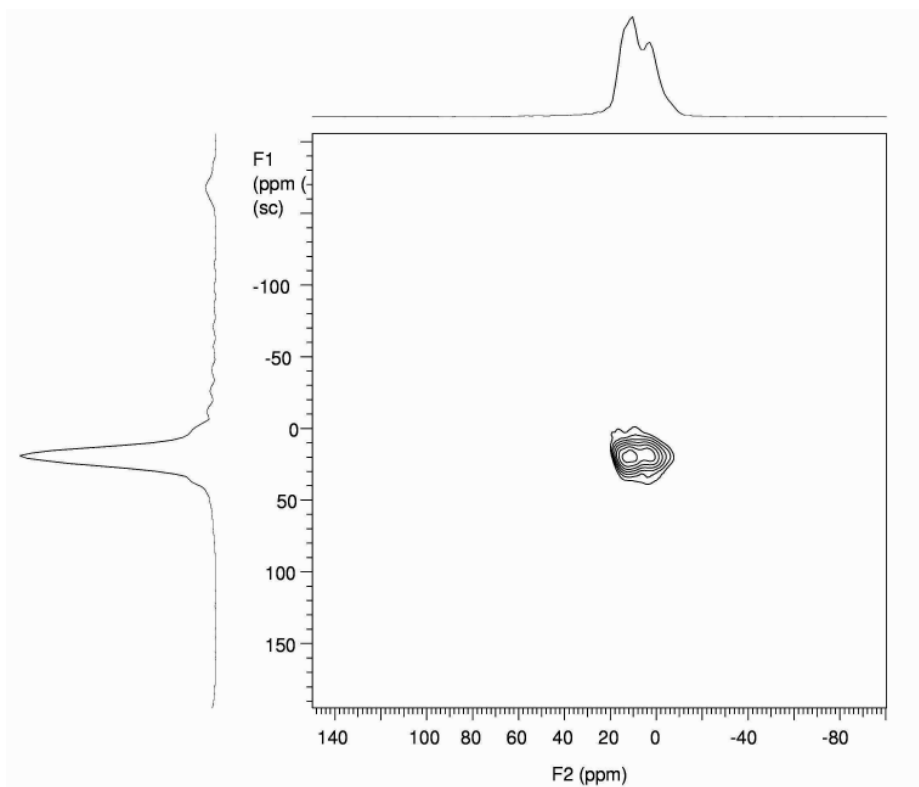


Figure 4.11: ^{45}Sc MQMAS MAS NMR spectra for structure **8**, clearly showing no separation in the intense signal described in figure 4.10, suggesting the presence of a single scandium site within structure **8**.

4.3.2 [(H₃N(CH₂)₂NH₃)₂][Sc₄(HPO₃)₈] – Structure 9

Structure **9**, [(H₃N(CH₂)₂NH₃)₂][Sc₄(HPO₃)₈], was solved by direct methods and Fourier syntheses, using the SHELXS program⁸¹, from laboratory single crystal X-ray data collected on a small crystal, the crystallographic information is outlined in table 4.1, with the atomic co-ordinates are listed below in table 4.5.

Atom	x	y	z	Occ	U _{iso}	Multiplicity
Sc(1)	0.75	0.39686(9)	0.75	1	0.0056(2)	2
Sc(2)	0.75	-0.10591(9)	0.25	1	0.0072(2)	2
P(1)	0.82178(9)	0.10196(9)	0.56649(9)	1	0.0089(2)	4
P(2)	0.35374(9)	0.33235(9)	0.52627(9)	1	0.0109(2)	4
O(1)	0.7538(3)	-0.2579(3)	0.4129(2)	1	0.0147(5)	4
O(2)	0.7487(3)	0.0697(2)	0.3925(3)	1	0.0137(5)	4
O(3)	0.7420(3)	0.2366(3)	0.5930(3)	1	0.0166(5)	4
O(4)	0.4991(2)	0.4085(2)	0.6508(2)	1	0.0114(5)	4
O(5)	0.7515(3)	0.5635(3)	0.6042(3)	1	0.0181(5)	4
O(6)	1.0026(3)	0.1150(3)	0.6383(3)	1	0.0229(6)	4
C(1)	0.1672(4)	0.5863(3)	0.6815(4)	1	0.0129(6)	4
N(1)	0.0583(3)	0.6970(3)	0.6985(3)	1	0.0158(6)	4
H(1)	0.7801	-0.0215	0.6245	1	0.024	4
H(2)	0.4168	0.2315	0.4597	1	0.019	4

Table 4.5: Atomic co-ordinates for structure **9**

The positions of the hydrogen atoms within the structure and on the template molecule were assigned using a combination of valence bond calculations¹³⁴ and difference Fourier maps.

Structure **9** presents a novel three dimensional scandium phosphite framework (Sc:P ratio of 1:2), containing isolated ScO₆ octahedra connected to 6 HPO₃ pseudo pyramids, figure 4.12. There are channels running in 2 dimensions through structure **8**, occupied by ethylenediamine template molecules, which is fully protonated.

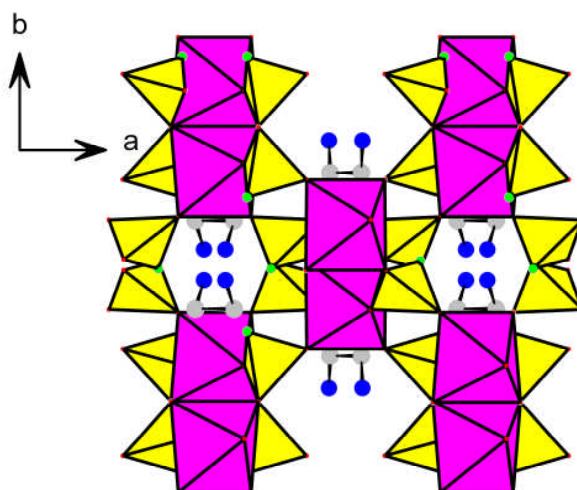


Figure 4.12: Projection down [001] of structure **9**, showing channels in which ethylenediamine molecules are located. The phosphite hydrogen atoms have been coloured green and hydrogen atoms attached to the organic have been omitted, for clarity.

The framework of structure **9** is related to that of structure **8**, but without disorder of the phosphite pseudo pyramids, and as a result can be described using the same views as those used for structure **8**. Structure **8** and **9** crystallise in different spacegroups ($I 4_1/amd$ and $P2/c$ respectively), and the difference in symmetry must arise from differences in interactions of the lithium ions and the template ethylenediamine ions with the framework. The $M_9(HPO_3)_{18}$ units present within structure **8** are also the building units present within structure **9**, creating a two dimensional channel system within which the ethylenediamine molecules can be located, figure 4.13. The manner in which these $M_9(HPO_3)_{18}$ building units stack within the framework is shown schematically in figure 4.14, which can be compared to the corresponding figure illustrating the stacking of the $M_9(HPO_3)_{18}$ building units in structure **7**, figure 4.5.

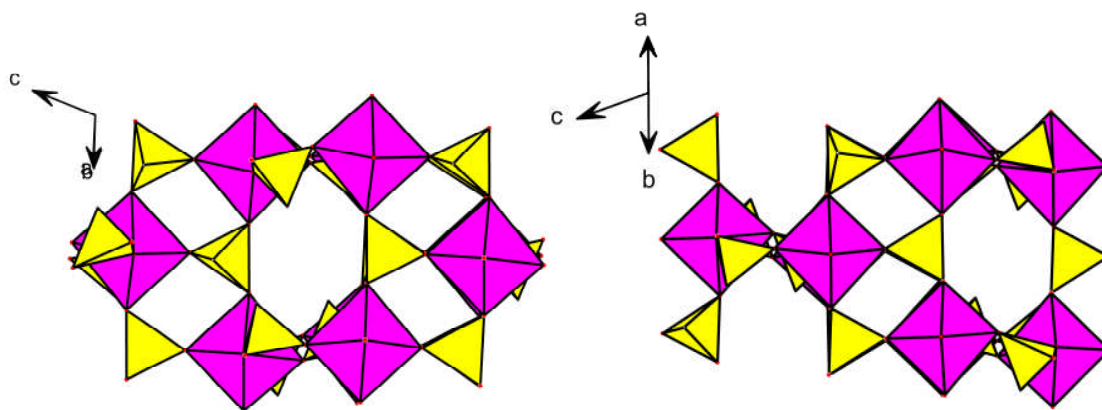


Figure 4.13: Two different projections of the $M_9(HPO_3)_{18}$ building units present within structure **9**. The left and right image can be directly compared to the respective images in figure 4.4.

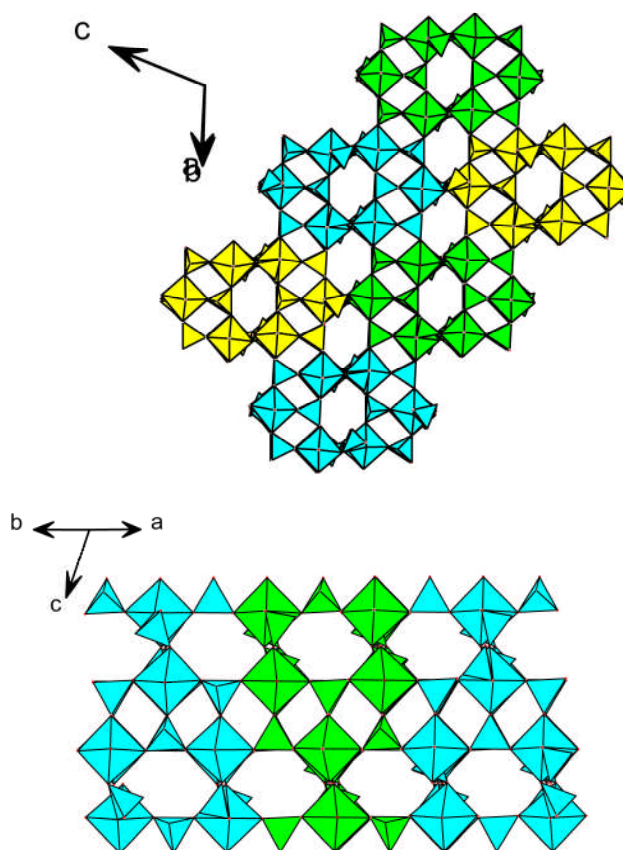


Figure 4.14: Different projections onto structure **9** highlighting different $M_9(HPO_3)_{18}$ building units and how they stack in respect to each other. The different polyhedral colours with the figures complement those used in figure 4.5 for comparison.

The interatomic distances and bond angles in the inorganic framework are as expected: Sc-O bond distances are between 2.059(7) and 2.132(8)Å and P-O distances are from 1.474(9) to 1.607(8)Å.

Structure **9** can be considered isomorphous to the ethylenediamine templated scandium phosphate structure reported by Riou *et al.*⁴⁵ The templating effect of the ethylenediamine molecule within the scandium phosphate and scandium phosphite system results in the formation of scandium phosphate or phosphite layers which have two different types of 8MRs. The first 8MR is occupied by the template molecule, which in turn positions the P-H or P-OH away from the template, creating void space for the template. The second 8MR results from the positions of four terminal phosphite or phosphate groups creating a small pore. This is shown for both structures **9** and Riou's scandium phosphate in figure 4.15. Although similar, there are differences in tilts for the two structures, which manifest themselves in a difference in the unit cell dimensions

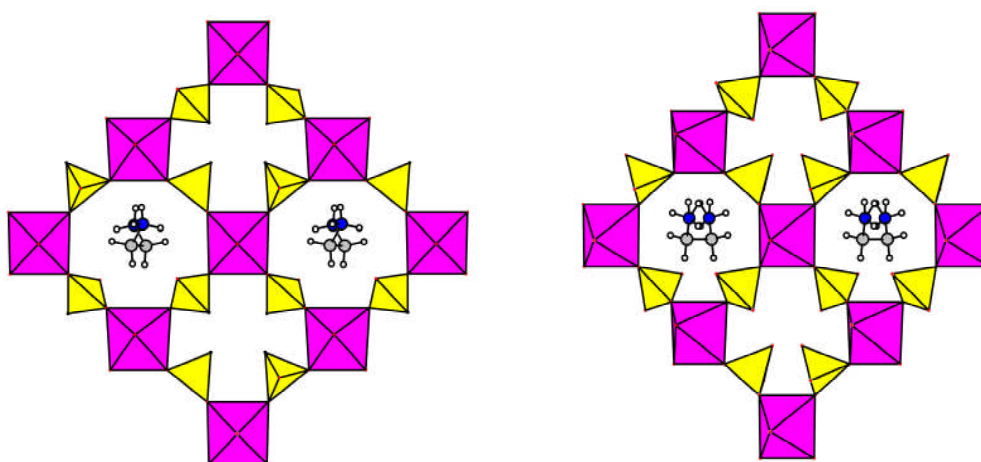


Figure 4.15: (Left): Structure **9** showing the situation of the amine and the different pore topologies within the layers. (Right): Riou's scandium phosphate showing the large and small pore system, similar to structure **9**.

The final charge balanced structural formula is $[(\text{H}_3\text{N}(\text{CH}_2)_2\text{NH}_3)_2][\text{Sc}_4(\text{HPO}_3)_8]$, with both amine groups of the diamine being protonated. CHN analysis, weight %, calculated, C, 2.55%, H, 1.07%, N, 2.97%; measured, C, 2.43%, H, 1.16%, N, 2.93%.

Solid state ^{31}P MAS NMR (figure 4.16) gives two distinct peaks at -5.57 and -11.00ppm, which is consistent with the two crystallographically unique phosphorus sites located in the single crystal structure.

^{45}Sc MAS NMR (figure 4.17) shows two intense signals at 14.00 and 3.95ppm which can be attributed to the two crystallographically unique scandium sites within the framework.

^{13}C CP MAS NMR shows a single peak 39.86ppm

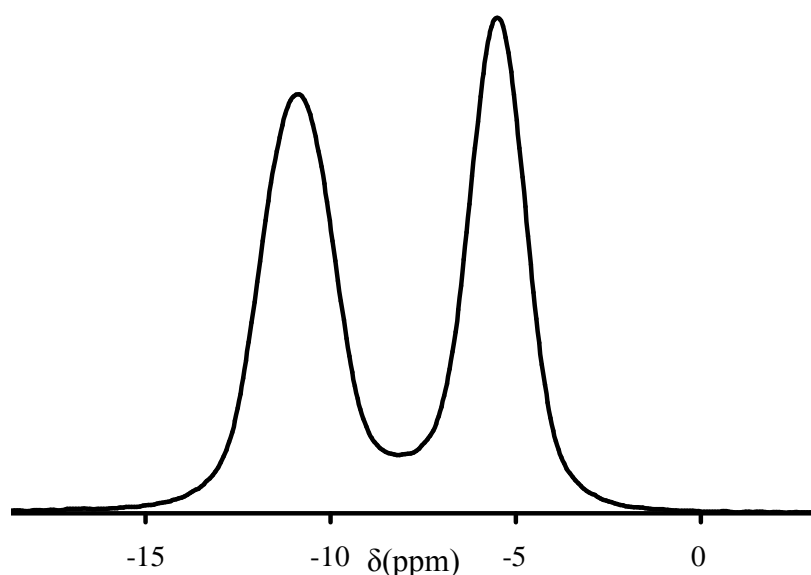


Figure 4.16: ^{31}P DP MAS NMR spectra for structure **9**, showing two distinct peaks at -5.57 and -11.00ppm, which correspond to the two crystallographically unique phosphorus atoms within the structure

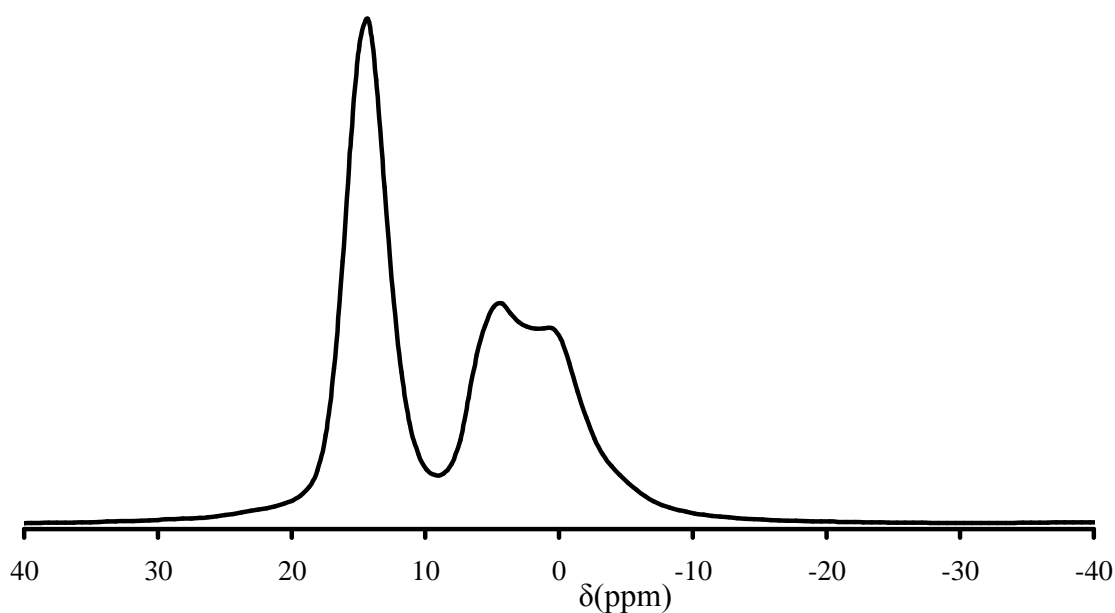


Figure 4.17: ^{45}Sc MAS spectra for structure **9**, showing intense signals at 14.00 and 3.95ppm.

Thermogravimetric analysis shows a significant weight loss (experimental, 13.4%) occurring between 150 and 330°C due to combustion of the organic (theoretical, 13.16%). The material did not retain its crystallinity upon removal of the organic moiety.

4.3.3 [(H₃N(CH₂)₄NH₃)₂][Sc₅F₄(HPO₃)₆(H₂PO₃)₂(PO₄)] – Structure 10

Structure **10**, [(H₃N(CH₂)₄NH₃)₂][Sc₅F₄(HPO₃)₆(H₂PO₃)₂(PO₄)], was solved by direct methods and Fourier syntheses, using the SHELXS program⁸¹, from single crystal X-ray diffraction data collected on station 9.8 at the synchrotron radiation facility, Daresbury. The crystallographic information is outlined in table 4.3, with the atomic co-ordinates for structure **10** being listed in table 4.6

Table 4.6: Atomic coordinates for structure **10**

Atom	x	y	z	Occ	U _{iso}	Multiplicity
Sc(1)	0.5	0	0.5	1	0.0125(4)	2
Sc(2)	0.11057(7)	0.12540(6)	0.39971(10)	1	0.0132(2)	8
P(1)	0.65712(9)	0.15152(8)	0.36491(13)	1	0.0136(3)	8
P(2)	-0.06953(14)	0	0.1920(2)	1	0.0181(4)	4
P(3)	0.27541(13)	0	0.26139(19)	1	0.0137(4)	4
H(1)	0.6527	0.1178	0.2838	1	0.016(3)	8
H(2)	-0.142	0	0.2066	1	0.022(3)	4
O(1)	-0.0816(5)	0	0.0445(6)	1	0.0309(14)	4
O(2)	0.7742(3)	0.1562(2)	0.4321(4)	0.5	0.0179(7)	8
O(3)	0.3947(4)	0	0.3146(5)	1	0.0172(10)	4
O(4)	0.2230(3)	0.0854(2)	0.2989(4)	1	0.0177(7)	8
O(5)	0.6113(3)	0.2447(2)	0.3259(4)	1	0.0180(8)	8
O(6)	-0.0171(3)	0.0852(2)	0.2548(4)	1	0.0207(8)	8
O(7)	0.5893(3)	0.1017(3)	0.4407(4)	1	0.0252(9)	8
O(8)	0.264(2)	0	0.113(3)	1	0.217(11)	4
F(1)	0	0.1688(3)	0.5	1	0.0164(8)	4
F(2)	0.1107(3)	0	0.4755(4)	1	0.0158(8)	4
C(1)	0.2572(4)	0.2525(4)	0.0724(6)	1	0.0248(12)	8
C(2)	0.3680(4)	0.2216(4)	0.1429(6)	1	0.0231(11)	8
N(2)	0.3780(3)	0.2202(3)	0.2863(5)	1	0.0204(9)	8

The positions of the hydrogen atoms within the structure and on the template molecule were assigned using a combination of valence bond calculations¹³⁴ and Fourier mapping.

As with structure **3**, analysis of thermal parameters from single crystal refinements along with semi-quantitative energy dispersive x-ray analysis, figure 4.18, indicated the presence of fluorine within the sample. These were included in the structural refinement, allowing for more appropriate thermal parameters and closer fit.

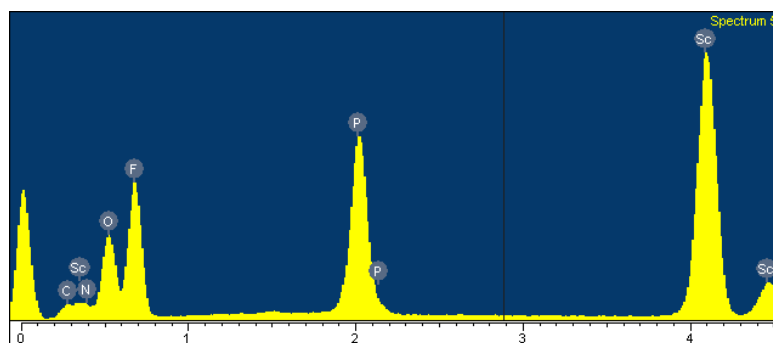


Figure 4.18: EDX analysis of structure **10**, clearly showing the presence of fluorine within the structure.

Structure **10**, presents a novel layered scandium phosphite – phosphate material which is composed of scandium fluoride phosphite – phosphate layers bridged by protonated diaminobutane molecules, figure 4.19.

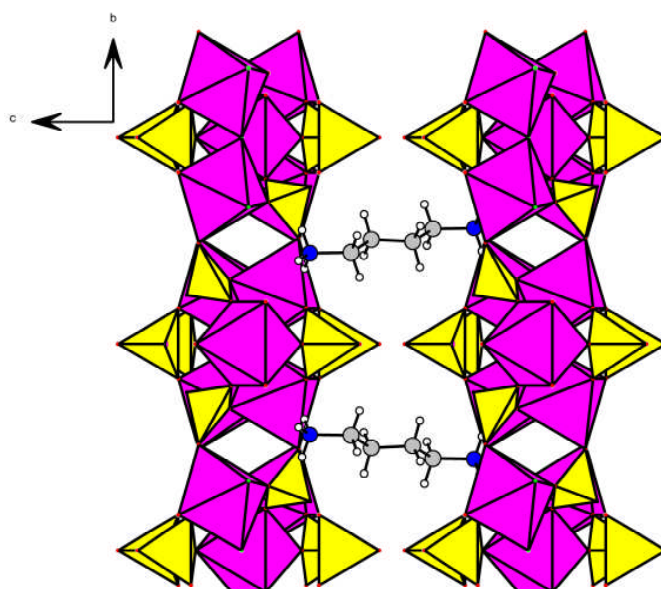


Figure 4.19: Projection down [100] of structure **10**, showing scandium phosphite – phosphate layers separated by protonated 1,4-diaminobutane molecules. Some 1,4-diaminobutane molecules have been omitted for clarity.

Each layer of structure **10** consists of isolated ScO_6 octahedra linked via phosphite groups to tetramers of corner-sharing ScO_4F_2 octahedra, which are linked through fluoride ions. The isolated ScO_6 octahedra are linked to the tetrameric squares through corner-sharing HPO_3 pseudo pyramids which bond to scandium atoms by their three apical oxygen atoms, the hydrogen projecting into the interlayer space.

Although structure **10** is a scandium phosphite – phosphate structure no phosphoric acid was included as a reactant. An explanation for the presence of the phosphate group is the oxidation of the phosphorous acid to give phosphoric acid during the hydrothermal reaction. This behaviour has been observed previously during the investigations of phosphite systems, in which the use of a single phosphorus source has yielded mixed phosphite – phosphate systems.¹³⁵⁻¹³⁸ The presence of the phosphate group is shown by the location of an additional oxygen O(2) in the Fourier maps, which was refined at 50% occupancy, suggesting that the phosphorus is 50% phosphate and 50% phosphite, the location of which in respect to the layers is shown in figure 4.20.

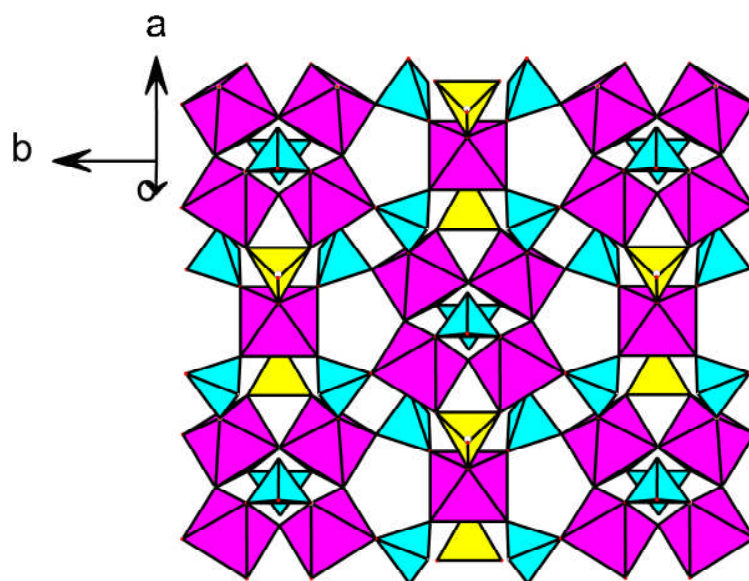


Figure 4.20: Representation of part of the layer of structure **10** illustrating the phosphite pseudo pyramids (cyan) and the mixed phosphite – phosphate polyhedra (yellow)

Structure **10** can be described as being isomorphous to structure **3**, $[(\text{H}_3\text{NC}_4\text{H}_8\text{NH}_3)_2(\text{H}_3\text{O})][\text{Sc}_5\text{F}_4(\text{HPO}_4)_8]$, differing only slightly in the dimensions of the unit cell, see table 4.7 for comparison.

Table 4.7: Unit cells of structure **3** and structure **9**

	a(Å)	b(Å)	c(Å)	β	spacegroup
Structure 3	12.8538(36)	14.9106(46)	10.1906(34)	101.17	C2/m
Structure 10	12.8880(16)	14.8350(11)	10.531(2)	103.09(0)	C2/m

A comparison of the layers which make up structure **3** and structure **10** are shown below in figure 4.21. Structure **3** contains phosphate tetrahedra which have two oxygen atoms which are only bound to the phosphorus, P(1). These are replaced by phosphite groups within structure **10**, with the only phosphate tetrahedra in the structure only having one free oxygen atom which is pointing into the free space between the layers.

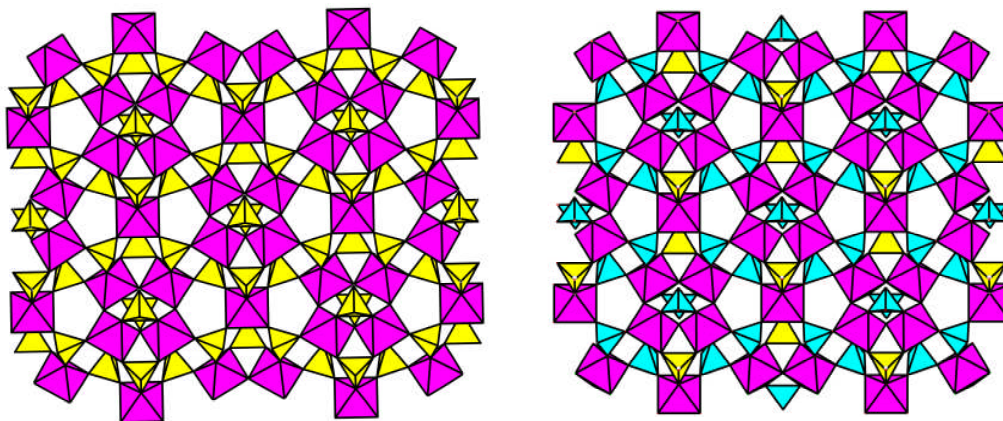


Figure 4.21: left: Scandium phosphate layer found within structure **3**; right: scandium phosphate/phosphite layer found within structure **10**. The yellow tetrahedral represent the phosphate units located in structure **10** whereas the cyan pseudo pyramids represent the phosphite units

The final charge balanced structural formula is therefore $[(\text{H}_3\text{N}(\text{CH}_2)_4\text{NH}_3)_2][\text{Sc}_5\text{F}_4(\text{HPO}_3)_7(\text{HPO}_4)]$. CHN analysis, weight %, calculated, C, 8.47%, H, 2.49%, N, 4.94%; measured, C, 8.56%, H, 2.75%, N, 5.03%.

Solid state ^{31}P MAS NMR (figure 4.22) shows four peaks at -1.1, -4.2, -9.2 and -12ppm which can be attributed to the three crystallographically unique phosphorus positions within structure **10**, with P(3) being at the centre of phosphate and phosphite polyhedral units, giving four distinct peaks overall.

^{45}Sc MAS NMR shows three peaks, believed to be signals from two different scandium sites present within structure **10**. The peaks at 3.32 and 1.08ppm are believed to be from the same scandium site which generated a typical quadrupolar line shape, and the peak 7.36ppm has been attributed to the other crystallographically unique scandium site present within structure **10**.

^{13}C CP MAS NMR shows two peaks at 40.17 and 25.88ppm which correspond to the two crystallographically unique carbon atoms of the diamminobutane template.

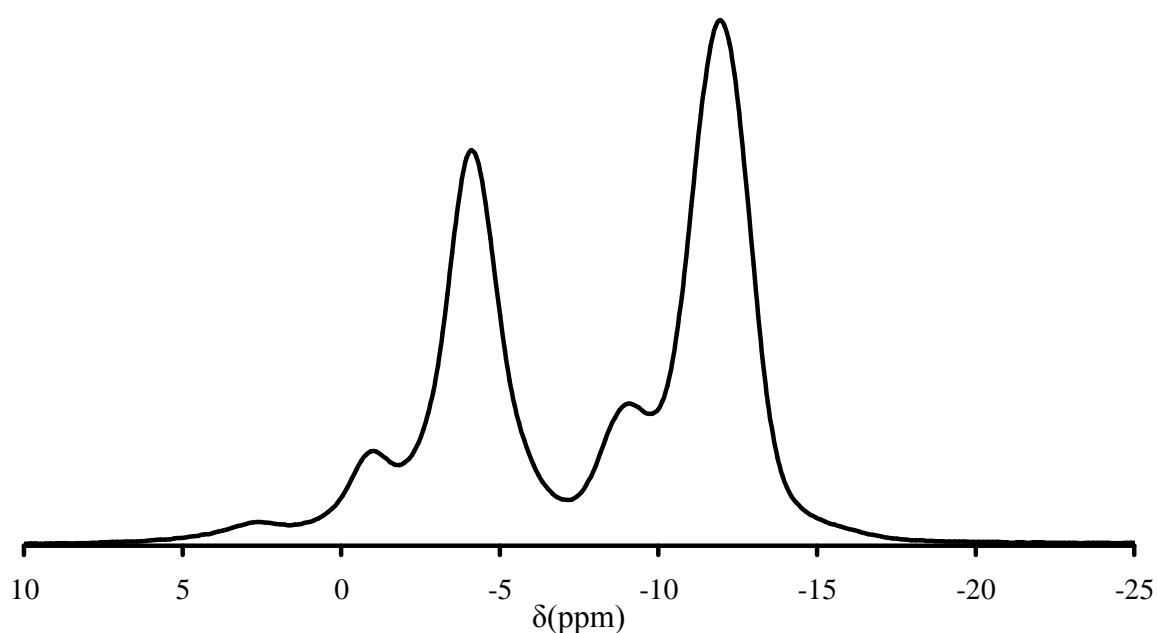


Figure 4.22: ^{31}P MAS NMR spectra of structure **10**, showing 4 main peaks at -1.1, -4.2, -9.2 and -12ppm.

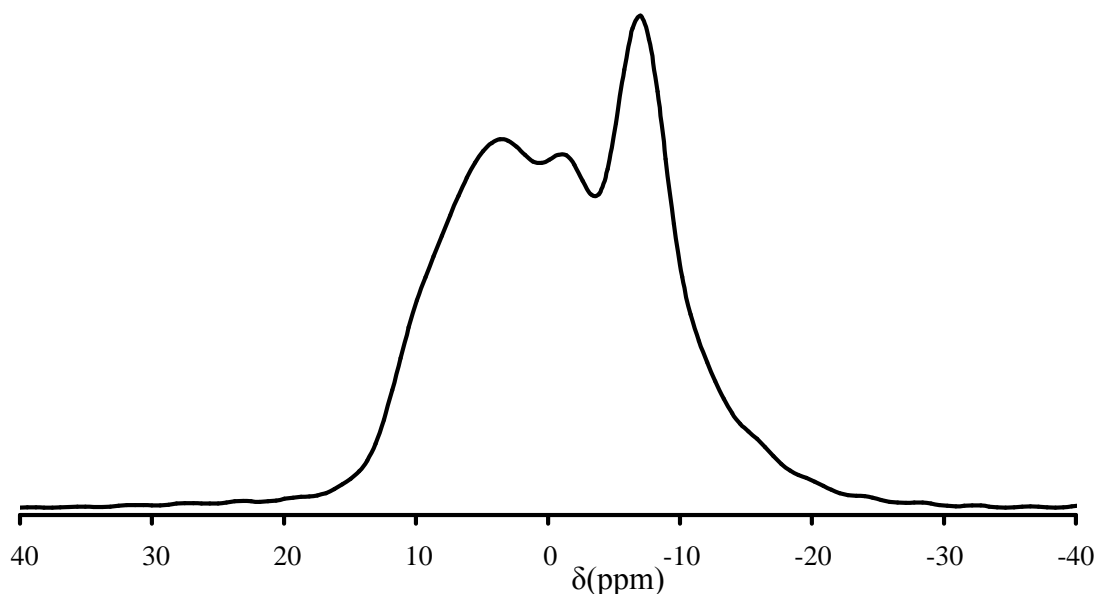


Figure 4.23: ^{45}Sc MAS NMR spectra from structure **10**, showing peaks at 3.32, 1.08 and 7.36ppm.

Thermogravimetric analysis shows a significant weight loss (experimental, 15.63 %) occurring between 420 and 600°C due to combustion of the organic (theoretical, 15.89%).

4.3.4 $\text{Sc}_2(\text{HPO}_3)_3$ – Structure **11**

Structure **11** was solved by direct methods and Fourier syntheses from single crystal X-ray data collected on a small crystal at the synchrotron radiation source, Daresbury, using the SHELXS program.⁸¹ The crystallographic information is outlined in table 4.8.

Table 4.8: Atomic coordinates for structure **11**

Atom	x	y	z	U_{iso}	Occ	Multiplicity
Sc(1)	0.66667	0.33333	0.45402(5)	0.0078(17)	1	4
P(1)	0.04228(6)	0.35122(5)	0.25	0.0069(18)	1	6
O(1)	0.84879(13)	0.56378(13)	0.58506(12)	0.0074(2)	1	12
O(2)	0.8597(17)	0.35723(18)	0.25	0.0120(3)	1	6
H(1)	0.00203(4)	0.18132(4)	0.25	0.0155(7)	1	6

Structure **11** presents a three dimensional framework with scandium to phosphorus ratio of 2:3. The structure contains a one dimensional infinite channel system running along [001],

with a small pores (approximately 3\AA in diameter), which is lined by six symmetry equivalent phosphite pyramids, see figure 4.24. The phosphite groups are positioned on two different levels, shown in figure 4.25.

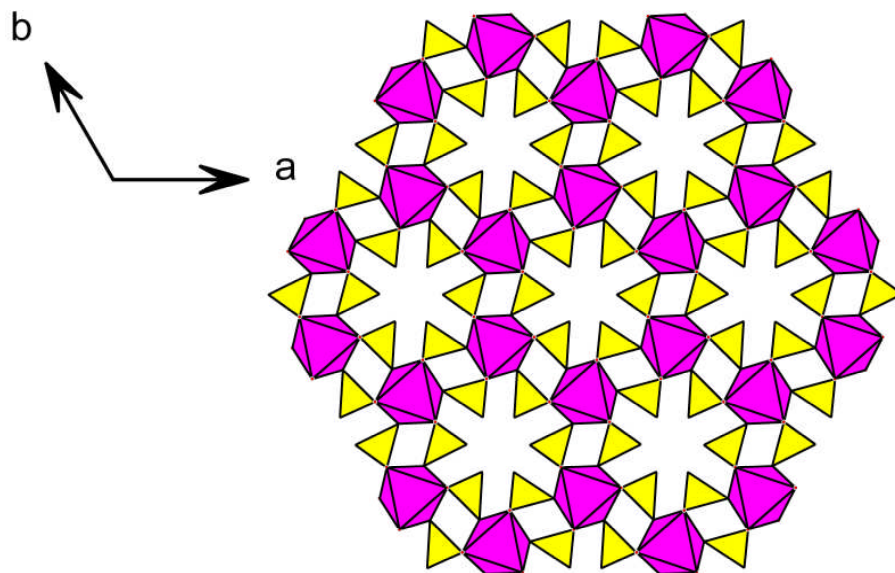


Figure 4.24: Projection down $[001]$ of structure **II**, showing small 12MR pores.

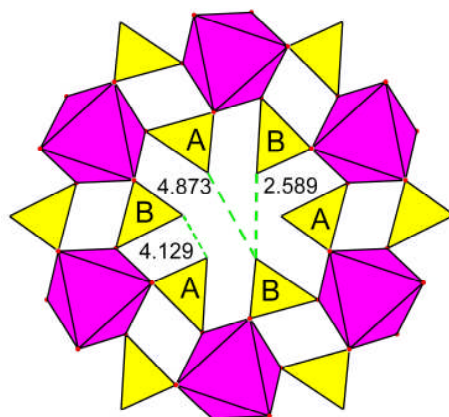


Figure 4.25: Representation of a single pore of structure **II**, highlighting the two different levels at which the phosphite pseudopyramids are situated (designated 'A' and 'B'), and also showing the distance between the hydrogen atoms of the phosphite groups

Each ScO_6 octahedra shares two coplanar and one apical oxygen with phosphite pseudo pyramids and face share the other two coplanar and one apical oxygen with another scandium octahedra, creating disordered Sc_2O_9 dimers, shown in figure 4.26.

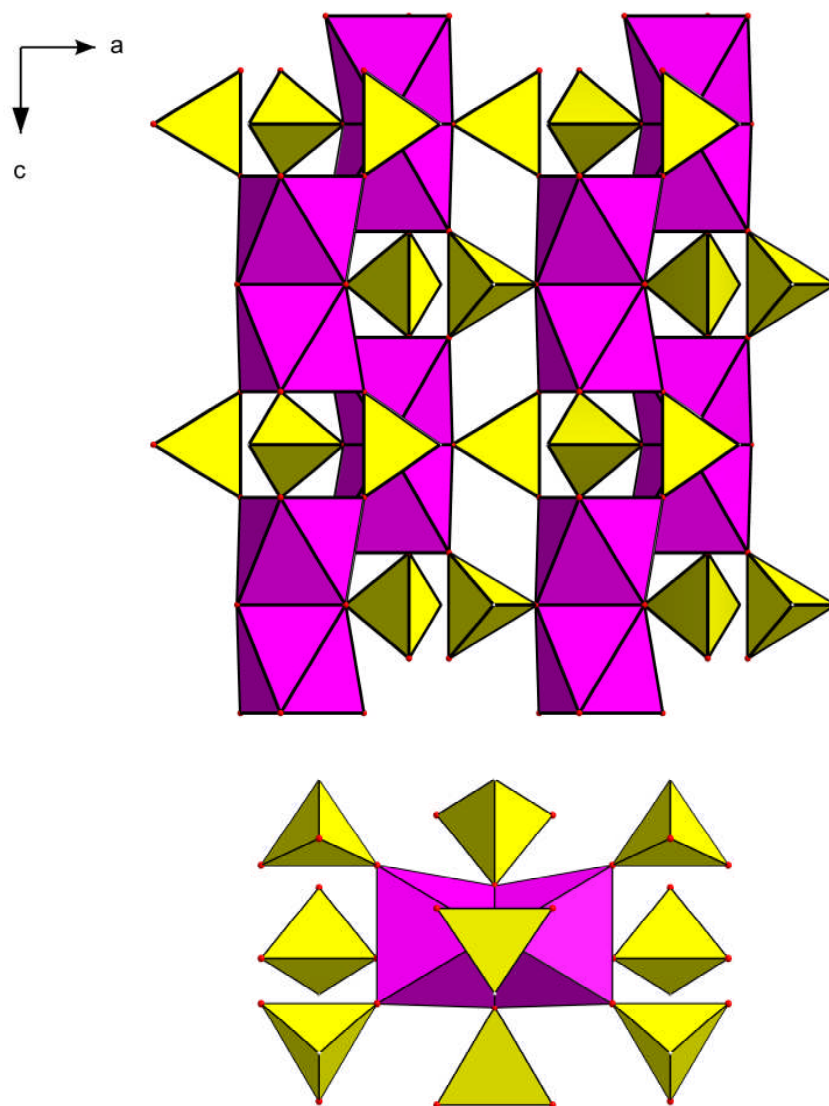


Figure 4.26: (top) Projection onto $[010]$ axis of structure **11**, showing the connectivity of the structure. (bottom) Illustration of the Sc_2O_9 units which act as building units for **11**. The dimer is viewed along the $[100]$ axis and a phosphite group has been removed to allow a clear view of the Sc_2O_9 face-sharing dimer.

$\text{Sc}_2(\text{HPO}_3)_3$ is isostructural to a scandium phosphite reported by Ewald *et al*¹³² which was synthesised as a by-product during investigations of the system Na–Sc–B–P–O(–H) under mild hydrothermal conditions. There are also isostructural aluminium, gallium¹³¹ and iron

phosphites¹³⁰ reported in the literature. The interatomic distances measured in this work agree with the values previously seen with Ewald's scandium phosphite and are slightly longer than those reported for the aluminium, gallium and iron (1.82(2) to 1.97(4)Å). The Sc—O bond distance range from 2.012(3) to 2.191(2)Å, whereas the P—O bonds involved in framework bonding range from 1.514(2) to 1.555(4)Å.

Solid state ³¹P MAS NMR (figure 4.27) gives a single peak at δ -11.27ppm, which is attributed to the single phosphorus site. ⁴⁵Sc MAS NMR (figure 4.28.) gives a single peak at 31.4ppm, again consistent with the one unique scandium site in the structure.

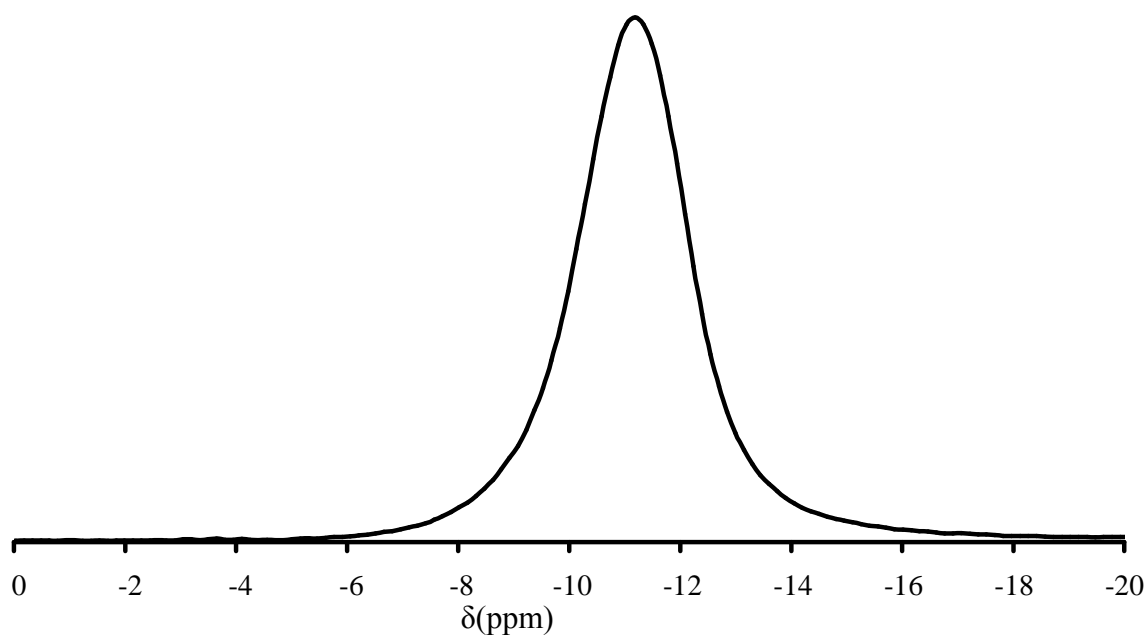


Figure 4.27: ³¹P MAS NMR for structure **11** showing a single resonance at -11.27ppm.

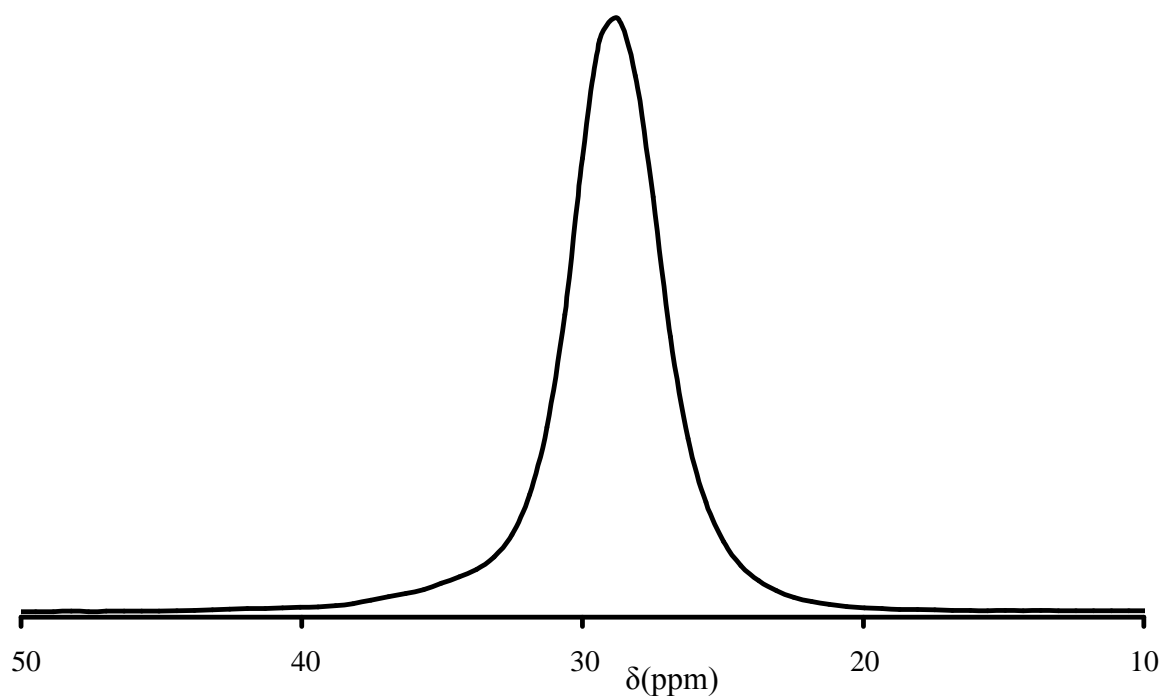


Figure 4.28: ^{45}Sc MAS NMR spectra for structure **11** showing a single resonance peak at 31.8 ppm.

4.4 Conclusions

The hydrothermal chemistry of scandium phosphites has been examined using amines, alkyl ammonium salts and alkali metal hydroxides as additives. It was thought that due to the reduced amount of oxygen atoms present in the phosphite pseudo pyramid, in comparison to the phosphate tetrahedra, there would be less opportunity for phosphite structures to be stabilised by hydrogen bonding networks, leading to the formation of structures which would remain intact after template removal.

Within the structures reported in this chapter only structure **10** is not a three dimensional framework material. Instead structure **10**, isostructural to the scandium phosphate structure (structure **3**), is a layered phosphite – phosphate structure which contains POH groups on the phosphate tetrahedra present in the structure to form a hydrogen bonding network between the template molecules and the layers. The formation of structure **10** indicates that there is a possibility for oxidation of the phosphoric acid to occur within the reaction conditions applied, which has been noted in other phosphite systems.

The other structures reported within this chapter are all fully-connected framework structures, indicating a potential route towards the synthesis of three dimensional porous scandium-bearing solids, i.e. reduce the ability for hydrogen bonding within the structure. However, the pore sizes are too small for adsorption of molecules, and these materials are more likely to be of interest as ionic conductors

Similar to chapter 3, the structures reported in this chapter show scandium occupying a variety of environments including isolated ScO_6 octahedra, $\text{Sc}_4\text{F}_4\text{O}_{16}$ tetramers and Sc_2O_9 dimers. The key SBUs within the phosphite structures reported in this chapter are shown in figure 4.29.

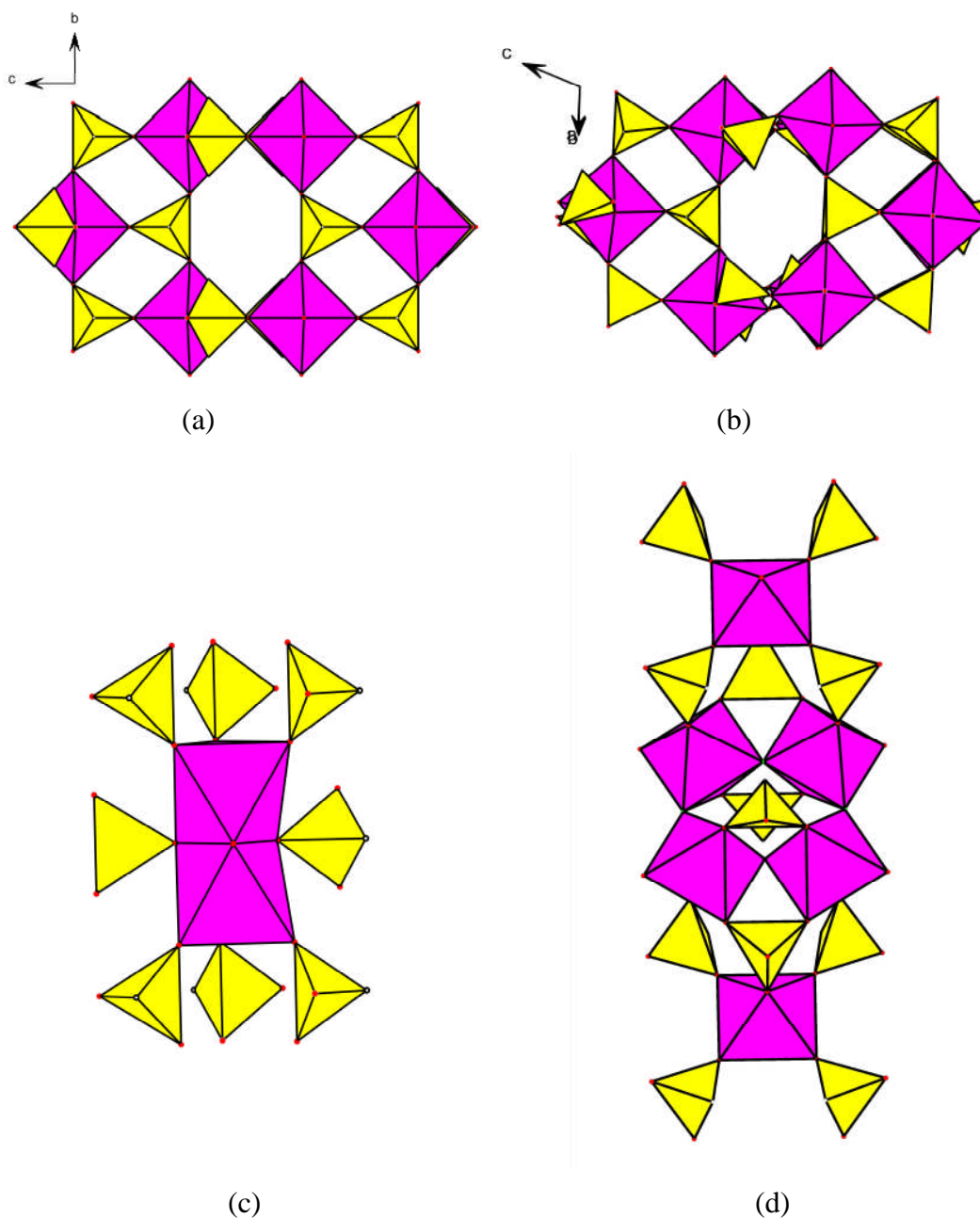


Figure 4.29: Secondary building units present within the scandium phosphite materials reported within this chapter. SBU's a – d are found within structures **8 - 11** respectively

As noted within the introduction to this chapter, the phosphite unit can be considered as the simplest member of the phosphonate family, PO_3R (where $\text{R} = \text{H}$). This led to the hypothesis that changing the functional group, R , to something other than hydrogen, could give stable, three dimensional structures without the addition of a templating agent and might then produce porous, thermally stable, scandium-bearing frameworks.

Chapter 5:

Scandium Phosphonates

5.1 Aims

Chapters 3 and 4 have shown scandium to be a versatile framework constituent of phosphate and phosphite systems. The structures described in previous chapters either lose their structural integrity upon removal of the organic template or possess pores too small for adsorption. The loss of structural integrity of organically templated phosphates is believed in part to be due to the breakdown of hydrogen bonding networks which exist between the phosphate oxygen atoms of the frameworks and the amine groups of the organic template as the organic is removed. Reducing the potential for the formation of hydrogen bonding networks by replacing PO_4 tetrahedra with HPO_3 pseudo pyramids tends to favour the formation of three dimensional scandium phosphite framework materials. Replacing the hydrogen atom of the phosphite pseudo pyramid with an organic moiety, (R), may result in the formation of microporous framework materials. The aim of this chapter is therefore to investigate the behaviour of the Sc^{3+} cation as a framework element within novel scandium phosphonate materials, aspiring to synthesise microporous and thermally stable phosphonates.

5.2 Introduction

The simplest member of the phosphonate family (RPO_3) is methyl phosphonate, where R is a methyl group, $-\text{CH}_3$. There has been significant research into the synthesis and structural behaviour of metal methylphosphonates in recent years, in particular of aluminium¹³⁹⁻¹⁴⁶ and gallium¹⁴⁷ methyl phosphonates.

During the mid-1990s, two aluminium phosphonate materials, $\text{AlMePO-}\alpha$ and $\text{AlMePO-}\beta$, reported by Maeda and co-workers were reported to have similar pore sizes to those of medium pore zeolites such as ZSM-5.^{140, 148, 149} The two phases are polymorphs, with the general composition $\text{Al}_2(\text{PO}_3\text{CH}_3)_3$, and possess one dimensional pore systems with a free diameter of *ca.* 6.5Å.

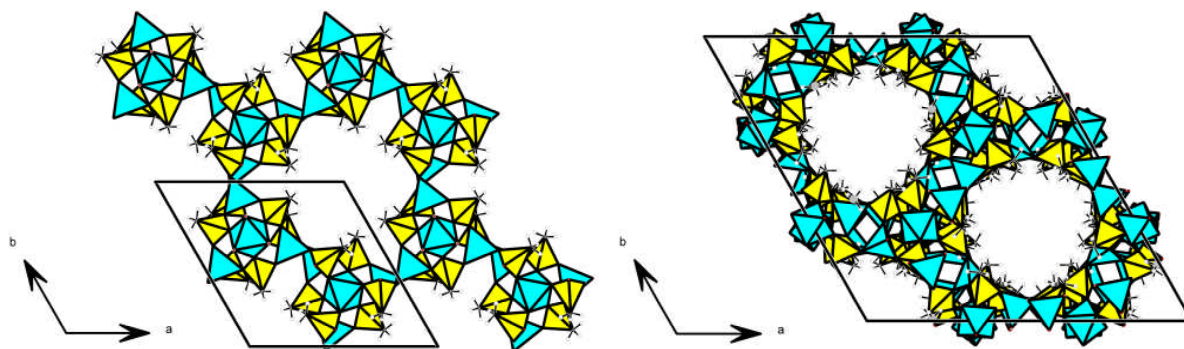


Figure 5.1: Projection down $[001]$ for α - and β -AlMePO (left and right images respectively)

These solids exhibit adsorption properties different to those of conventional zeolites owing to the methyl groups lining the pores, which make the pores hydrophobic, with both polymorphs exhibiting little water adsorption at low relative pressures.¹⁴⁸

The energy / temperature associated with breaking a P – C bond is known to be relatively high and consequently the use of phosphonic acids within the hydrothermal synthesis of materials is likely to produce thermally stable materials.¹⁵⁰ Unlike metal phosphate and phosphite systems, the use of organic species as structural directing agents is not essential to produce different framework architectures owing to the presence of the organic group on the phosphonic acid, which does not interact with charged amines. The framework geometries are more strongly determined by the coordination geometry of the phosphonate group and the tendency for organic and inorganic groups to arrange themselves into separate regions in the structure.

Recent studies into the reactions of N,N'-piperazinebismethylenephosphonic acid (H_4L), and 2-methyl-N,N'-piperazinebismethylenephosphonic acid (H_4L'), figure 5.2, with transition metals have led to the isolation and characterisation of several porous framework materials, which show great potential for adsorption.^{60, 67-69}

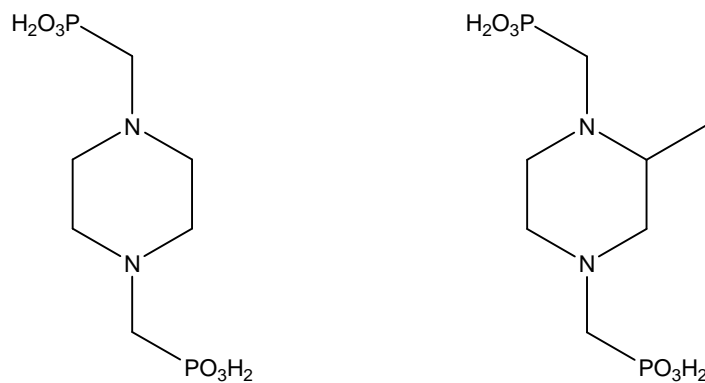


Figure 5.2: (left) *N,N'*-piperazinebismethylenephosphonic acid (H_4L) and (right) its racemic 2-methylated derivative (H_4L')

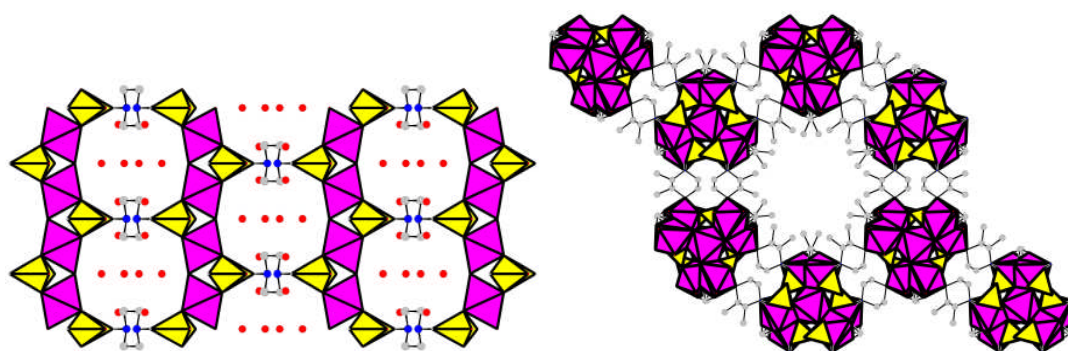


Figure 5.3: Two examples of structures which have been synthesised with the H_4L bisphosphonate ligand (MIL-91, $AlOH(H_2L).nH_2O$ or $TiO(H_2L).nH_2O$ where $n \approx 3$ or 4.5 respectively, left)⁶⁹ and the H_4L' 2-methylated derivative (cobalt bisphosphonate, $Co_4L'_{1.5}(CH_3CO_2)_{1.5}(OH,H_2O)_3$, right).⁶⁰ Note that the methyl group in the cobalt bisphosphonate can occupy one of two equivalent positions per group protruding into the pores

5.3 Experimental

A range of different phosphonic and bisphosphonic acids were used to investigate the resulting structural motifs of associated scandium phosphonate systems. Scandium phosphonate-based gels were prepared, examining a variety of reactant ratios, and treated hydrothermally over a range of times and temperatures. The reaction stoichiometries are listed in table 5.15, together with the phases formed. The structures are described throughout

this chapter. Syntheses were performed hydrothermally in 25 ml Teflon-lined Parr autoclaves using following reactants as required. Scandium oxide, was used as the scandium source in all structures reported in this chapter, unless stated otherwise, with HF or NaOH being added as required. Phosphonic acid used were methylphosphonic acid (Aldrich, 98%), ethylene bisphosphonic acid (Aldrich 99%), N,N'-piperazinebis-(methylenephosphonic acid) and N,N'-2-methylpiperazinebis(methylene-phosphonic acid), shown below in figure 5.4.

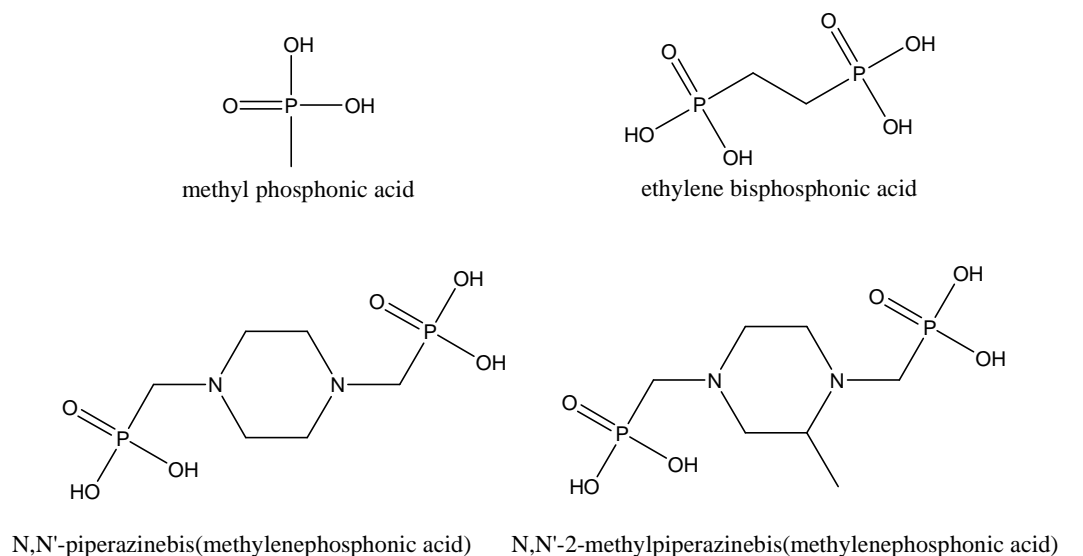


Figure 5.4: Schematic representation of the phosphonic acids discussed within the structures of this chapter

Both piperazine-based bisphosphonic acids were prepared via a modified Mannich¹⁵¹ type reaction. Piperazine (99%), phosphorous acid (98%), formaldehyde (37%, in solution) and hydrochloric acid (18%, in solution) were obtained from Fisher Scientific and used as received. Piperazine (0.1 mol) was mixed with phosphorous acid (0.2 mol) and 100cm³ of hydrochloric acid. Formaldehyde (0.4 mol) was added dropwise over one hour and the mixture was refluxed at 120°C. After 4 hours a white solid had precipitated which was filtered, washed and dried. Analysis was based on one HCl associated with the product. CHN analysis, weight %, measured: C, 23.27%, H, 5.51%, N, 8.81%. Calculated for C₆H₁₇N₂P₂O₆Cl: C, 23.20%, H, 5.52% and N 9.02%. The N,N'-2-methylpiperazinebis(methylenephosphonic acid) was kindly supplied by J. P. S. Mowat.

5.4 Results

The experimental program described gave rise to 7 crystalline scandium phosphonate-based materials. The crystal structures of four of these materials were fully solved and refined from single crystal diffraction data. One of the structures was partially solved from single crystal diffraction data, and then refined from powder diffraction data, with another two materials being solved and refined from powder diffraction data alone. The crystallographic information for each structure is listed in Tables 5.1 and 5.2.

The positions of the hydrogen atoms in these structures were located through a combination of valence bond sum calculations and Fourier mapping, with their positions being fixed to 0.98(1)Å for a C-H with $U_{\text{iso}}(\text{H})$ being 1.2 times the parent carbon atoms, 0.85(1)Å for a N-H bond with $U_{\text{iso}}(\text{H})$ being 1.5 times the parent nitrogen atom and 0.98(1)Å for a O-H bond with $U_{\text{iso}}(\text{H})$ being 1.5 equivalents of the parent oxygen atom.

Structures **12-15** and **17** were solved from single crystal data and structures **16** and **18** were solved by powder diffraction methods. Wherever possible, phase purity of bulk samples was confirmed by Rietveld refinement of structural (and instrumental) parameters against powder diffraction data. Rietveld refinement was performed with the GSAS program suite⁷⁵ using the atomic co-ordinates determined by the single crystal structure solution as a starting point. Instrumental parameters (background, zero-point, peak profile coefficients) and structural parameters (unit cell, atomic co-ordinates, thermal parameters) were refined, keeping constraints on the bond distances and angles. Close final fits to the observed data were achieved, with R_{wp} values between 6 and 12%, starting from structures determined from the single crystal experiments where ever possible. In order to characterise the materials further, TGA was performed and ⁴⁵Sc MAS NMR spectra measured for phase pure samples to determine the NMR properties of scandium in phosphonate frameworks. ⁴⁵Sc MAS NMR spectra are presented with the structures with the experimental conditions given in Chapter 2. Further analysis of ⁴⁵Sc NMR is given in chapter 7

Table 5.1: Crystallographic information for structures 12 - 15

		Structure 12	Structure 13	Structure 14	Structure 15
Empirical Formula		$\text{Al}_x\text{Sc}_{1-x}\text{Al}_3(\text{CH}_3\text{PO}_3)_6$	$\text{ScAl}_3(\text{PO}_3\text{CH}_3)_6$	$\text{ScF}(\text{H}_2\text{O})\text{CH}_3\text{PO}_3$	$\text{NaSc}(\text{CH}_3\text{PO}_3)_2 \cdot \text{H}_2\text{O}$
Formula Weight		310.93	546.63	145.0	264.97
Temperature (K)		123	123	93	298
Wavelength (Å)/ Diffractometer		0.71073 / Saturn	0.69901 / 9.8 SRS	0.71073 / Saturn	0.6325 / ID-31, ESRF, Grenoble
Crystal System / Space group		Trigonal / P 3 ₁ c	Monoclinic / P 2/c	Orthorhombic / P 2 ₁ 2 ₁ 2 ₁	Tetragonal / P 4 ₂ /n
Unit Cell Dimensions	a (Å)	14.1880(16)	17.285(4)	7.532(2)	17.7934(8)
	b (Å)	-	9.210(6)	8.081(3)	-
	c (Å)	8.7701(9)	16.507(3)	8.721(3)	5.38859(3)
	α (°)	-	-	-	-
	β (°)	-	110.71(8)	-	-
	γ (°)	-	-	-	-
Volume		1528.9(3)	2458.03(4)	530.8(3)	1706.81(2)
Z		6	4	4	8
Number of reflections		18908	9380	3156	973
Number of unique reflections		1770	6654	908	-
2θ range (°)		1.66 – 25.26	2.15 – 30.05	3.44 – 25.34	2-38
Variables / Restraints		105	314	82	38
R1 (I>2σI)		0.117	0.0957	0.0157	0.062
R1 (all data)		0.1195	0.1417	0.0169	0.082
Max., Min. difference in electron density (eÅ ⁻³)		1.09, -0.87	0.796, -1.520	0.264, -0.220	-

Table 5.2: Crystallographic information for structures **16 - 18**

	Structure 16	Structure 17	Structure 18
Empirical Formula	Sc(H ₂ O)Sc(H ₂ O) ₂ (CH ₃ PO ₃) ₃	Sc ₃ (O ₃ PC ₂ H ₄ PO ₃)- (HO ₃ PC ₂ H ₄ PO ₃ H) ₃ .H ₃ O	Sc ₂ (O ₃ PCH ₂ (NHC ₅ H ₁₀ NH)- CH ₂ PO ₃) ₃ 4H ₂ O
Formula Weight	425.97	443.36	326.67
Temperature (K)	150	123	273
Wavelength (Å)/ Diffractometer	0.8002 / ID31	0.69013 / Station 9.8 SRS	0.8002 / ID31
Crystal System / Space group	Monoclinic / I a	Rhombohedral / R $\bar{3}c$	Trigonal / P $\bar{3}$
Unit Cell Dimensions			
a (Å)	15.84964(10)	9.998(3)	16.0314(11)
b (Å)	9.42885(5)	-	-
c (Å)	10.02195(5)	46.935(11)	9.6921(8)
α (°)	-	-	-
β (°)	102.0372(3)	-	-
γ (°)	-	-	-
Volume	1464.79(2)	4063.1(1)	2157.21(34)
Z	4	12	6
Number of reflections	15990	12415	4250
Number of unique reflections	201	1384	1169
2θ range (°)	5 – 38	2.51 – 30.87	5.0 – 90.0
Variables / Restraints	67	68	59
R1 (I>2σI)	0.0514	0.2113	0.0487
R1 (all data)	0.0673	0.2184	0.0763
Max., Min. difference in electron density (eÅ ⁻³)	-	3.028, -3.650	-
Max., mean shift/su	0.08 / 0.00	-	0.05 / 0.01

5.4.1 Mixed scandium / aluminium methyl phosphonates

Isovalent substitution of scandium into well known phosphonate framework materials was chosen as a suitable starting point for the synthesis of scandium-bearing phosphonate frameworks. Amongst the most studied phosphonate materials are α and β -AlMePO, which were first synthesized by Maeda *et al.* The ' α ' and ' β ' phases are closely related, mixed coordination, microporous framework materials, and both contain aluminium in tetrahedral and octahedral sites. Experiments were performed in an attempt to replace the aluminium cation occupying the octahedral site by scandium. As aluminium sites within both α and β -AlMePO, are in a ratio of 1:3 (octahedral : tetrahedral), the scandium to aluminium ratio in the reaction must be 1:3 to allow all octahedral aluminium sites to be replaced by scandium. Reactions were based on the conditions reported for the synthesis for AlMePO- β , modified to include scandium within the preparation.

Table 5.3: Reaction conditions employed to substitute scandium into α and β AlMePO's

Al(OH) ₃	Sc ₂ O ₃	Sc(NO ₃) ₃	Theoretical Al _{oct} replaced by Sc	Phase formed
1	0.167	-	100	Structure 12
1	-	0.33	100	Structure 13
1	-	-	-	AlMePO- β

Methylphosphonic acid, aluminium hydroxide, scandium oxide, 1,4-dioxane and water were mixed together, in the molar ratio 1.5 : 1 : 0.167 : 0.5 : 40, using a magnetic stirrer at room temperature until the gel was homogeneous. Using Sc(NO₃)₃ as the scandium source, the ratio was 1.5 : 1 : 0.33 : 0.5 : 40. The gel was then placed in a PTFE-lined stainless steel acid digestion bomb (Parr type, 23ml) and placed in a 160°C oven for 48h. The resultant product was filtered and dried in air at 60°C overnight. Single crystals were selected for EDX analysis in order to confirm the presence of scandium within the sample.

The x-ray diffraction patterns are shown below (figure 5.5). Straightforward inclusion of scandium oxide gives a mixture of phases, including AlMePO- α and AlMePO- β , but also with at least one other, with a main peak at 10° 2 θ . EDX on the powder indicates that all the single crystals contain both scandium and aluminium; with ratios of $\frac{Sc}{Sc + Al}$ in the range of 0.11 to 0.34. X-ray diffraction on a single crystal of the mixture indicates that it is AlMePO- α (structure **12**).

It is clearly shown that the use of scandium nitrate in the synthesis instead of scandium oxide results in the formation of a different phase. Scandium oxide is relatively insoluble in water whereas scandium nitrate is very soluble, so the synthesis using scandium oxide would have a lower concentration of Sc^{3+} cations in solution at the beginning of the hydrothermal reaction, whereas those reactions containing scandium nitrate would have all the starting materials in solution prior to hydrothermal treatment.

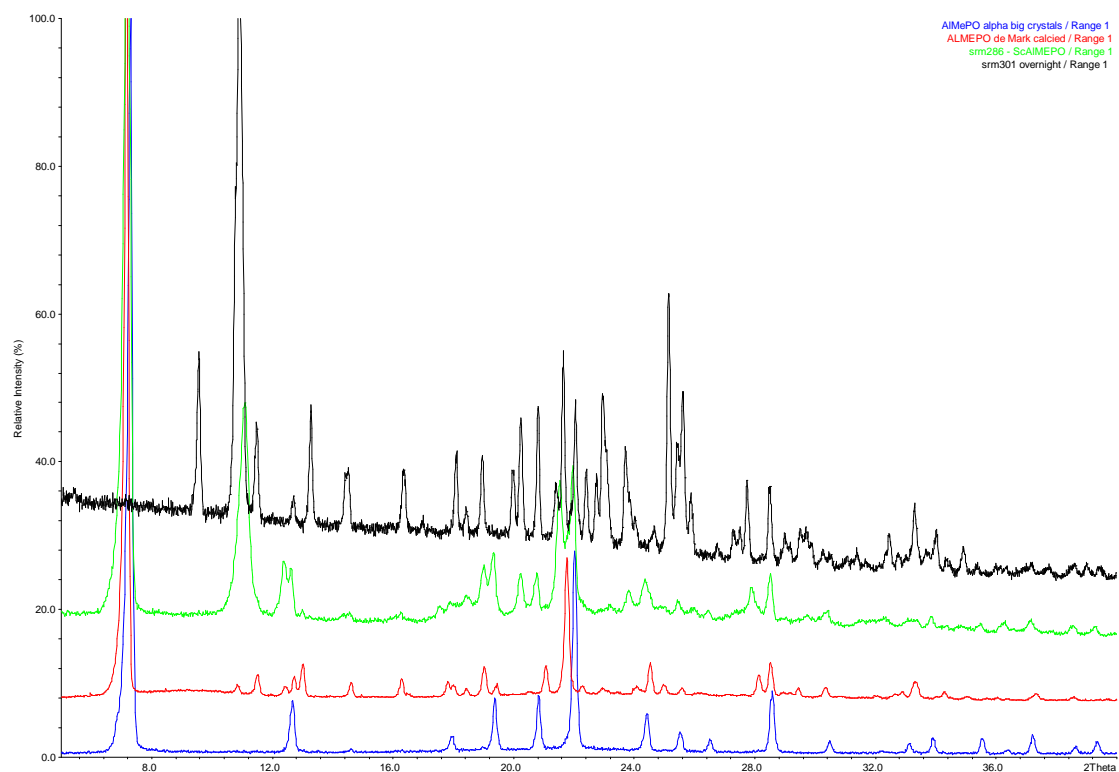
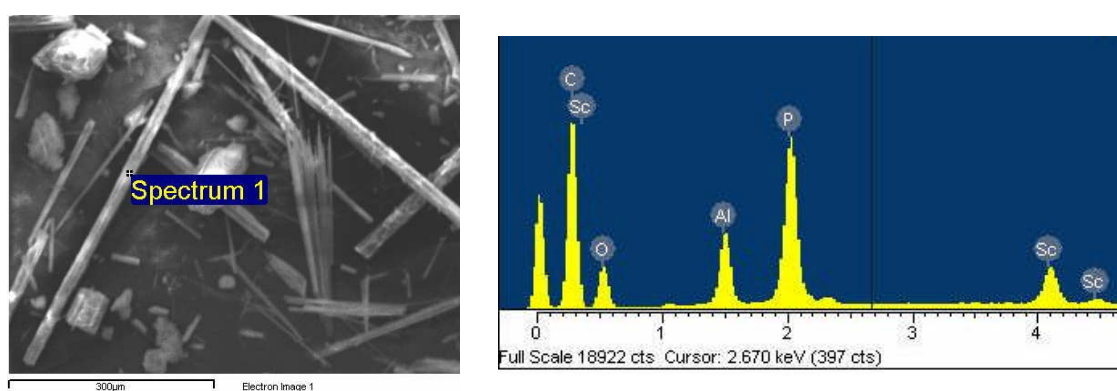


Figure 5.5: Powder X-ray diffraction patterns for the products of mixed aluminium / scandium methyl phosphonate preparations, compared with the known patterns of: AlMePO- α ; (blue trace); AlMePO- β (red trace); preparation including scandium from scandium oxide (green trace); preparation including scandium from scandium nitrate (black trace).

5.4.2 $\text{Al}_{1-x}\text{Sc}_x\text{Al}_3(\text{CH}_3\text{PO}_3)_6$ – Structure 12

Structure **12**, $\text{Al}_{1-x}\text{Sc}_x\text{Al}_3(\text{CH}_3\text{PO}_3)_6$, was prepared using reactions conditions outlined by Gonzalez *et al.*,¹⁵² as discussed above.

EDX analysis for structure **12**, figure 5.6, confirms the presence of scandium and aluminium within the same needle-like hexagonal crystals, which are assumed to be the phase discussed within this text. The ratio of scandium to aluminium within the sample calculated by the energy dispersive x-ray analysis are in very close agreement with those predicted by the single crystal analysis of a crystal from the product.



Element	Atomic%
Phosphorous	59.5
Aluminium	34.1
Scandium	6.4

Figure 5.6: Scanning electron microscope image of structure **12**, showing hexagonal needle-like crystals. EDX analysis of the crystals confirm a scandium : aluminium ratio close to that which was estimated from single crystal analysis.

A comparison of the unit cell parameters obtained in the analysis of the selected single crystal (structure **12**) with those of $\text{AlMePO-}\alpha$ and $\text{AlMePO-}\beta$, clearly indicates that phase analysed is the α -polymorph, with the larger cell dimensions including substitution of $\text{Al}^{3+}_{(\text{oct})}$ ($r = 0.67\text{\AA}$) with the larger $\text{Sc}^{3+}_{(\text{oct})}$ ($r = 0.88\text{\AA}$)

Table 5.4: Comparison of the unit cells for AlMePO- α and AlMePO- β with that of structure **11**, which is close to that of α -AlMePO.

Material	Unit cell Parameters			Spacegroup
	a (Å)	b (Å)	c (Å)	
AlMePO- α	13.9949(13)	13.9949(13)	8.5311(16)	P 3 ₁ c
AlMePO- β	24.650(2)	24.650(2)	25.299(5)	R 3c
Structure 12	14.1880(16)	14.1880(16)	8.7701(9)	P 3 ₁ c

Structure **12** was solved by direct methods and Fourier syntheses, using the SHELXS program⁸¹, from laboratory single crystal X-ray data collected on a small crystal, the crystallographic information is outlined in table 5.1. Atomic co-ordinates for structure **12** are given in table 5.4

Table 5.5: Atomic co-ordinates for structure **12**, formula Sc_{0.7}Al_{1.3}.

Atom	x	y	z	Occ	Uiso	Multiplicity
Sc(1)	0.6667	0.3333	0.6049(5)	0.64	0.0354(18)	2
Al(1)	0.6667	0.3333	0.6049(5)	0.36	0.0354(18)	2
Al(2)	0.4907(4)	0.3917(4)	1.0368(5)	1	0.0439(12)	6
P(1)	0.3478(3)	0.4740(3)	0.8877(4)	1	0.0353(10)	6
P(2)	0.7169(3)	0.5313(3)	0.8806(4)	1	0.0364(9)	6
O(1)	0.7063(11)	0.4677(10)	0.7416(13)	1	0.065(4)	6
O(2)	0.3796(10)	0.5759(10)	0.9698(14)	1	0.057(3)	6
O(3)	0.3821(11)	0.4026(11)	0.9768(14)	1	0.067(4)	6
O(4)	0.6093(11)	0.4934(11)	0.9584(17)	1	0.069(4)	6
O(5)	0.4015(11)	0.4992(12)	0.7285(14)	1	0.064(4)	6
O(6)	0.4656(18)	0.2585(14)	0.9940(16)	1	0.098(6)	6
C(1)	0.2053(18)	0.3921(14)	0.867(2)	1	0.065(5)	6
C(2)	0.760(3)	0.662(3)	0.815(4)	1	0.126(12)	6

Both scandium and aluminium were refined on the octahedral site within the structure, with their occupancies allowed to refine, while their sum was constrained to sum to 1.0, and their displacement parameters were constrained each other, *i.e.* $U_{\text{iso}}(\text{Sc}(1)) = U_{\text{iso}}(\text{Al}(1))$. The occupancy refined to suggest that approximately 64% of the octahedral site is occupied by scandium. The high degree of scandium occupancy in the octahedral site is confirmed by the

M-O bond lengths which surround the octahedral site, ($M-O \approx 2.07\text{\AA}$, which is a typical value for a Sc-O (2.05\AA) bond, in comparison to approximately 1.8\AA for an octahedral Al-O bond.

Structure **12** is a fully connected, porous, framework material, comprising of alternating metal / phosphonate polyhedral units, figure 5.7. The connectivity scheme along the *c*-axis can be represented by pillars of $[-M-O-P-O-Al-O-P-O-]$, where M represents an octahedral metal position which can be occupied by scandium or aluminium, with the pillars being connected with a ‘crankshaft-like’ aluminium phosphonate chain, shown in figure 5.8.

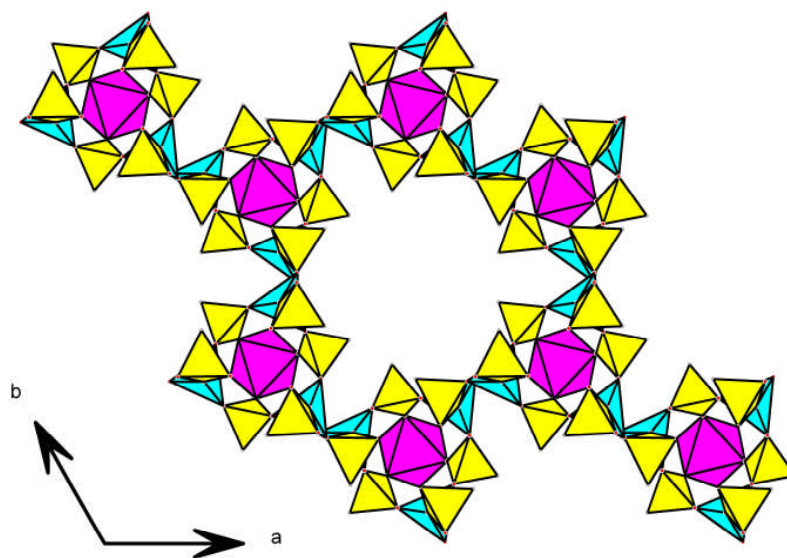


Figure 5.7: Projection down $[001]$ of structure **12**, showing

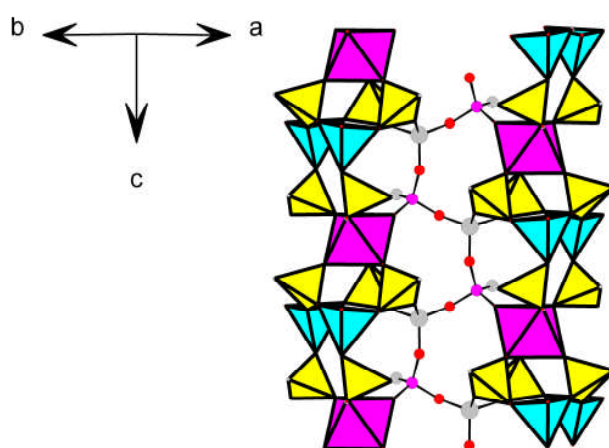


Figure 5.8: Representation of the connectivity scheme present within structure **12**, showing columns of isolated ‘M’ octahedra which are separated by aluminium and methyl phosphonate tetrahedra and connected through a ‘crankshaft-like’ aluminium / phosphonate chain

Substituting scandium into the octahedral metal sites within the AlMePO- α structure results in a slightly larger free pore diameter when compared to the pure aluminium AlMePO- α , details of both are given in figure 5.9 and table 5.6. The larger pore aperture is due to the difference in M – O bond distances, and could result in slightly different adsorption properties and selectivities.

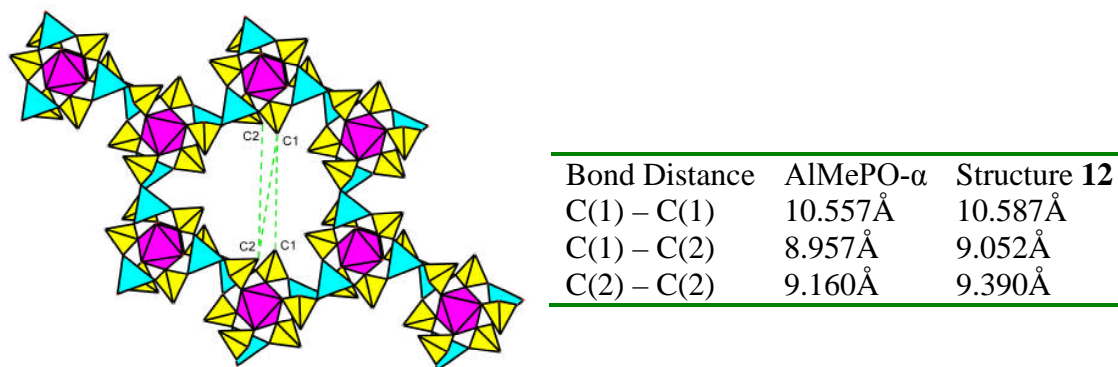


Figure 5.9 and table 5.6: Projection down [001] of the AlMePO- α , showing distances across the pore, the values for which are given in table 5.6. (right).

The ^{45}Sc MAS NMR spectra for structure **12** shows one very narrow line at -14.3ppm and a very broad resonance at 20.3ppm, the latter of which is only just detected in an MQMAS experiment, however only two independent species can be found, figure 5.11. The sharper resonance, which is determined from MQMAS to have an isotropic chemical shift of -13.9ppm is attributed to scandium substitution in the octahedral sites of AlMePO- α and AlMePO- β structures.

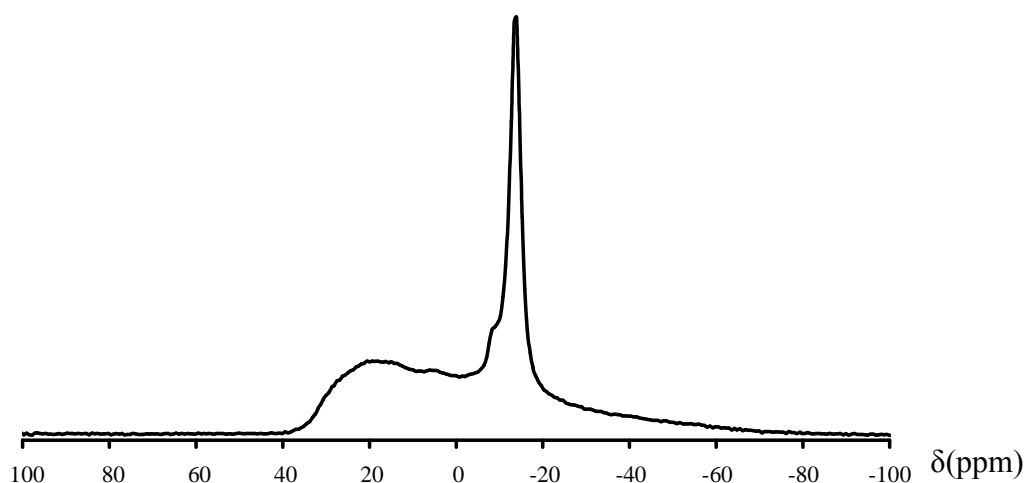


Figure 5.10: ^{45}Sc MAS NMR spectra for structure **12**, showing a very sharp resonance at -14.3ppm and a broad resonance at 20.3ppm

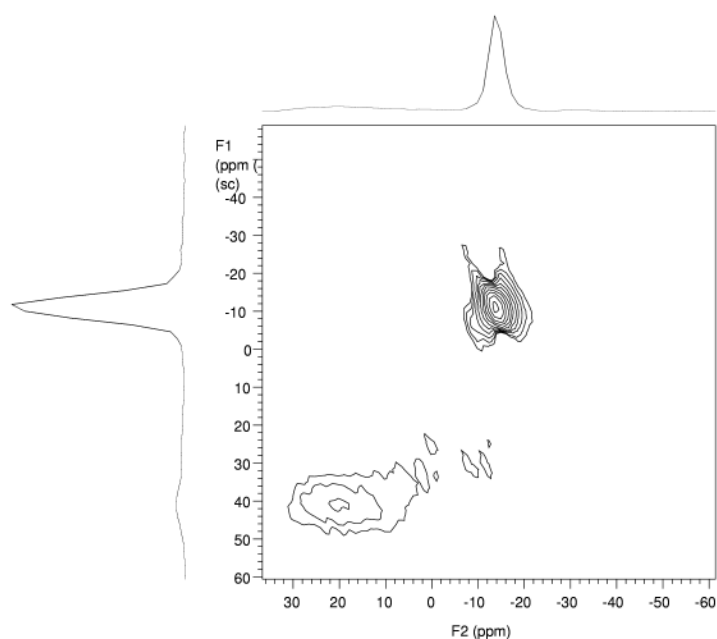


Figure 5.11: MQMAS spectra for structure **12** showing that there are only two independent resonances within the spectrum.

When the AlMePO- β synthesis was modified to include scandium nitrate instead of scandium oxide, with the objective of replacing all octahedral aluminium sites within the AlMePO framework, a new phase was prepared, and neither AlMePO- α or AlMePO- β crystallised. This new phase was prepared as small crystals suitable for microcrystal diffraction at the synchrotron radiation source, and solved as described below.

To determine whether formation of this new material resulted from the presence of scandium, or whether the use of nitrate ions within the synthetic preparation was more important, experiments were performed in which aluminium nitrate was added in the same stoichiometry as scandium nitrate while keeping all other conditions the same. In this case the crystallising phase was identified as the layered phase $\text{Al}(\text{OH})\text{CH}_3\text{PO}_3$ indicating that both the metal source and type influence the crystallisation behaviour in this system.¹⁵³

5.4.3 $\text{ScAl}_3(\text{PO}_3\text{CH}_3)_6$ - Structure 13

Structure **13**, $\text{ScAl}_3(\text{PO}_3\text{CH}_3)_6$, was solved by direct methods and Fourier syntheses, using the SHELXS program⁸¹, from single crystal X-ray diffraction data collected on station 9.8 at the synchrotron radiation facility, Daresbury. The crystallographic information is outlined in table 5.1, with the atomic co-ordinates for structure **13** being listed in table 5.7

Table 5.7: Atomic coordinates for structure **13**

Atom	x	y	z	Occ	Uiso	Multiplicity
Sc(1)	-0.22270(8)	0.36484(13)	-0.34450(7)	1	0.0221(3)	4
Al(2)	-0.20099(13)	-0.1619(2)	-0.10118(11)	1	0.0241(4)	4
Al(3A)	-0.4222(2)	0.4675(4)	-0.0523(2)	0.5	0.0233(7)	4
Al(3B)	-0.4135(3)	0.4704(4)	-0.1219(2)	0.5	0.0247(8)	4
Al(4)	-0.18087(13)	0.8797(2)	-0.35399(11)	1	0.0256(5)	4
P(1)	-0.25397(11)	0.64940(19)	-0.49770(9)	1	0.0243(4)	4
P(2)	-0.12188(11)	0.64530(19)	-0.20929(10)	1	0.0252(4)	4
P(3)	-0.25565(11)	0.06442(19)	-0.24748(10)	1	0.0244(4)	4
P(4)	-0.09121(10)	0.15041(19)	-0.40205(9)	1	0.0232(4)	4
P(5)	-0.34679(10)	0.22053(19)	-0.53653(9)	1	0.0239(4)	4
P(6A)	-0.4087(2)	0.5127(4)	-0.3612(2)	0.5	0.0256(7)	4
P(6B)	-0.4019(2)	0.4965(4)	-0.3087(2)	0.5	0.0246(6)	4
O(1)	-0.2365(3)	0.5265(6)	-0.4350(3)	1	0.0351(12)	4
O(2)	-0.2346(3)	0.7967(6)	-0.4527(3)	1	0.0338(12)	4
O(3)	-0.1204(3)	0.7572(5)	-0.2774(3)	1	0.0292(11)	4
O(4)	-0.2537(3)	-0.0485(5)	-0.3149(3)	1	0.0301(11)	4
O(5)	-0.2133(3)	0.2030(5)	-0.2565(3)	1	0.0264(10)	4
O(6)	-0.2128(3)	0.0012(5)	-0.1562(3)	1	0.0326(12)	4
O(7)	-0.1756(3)	0.7033(5)	-0.1603(3)	1	0.0323(11)	4
O(8)	-0.1520(3)	0.5002(5)	-0.2471(3)	1	0.0312(11)	4
O(9)	-0.1237(3)	0.1449(6)	-0.5018(3)	1	0.0339(12)	4
O(10)	-0.2959(3)	0.2039(7)	-0.5944(3)	1	0.0391(13)	4
O(11)	-0.1148(3)	0.0085(6)	-0.3685(3)	1	0.0347(12)	4
O(12)	-0.1206(3)	0.2808(5)	-0.3678(3)	1	0.0291(10)	4
O(13)	-0.2943(3)	0.2263(6)	-0.4426(3)	1	0.0335(12)	4
O(14)	-0.4009(3)	0.3536(6)	-0.5685(3)	1	0.0363(12)	4
O(15)	-0.4840(3)	0.4279(5)	-0.3603(3)	1	0.0335(12)	4
O(16A)	-0.4307(6)	0.5670(12)	-0.4530(6)	0.5	0.032(2)	4
O(16B)	-0.3913(7)	0.4744(15)	-0.2137(6)	0.5	0.041(3)	4
O(17)	-0.3316(3)	0.4262(6)	-0.3295(3)	1	0.0367(12)	4
O(18)	-0.3452(3)	0.6514(6)	-0.5583(3)	1	0.0332(12)	4
C(1)	-0.1928(5)	0.6330(9)	-0.5628(4)	1	0.0381(18)	4
C(2)	-0.0201(5)	0.6298(10)	-0.1331(5)	1	0.044(2)	4
C(3)	-0.3609(5)	0.0938(9)	-0.2635(6)	1	0.0413(19)	4
C(4)	0.0183(5)	0.1542(10)	-0.3688(5)	1	0.0385(18)	4
C(5)	-0.4144(5)	0.0668(9)	-0.5555(6)	1	0.046(2)	4
C(6)	-0.4004(6)	0.6802(11)	-0.3085(9)	1	0.071(4)	4

Structure **13**, $\text{ScAl}_3(\text{PO}_3\text{CH}_3)_6$, presents a novel layered scandium aluminium methylphosphonate material, figure 5.12. The metal to phosphorus ratio within the layers is observed as being 2:3, the same ratios as observed with the AlMePO- α and AlMePO- β

structures. The scandium to aluminium ratio is 1:3, which is the same ratio that would be present in the idealised $\text{ScAl}_3(\text{CH}_3\text{PO})_6$ - α and - β structures. This gives a scandium to phosphorus ratio of 1:6 and aluminium to phosphorus ratio of 1:2.

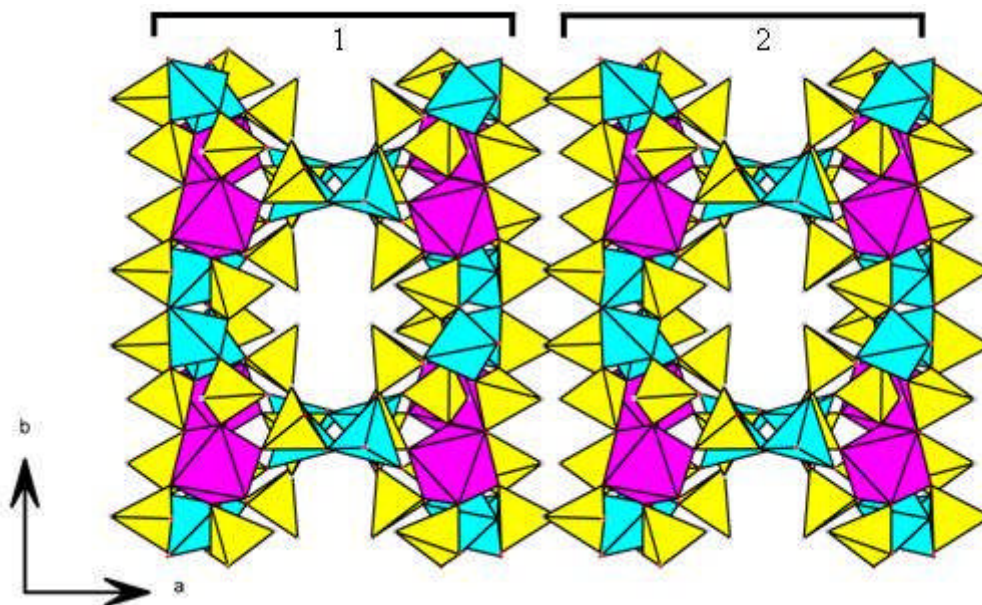


Figure 5.12: Projection down [001] of structure 13, showing two ‘double-sheet’ scandium-aluminium methylphosphonate layers (‘1’ and ‘2’), which are separated by the methylphosphonate tetrahedral units with methyl groups pointing towards each other. Hydrogen atoms have been omitted for clarity.

The ‘double-sheet’ layers are composed of $\text{ScAl}_3(\text{PO}_3\text{CH}_3)_6$ which are linked to create ‘dimeric’ building units, figure 5.13.

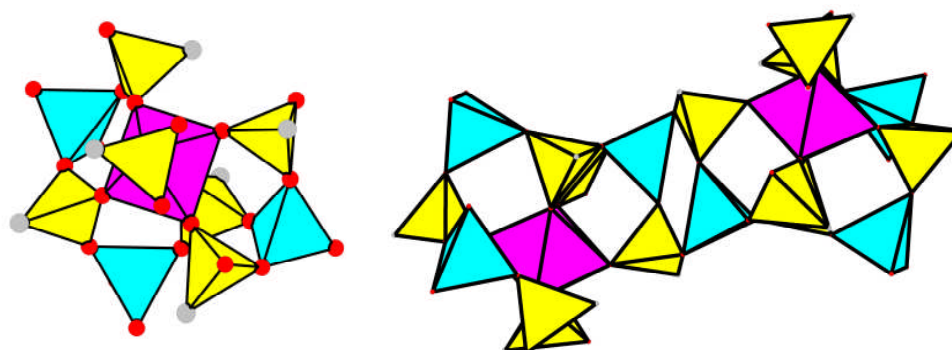


Figure 5.13: (left) $\text{ScAl}_3(\text{PO}_3\text{CH}_3)_6$ building units showing the oxygen and carbon atoms as large red and grey spheres respectively. (Right): Dimeric building units.

The dimeric building units are stacked along the c -axis through corner-sharing tetrahedrally coordinated aluminium to give chains. Each aluminium atom is connected to four phosphonate groups.

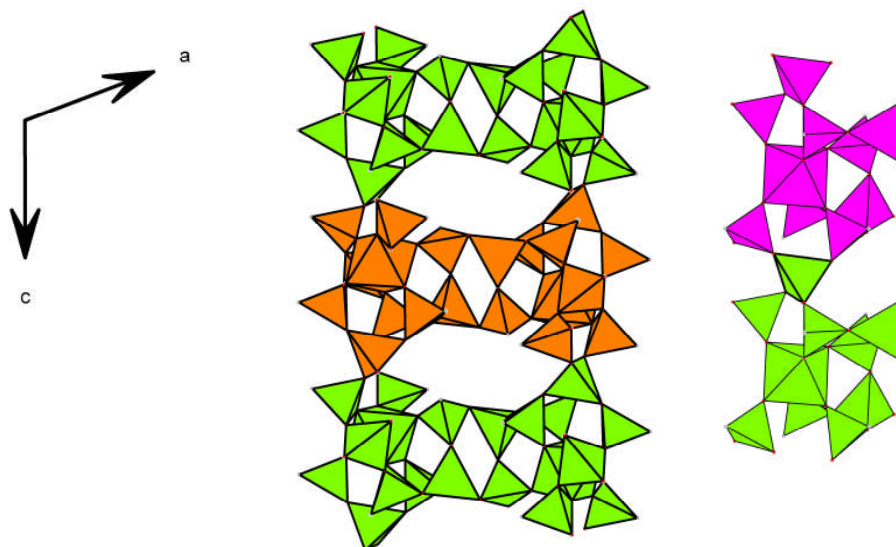


Figure 5.14: (Left) Stacking of dimeric building units shown in figure 5.13. (Right) Stacking of building units along the c -axis, highlighting the aluminium tetraheda (outlined in bold) through which the building units are connected.

Within the overall framework structure, there is a disorder of aluminium and phosphorus over two sites, Al(3A) and (3B) and P(6A) and (6B). This disorder results in different possible ways in which the framework within the layers can be arranged. The first manner in which the disorder of the aluminium and phosphorus can be modelled is having a ‘crankshaft-like’ connectivity, shown in figure 5.15. This again leads to two different modelling schemes, which are shown. The different schemes results in two different local environment for the scandium atom, with the Sc – P(6A) and (6B) and Sc – Al(3A) and (3B) distances varying depending upon whether the ‘A’ or ‘B’ atoms are present. Table 5.8 lists the different distances between the scandium atoms and the disordered aluminium and phosphorus atoms. The disorder can also be modelled from the crystallographic structure using an ‘interrupted’ modelling scheme, in which the Al(3) and P(3) tetrahedra are connected in such a way that they form 4MRs, instead of a continual ‘crankshaft’. The local environment of the scandium atom is affected in a similar manner to that possible with the ‘crankshaft-like’ connectivity scheme.

Table 5.8: Selected bond distances within structure 13

Atoms	Distance (Å)
Sc – Al(3A)	4.204
Sc – Al (3B)	4.844
Sc – P(6A)	3.412
Sc – P(6B)	3.565

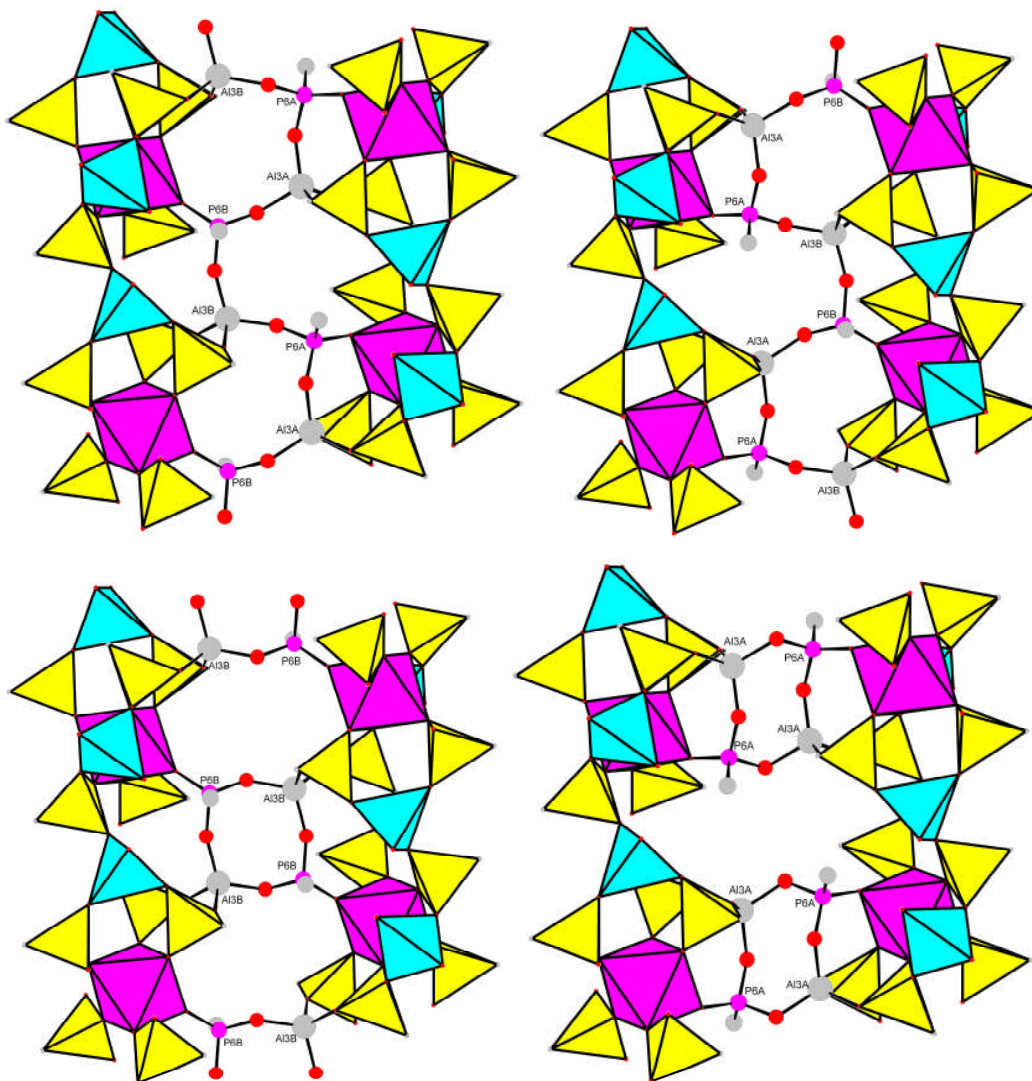


Figure 5.15: Different modelling representations of the disorder within structure 13. The top images show the two different ways the disorder can be modelled using a continual chain between Al(3) and P(6) atoms. The bottom two images show the formations of 4MRs to model the disorder.

Owing to a combination of the 6 independent phosphorus sites within structure **13** and the disorder present within the framework, the ^{31}P MAS NMR shows seven peaks at 17.8, 15.4, 13.4, 12.3, 9.2, 6.4 and 0.7 ppm which can be deconvoluted into 13 independent ^{31}P signals.

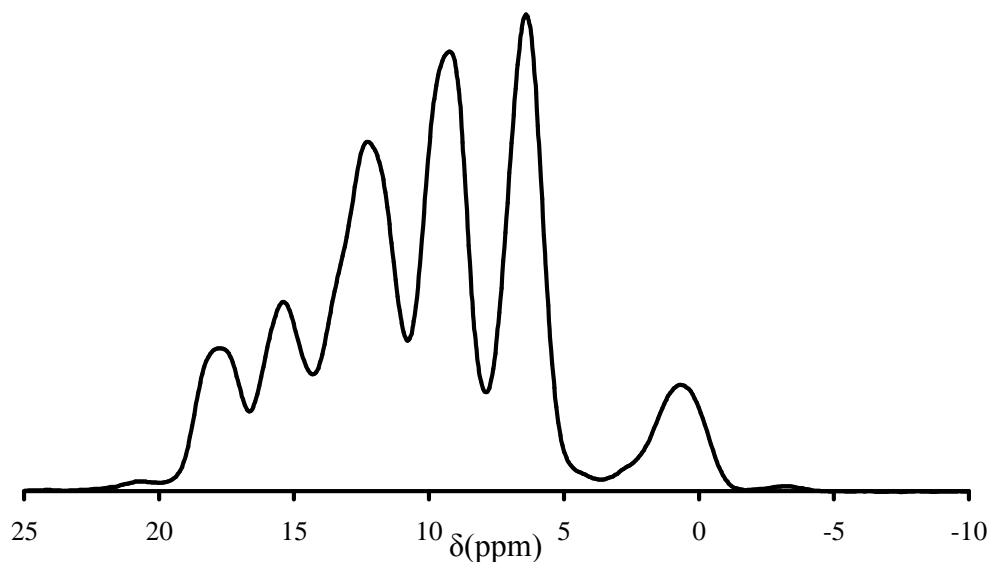


Figure 5.16: ^{31}P MAS NMR spectra for structure **13**, showing seven peaks at 17.8, 15.4, 13.4, 12.3, 9.2, 6.4 and 0.7 ppm.

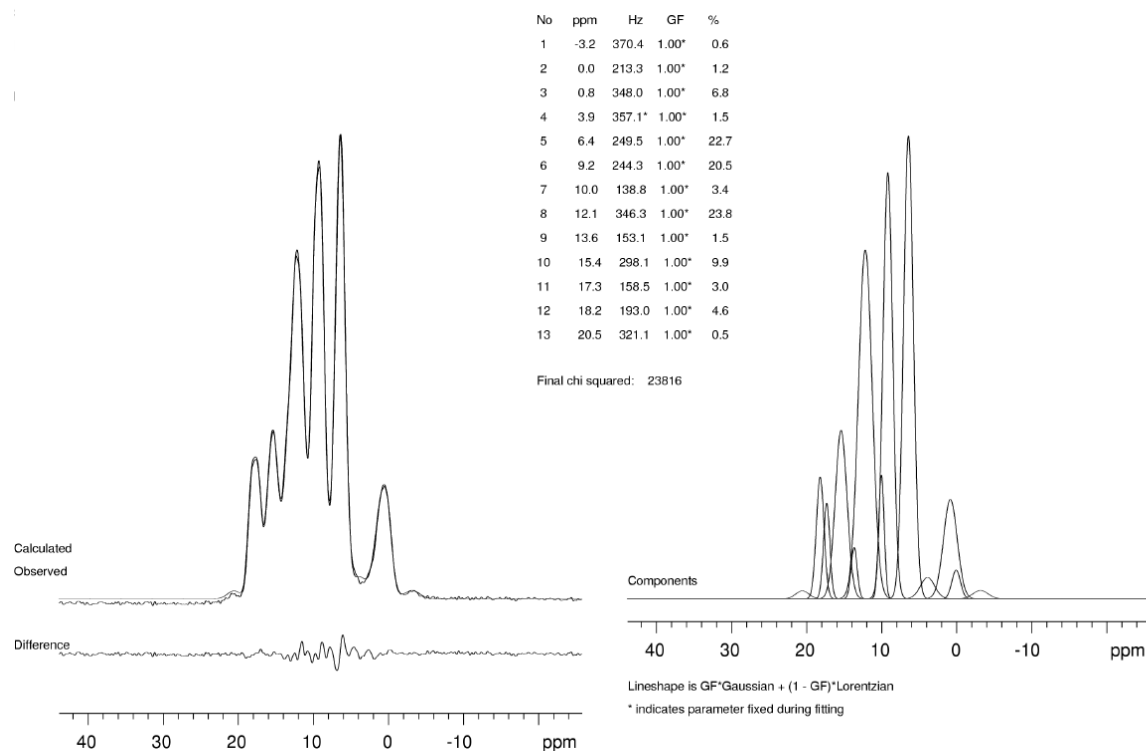


Figure 5.17: ^{31}P MAS NMR spectra for structure **13**, showing deconvolution into 13 different signals.

^{45}Sc MAS NMR gives an intense signal with two peaks at -5.8 and -14.8ppm (figure 5.19) which can be clearly resolved in the MQMAS experiment as they have different isotropic chemical shifts and therefore result from different scandium environments (figure 5.20). As there is only one crystallographically unique scandium site located via single crystal investigations, it is believed that the disorder of Al(3) and P(6), discussed previously, is responsible for the different chemical shifts. In particular it is likely that the configuration of aluminium in the second coordination shell of scandium is important here, figure 5.18 gives the possible positions of aluminium sites in relation to the octahedral scandium site.

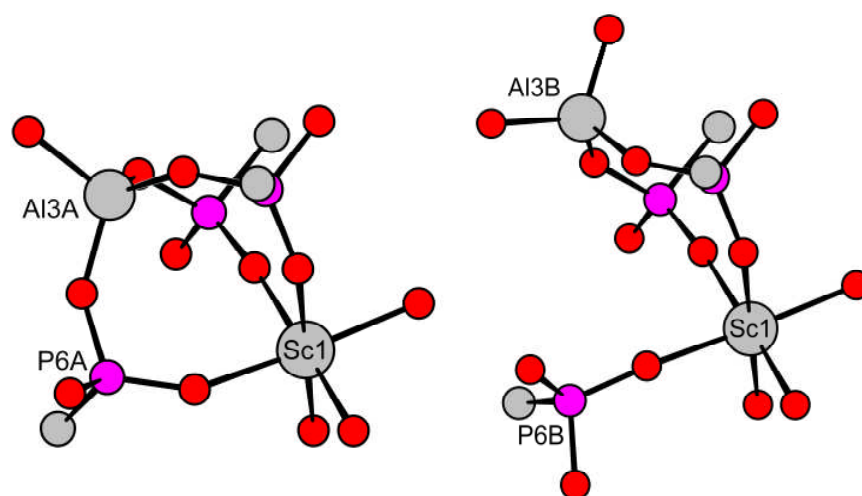


Figure 5.18: Representation of the possible local environment of the only crystallographically unique scandium site within structure **13**, showing Al(3) and P(6) disordered over two sites (A and B).

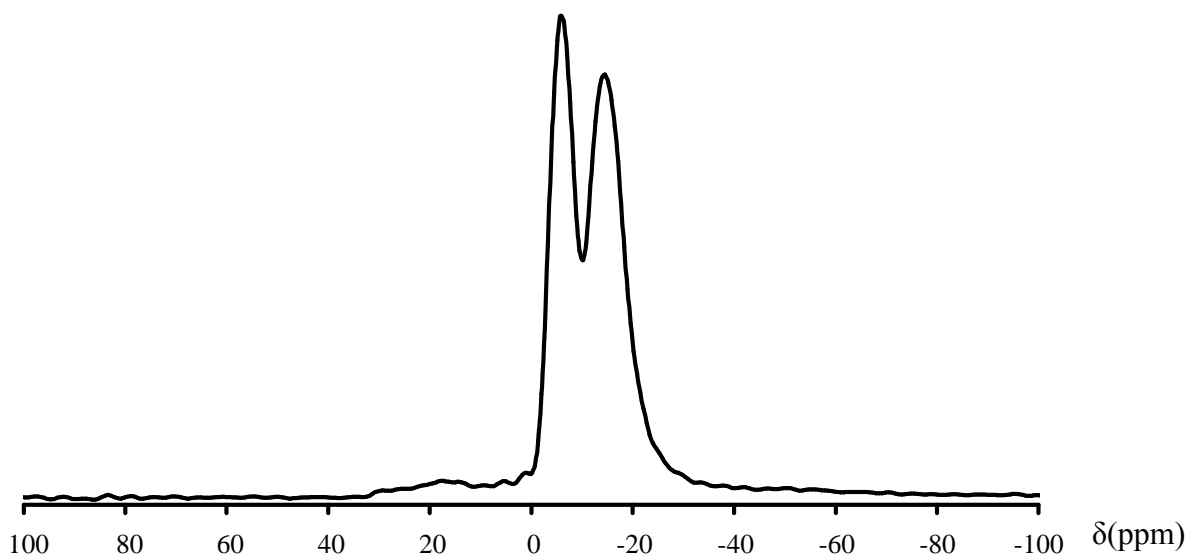


Figure 5.19: ^{45}Sc MAS NMR spectra for structure **13**, showing 2 distinct peaks at -5.8 and -14.8ppm. Although there is only one crystallographically unique scandium position within the structure, the ^{45}Sc MAS NMR is affected by the disorder in $P(6)$ and $\text{Al}(3)$

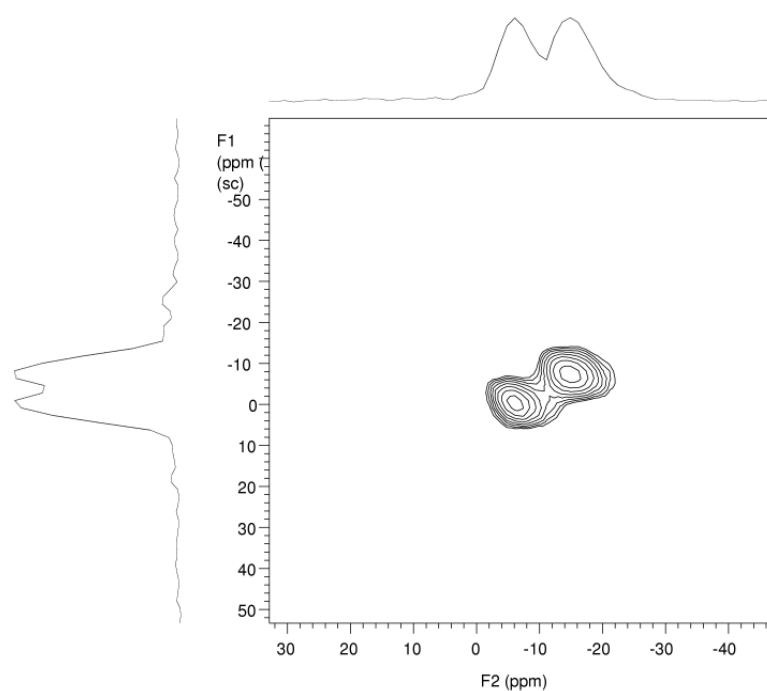


Figure 5.20: ^{45}Sc MQMAS NMR spectra for structure **13** clearly shows that the 2 peaks shown in figure 5.19 can be separated into different scandium sites, which can be rationalized by the disorder within the structure.

^{27}Al MAS NMR for structure **13**, shows an intense signal at 40.5ppm which is believed to be from the tetrahedrally coordinated aluminium present within the layers. There is also a small

signal at -21.5ppm which suggests the presence of a small amount of octahedrally coordinated aluminium, indicating that a very small amount of the octahedral sites within the layers may be occupied by aluminium instead of scandium.

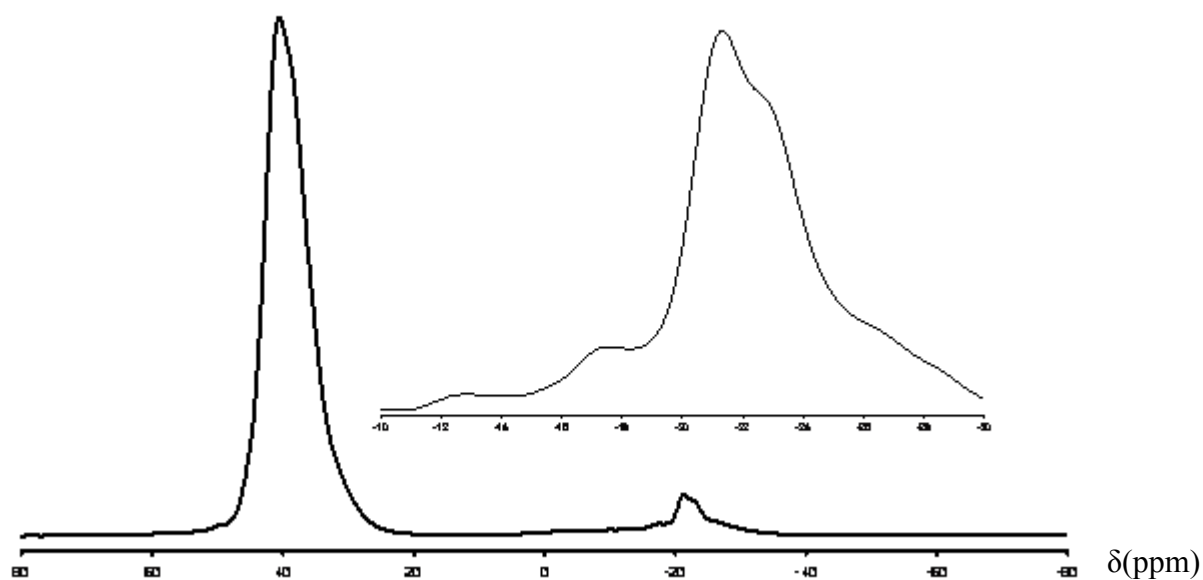


Figure 5.21: ^{27}Al MAS NMR spectra for structure **13**, showing an intense signal at 40.5ppm believed to be from the tetrahedrally-coordinated aluminium present within the layers, and a small signal at -21.5ppm, suggesting the presence of a small amount of octahedrally coordinated aluminium.

Having found it is possible for scandium to act as a framework element in aluminium methylphosphonate systems, it is appropriate to investigate methyl phosphonate systems in which scandium is the only metal included in the synthesis.

A series of experiments were performed investigating different reaction conditions, listed in table 5.9. From the relating powder X-ray diffraction patterns shown in figure 5.22, it is evident that novel crystalline scandium methylphosphonate phases are being formed (phase 'a'), however no single crystals were obtained for analysis.

The reaction conditions used to synthesis phase 'a' were investigated further in an attempted to grow larger single crystals for analysis. A series of experiments were performed in which metal hydroxides or HF was added to the reaction in order to promote crystallisation. Table 5.9 lists reactions which include lithium, sodium or potassium hydroxide, or hydrofluoric acid and relates them to phases or structures discussed later in the text.

Table 5.9: Selection of reaction conditions used to investigate scandium methyl phosphonates. * Initial pH adjusted using 10M alkali hydroxide

Reactants				Temp	Time	pH _i	pH _f	Diffraction
Sc ₂ O ₃	MePO ₃ H ₂	HF / alkyl hydroxide	H ₂ O	°C	(days)			pattern
1	1.5	-	40	160	6	3	6	Phase 'a'
0.5	3	NaOH	40	160	6	4*	7	Structure 15 + Sc ₂ O ₃
0.5	3	KOH	40	160	6	4*	6	Phase 'b'
0.3	3	NaOH	40	220	2	4*	7	Structure 15
0.3	3	LiOH	40	220	2	4*	7	Structure 16
0.5	3	HF 2eq	200	220	2	1	4	Structure 14

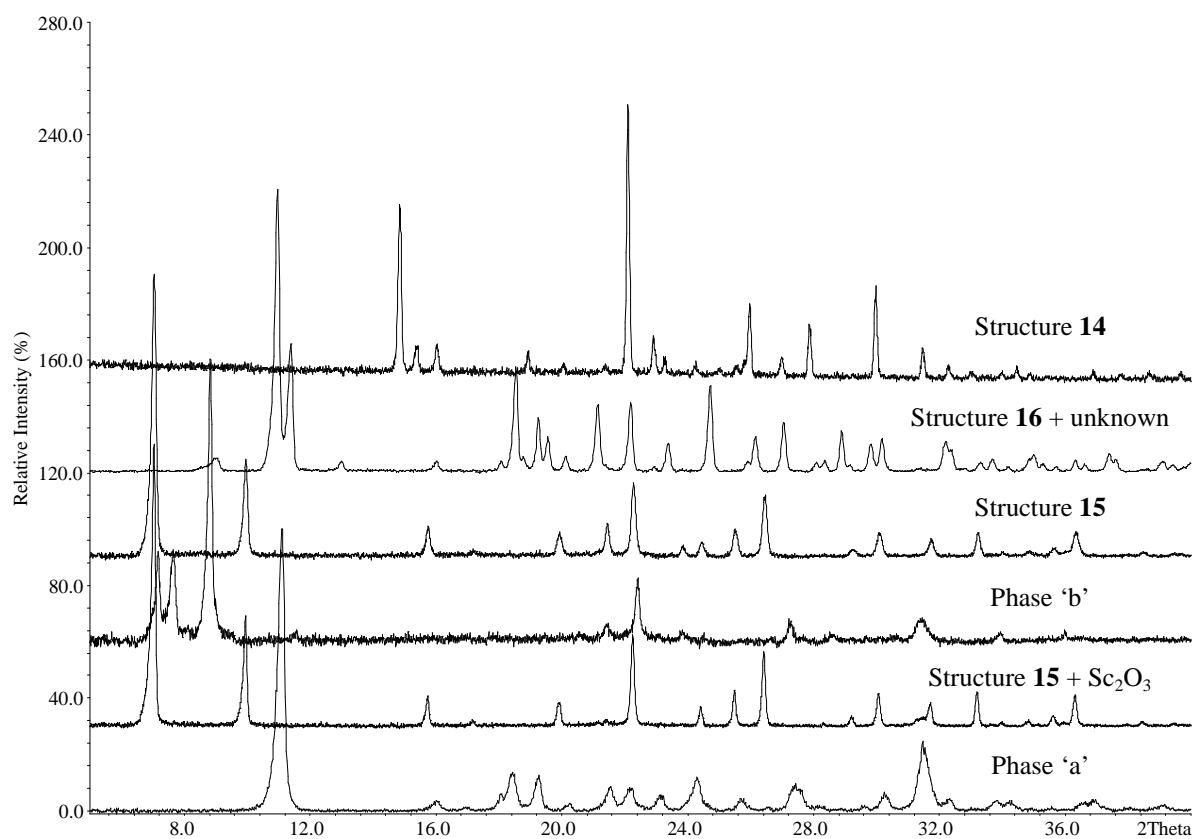


Figure 5.22: X-ray diffraction patterns of scandium methylphosphonate materials synthesised in the course of this work

5.4.4 ScF(H₂O)CH₃PO₃ – Structure 14

Structure **14**, ScF(H₂O)CH₃PO₃, was solved by direct methods and Fourier syntheses, using the SHELXS program⁸¹, from laboratory single crystal X-ray data collected on a small crystal, the crystallographic information is outlined in table 5.1. The atomic co-ordinates for structure **14** are listed below in table 5.10

Table 5.10: Atomic co-ordinates for structure 14

Atom	x	y	z	Occ	Uiso	Multiplicity
Sc(1)	0.8679(5)	0.7455(3)	0.5094(3)	1	0.00425(2)	4
P(1)	0.6168(6)	1.0424(5)	0.6705(8)	1	0.00606(8)	4
O(1)	0.7754(9)	0.9251(2)	0.6565(2)	1	0.01190(9)	4
O(2)	0.4447(3)	0.9603(2)	0.6139(9)	1	0.00930(3)	4
O(3)	0.5912(2)	1.0962(1)	0.8358(3)	1	0.01032(8)	4
O(4)	0.8567(4)	0.5767(4)	0.7098(5)	1	0.01590(5)	4
C(1)	0.6588(6)	1.2189(3)	0.554(3)	1	0.01264(6)	4
F(1)	1.1202(9)	0.7943(4)	0.5739(8)	1	0.00600(7)	4

Structure **14**, ScF(H₂O)CH₃PO₃, is composed of undulating chains of ScF₂O₄ octahedra which are linked through fluoride ions along the *a* axis. Each scandium is coordinated by two fluoride ions, a water molecule and three oxygens from methylphosphonate groups. Adjacent chains are linked by phosphonate groups and the fluoride ions of one chain form weak bonds to protons belonging to water bound to scandium of the adjacent chain, see figure 5.23. The chains are arranged in groups of four along [100] (figure 5.24), with methyl groups of the linking phosphonates projecting into the spaces between the chains, so that methyl groups project from alternate sides of the ‘channels’ going along [100]. Owing to the directions of the phosphonate tetrahedra, there is no free volume.

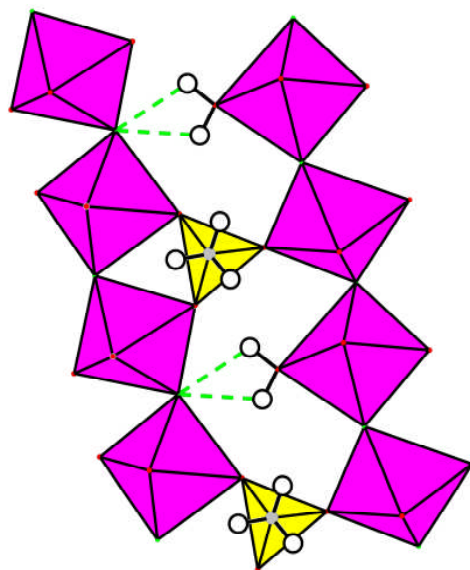


Figure 5.23: Adjacent chains of the $\text{ScF}(\text{H}_2\text{O})\text{CH}_3\text{PO}_3$ structure. The hydrogen atoms have been increased in size in respect to the other atoms for clarity purposes. The broken green line represents hydrogen bonding between the H_2O on the scandium with the fluorine atoms of adjacent octahedra.

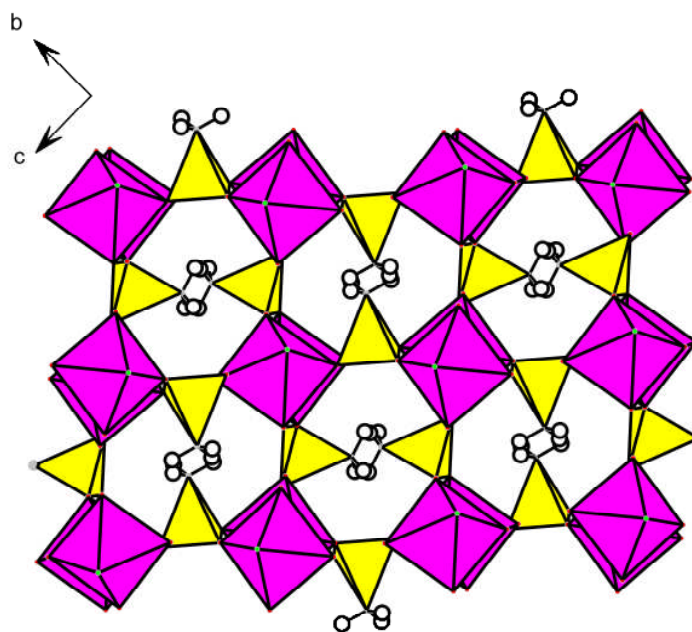


Figure 5.24: Projection down $[100]$ of structure 14 showing methyl groups projecting into the spaces between the chains.

Thermogravimetric analysis reveals two individual weight loss events, one of 10% at 300 °C and a second, of 8%, at 600 °C. X-ray analysis of powder diffraction patterns of the sample

heated at 400 °C, *i.e.* to allow the first event but not the second, indicates the material has converted partly to a highly crystalline solid that can be identified by its powder XRD pattern to be ScF₃ and partly to a poorly crystalline phase, assumed to be a scandium methylphosphonate. The first step can therefore be approximated by:



The final charge balanced structural formula for structure **14** is therefore ScF(H₂O)CH₃PO₃. Elemental analysis, weight %, calculated, C, 6.825%, H, 2.86%; measured, C, 6.78%, H, 2.63%.

5.4.5 NaSc(CH₃PO₃)₂·H₂O – structure 15

Raising the initial pH of the scandium oxide/methylphosphonic acid synthesis mixture with sodium hydroxide resulted in the crystallisation of a different phase, structure **15** (NaSc(CH₃PO₃)₂·H₂O). In the first experiments, performed with Sc:P of 2:3, some unreacted Sc₂O₃ remains. Once the pattern was indexed and the structure solved it was possible to adjust synthesis conditions until the pure phase was obtained (synthesis conditions are given in the experimental section).

Single crystal x-ray diffraction data could not be collected for structure **15** because the sample was micro crystalline, and consequently the structure was solved from high resolution powder x-ray diffraction data was collected on ID31 at the ESRF, Grenoble. The atomic coordinates from the structure solution are given below in table 5.11

Table 5.11: Atomic coordinates for structure 15

Atom	x	y	z	Ueq	Occ	Multiplicity
Sc(1)	0.57778(15)	0.09480(15)	0.7391(7)	0.0214(3)	1	8
P(1)	0.7037(2)	0.0662(2)	0.2404(11)	0.0241(3)	1	8
P(2)	0.45911(20)	0.0955(2)	0.2540(11)	0.0241(3)	1	8
Na(1)	0.6114(3)	0.2140(2)	0.2566(15)	0.0241(3)	1	8
O(1)	0.6752(5)	0.0935(6)	0.9937(15)	0.0241(3)	1	8
O(2)	0.6562(5)	0.0964(6)	0.4482(16)	0.0241(3)	1	8
O(3)	0.5912(4)	0.2153(4)	0.7796(19)	0.0241(3)	1	8
O(4)	0.4856(5)	0.0961(5)	0.5118(14)	0.0241(3)	1	8
O(5)	0.5116(5)	0.1148(5)	1.0449(15)	0.0241(3)	1	8
O(6)	0.5701(5)	-0.0225(4)	0.7890(18)	0.0241(3)	1	8
C(1)	0.7031(7)	-0.0341(6)	0.288(3)	0.0241(3)	1	8
C(1)	0.3806(5)	0.1634(6)	0.236(3)	0.0241(3)	1	8
O(w)	0.75	0.25	0.227(6)	0.0241(3)	0.5	4

Structure 15 was determined by Nathalie Guillou, Institut Lavoisier, University of Versailles, from powder diffraction data as single crystals of analysis of the material was not possible owing to its micro-crystalline nature. Figure 5.25, an SEM image of the sample, shows a needle-like morphology, with the crystallites approximating 10 μ m in length.

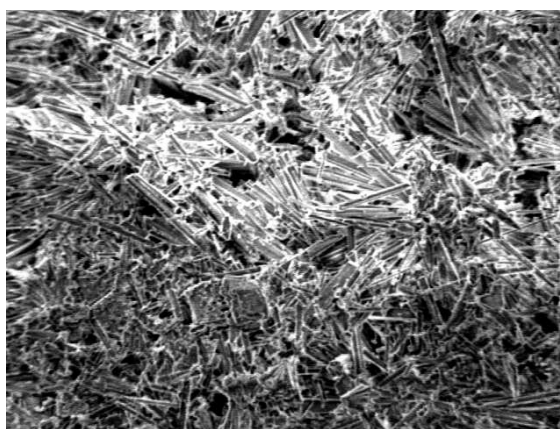


Figure 5.25: Needle-like morphology of structure 15.

The structure of as prepared NaSc(CH₃PO₃)₂H₂O was determined from X-ray synchrotron powder diffraction data obtained at station ID-31 at the ESRF, Grenoble.¹⁵⁴ Data collection was carried out at room temperature in Debye–Scherrer geometry, with the sample in a sealed quartz glass capillary, with 2 θ of 2–38° and using monochromated radiation with a wavelength of 0.63248Å. The structure was observed to change gradually in the intense X-ray beam, so four data collections over 170s were performed on freshly exposed portions of the sample and the data sets were summed. The diffraction pattern of the sample did not

change in this period. Subsequent structure solution calculations were performed with the EXPO¹⁵⁵ package. Sc₂O₃ was considered as a second phase and its scale factor, as well as its profile factors (one cell parameter, two halfwidth and two variables for the angular variation of θ) were refined using the Fulprof program suite. The final fit obtained between calculated and observed patterns is shown below in figure 5.26.

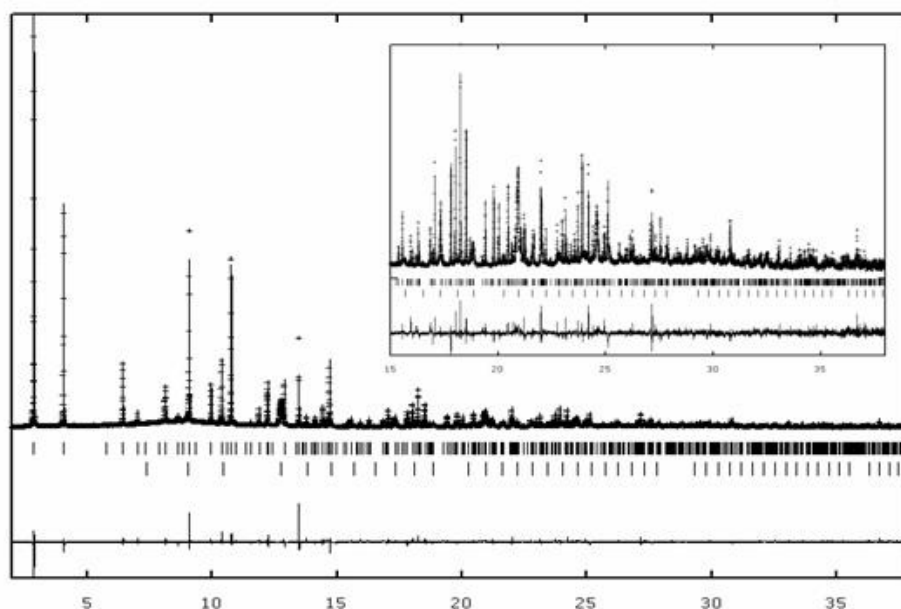


Figure 5.26: Rietveld refinement of structure **15**.⁴⁷

The reaction conditions used to prepare structure **15** were modified to include less Sc₂O₃ (table 5.9) which led to the isolation of the phase pure material. Rietveld refinement of powder x-ray diffraction data from this sample was performed with the GSAS program suite using the atomic co-ordinates determined by Nathalie Guillou as a starting point in order to confirm the purity of the phase. Instrumental parameters (background, zero-point, peak profile coefficients) and structural parameters (unit cell, atomic co-ordinates, thermal parameters) were refined, with no constraints on the bond distances or angles. A close final fit to the observed data was achieved, the $R_{wp} = 7.1\%$, (figure 5.27) with the structure determined from the powder diffraction data.

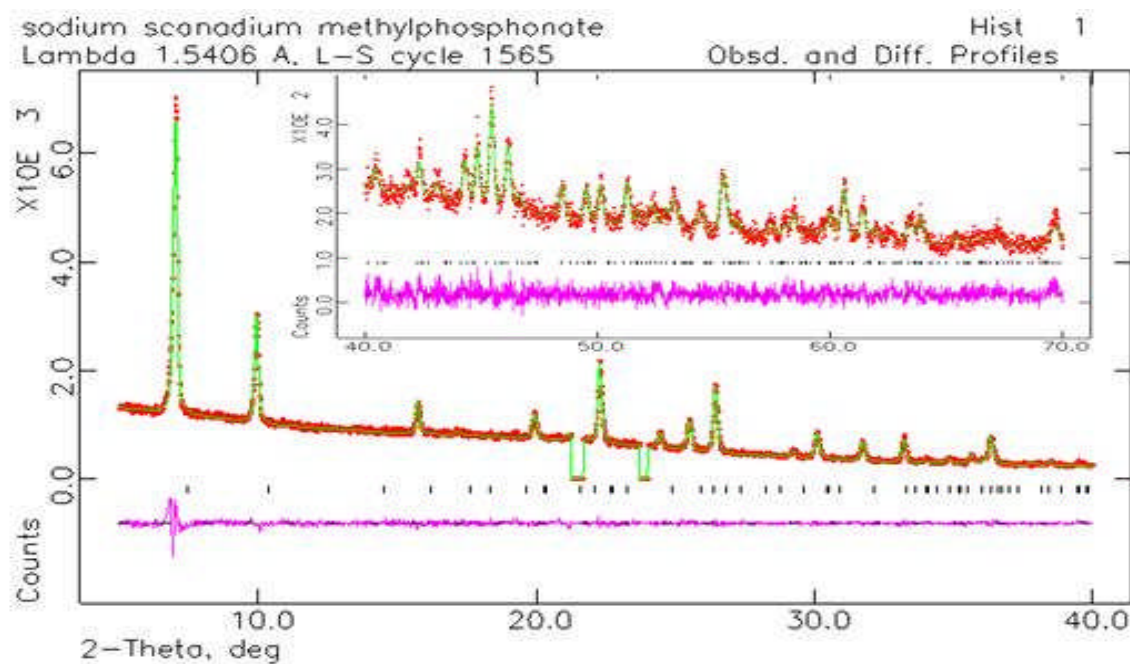


Figure 5.27: Final Rietveld refinement of structure **15** without the presence of any impurities, i.e. scandium oxide, in the sample (excluded regions correspond to peaks inherent to the diffractometer)

Structure **15** has an inorganic framework within which the scandium and phosphonate groups are fully linked into the network: each scandium links through six oxygens to phosphorus atoms, each phosphorus atom links through three oxygens to scandium atoms. There are two channel systems in the inorganic framework running parallel to the c axis, one surrounded by 4 Sc and 4 P, the other by 8 Sc and 8 P, figure 5.28.

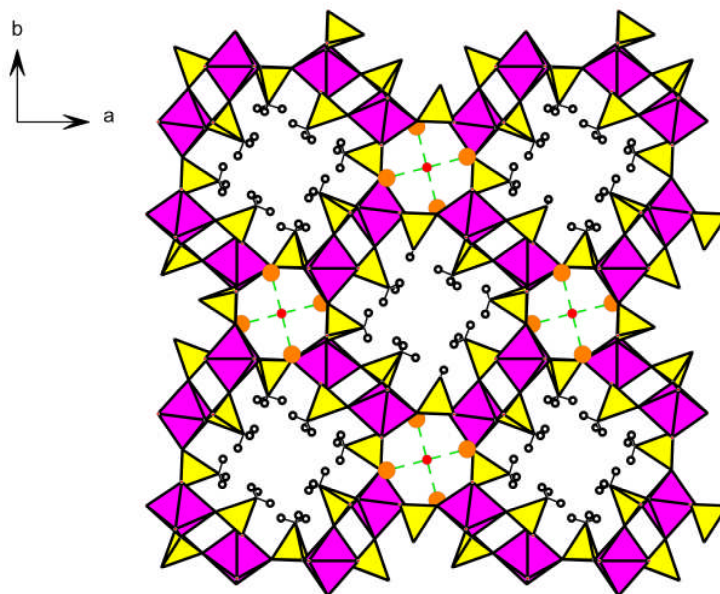


Figure 5.28: Projection down [001] of structure 15, showing two channel systems, the larger, organic, channel is lined with methyl groups, whereas the small, inorganic, channel is lined with sodium cations and has a water molecule bound within it.

The channel ringed by 8 Sc and 8 P is lined by methyl groups, leaving little void space. Allowing for the H atoms to have a van der Waals radius of 1.2\AA , then these channels only have a free diameter of around 2\AA . The channels surrounded by 4 Sc and 4 P are fully inorganic in nature, and are large enough to accommodate water bound to extra framework sodium cations. The sodium cations occupy six-membered ring window sites in the smaller channels. There are eight Na–O distances between 2.47 and 2.87\AA . Attempts to exchange the sodium cations (for example by extended stirring in aqueous 0.1 M solutions of potassium, copper or zinc salts at $70\text{ }^\circ\text{C}$) were unsuccessful.

TGA indicates that the coordinated water is lost from the structure at $100\text{ }^\circ\text{C}$ (weight loss observed, $3.5\text{ wt}\%$; expected, $3.4\text{ wt}\%$). The sodium cation remains in the same site, but neutron diffraction studies on a deuterated sample shows that on losing the coordinating water molecule it has moved away from the centre of the small channel to achieve better coordination with the framework oxygens, and displays six Na–O bond distances between 2.27 and 2.88\AA (figure 5.29).⁴⁷

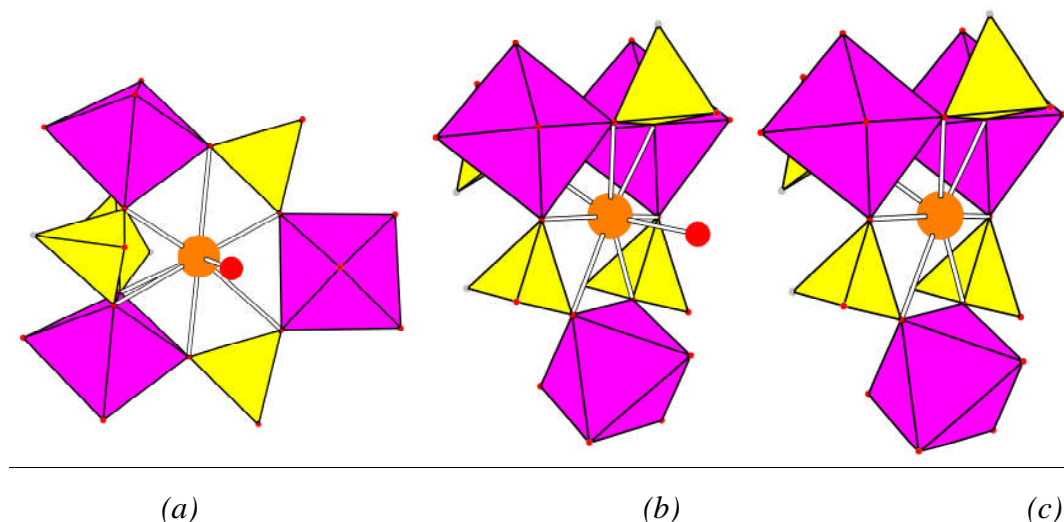


Figure 5.29: (a) and (b) Details of the sodium cation site in the hydrated solid. (c) Environment of the sodium cation in the dehydrated solid.⁴⁷

Solid state ^{31}P MAS NMR (figure 5.30) gives two distinct peaks at 16.8 and 1.7ppm, corresponding to the two crystallographically unique phosphorus sites within the structure. ^{45}Sc MAS NMR (figure 5.31) shows a single peak at 7.1ppm, which corresponds to the only scandium site present within the framework and confirms that the solid has been prepared without the Sc_2O_3 impurity.

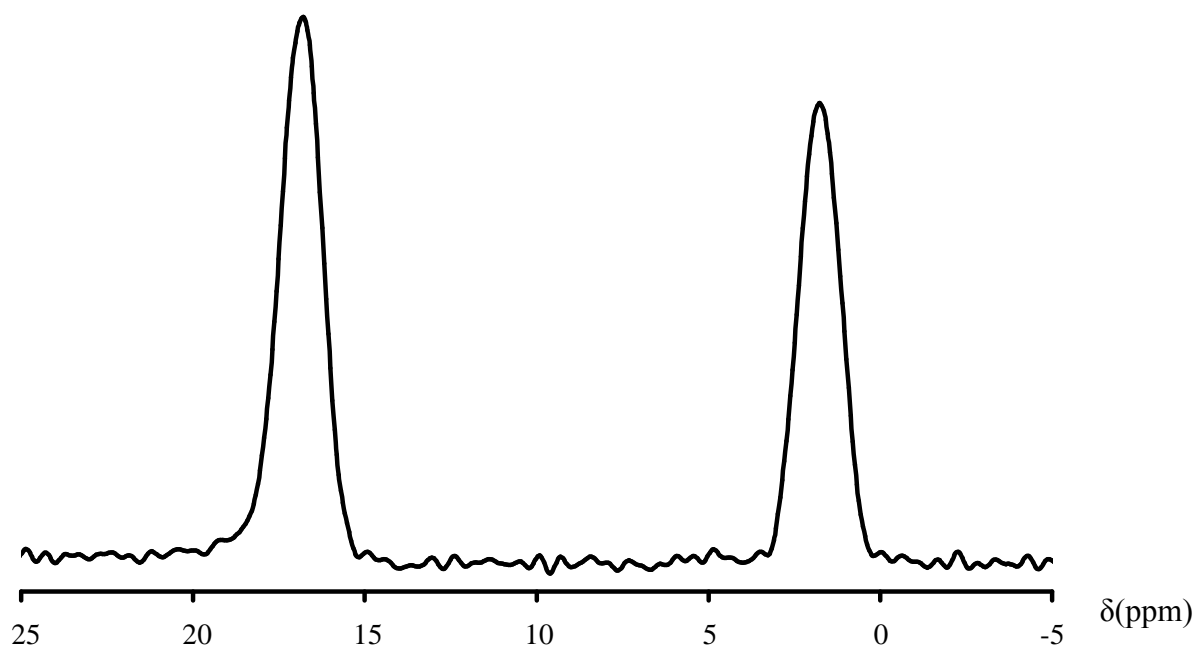


Figure 5.30: ^{31}P DP MAS NMR spectra for structure **15** showing two peaks, at 16.8 and 1.7ppm, corresponding to the 2 unique phosphorus sites present within the structure.

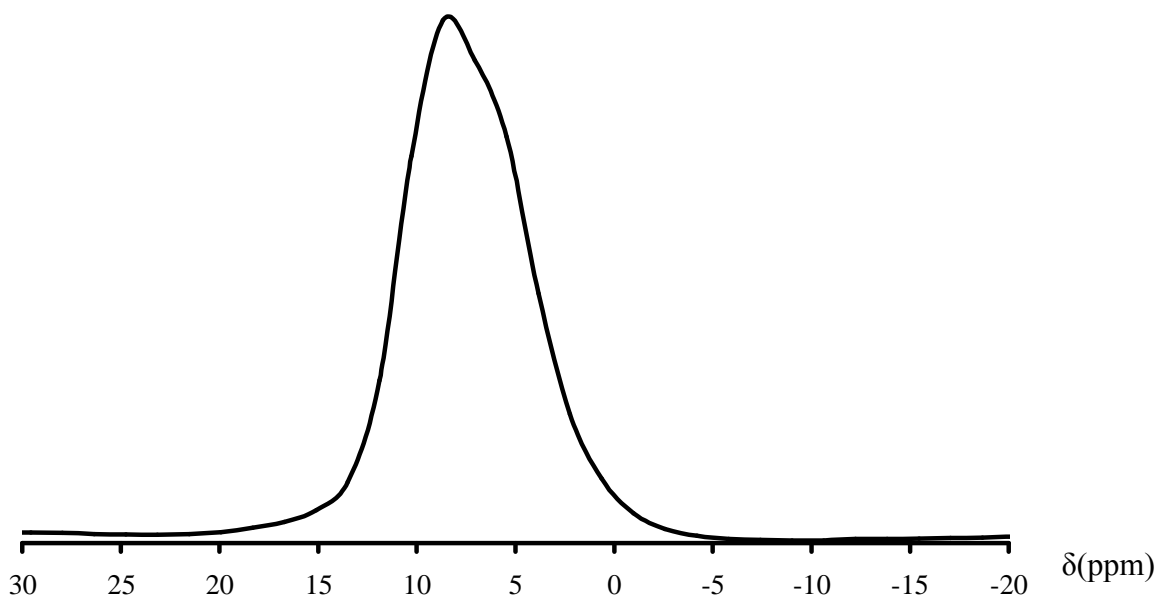


Figure 5.31: ^{45}Sc MAS NMR spectra for structure **15** showing a single intense peak at 7.1ppm which corresponds to the single crystallographically unique scandium site within the structure.

5.4.6 $\text{Sc}(\text{H}_2\text{O})\text{Sc}(\text{H}_2\text{O})_2(\text{CH}_3\text{PO}_3)_3$ – structure **16**

Changing the alkali metal hydroxide used to raise the initial pH of the scandium oxide/methylphosphonic acid synthesis mixture from sodium hydroxide to lithium hydroxide resulted in the crystallisation of a different phase, structure **16**, $\text{Sc}(\text{H}_2\text{O})\text{Sc}(\text{H}_2\text{O})_2(\text{CH}_3\text{PO}_3)_3$. Structure **16** has only been formed in the presence of lithium hydroxide however lithium is neither part of the structure nor does it occupy interstitial sites within the framework. The lithium is believed to be included in another, unidentified phase, traces of which have been found in all synthetic attempts to make structure **16** phase pure. It is therefore the pH-controlling role of the LiOH additive that is thought to be more important in the crystallization of structure **16**.

Single crystal x-ray diffraction data could not be collected for structure **16** because the sample was micro crystalline, as shown in figure 5.32.

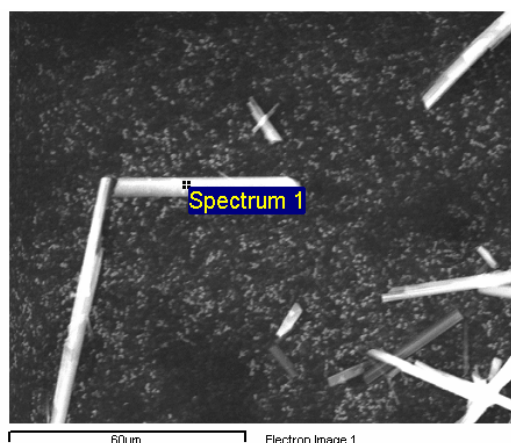


Figure 5.32: Needle-like morphology of structure 16.

The structure of the as-prepared $\text{Sc}(\text{H}_2\text{O})\text{Sc}(\text{H}_2\text{O})_2(\text{CH}_3\text{PO}_3)_3$ was therefore determined from X-ray synchrotron powder diffraction data obtained at station ID-31 at the ESRF, Grenoble. data collection was performed at 150 K in Debye–Scherrer geometry, with the sample in a sealed quartz glass capillary, with 2θ of $0\text{--}40^\circ$ and using monochromated radiation with a wavelength of 0.80018\AA . The structure was observed to change gradually in the intense X-ray beam, so fourteen data collections over 170s were performed on freshly exposed portions of the sample and the data sets were summed. The diffraction pattern of the sample did not change in this period.

The extraction of the peak positions for indexing was performed using the EXPO2004 suite. Pattern indexing was carried out within EXPO2004 using the computer program TREOR from sixty lines, with an absolute error on peak positions of $0.01^\circ 2\theta$. A monoclinic solution was found with satisfactory figures of merit. Systematic absences were consistent with several spacegroups. The spacegroups in which fewer symmetry operators were present were chosen as a starting point for structure solution using the EXPO2004 suite.

A list of 201 reflections was extracted in the angular range $5\text{--}38^\circ 2\theta$. According to the degree of diffraction overlap, 49.03% of these reflections were statistically considered as independent. The Sc, P, O and C atoms were found from the E-map with the highest figure of merit.

The corresponding atomic co-ordinates were used as the starting model for Rietveld refinement, using the GSAS program suite. The refinement excluded the region below $5^\circ 2\theta$, as this was attributed to the presence of an impurity phase. A pseudo-Voigt function was selected to describe individual line profiles. Unit cell and instrumental parameters were allowed to vary from time to time during the refinement process, as well as atomic co-

ordinates, initially with soft distance restraints. At this stage $R_{wp} = 0.085$ with all peaks included between $5 - 38^\circ 2\theta$, figure 5.33, however owing to difficulties modeling the line shapes of the first two peaks, at 5.7 and $5.9^\circ 2\theta$ a closer fit was achieved, $R_{wp} = 0.067$, by omitting these reflections, figure 5.34.

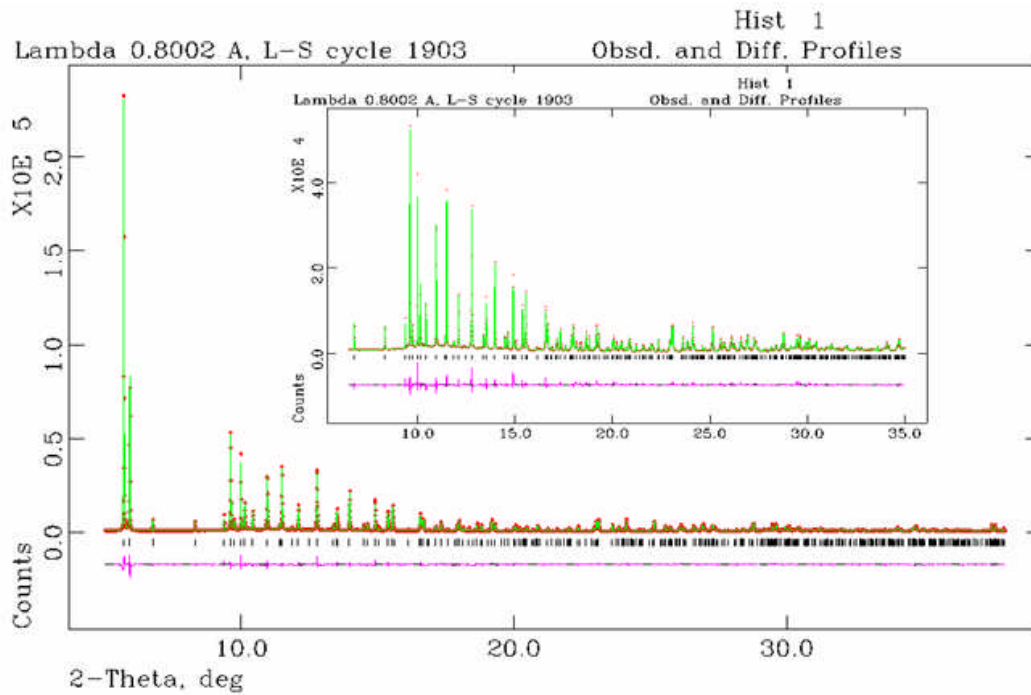


Figure 5.33: Rietveld plot for structure 16 including the first two reflections, shown at 5.7 and 5.9° , where $R_{wp} = 0.0856$

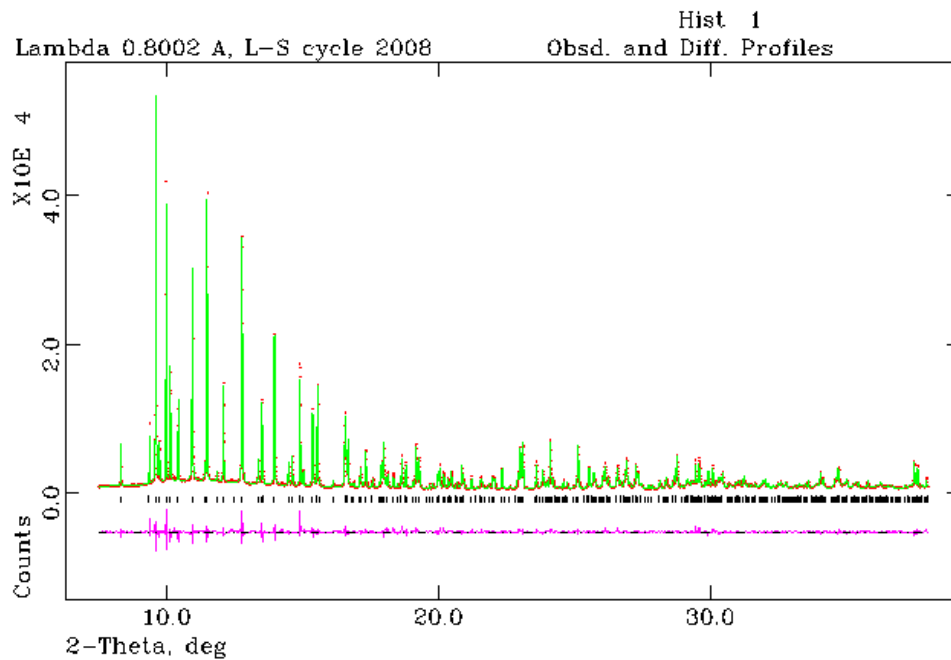


Figure 5.34: Rietveld plot for structure 16 in which the first two reflections (5.7 and 5.9°) have been omitted.

In order to ensure that the space group selection was correct, the atomic coordinates were input into the PLATON program suite, and additional symmetry sought. The symmetry remained unchanged however, suggesting that the structure is in the correct spacegroup.

Table 5.12: Atomic coordinates for structure **16**

Atom	x	y	z	Occ	Uiso	Multiplicity
Sc(1)	0.29050(16)	0.24666(30)	-0.46821(21)	1	0.0027(3)	4
Sc(2)	0.44719(16)	-0.24395(32)	-0.24473(23)	1	0.0027(3)	4
P(1)	0.44746(24)	0.49617(30)	-0.4867(4)	1	0.0027(3)	4
P(2)	0.32472(20)	-0.09670(33)	-0.53350(32)	1	0.0027(3)	4
P(3)	0.14965(21)	0.13854(34)	-0.26284(31)	1	0.0027(3)	4
O(1)	0.4653(4)	0.5785(5)	-0.6129(5)	1	0.0027(3)	4
O(2)	0.4196(4)	-0.4067(5)	-0.3789(5)	1	0.0027(3)	4
O(3)	0.38010(32)	0.3722(6)	-0.5278(6)	1	0.0027(3)	4
O(4)	0.3155(4)	0.0657(4)	-0.5626(5)	1	0.0027(3)	4
O(5)	0.35894(32)	-0.3211(6)	-0.1424(5)	1	0.0027(3)	4
O(6)	0.38026(35)	-0.1128(6)	-0.3885(4)	1	0.0027(3)	4
O(7)	0.2042(4)	0.1567(7)	-0.3725(5)	1	0.0027(3)	4
O(8)	0.19378(29)	0.2118(6)	-0.1297(4)	1	0.0027(3)	4
O(9)	0.05597(26)	0.1916(7)	-0.3107(5)	1	0.0027(3)	4
O(10)	0.2810(4)	0.4408(7)	-0.3395(6)	1	0.0027(3)	4
O(11)	0.3949(4)	0.1654(7)	-0.3032(6)	1	0.0027(3)	4
O(12)	0.5451(4)	-0.3695(7)	-0.0877(6)	1	0.0027(3)	4
C(1)	0.5471(4)	0.4114(9)	-0.4095(8)	1	0.0027(3)	4
C(2)	0.21786(34)	-0.1627(9)	-0.5354(9)	1	0.0027(3)	4
C(3)	0.1457(6)	-0.0486(5)	-0.2294(9)	1	0.0027(3)	4

Hydrogen atoms were added to the water molecules attached to the scandium cations and to the methyl groups. The position of the hydrogen atoms were fixed using the SHELXL program suite with The O-H bond distances being restrained to be 0.98(1)Å with U_{iso}(H) set to 1.5 times that of the parent oxygen atom and C-H bond distances being restrained to 0.98(1)Å with U_{iso}(H) set to 1.2 times that of the parent carbon atom.

Structure **16**, Sc(H₂O)Sc(H₂O)₂(CH₃PO₃)₃, presents a novel framework scandium methylphosphonate material, which consists of an inorganic framework within which the scandium to phosphorus ratio is 2:3. The framework is built from two different scandium phosphonate chains, six of which are arranged to form a channel which is lined with methyl groups, figure 5.35.

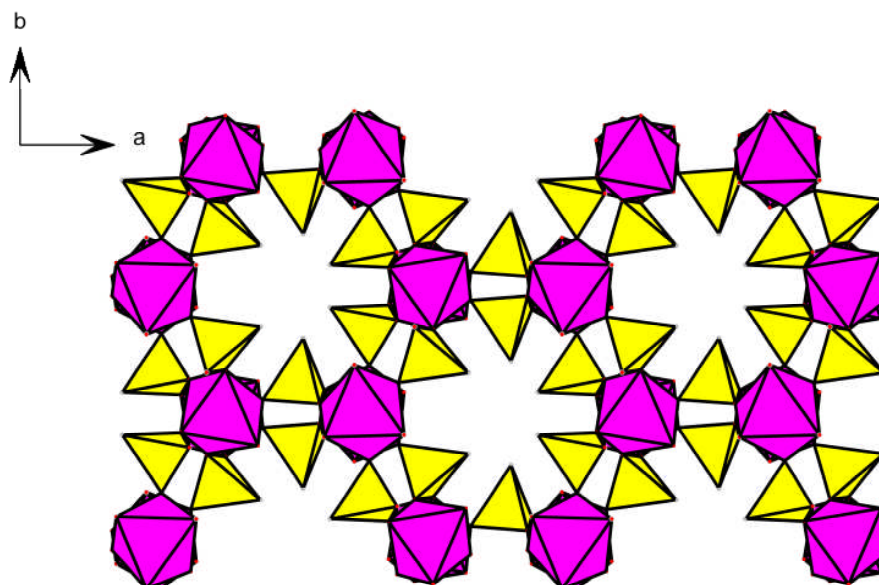


Figure 5.35: Projection down [001] of structure **16** showing channels which are lined by six methyl groups.

The main structural feature of structure **16** is a channel system running parallel to the *c*-axis. The framework consists of rows of isolated scandium octahedral units which are separated by phosphonate groups, the methyl groups of which point into the channels. There are two crystallographically unique scandium atoms in structure **16**, with different coordination environments, Sc(1) is bonded to four framework oxygen atoms and two water molecules, whereas Sc(2) is bonded to five framework oxygen atoms and one water molecule. This is shown in figure 5.36.

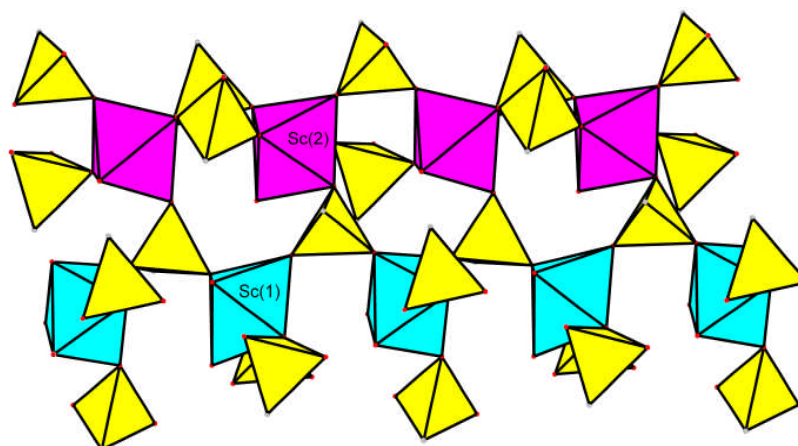


Figure 5.36: Representation of the two different scandium phosphonate chains present within structure **16**, which shows the top row (purple) of scandium octahedra connected via five methyl phosphonate groups, whereas the bottom row (cyan) are connected via four methyl phosphonate groups

The interatomic bond distances and angles in the framework are as expected: Sc - O bond distances are between 2.02(1) and 2.035(2)Å with Sc - OH₂ bond distances between 2.203(2) and 2.325(1)Å, which is comparable other materials reported in this work.

NMR information was not collected for this sample as it could not be synthesised as a pure phase.

Thermogravimetric analysis was collected despite the impurities present within the sample and a significant weight loss (experimental, 9.53%) occurring between and 230 and 270°C owing to the loss of water from the Sc³⁺ cations (theoretical, 12.69%). The material did not retain its crystallinity upon removal of the water molecules.

5.4.7 Scandium ethylenebisphosphonate Sc₃(O₃PC₂H₄PO₃)(HO₃PC₂H₄PO₃H)₃.H₃O Structure 17

Structure **17**, Sc₃(O₃PC₂H₄PO₃)(HO₃PC₂H₄PO₃H)₃.H₃O, was solved through a combination of single crystal diffraction data collected at the synchrotron radiation facility, Daresbury, and powder diffraction refinements. Once the data had been collected at the synchrotron source, the structure was solved in R $\bar{3}$ c, giving a residual value of 20%, with all atoms being refined anisotropically. The position of one of the carbons atoms, C(1), which was located on a three fold axis, gave unfavourable bond lengths and angles (with its symmetry generated neighbours), and also high thermal parameters suggesting that the position was incompletely characterised. Consequently, the carbon atom C(1) was split into three different sites, situated close to, but not on the three fold axis, each with their occupancy set at 0.33

A closer examination of the frames collected during the single crystal experiment indicated the possibility of multiple peaks per spot, suggesting that the crystal on which the data was collected for was not single, i.e. twinned, or more than one crystal was present on the goniometer head. Two more data collections were performed on crystals from different samples of the same material, but the result remained unchanged. This, supported by SEM images of the material (figure 5.37), suggesting the presence of only one crystal on the goniometer, but which was twinned. The atomic co-ordinates are given below in table 5.13.

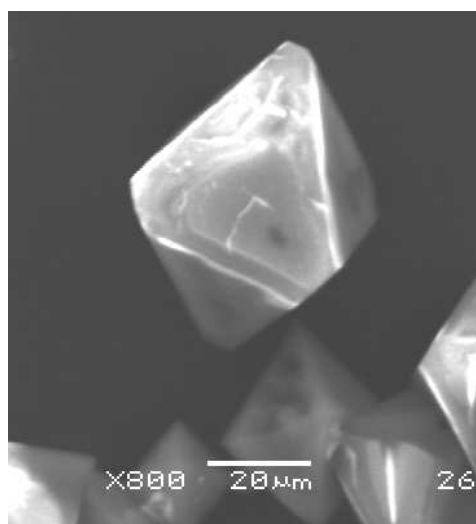


Figure 5.37: SEM image for structure **17** showing apparently a single crystal with a bipyramidal morphology.

Table 5.13: Atomic co-ordinates for structure **17**

Atom	x	y	z	Ueq	Occ	Multiplicity
Sc(1)	0.24756(4)	0.33333	0.08333(16)	0.0229(9)	1	18
P(1)	0.33333	0.66667	0.1195(12)	0.0272(9)	1	12
P(2)	0.55905(4)	0.58427(13)	0.04389(11)	0.0233(11)	1	36
O(1)	0.62847(13)	0.29514(12)	0.08333(9)	0.0952(12)	1	18
O(2)	0.45235(14)	0.43757(12)	0.05934(13)	0.0263(8)	1	36
O(3)	0.15004(12)	0.42355(15)	0.05649(14)	0.0275(9)	1	36
O(4)	0.35622(14)	0.53134(16)	0.10982(15)	0.03(13)	1	36
C(1)	0.49689(18)	0.56872(19)	0.00788(12)	0.0273(6)	1	36
C(2)	0.34189(12)	0.61614(12)	0.15563(12)	0.0565(15)	0.3333	36
O(100)	0.72045(14)	0.59091(12)	0.04249(13)	0.0303(11)	0.3333	36

A Rietveld refinement was performed with the GSAS program suite⁷⁵ using the atomic co-ordinates determined by the single crystal structure solution as a starting point in order. Instrumental parameters (background, zero-point, peak profile coefficients) and structural parameters (unit cell, atomic co-ordinates, thermal parameters) were refined, keeping constraints on the bond distances and angles. A close final fit to the observed data was achieved, with $R_{wp} = 11.5\%$, (figure 5.38) with the structure determined from the single crystal experiment, with atomic positions refining to positions very close to the values determined from single crystal diffraction.

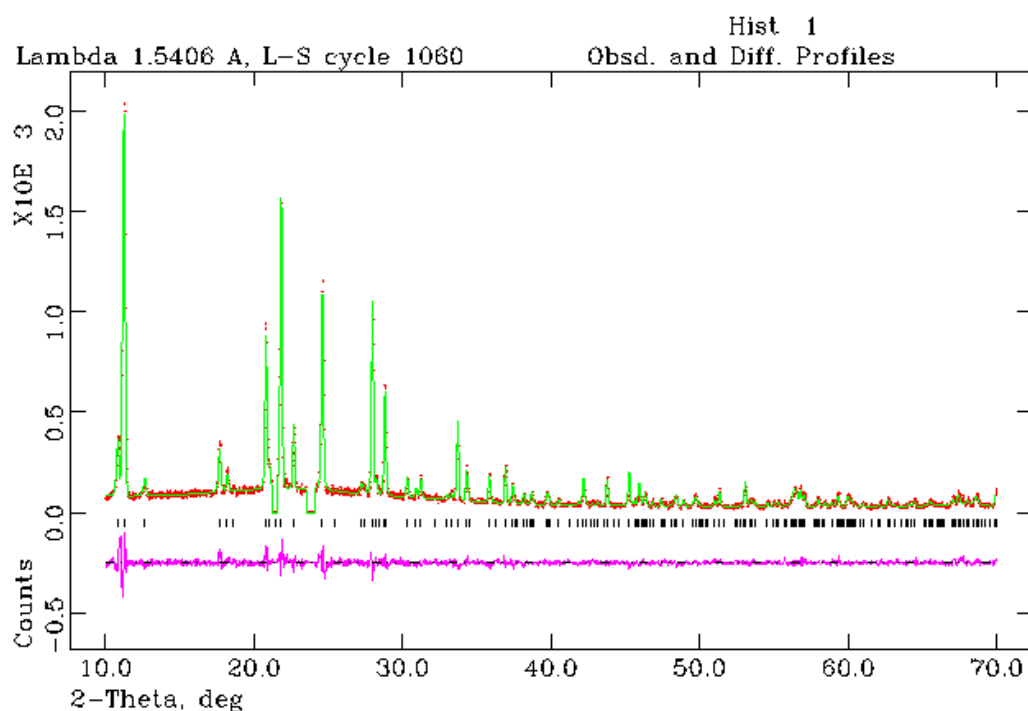


Figure 5.38: Rietveld refinement of structure **17**.

Structure **17**, $[\text{Sc}_3(\text{O}_3\text{PC}_2\text{H}_4\text{PO}_3)(\text{HO}_3\text{PC}_2\text{H}_4\text{PO}_3\text{H})_3 \cdot \text{H}_3\text{O}]$, is a pillared layered scandium ethylene-bisphosphonate. The scandium-to-phosphorus ratio is 3:8, with a strict alternation between scandium and phosphorus and no Sc – O – Sc bonds. The structure consists of inorganic layers of scandium octahedra, bonded to 6 phosphonate tetrahedra. The ethylene linker within the bisphosphonate separates the inorganic layers within the structure, giving an interlamellar distance of approximately 8\AA , shown in figure 5.39.

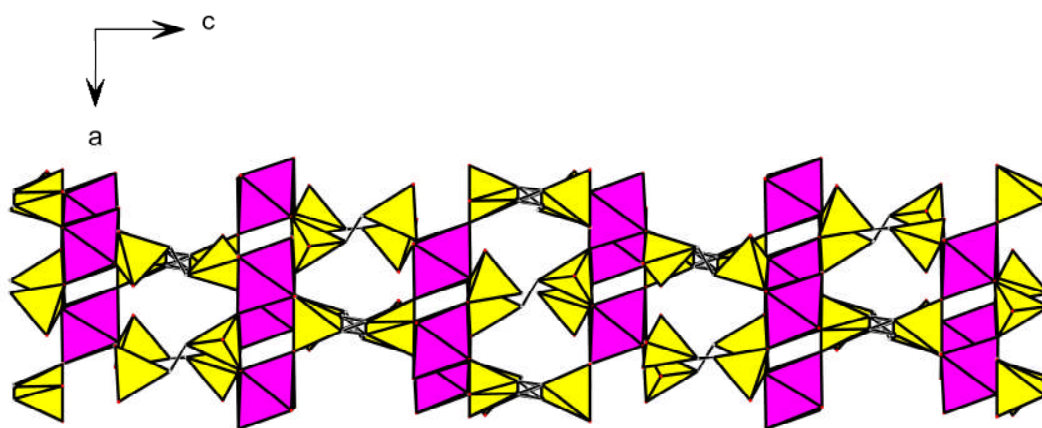


Figure 5.39 Projection down $[010]$ of structure **17**, showing layers of scandium and phosphorus polyhedra separated by the ethylene linkers.

There are cavities present within the scandium phosphonate layers, which are created by 12MRs consisting of 6 ScO_6 octahedra and 6 phosphonate tetrahedra, as shown in figure 5.40.

There is a disorder of the C(1) site about the $\bar{3}$ axis.

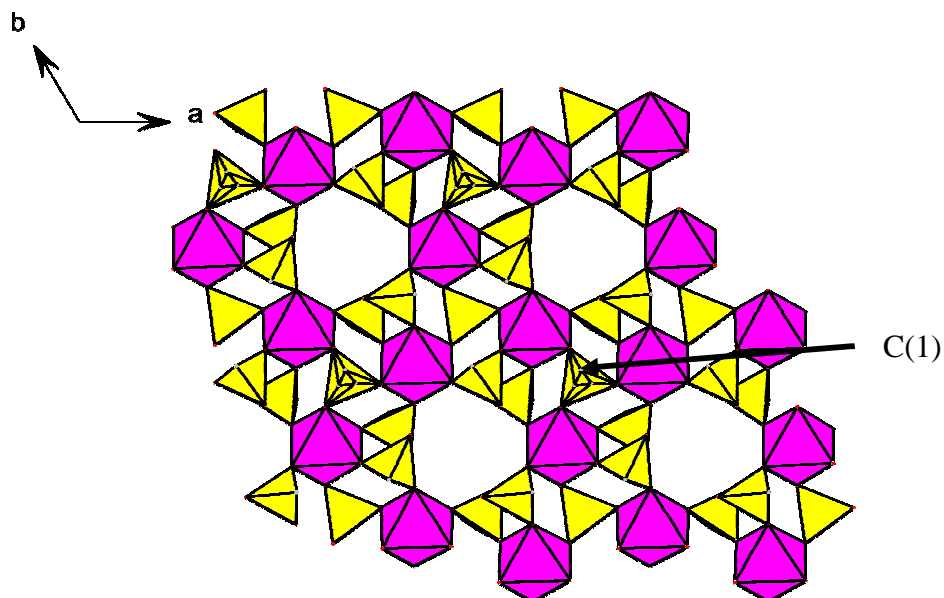


Figure 5.40: Projection down [001] of a single layer of structure 17, showing cavities formed by the presence of 12MRs. C(1) is labelled in order to show the disorder present about the $\bar{3}$ axis

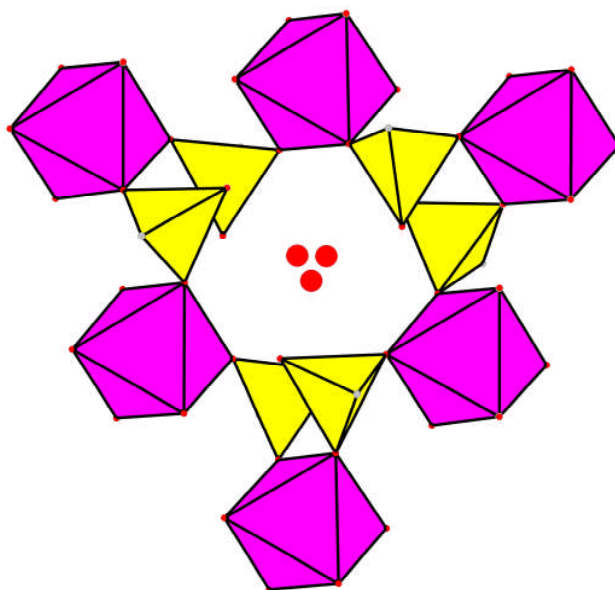


Figure 5.41: Projection onto a single cavity created by the formation of 12MR's of scandium and phosphonate polyhedra. Disordered water within the cavity is shown.

Structure **17** is isostructural with a vanadium phosphonate reported as a minority phase by Zubieta *et al.*¹⁵⁶ Unit cell parameters for structure **17** are listed with those from the phase reported by Zubieta *et al* in table 5.14.

Table 5.14: Comparison of crystallographic parameters of structure **17** and the vanadium phosphonate published by Zubieta *et al*

Material	Unit cell Parameters		Spacegroup
	a (Å)	c(Å)	
$(\text{H}_3\text{O})_3(\text{O}_3\text{PCH}_2\text{CH}_2\text{PO}_3)(\text{HO}_3\text{PCH}_2\text{CH}_2\text{PO}_3\text{H})$ ¹⁵⁷	9.863(1)	46.403(9)	$\bar{R}3c$
Structure 17	10.016(2)	47.084 (4)	$\bar{R}3c$

Solid state ³¹P MAS NMR (figure 5.42) shows one intense signal at 6.4ppm. Although there are two crystallographically unique phosphorus atoms in the crystal structure, they have similar local environments, and therefore similar chemical shifts would be expected. ⁴⁵Sc MAS NMR (figure 5.43) shows one peak at 9.8ppm which corresponded to the single scandium position within structure **17**.

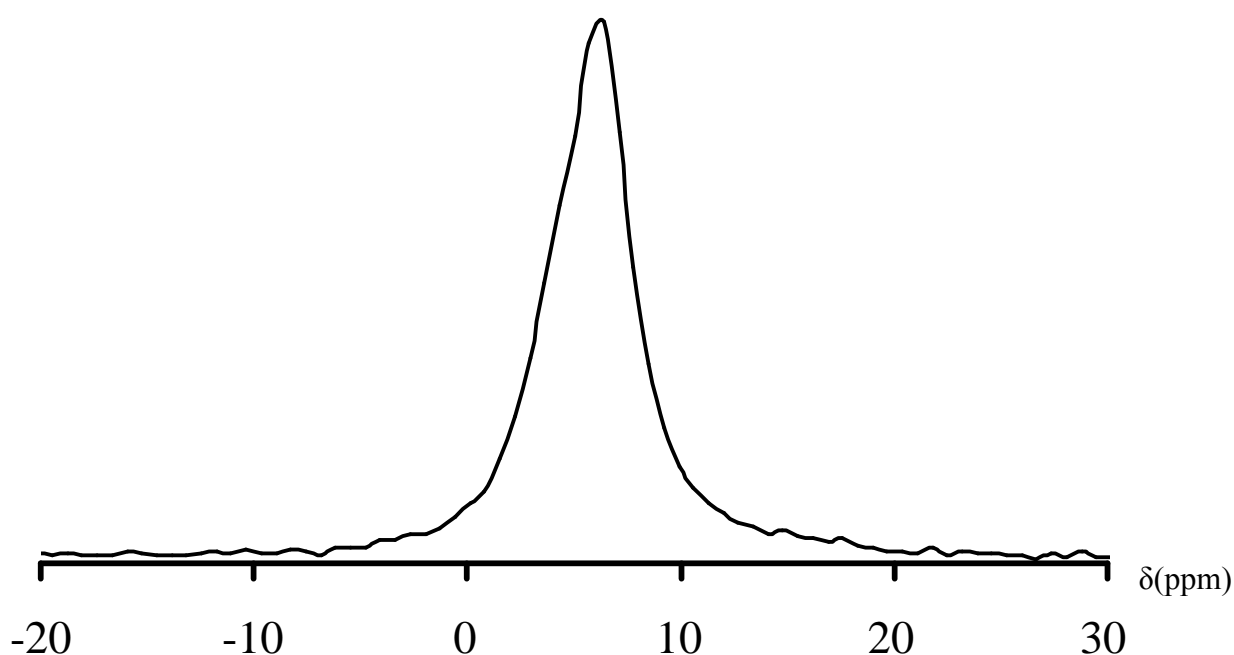


Figure 5.42: ³¹P MAS NMR spectra for structure **17**, showing a single intense signal at 6.4ppm, which corresponds to the two phosphorus sites in the sample.

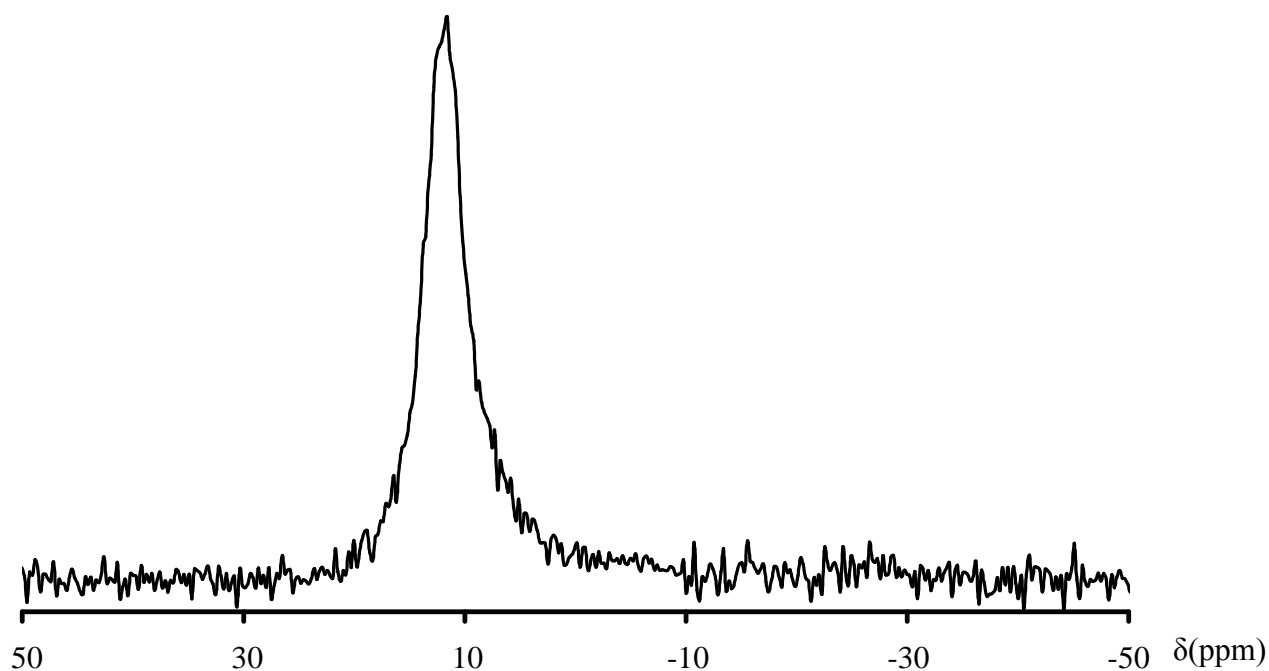


Figure 5.43: ^{45}Sc MAS NMR spectra for structure **17** showing an intense signal at 9.8ppm which can be attributed to the single independent scandium site located in by crystallography

Thermogravimetric analysis of structure **17** shows a weight loss occurring between 380 and 450°C, 9.2%, which corresponds to loss of water (4.2%) and a further weight loss of approximately 5% thought to be breakdown of the framework in order to allow removal of the water molecule. The product after heating is amorphous.

5.4.8 Scandium bisphosphonates templated with piperazine-based bisphosphonate ligands

The use of methyl phosphonic acid and ethylenebisphosphonic acid has led to the formation of five novel microporous scandium phosphonates, but the pores possessed by these materials are very small, and do not show substantial porosity for molecules other than water.

Here the structure directing effects of scandium is examined within piperazine-bis-methylenephosphonate systems in an attempt to synthesise porous scandium bisphosphonates. During the investigation of piperazine-based bisphosphonate systems, different piperazine bisphosphonic acids were used in the synthesis, in order to investigate their structure directing

effects. A diagram of the bisphosphonic acids used during this investigation are shown in figure 5.4 (section 5.3), which correspond to the nomenclature used in the synthesis conditions, listed in table 5.15.

It was observed that the use of certain piperazine-based bisphosphonic acids in the reaction gel favoured the formation of certain phases. Unfortunately none of the samples prepared yielded single crystals for structural analysis. The powder diffraction patterns obtained from using some of the different bisphosphonic acids, are shown below in figure 5.44

Table 5.15: Reaction conditions which yielded crystalline solids whilst investigating piperazine-based bisphosphonate, where *L* denotes *N,N'*-piperazinebismethylenephosphonic acid and *L'* its racemic 2-methylated derivative

Reactants			T (°C)	Time	pH _i	pH _f	Product
Sc ₂ O ₃	Ligand	H ₂ O		(days)			
0.25	L' 1eq	300	220	2	2	2	Structure 18
0.25	L 2eq	400	220	2	1	4	Unknown 'a'
0.5	L 1eq	400	220	2	2	5	Unknown 'b'

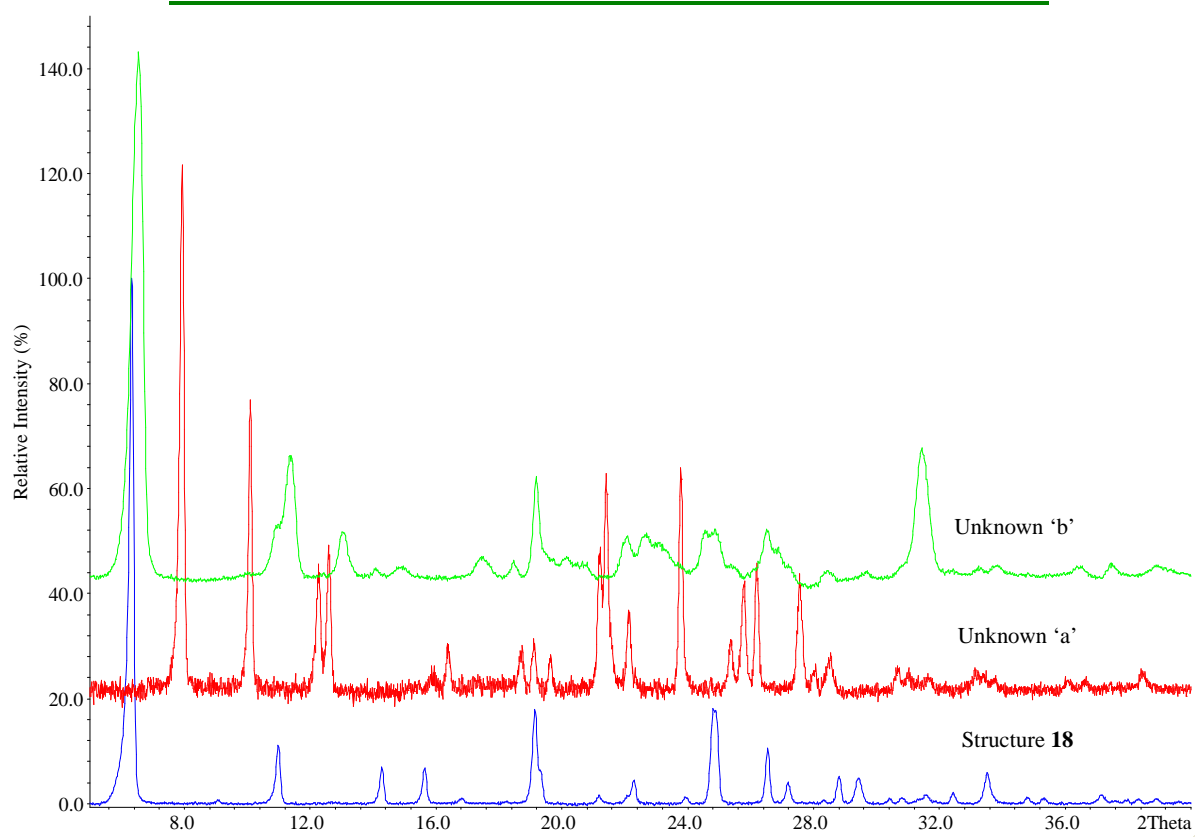


Figure 5.44: Powder X-ray diffraction patterns of crystalline phases formed during the investigation of piperazine-based bisphosphonates.

5.4.9 $\text{Sc}_2(\text{O}_3\text{PCH}_2(\text{NHC}_5\text{H}_{10}\text{NH})\text{CH}_2\text{PO}_3)_3 \cdot 4\text{H}_2\text{O}$ – Structure 18

Structure **18** was synthesised using the reaction conditions outlined in table 5.15. using N,N'-2-methylpiperazinebis(methylenephosphonic acid). The product was collected as a fine microcrystalline powder, with no crystals being suitable for single crystal analysis. The powder x-ray diffraction pattern was indexed to give a hexagonal unit cell ($a = 16.03\text{\AA}$ and $c = 9.69\text{\AA}$) however the reflections present in the diffraction pattern were consistent with 16 spacegroups, listed in table 5.16.

Table 5.16: Possible space groups for structure 18

Trigonal space groups	Hexagonal space groups
P3, $\bar{P}3$, P321, P3m1,	P6, $\bar{P}6$, P6/m, P622,
$\bar{P}3m1$, P312, P31m, $\bar{P}31m$	P6mm, $\bar{P}62m$, $\bar{P}6m2$, P6/mmm

The powder x-ray diffraction pattern for structure **18** and unit cell parameters were found to be similar to those of an yttrium phase prepared in the same laboratory by J. A. Groves. Figure 5.45 shows the experimental powder X-ray diffraction patterns for structure **18** and its yttrium analogue.

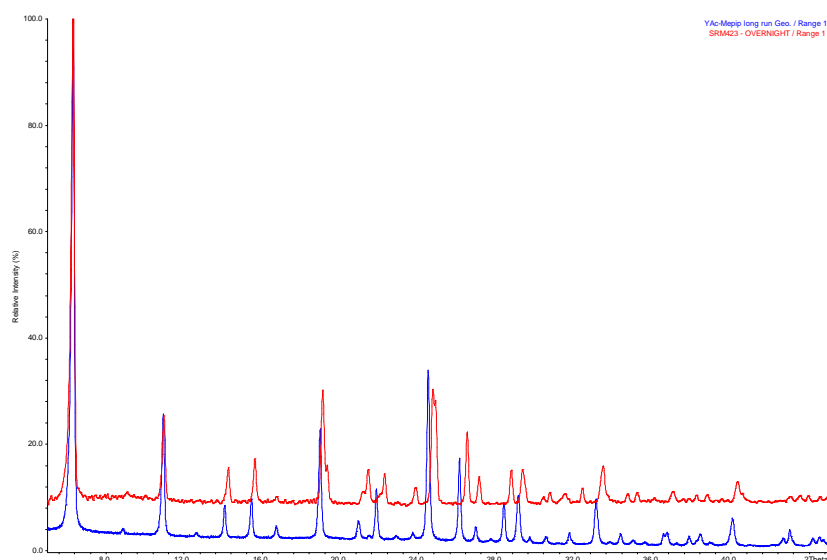


Figure 5.45: Experimental powder X-ray diffraction patterns for $[\text{Y}_2(\text{O}_3\text{PCH}_2(\text{NHC}_5\text{H}_{10}\text{NH})\text{CH}_2\text{PO}_3)_3] \cdot 4\text{H}_2\text{O}$ (blue) and its scandium analogue, structure **18** (red).

In order to obtain a suitable structural model for structure **18** which could be refined against the powder x-ray diffraction data two routes were pursued. Initially only powder data was available so that attempts were made via modelling and using the FOX program with a high degree of success. Independently a single crystal of the yttrium form became available that yielded a structure solution. Both methods of structure solution are described here.

A small crystal of the yttrium bisphosphonate yielded single crystal data, from which a partial structure was obtained, ($R_1 = 32\%$). From the single crystal information, the unit cell was confirmed, previously established from powder diffraction data, as well as a spacegroup. Assigning a specific spacegroup unambiguously had not been possible from the scandium or yttrium bisphosphonate data, and sixteen space groups (given in table 5.16) were possible on the basis of the observed reflections. Atomic co-ordinates were taken from the partial model, obtained from the yttrium single crystal diffraction data, and refined against the powder diffraction data. The Rietveld refinement of the powder data, collected on the as prepared sample, was performed with the GSAS program suite.⁷⁵ Firstly, instrumental parameters (background, zero-point, peak profile coefficients) were refined followed by structural parameters (unit cell, atomic co-ordinates, thermal parameters). Bond restraints were placed on the structure in order to direct the refinement of the data, as initially, refinement of the structure without bond constraints often led to atoms moving towards the centre of the pore. Positioning water molecules within the pores allowed the data to refine to give a close final fit to the observed data, with $R_{wp} = 4.6\%$.

For the structural solution from powder diffraction data alone, the yttrium bisphosphonate powder diffraction pattern and unit cell parameters, derived by indexing the powder data, were input in the EXPO2004 program suite. Only four different spacegroups were used whilst trying to propose a model by this method ($P3$, $P\bar{3}$, $P6$ and $P\bar{6}$) as any additional symmetry should be obvious from the final model. The trigonal spacegroup $P\bar{3}$ gave the most promising results, with the yttrium, phosphorus and oxygen atoms of the inorganic chains being located. As the bisphosphonate linker has been studied previously^{60, 69, 158-160} the interatomic distances are well known. From the phosphorus – phosphorus distances obtained from the EXPO2004 model, one sensible position for the bisphosphonate linker was located. The atomic coordinates of the inorganic chains were used in the GSAS program suite, and Fourier difference maps were generated in order to locate the organic. No sensible atomic coordinates were obtained by this method and consequently the atomic coordinates for the inorganic chains were input into Cerius², a molecular modelling / minimisation program suite.

This allowed the linker to be manually placed and fixed in the presence of symmetry constraints and then energy minimised free from all symmetry constraints. The resultant 'energy minimised' model was in P1, and high symmetry was searched for using the PLATON program suite, which suggested that the symmetry remained $P\bar{3}$. This process did not take into consideration any water molecules which could reside within the pores. The final models obtained from both the partial single crystal structure solution and the energy minimisation procedure were refined independently against the powder diffraction data using the GSAS program suite.

A Rietveld refinement of structure **18** was performed using GSAS, using the atomic coordinates of the yttrium material as a starting point. The bond distances and angles within the structures were all assumed to be similar to that of the yttrium sample, with the exception of the M – O bond length. In the case of octahedrally co-ordinated yttrium, the Y – O bond length is found to be approximately 2.35Å, in comparison with a standard Sc – O bond length of 2.05Å. Constraints were therefore placed upon all Sc – O bond lengths, as well as O – O bond lengths within scandium octahedra, during the refinement.

Instrumental parameters (background, zero-point, peak profile coefficients) and structural parameters (unit cell, atomic co-ordinates, thermal parameters) were refined, keeping constraints on the bond distances and angles. There was difficulty fitting the asymmetry of the first peak during the Rietveld refinement of the sample, with $R_{wp} = 8.2\%$, figure 5.46. Excluding the first peak from the refinement gives a R_{wp} value of 4.2%, figure 5.47.

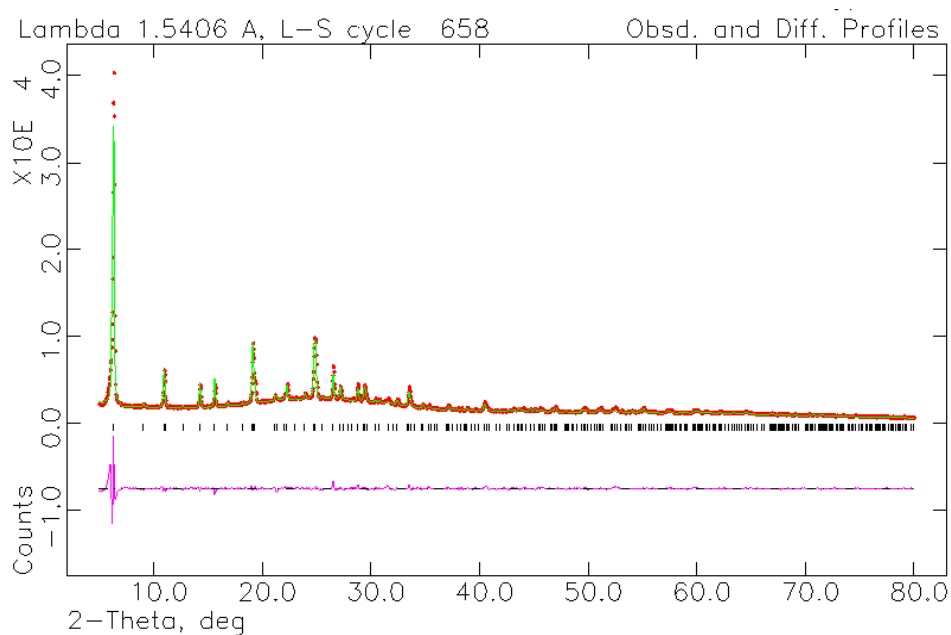


Figure 5.46: Rietveld refinement of structure **18** showing significant difference of the first peak between the experimental pattern (red) and the theoretical pattern (green). The difference plot is shown in purple.

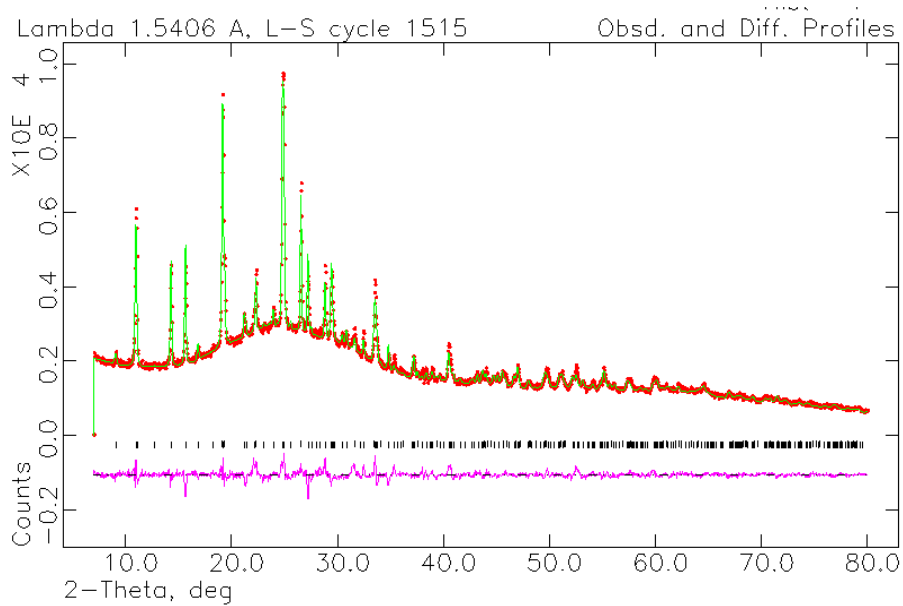


Figure 5.46: Rietveld refinement of structure **18** shown x-ray diffraction pattern with the first peak omitted from the refinement.

Table 5:17 Atomic coordinates for structure **18**

Atom	x	y	z	Occ	Ueq	Multiplicity
Sc(1)	0.6667	0.3333	0.30729(3)	1	0.0131(2)	2
Sc(2)	0.6667	0.3333	-0.20145(3)	1	0.0131(2)	2
P(1)	0.60878(2)	0.45496(2)	0.05577(3)	1	0.0131(2)	6
P(2)	0.77512(3)	0.51588(2)	0.54045(4)	1	0.0131(2)	6
O(1)	0.6518(3)	0.43367(2)	0.18071(4)	1	0.0131(2)	6
O(2)	0.62454(3)	0.41379(3)	-0.07521(3)	1	0.0131(2)	6
O(3)	0.64615(2)	0.56186(3)	0.0423(2)	1	0.0131(2)	6
O(4)	0.77367(3)	0.44837(4)	0.42891(3)	1	0.0131(2)	6
O(5)	0.53951(3)	0.27819(2)	-0.32348(2)	1	0.0131(2)	6
O(6)	0.87314(4)	0.60554(3)	0.55302(2)	1	0.0131(2)	6
O(7)	0.25005(2)	0.24581(3)	-0.14919(1)	1	0.0131(2)	6
O(8)	0	0	0.21842(2)	1	0.0131(2)	2
O(9)	0.14904(2)	0.08(3)	0.52909(3)	0.215	0.0131(2)	6
O(10)	0.31859(3)	0.0022(3)	0.27033(2)	0.215	0.0131(2)	6
N(1)	0.3918(3)	0.37919(3)	0.16717(3)	1	0.0131(2)	6
N(2)	0.30394(2)	0.36821(2)	0.41951(3)	1	0.0131(2)	6
C(1)	0.26582(3)	0.29728(3)	0.30065(2)	1	0.0131(2)	6
C(2)	0.16039(2)	0.22323(3)	0.28156(2)	1	0.0131(2)	6
C(3)	0.40597(4)	0.44276(4)	0.38048(4)	1	0.0131(2)	6
C(4)	0.47903(2)	0.39616(2)	0.08424(3)	1	0.0131(2)	6
C(5)	0.69199(2)	0.5566(2)	0.48143(2)	1	0.0131(2)	6
C(6)	0.3305(3)	0.27482(2)	0.20928(2)	1	0.0131(2)	6
C(7)	0.46867(3)	0.42644(2)	0.27702(2)	1	0.0131(2)	6

Thermal analysis of structure **18** was used to determine the number of water molecules present within the pores and shows a weight loss of 9% between room temperature and 100°C, which can be attributed to a loss of water molecules from within the pores.

Structure **18** is a porous framework bisphosphonate structure. The framework is built from chains of isolated ScO₆ octahedra which are bonded to each other via by three phosphonate tetrahedra. The chains, running parallel to the *c*-axis, are joined together by the piperazine moiety, with each inorganic chain being connected to three other chains. The arrangement of 6 inorganic chains connected by the organic moiety creates a channel system, down [001], with the inside of the channel being lined by the methyl group of the ligand, figure 5.47.

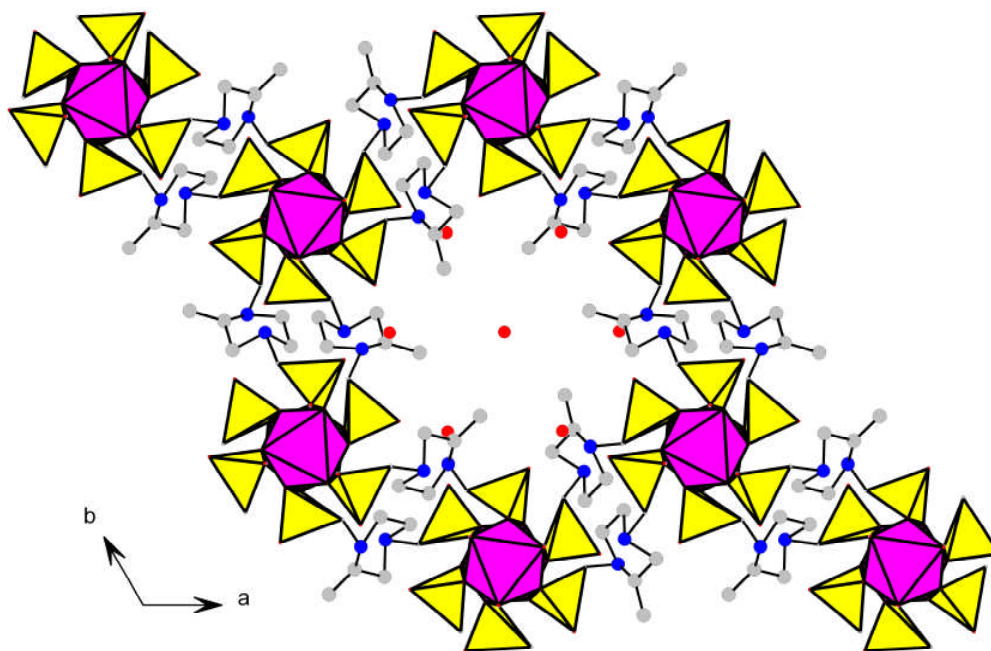


Figure 5.47: Projection down $[001]$ of structure **18**, showing a channel formed by six different scandium phosphonate chains, linked via methyl piperazine moiety. Water molecules can be seen situated within the pore, which is lined with methyl groups. Hydrogen atoms have been omitted for clarity.

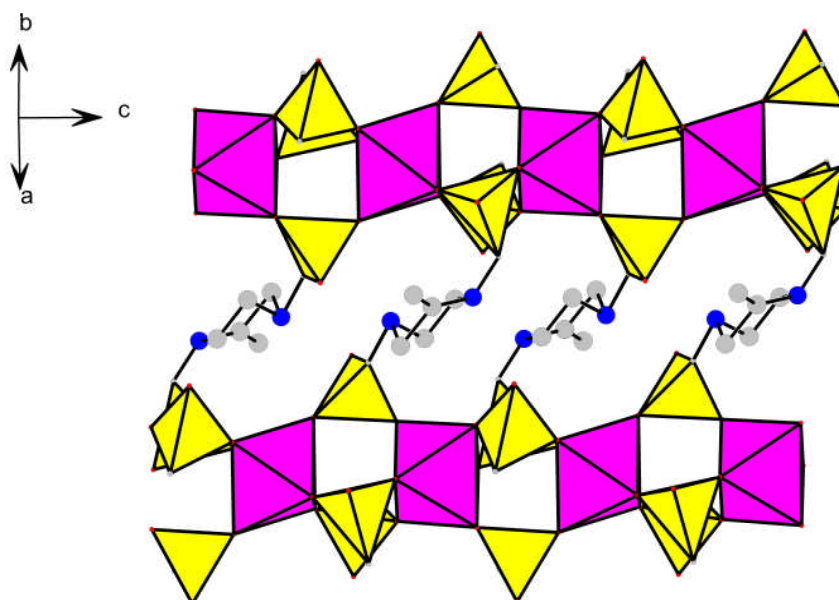


Figure 5.48: projection down $[110]$ showing chains of scandium phosphonate polyhedra linked via the piperazine moiety.

The channel, which is formed by six scandium phosphonate chains, is lined by methyl groups from the piperazine moiety. The methyl groups protrude into the pore of the structure at two different heights within the unit cell, with three methyl groups at each height, and the two sets of methyl groups are staggered in respect to each other. Allowing for the H atoms to have a van der Waals radius of 1.2Å, then these channels have a free diameter of around 3Å. The structural information strongly suggesting that there is only one carbon within the piperazine ring which is bonded to a methyl group, C(5). Electron density was not found in order to locate methyl groups attached to carbons atoms C(2) and C(3). A reason for this is believed to be steric hinderance.

In order to determine if it were possible for structure **18** to accommodate a methyl group at another position within the framework, attempts were made to synthesise the same material using both a chiral version of the ligand, and the 2,5-dimethyl version. Synthetic attempts using the 2,5-dimethyl and chiral 2-methyl version of the piperazine-based ligand proved only to yield the recrystallised ligand. Consequently it is believed that the methyl group must protrude into the pore of the material in order to form this solid. Methyl groups positioned pointing into the pore are less hindered sterically in comparison to those which would be positioned pointing away from the pore.

The final charge balanced structural formula is $[\text{Sc}_2(\text{HO}_3\text{PCH}_2(\text{NC}_5\text{H}_{10}\text{N})\text{CH}_2\text{PO}_3\text{H})_3]\cdot 4\text{H}_2\text{O}$. CHN analysis, weight %, calculated, C, 22.4%, H, 4.29%, N, 7.5%; measured, C, 22.9%, H, 4.7%, N, 7.7%.

Solid state ^{31}P MAS NMR, figure 5.49, shows a single intense peak at -3.2ppm which can be attributed to the two crystallographically unique but chemically similar phosphorus sites present within structure **18**. ^{45}Sc MAS NMR, figure 5.50, shows two distinct peaks at 14.3 and -12.7ppm which corresponds to the two crystallographically unique scandium sites present within structure **18**. ^{13}C CP MAS NMR shows several signals at 59.8, 56, 52.5, 44.4 and 15.4 ppm

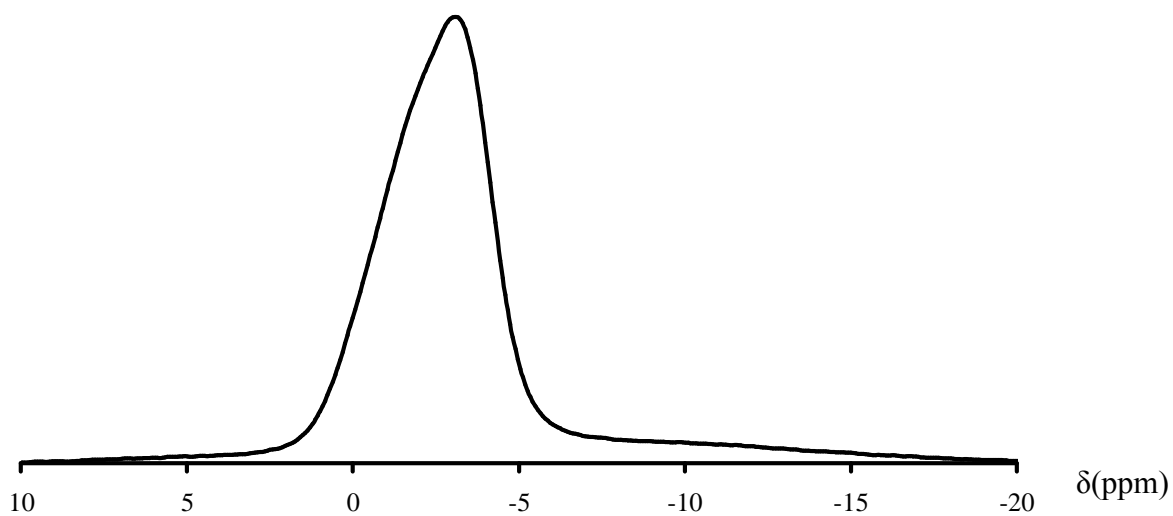


Figure 5.49: ^{31}P MAS NMR spectra for structure **18**, showing a single an intense peak at -3.16ppm corresponding to the two crystallographically unique phosphorus sites present.

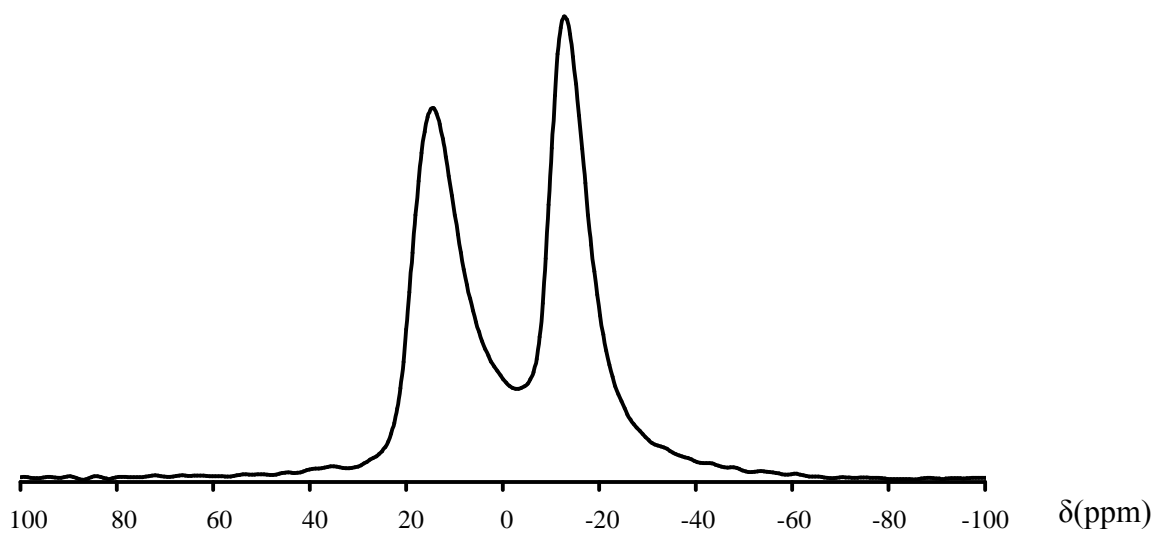


Figure 5.50: ^{45}Sc MAS NMR spectra of structure **18**, showing two peaks with maximum values at 14.3 and -12.7ppm

5.5 Discussion

The aim of this chapter was to utilise the structure directing potential of the Sc^{3+} cation, already mentioned in chapters 3 and 4, within scandium phosphonate systems. Previous chapters have discussed the formation of scandium phosphates and phosphites which demonstrated the potential of scandium as a framework element within microporous materials. However, an issue with these systems was the thermal stability, with framework integrity being lost with the loss of any organic template present within the structure.

In chapter 4, scandium phosphite systems were examined, with the hypothesis that reducing the number of oxygen atoms to which the phosphorus was bonded would reduce the potential for the formation of hydrogen bonding networks through POH groups, and thus lead to the formation of three dimensional framework materials. The structures reported in chapter 4 supported this hypothesis, with only a phosphite / phosphate structure (structure 8), not forming a three dimensional framework. All the materials reported within this chapter were 3 dimensional framework materials.

Chapter 5 has investigated the structural potential of scandium within phosphonate systems. Replacing the hydrogen present on the phosphite pseudo pyramid with an organic group, R, has led to the formation of several different novel scandium phosphonate and bisphosphonate systems.

Scandium phosphonates can form three-dimensionally connected porous frameworks which can be neutral or negatively charged. In all phosphonate frameworks described in this chapter, building blocks are arranged so that the structures are divided up into separate inorganic and organic regions, as usually seen for such hybrid phosphonate solids.

The inclusion of fluoride as a mineralising agent resulted in the formation of a dense three dimensional scandium phosphonate structure, $\text{ScF}(\text{H}_2\text{O})\text{CH}_3\text{PO}_3$, in which scandium fluoride chains are linked by phosphonate groups, with water making up the sixth coordination site on the scandium. Thermal treatment results in loss of water and subsequent solid state reaction at 300 °C. For $\text{NaSc}(\text{CH}_3\text{PO}_3)_2 \cdot \text{H}_2\text{O}$, which crystallises if sodium hydroxide is added to the synthesis gel, the scandium and methylphosphonate groups are fully linked in the inorganic network and so the solid is thermally stable to 400°C. The framework is anionic, and the charge is balanced in the as-prepared form by extra-framework sodium cations which occupy sites within six-membered rings in the walls of inorganic channels in the structure and coordinate to water within the channels. Although it does not adsorb nitrogen, it does exhibit reversible dehydration/rehydration behaviour.

Using phosphonic acids with a variety of different organic groups, such as phenyl, benzyl groups rather than methyl, resulted in the formation of a poorly microcrystalline products which could not be fully characterised.

Ethylenebisphosphonic acid was the first bisphosphonate system to be investigated, yielding a layered bisphosphonate pillared by the ethylene linker, with hydronium ions located in cavities within the layers. Thermal analysis suggests that the hydronium ion can not be removed from the cavities within destroying the framework.

The use of piperazine-based bis-phosphonic acids yielded three different crystalline materials, however none of these materials contained crystallites large enough for single crystal analysis. The structures of the two materials, which were synthesised using N,N'-piperazinebismethylenephosphonic acid have not yet been solved. The structure of the material synthesised using N,N'-2-methylpiperazinebis(methylene-phosphonic acid), structure **18**, was solved by a combination of single crystal analysis, direct methods from powder diffraction and molecular modeling, revealing a framework material with a one dimensional pore system. The pore size is relatively small, with an estimated free diameter of 3Å, however the structure shows reversible dehydration / hydration.

Key SBUs within the phosphonate structures reported in this chapter are shown in figure 5.51.

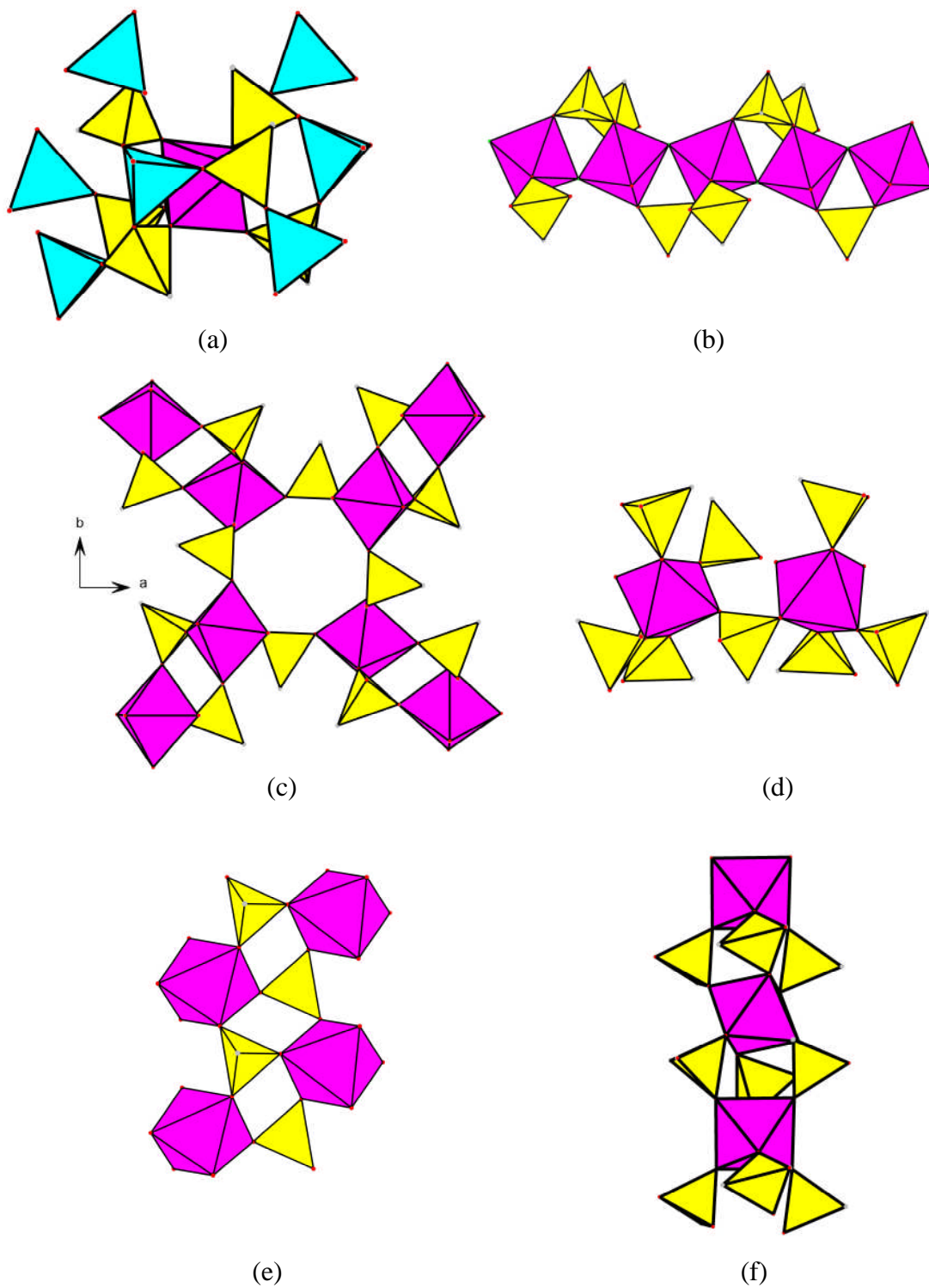


Figure 5.51: Secondary building units present within the scandium phosphite materials reported within this chapter. SBU's (a) – (f) are found within structures **13** - **18** respectively

Chapter 6

Scandium Carboxylates

6.1 Aims

Recently there has been a remarkable progress in the synthesis of porous metal di- and tri-carboxylates, with numerous novel structures with high thermal stability and large internal surface areas. The aim of this chapter is to investigate the crystal chemistry of scandium in carboxylate systems.

6.2 Introduction

As described previously, the design and synthesis of porous hybrid materials with high internal volumes and high thermal stability is a challenge which has been an intriguing area of research in recent years. Much 'MOF-related' research has been performed on metal carboxylates, investigating many possible combinations of different metals and carboxylate linkers. Among the carboxylate frameworks reported, most of the transition metal elements and an increasing number of f-block metals have been included as the main metal framework constituents. Within such systems, metals have been observed as isolated monomeric units, dimers, trimers, chains, layers and polymeric clusters and a variety of organic moieties have been used as the carboxylate linkers, from simple aliphatic to complex aromatic molecules.^{1,}

161-172

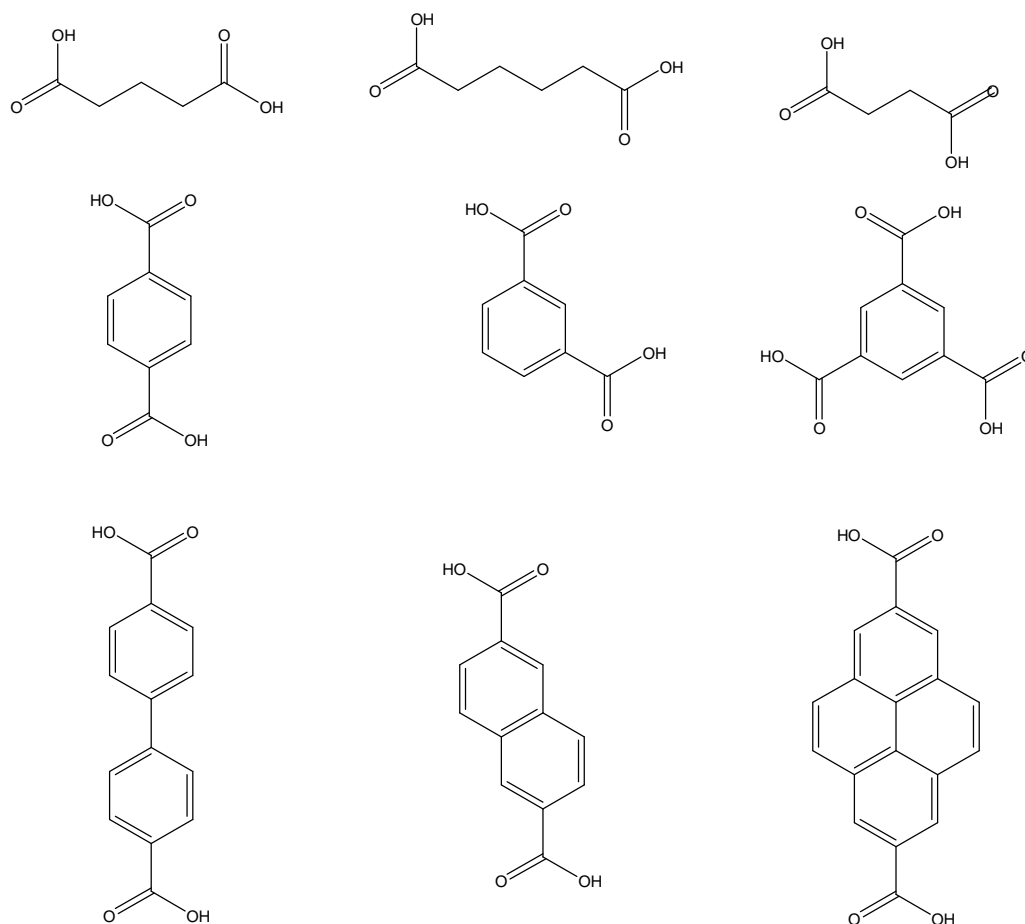


Figure 6.1: Possible di- and tricarboxylic acids which have been used within MOFs

Taking into account this variety of building units and the synthesis variables listed in chapter 1 (pH, temperature, time, etc), it is likely that very many more framework topologies are still to be discovered. The main approach to the synthesis of novel MOFs has been via exploratory synthesis, investigating a wide ‘composition space’. This is the approach that is adopted in this work for scandium. Nevertheless, there are current efforts to design MOFs with particular pore sizes and surface areas. Yaghi *et al.*,¹⁷³ for instance, have published a well established family of hybrid materials which yield the same framework topology with different linking units. These isorecticular metal organic frameworks, IRMOFs, clearly show the possibility of manipulating desirable physical qualities within a structure, e.g. pore size or internal volume. Also, Férey *et al* have introduced a computational approach to the design of hybrid frameworks, using global optimisation techniques.^{32, 174} The method applies the processing power of a computer to sift through a finite number of predefined building units, within a unit cell which is allowed to vary freely, focusing on the overall topology for the final lattice. This approach is known as the AASBU (automated assembly of secondary

building units) method and has been used successfully in structure solution and prediction of novel materials.¹⁷⁵⁻¹⁷⁷

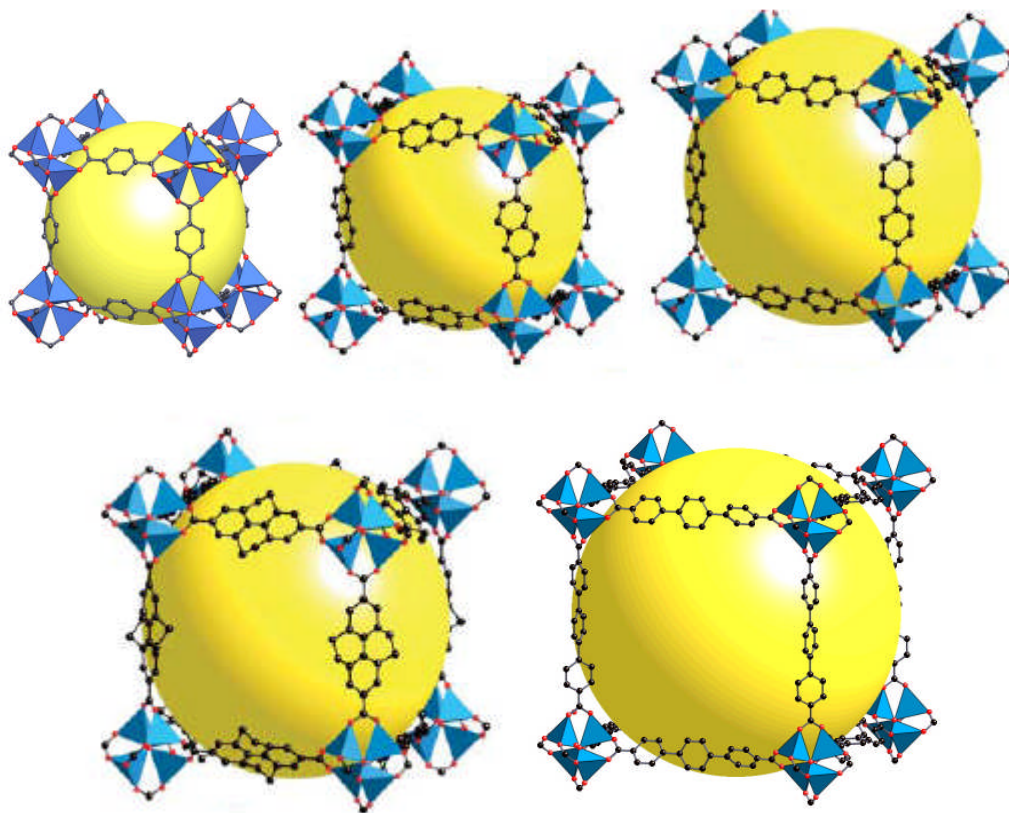


Figure 6.2: Isorecticular metal organic frameworks, IRMOFs. Each MOF consists of a cluster of four zinc tetrahedral sharing one oxygen atom, which are separated by dicarboxylic acids.

The main advantage to approaches such as these is that the specific chemistry of the solid could be determined prior to its synthesis. This implies that physical properties of MOFs, such as the chemistry of the internal surface, the volume of the pore, the opening size of the window and catalytic activity, can be deliberately imparted on a framework, rather than relying on a ‘luck of the draw’ approach. Nevertheless, empirical approaches remain important to indicate what chemistry is possible, and these are outlined for scandium carboxylates below.

There are a few scandium carboxylates reported in the literature.^{51-53, 178} Prior to the studies reported in this thesis, Perles *et al* had reported the synthesis and catalytic activity of a scandium succinate, $\text{Sc}_2(\text{O}_2\text{CC}_2\text{H}_4\text{CO}_2)_3$, and also suggested the potential for such materials in the area of Lewis acid catalysis.^{53, 178} Dietzel *et al* also reported a scandium coordination

polymer, synthesised using 2,5-dihydroxyterephthalic acid.⁵¹ The conditions used in the synthesis of this material resulted in the formation of a trimeric inorganic building block, within which three scandium cations are coordinated to the same μ_3 oxygen atom. This cluster has been observed previously in other MOF materials, such as the large pore materials MIL-100 and MIL-101.^{161, 179} It was thought that the higher charge associated with a trivalent Sc^{3+} cation could result in structures which are more thermally and hydrothermally stable than structures synthesised using divalent metals, such as zinc (MOF-5),¹⁷³ so the scandium carboxylates system was investigated

6.3 Experimental

To investigate further the structural variety of scandium-bearing carboxylates reaction compositions were examined using different scandium sources and carboxylate linkers. Aliphatic carboxylic acids were the investigated first, with initial reaction conditions chosen to be similar to those reported in other scandium carboxylate preparations.⁵³ Further experiments were performed with aromatic carboxylate linkers, initially using reaction stoichiometries similar to those used for reactions with aliphatic carboxylic acids. These were then modified to optimise product crystallinity and purity. The synthesis and structures of materials are discussed in two sections. Scandium carboxylates synthesised using aliphatic carboxylic acids are discussed in section 6.4 of this chapter and those synthesised using aromatic carboxylic acids in section 6.5. Details of the synthetic conditions are given in tables within the relevant parts of the chapter.

The positions of the hydrogen atoms in these structures were located through a combination of valence bond sum calculations and Fourier mapping, with their positions being fixed to 0.98(1)Å for aliphatic C-H with $U_{\text{iso}}(\text{H})$ being 1.2 times the parent carbon atoms, 0.93(1)Å for aromatic C-H bond with $U_{\text{iso}}(\text{H})$ being 1.2 times the parent carbon atom and 0.98(1)Å for a O-H bond with $U_{\text{iso}}(\text{H})$ being 1.5 equivalents of the parent oxygen atom.

All structures in this chapter were solved from single crystal data, and the crystallographic data are reported in Table 6.1-6.3. Wherever possible, phase purity of bulk samples was confirmed by Rietveld refinement of structural (and instrumental) parameters against powder diffraction data. Rietveld refinement was performed with the GSAS program suite⁷⁵ using the atomic co-ordinates determined by the single crystal structure solution as a starting point. Instrumental parameters (background, zero-point, peak profile coefficients) and structural parameters (unit cell, atomic co-ordinates, thermal parameters) were refined, keeping

constraints on the bond distances and angles. Close final fits to the observed data were achieved, with R_{wp} values between 7 and 10%, starting from structures determined from the single crystal experiments for structures **19**, **21-24**, **26** and **27**. In order to characterise the materials further, TGA was performed and ^{45}Sc MAS NMR spectra measured for phase pure samples to determine the NMR properties of scandium in carboxylate frameworks. ^{45}Sc MAS NMR spectra are presented with the structures with the experimental conditions given in Chapter 2. Further analysis of ^{45}Sc NMR is given in chapter 7.

Table 6.1: Crystallographic information for structures **19 - 21**

	Structure 19	Structure 20	Structure 21
Empirical Formula	Sc ₂ (O ₂ CC ₂ H ₄ CO ₂) ₃	Sc ₂ (OH)[O ₂ CC ₂ H ₄ CO ₂] _{2.5}	Sc ₂ (O ₂ CC ₃ H ₆ CO ₂) ₃
Formula Weight	219.07	386.02	222.09
Temperature (K)	150	93	150
Wavelength (Å)/ Diffractometer	0.69100 (16.2SMX)	0.71073 / (Sat)	0.67130 / (9.8)
Crystal System / Space group	Orthorhombic / Fdd2	Monoclinic / P2 ₁ /c	Monoclinic / C2/c
Unit Cell Dimensions			
a / Å	23.2913(16)	9.2150(11)	15.0920(51)
b / Å	15.9115(11)	7.7690(10)	8.2965(28)
c / Å	8.4090(6)	19.9180(15)	15.3829(50)
β (°)	-	95.91 (46)	91.9666(55)
Volume Å ³	3116.4(4)	1418.4(17)	1924.0(19)
Z	16	4	8
Number of reflections	7440	9958	5760
Number of unique reflections	2201	2755	1315
2θ range (°)	3.01 – 29.98	2.87 – 27.24	2.50 – 21.54
Variables / Restraints	118	208	113
R1 (I>2σI)	0.0234	0.1834	0.1184
R1 (all data)	0.0622	0.1858	0.1291
Max., Min. difference in electron density (eÅ ⁻³)	0.286, -0.226	1.789, -1.515	1.176, -1.102

Table 6.2: Crystallographic information for structures 22 - 24

		Structure 22	Structure 23	Structure 24
Empirical Formula		Sc(O ₂ CC ₁₂ H ₈ CO ₂) _{1.5} ·(H ₂ O) _{0.125}	Sc ₂ (O ₂ CC ₆ H ₄ CO ₂) ₃	Sc(OH)[O ₂ CC ₆ H ₄ CO ₂] ₃
Formula Weight		826.53	582.26	226.08
Temperature (K)		150	93	93
Wavelength (Å)/ Diffractometer		0.67090 / (16.2SMX)	0.71073 / (Sat)	0.69990 / (9.8)
Crystal System / Space group		Triclinic / P $\bar{1}$	Cubic / P2 ₁ 3	Monoclinic / C2/c
Unit Cell Dimensions	a / Å	7.913 (6)	13.345(3)	6.6900(6)
	b / Å	8.529 (8)	-	17.7350(7)
	c / Å	13.913 (8)	-	7.5630(5)
	α (°)	74.196 (11)	-	-
	β (°)	88.593 (10)	-	113.171(4)
	γ (°)	69.695 (11)	-	-
Volume		844.8(11)	2376.6(9)	824.94(10)
Z		1	4	4
Number of reflections		7775	23854	4792
Number of unique reflections		3660	1459	1366
2 θ range (°)		1.44 – 25.49	2.16-28.15	3.67-31.39
Variables / Restraints		257	115	68
R1 (I>2 σ I)		0.1462	0.0330	0.0333
R1 (all data)		0.421	0.0728	0.1047
Max., Min. diff in electron density (eÅ ⁻³)		1.59, -0.84	0.201, -0.188	0.954, -0.749

Table 6.3: Crystallographic information for structures 25 - 27

		Structure 25	Structure 26	Structure 27
Empirical Formula		Sc(OH)[O ₂ CC ₆ H ₄ CO ₂]	Sc ₂ (O ₂ CC ₆ H ₄ CO ₂) ₃	ScF(O ₂ CC ₆ H ₄ CO ₂)
Formula Weight		225.07	582.26	114.04
Temperature (K)		93	93	93
Wavelength (Å)/ Diffractometer		0.7103Å / (Sat)	0.7103 / (Sat)	0.7103 / (Mer)
Crystal System / Space group		Orthorhombic / I mcm	Orthorhombic / Fddd	Monoclinic C2/c
Unit Cell Dimensions	a / Å	18.112(15)	8.7550(3)	19.116(12)
	b / Å	11.590(25)	20.7786(7)	4.0396(24)
	c / Å	7.225(39)	34.4075(13)	9.903(10)
	α (°)	-	-	-
	β (°)	-	-	98.226(65)
	γ (°)	-	-	-
Volume		1516.7(89)	6259.30(38)	756.9(12)
Z		16	8	8
Number of reflections		5093	41789	2293
Number of unique reflections		807	4213	679
2θ range (°)		2.09 – 25.65	2.37 – 40.31	2.15 – 25.29
Variables / Restraints		39	89	65
R1 (I>2σI)		0.2334	0.0315	0.1388
R1 (all data)		0.2707	0.0428	0.1245
Max., Min. difference in electron density (eÅ ⁻³)		1.311, -1.140	0.846, -0.679	2.637, -1.069

6.4 Scandium Carboxylates Synthesised using Aliphatic Carboxylic Acids

A series of experiments were performed to investigate the hydrothermal chemistry of scandium, using various different aliphatic dicarboxylic acids as linker molecules. It is known that the aliphatic dicarboxylic acids exhibit interesting complexing behaviour due to their inherent flexibility, allowing a diverse range of coordination to the metal cations, e.g. monodentate, polydentate and chelating. The aliphatic carboxylic acids which have been investigated in this chapter are given in table 6.4. The synthetic conditions explored in this work are shown in table 6.5, which refers to the aliphatic carboxylic acids listed in figure 6.4.

Table 6.4: Aliphatic carboxylic acids explored as potential linkers in scandium carboxylates

Carboxylic acid	Structural formula	Annotation
succinic acid	HO ₂ C-(CH ₂) ₂ -CO ₂ H	'a'
glutaric acid	HO ₂ C-(CH ₂) ₃ -CO ₂ H	'b'
adipic acid	HO ₂ C-(CH ₂) ₄ -CO ₂ H	'c'
pimelic acid	HO ₂ C-(CH ₂) ₅ -CO ₂ H	'd'
suberic acid	HO ₂ C-(CH ₂) ₆ -CO ₂ H	'e'

Table 6.5: Selection of synthesis of scandium carboxylates using aliphatic carboxylic acids. The crystallisation reactions listed here were carried out at 220°C for 48h

Reactants			Product (structure number)
Sc ₂ O ₃	L	H ₂ O	
0.5	2 'a'	400	Sc ₂ (O ₂ CC ₂ H ₄ CO ₂) ₃ (19)
0.5	3 'a'	400	Sc ₂ (O ₂ CC ₂ H ₄ CO ₂) ₃ + Sc ₂ (O ₂ CC ₂ H ₄ CO ₂) _{2.5} OH (19 + 20)
0.5	2 'b'	400	Sc ₂ (O ₂ CC ₃ H ₆ CO ₂) _{1.5} (21)
0.5	2 'c'	400	Unknown solid
0.5	2 'd'	400	Unknown solid
0.5	2 'e'	400	Unknown solid

Some aliphatic carboxylic acids investigated in these reactions yielded microcrystalline solids, the structures of which have not yet been determined. The diffraction patterns for products of some of the synthetic conditions listed in table 6.5 are shown in figure 6.3.

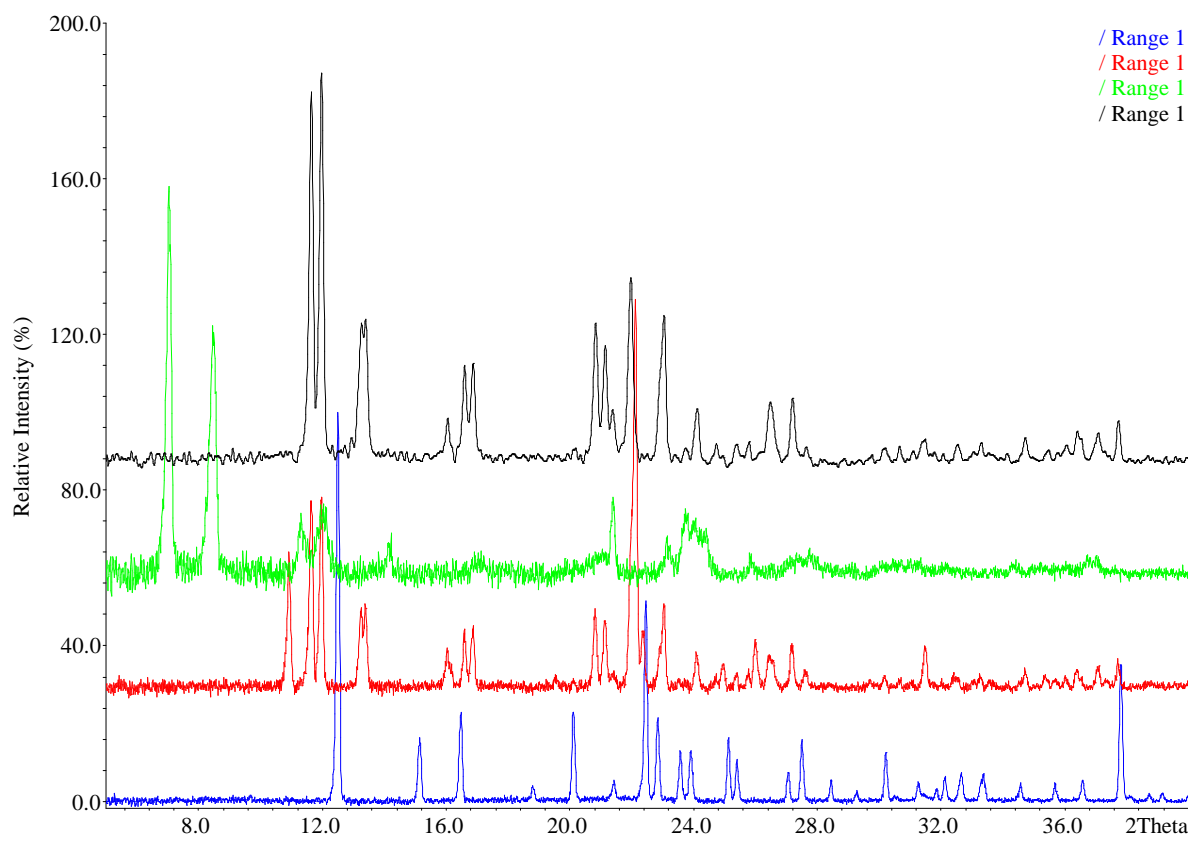


Figure 6.3: X-ray diffraction patterns for four scandium carboxylate materials prepared during this work. The different colour diffractograms, blue, red, green and black correspond to materials formed in the absence of hydrofluoric acid and using succinic, glutaric, adipic and pimelic acid, respectively.

6.4.1 Scandium succinate $\text{Sc}_2(\text{O}_2\text{CC}_2\text{H}_4\text{CO}_2)_3$ – Structure 19

Structure **19**, $\text{Sc}_2(\text{O}_2\text{CC}_2\text{H}_4\text{CO}_2)_3$, was solved from single crystal X-ray data collected on Station 16.2SMX at the synchrotron radiation facility, Daresbury, by direct methods and Fourier syntheses, using the SHELXS program.⁸¹ The crystallographic information is outlined in table 6.1, with atomic co-ordinates listed below in table 6.4.

Table 6.4: Atomic co-ordinates for structure **19**, $\text{Sc}_2(\text{O}_2\text{CC}_2\text{H}_4\text{CO}_2)_3$

Atom	x	y	z	U_{iso}	Occ	Multiplicity
Sc(1)	0.09096(2)	0.12120(1)	0.99993(4)	0.0077(1)	1	16
O(1)	0.14693(9)	0.04807(6)	1.10258(19)	0.0150(3)	1	16
O(2)	0.03335(9)	0.19348(6)	0.90767(18)	0.0147(3)	1	16
O(3)	0.20459(8)	0.15480(6)	0.93129(18)	0.0132(3)	1	16
O(4)	0.09553(9)	0.16223(7)	1.22348(19)	0.0181(3)	1	16
O(5)	-0.02409(10)	0.09033(8)	1.0664(2)	0.0212(3)	1	16
O(6)	0.08064(9)	0.07551(6)	0.78303(17)	0.0139(3)	1	16
C(1)	0.21443(11)	-0.02840(8)	1.2408(3)	0.0144(3)	1	16
C(2)	0.28536(11)	0.22729(8)	0.8051(2)	0.0095(3)	1	16
C(3)	0.12031(12)	0.19225(8)	1.4907(2)	0.0124(3)	1	16
C(4)	0.27260(11)	0.18271(7)	0.9337(2)	0.0088(3)	1	16
C(5)	0.14892(11)	0.17028(7)	1.3308(2)	0.0104(3)	1	16
C(6)	0.21441(11)	0.02953(8)	1.1610(2)	0.0099(3)	1	16

$\text{Sc}_2(\text{O}_2\text{CC}_2\text{H}_4\text{CO}_2)_3$, structure **19**, presents a novel three-dimensional scandium carboxylate framework, where the scandium to linker ratio is 2:3. The framework is made up of two different columns of isolated ScO_6 octahedra running parallel to [100].

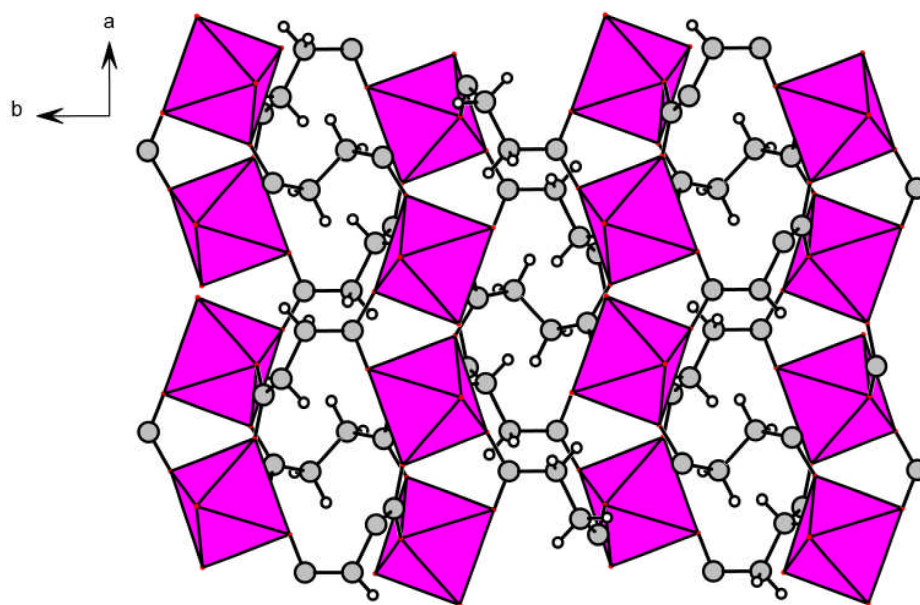


Figure 6.4: Projection down [001] of structure **19**, showing isolated scandium octahedra arranged in chains, running parallel to the a-axis. Each scandium octahedron is linked via the carboxylate linkers present on the succinic acid linkers.

In total, each ScO_6 octahedron is connected to eight other ScO_6 octahedra, via bridging carboxylate groups or succinate linkers, with only two lying within the same column. The other 6 octahedra are situated in columns which run perpendicular to the first column, shown in figure 6.5. The framework is non-porous.

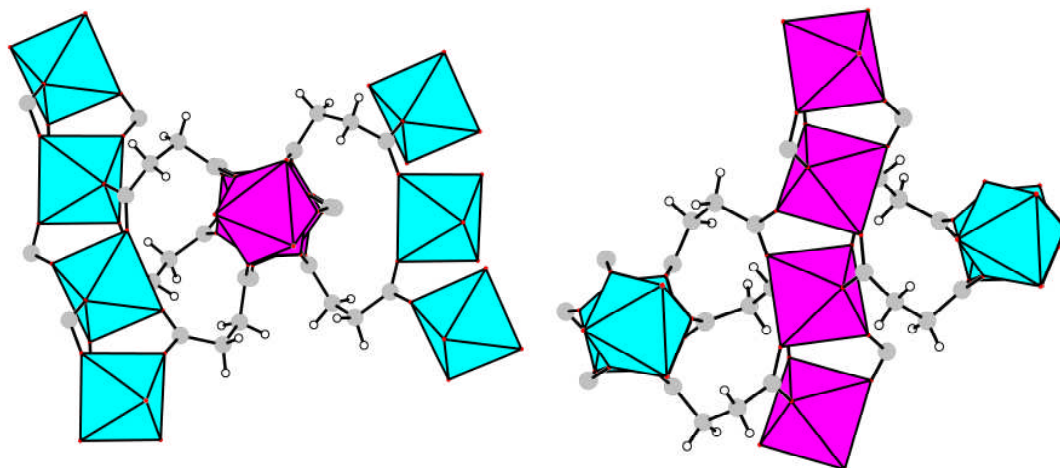


Figure 6.5: Representations of the local environment surrounding scandium octahedra. The portion of the structure on the left shows how one octahedral unit can link to six different octahedra out with the same chain. The portion of the structure on the right depicts how the octahedra join to each other within the same chain.

^{45}Sc MAS NMR (figure 6.6) shows a signal with maxima at -21.8 and -36.3ppm, with a typical quadrupolar line shape for a single ^{45}Sc species, which corresponds to the only scandium site present within the framework.

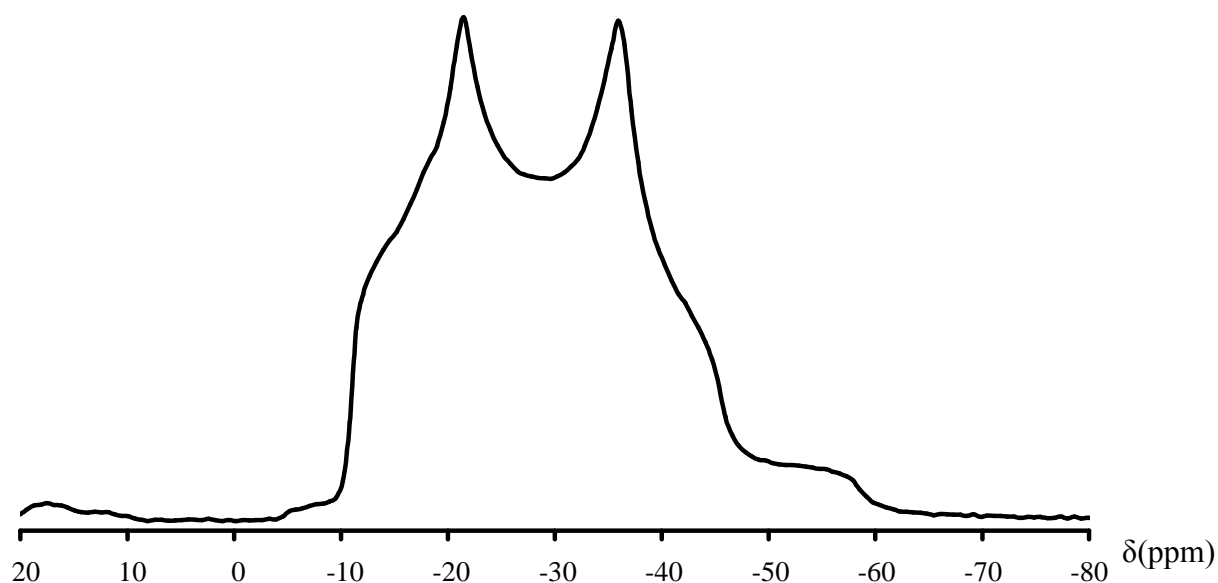


Figure 6.6: ^{45}Sc MAS NMR of structure **19** showing a signal with peaks at -21.8 and -36.3 ppm, with a typical quadrupolar line shape for a single ^{45}Sc species.

Thermogravimetric analysis shows a weight loss of 47.2% between 535 and 555°C which corresponds to the thermal decomposition of the framework.

6.4.2 Scandium succinate hydroxide $\text{Sc}_2\text{OH}(\text{O}_2\text{CC}_2\text{H}_4\text{CO}_2)_{2.5}$ – Structure **20**

Structure **20**, $\text{Sc}_2\text{OH}(\text{O}_2\text{CC}_2\text{H}_4\text{CO}_2)_{2.5}$, was recovered as a minority phase in the preparation of structure **19**. The structure was solved from single crystal X-ray data by direct methods and Fourier syntheses, using the SHELXS program.⁸¹ Owing to the small size of the crystals of structure **20** single crystal data collection was difficult. A structure was determined from the data although it had poor residual values. The crystallographic information is outlined in table 6.1, with atomic co-ordinates listed below in table 6.5.

Table 6.5: Atomic co-ordinates for structure **20**

Atom	x	y	z	U _{iso}	Occ	Multiplicity
Sc(1)	0.6880(3)	0.6913(4)	0.83030(15)	0.0110(8)	1	4
Sc(2)	0.2992(3)	0.6844(4)	0.85227(15)	0.0103(8)	1	4
O(1)	0.7155(12)	0.5832(14)	0.7360(6)	0.012(2)	1	4
O(2)	0.1764(13)	0.6195(15)	0.7635(6)	0.014(2)	1	4
O(3)	0.4722(13)	0.7605(14)	0.8018(5)	0.013(2)	1	4
O(4)	0.4217(13)	0.7424(16)	0.9467(5)	0.015(3)	1	4
O(5)	0.3910(13)	0.4392(14)	0.8642(6)	0.015(2)	1	4
O(6)	0.1329(12)	0.5975(15)	0.9068(6)	0.014(2)	1	4
O(7)	0.2026(13)	0.9327(14)	0.8474(6)	0.012(2)	1	4
O(8)	0.6553(13)	0.7592(16)	0.9309(6)	0.017(3)	1	4
O(9)	0.6320(13)	0.4358(16)	0.8595(6)	0.017(3)	1	4
O(10)	0.9043(13)	0.6403(16)	0.8601(6)	0.018(3)	1	4
O(11)	0.7512(13)	0.9379(16)	0.8109(6)	0.019(3)	1	4
C(1)	0.1668(15)	0.5558(18)	0.7069(7)	0.006(3)	1	4
C(2)	-0.0027(18)	0.5955(18)	0.9119(7)	0.009(3)	1	4
C(3)	0.5167(17)	0.3687(19)	0.8763(7)	0.008(3)	1	4
C(4)	-0.0609(17)	0.537(2)	0.9757(8)	0.012(3)	1	4
C(5)	0.0556(18)	0.630(2)	0.6532(8)	0.014(3)	1	4
C(6)	0.8021(17)	0.5619(19)	0.6907(7)	0.009(3)	1	4
C(7)	0.4065(18)	0.176(2)	0.9612(8)	0.013(3)	1	4
C(8)	0.5228(19)	0.198(2)	0.9119(8)	0.014(3)	1	4
C(9)	-0.0827(18)	0.698(2)	0.6816(8)	0.014(3)	1	4
C(10)	0.5561(18)	0.7682(19)	0.9674(8)	0.012(3)	1	4

Sc₂(O₂CC₂H₄CO₂)_{2.5}OH, structure **20**, presents a three-dimensional scandium succinate hydroxide framework where the scandium to linker ratio is 4:5. The structure consists of Sc₂O₁₀OH dimeric units which are linked to each other via succinate groups as shown in figure 6.7.

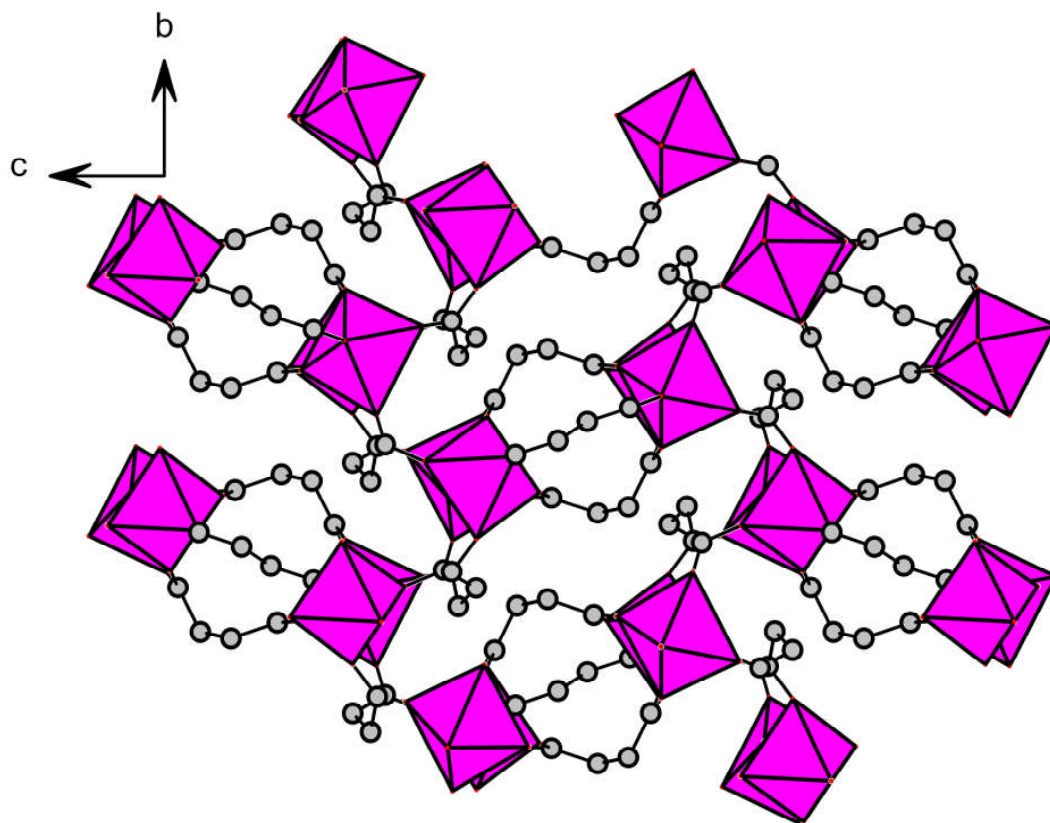


Figure 6.7: Projection down [100] of structure **20** showing scandium octahedral units linked via succinate linkers. Hydrogen atoms have been omitted for clarity.

Structure **20** has previously been reported by Perles *et al* and was noted for its high thermal stability and activity as a Lewis acid catalyst.⁵³ Within structure **20**, each scandium octahedron is bonded to five different succinic acid linkers, and another, crystallographically unique scandium atom, via a hydroxyl group. Every carboxylate terminus of the succinate linker is bonded to different scandium atoms, creating a bridging effect between scandium octahedral units, shown in figure 6.8.

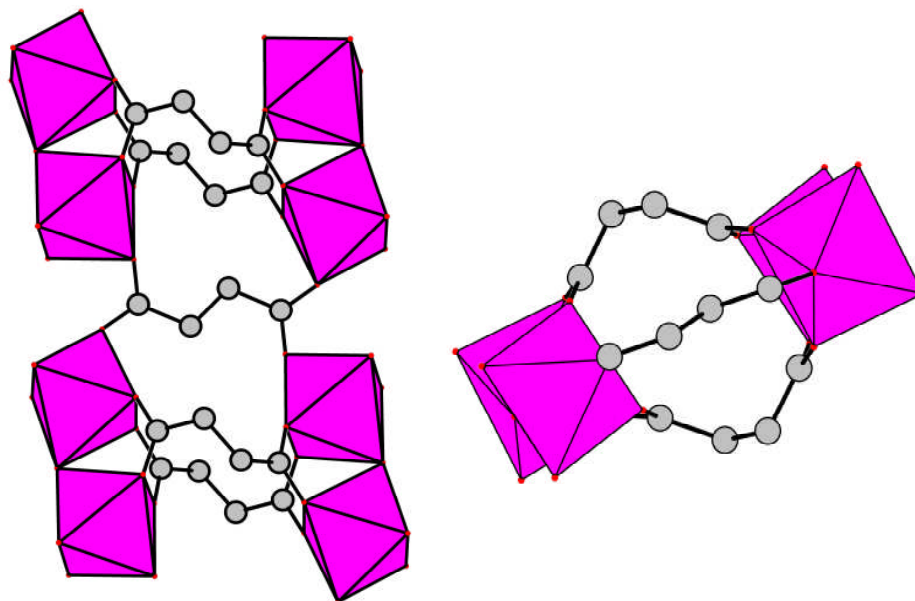


Figure 6.8: *Left; Dimeric $Sc_2O_{10}OH$ units linked together by three different succinate units. Right: An 'end-on' projection of the left hand image clearly showing the succinate linkers creating a bridge effect between the different dimeric units.*

6.4.3 Scandium glutarate, $Sc_2(O_2CC_3H_6CO_2)_3$ - Structure 21

Structure **21**, $Sc_2(O_2CC_3H_6CO_2)_3$, was solved from single crystal X-ray data collected on station 9.8 at the synchrotron radiation facility, Daresbury, by direct methods and Fourier syntheses, using the SHELXS program.⁸¹ The crystallographic information is outlined in table 6.1, with atomic co-ordinates listed below in table 6.6.

Table 6.6: Atomic co-ordinates for structure **21**

Atom	x	y	z	U _{iso}	Occ	Multiplicity
Sc(1)	0	0	0.5	0.0256(7)	1	4
Sc(2)	0.75	0.25	0.5	0.0686(13)	1	4
O(1)	0.9502(3)	-0.0926(9)	0.8802(4)	0.0475(19)	1	8
O(2)	0.8832(3)	-0.1006(7)	0.5326(4)	0.0313(15)	1	8
O(3)	0.0238(4)	-0.2053(8)	0.4296(5)	0.058(2)	1	8
O(4)	0.7656(4)	0.0343(12)	0.5681(4)	0.070(3)	1	8
O(5)	0.8180(5)	-0.1703(13)	0.8953(4)	0.092(4)	1	8
O(6)	0.1411(5)	-0.3536(13)	0.4338(4)	0.090(3)	1	8
C(1)	0.8102(5)	-0.0895(15)	0.5689(6)	0.047(3)	1	8
C(2)	0.8704(5)	-0.1621(11)	0.7514(6)	0.035(2)	1	8
C(3)	0	-0.3202(15)	0.25	0.039(3)	1	4
C(4)	0.8802(5)	-0.1398(11)	0.8483(6)	0.033(2)	1	8
C(5)	0.0675(7)	-0.3187(14)	0.4025(7)	0.060(3)	1	8
C(6)	0.7813(7)	-0.2048(18)	0.7160(7)	0.074(4)	1	8
C(7)	0.7783(7)	-0.2345(17)	0.6163(7)	0.072(4)	1	8
C(8)	0.0333(13)	-0.4167(15)	0.3272(9)	0.120(8)	1	8

$\text{Sc}_2(\text{O}_2\text{CC}_3\text{H}_6\text{CO}_2)_3$, structure **21**, presents a novel three-dimensional framework (2Sc:3L) containing isolated octahedra arranged in layers running perpendicular to the *c*-axis, figure 6.9. Each scandium octahedron is connected to two different scandium octahedra within the same row via three different bridging carboxylate groups, i.e. Sc(1) is connected to Sc(2) at opposing sides.

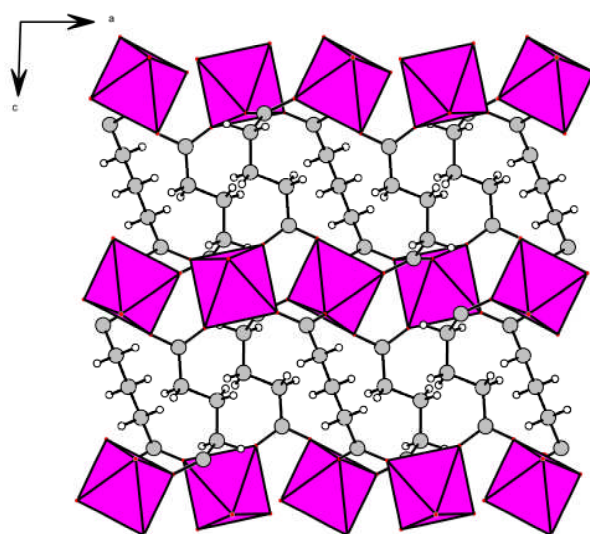


Figure 6.9: Projection down [010] of structure **21**, showing rows of isolated scandium octahedral units bridged by carboxylate linkers.

The layers of isolated scandium octahedral units contain the octahedra on rows, which adopt two different orientations as shown in figure 6.10.

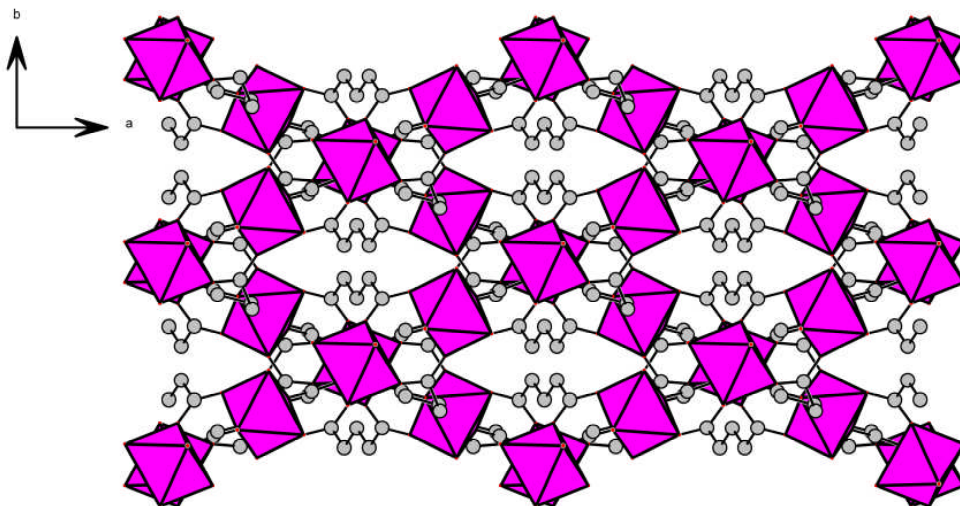


Figure 6.10: Projection down [001] of structure **21** showing the isolated scandium octahedral units aligning in rows. The rows are orientated in two different directions in alternate layers creating a diamond-like motif. Hydrogen atoms have been excluded for clarity.

Solid state ^{45}Sc MAS NMR (figure 6.11) shows an intense signal at -8.6ppm. This signal can be fitted to two independent scandium sites using the program DMFIT¹⁸⁰ with chemical shifts of -3.3 and -0.5 ppm which is consistent with the crystallography. (See chapter 7 for details)

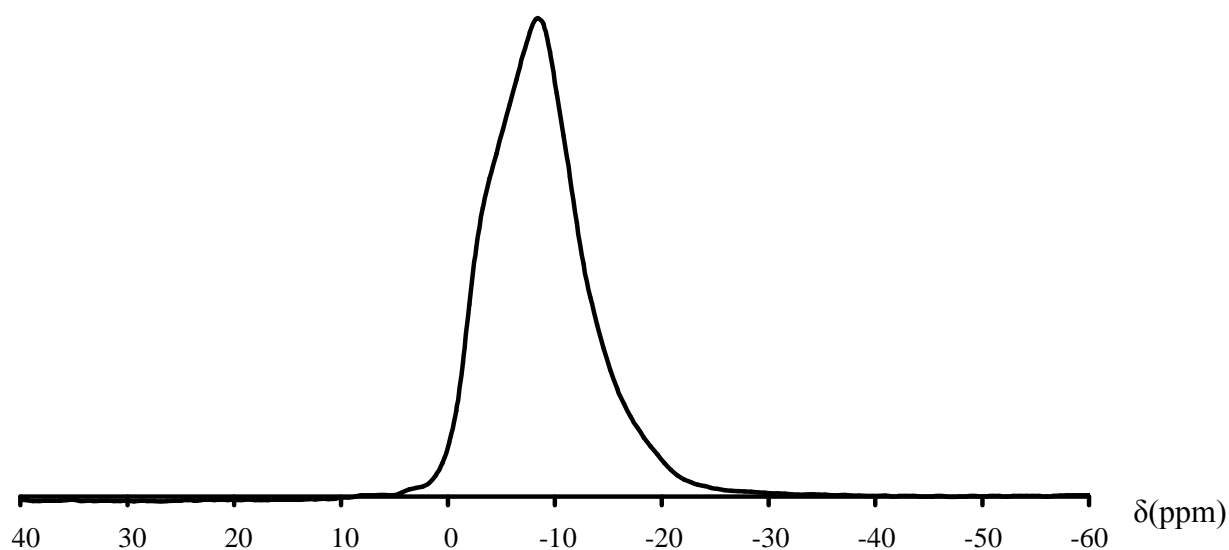


Figure 6.11: Solid state ^{45}Sc MAS NMR showing an maximum signal at -8.6ppm

Thermogravimetric analysis shows a weight loss of 57.2% between 525 and 560 °C, owing to the thermal decomposition of the material. The material is amorphous after heating.

6.5 Scandium Carboxylates Synthesised using Aromatic Carboxylic Acids

Although investigations into the synthesis of scandium carboxylate materials using aliphatic carboxylic acids as linker molecules has yielded novel structures, none of these materials shows any potential for adsorption or gas storage purposes owing to the lack of free space within the structures.

The use of aromatic based dicarboxylic acid has been shown to produce a plethora of solids, with varying topologies.^{34, 181-184} Substituting carboxylic acid groups at the 1,4-, 1,3- or 1,3,5-positions on a benzene ring, figure 6.12, gives simple di- and tri-carboxylic acids which have been used extensively with many different di- and trivalent transition metals, to give porous solids.

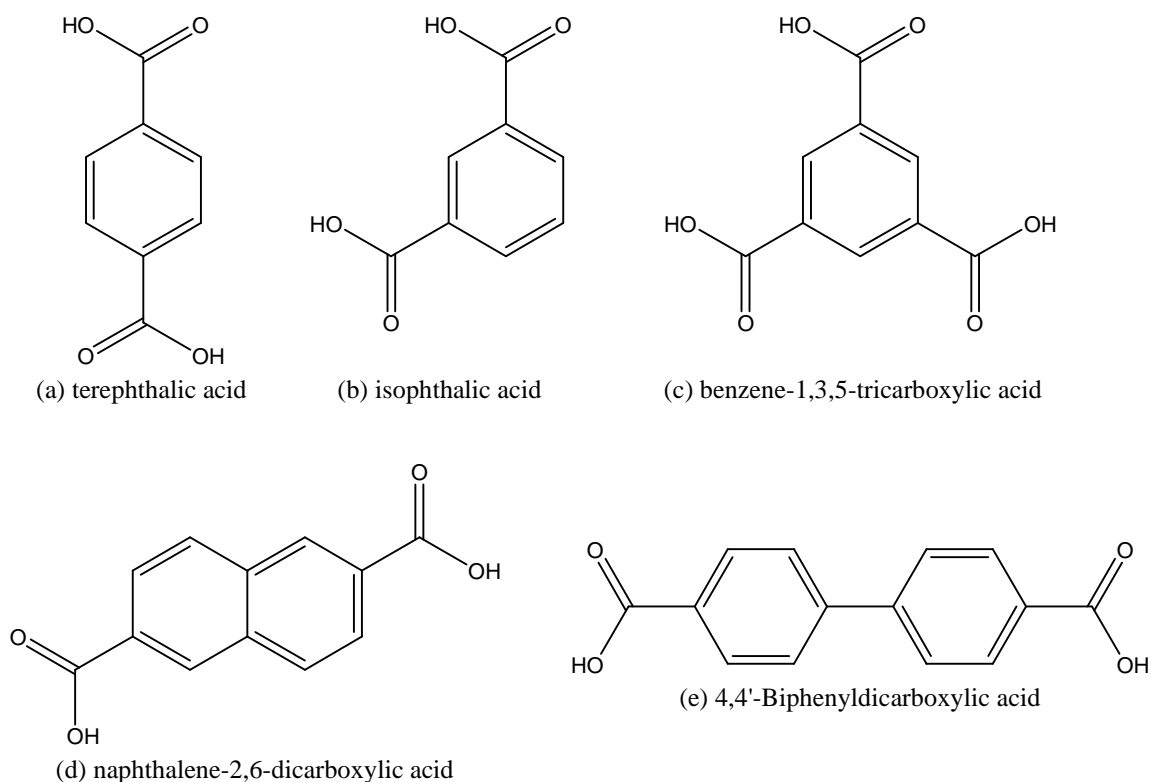


Figure 6.12: Aromatic di- and tri- carboxylic acids.

The use of aromatic carboxylic linkers within MOF materials can have advantages over their aliphatic counterparts. The structural properties of the moieties themselves are attractive as they can impart properties such as rigidity on new materials and there is free rotation of the carboxylic to aromatic carbon-carbon bond, which allows the linker to facilitate a variety of environments, for example bridging isolated polyhedra, clusters or chains.

A series of experiments were performed to investigate the hydrothermal chemistry of scandium with aromatic carboxylic acids as linker molecules, table 6.7. The chemistry of the scandium terephthalate system proved to be more complex than the other aromatic linkers examined. The effects of varying experimental conditions on the scandium terephthalate products are discussed later in this chapter.

Table 6.7: Selection of successful reaction conditions investigated using aromatic carboxylic acids. The reactions listed here were carried out at 220°C for 48h

Reactants			Product (structure number)
Sc ₂ O ₃	L	H ₂ O	
0.5	2 'b'	300	Sc ₂ (O ₂ CC ₆ H ₄ CO ₂) ₃ (23)
0.5	3 'b'	300	Sc ₂ (O ₂ CC ₆ H ₄ CO ₂) ₃ (23) + 'b'
0.5	2 'c'	400	'c'
0.5	3 'c'	300	'c'
0.5	2 'd'	300	Unknown 'a'
0.5	3 'd'	300	Unknown 'a'
0.5	2 'e'	300	Sc(O ₂ CC ₁₂ H ₈ CO ₂) _{1.5} .(H ₂ O) _{0.125} (22)
0.5	3 'e'	300	Sc(O ₂ CC ₁₂ H ₈ CO ₂) _{1.5} .(H ₂ O) _{0.125} (22) + unknown

6.5.1 Scandium 4,4'-biphenyldicarboxylate, Sc(O₂CC₁₂H₈CO₂)_{1.5}.(H₂O)_{0.125} (**22**)

Structure **22**, Sc(O₂CC₁₂H₈CO₂)_{1.5}.(H₂O)_{0.125}, was solved from single crystal X-ray data collected on station 9.8 at the synchrotron radiation facility, Daresbury, by direct methods and Fourier syntheses, using the SHELXS program.⁸¹ The crystallographic information is outlined in table 6.2, with atomic co-ordinates listed below in table 6.8.

Table 6.8: Atomic co-ordinates for structure **22**

Atom	x	y	z	U _{iso}	Occ	Multiplicity
Sc(1)	0.1773(3)	0.1922(3)	0.49597(16)	0.0224(6)	1	2
O(1)	0.6556(11)	0.0384(11)	0.4032(6)	0.0314(19)	1	2
O(2)	0.0156(11)	0.5838(10)	-0.4054(6)	0.0324(19)	1	2
O(3)	0.2234(10)	0.3321(10)	-0.4100(6)	0.0282(18)	1	2
O(4)	-0.0355(11)	0.1382(11)	0.5697(6)	0.033(2)	1	2
O(5)	-0.170(1)	-0.0587(10)	0.6117(6)	0.0284(18)	1	2
O(6)	0.3934(11)	0.2361(10)	0.4198(6)	0.0300(19)	1	2
O(7)	0.542(11)	0.415(11)	-0.452(6)	0.05(2)	0.125	2
C(11)	0.5173(15)	0.1650(14)	0.3664(9)	0.029(3)	1	2
C(12)	0.4856(15)	0.2376(14)	0.2541(9)	0.026(2)	1	2
C(13)	0.345(2)	0.3883(16)	0.2064(10)	0.045(4)	1	2
C(14)	0.311(2)	0.4377(17)	0.1029(10)	0.047(4)	1	2
C(15)	0.4086(15)	0.3350(14)	0.0432(9)	0.026(2)	1	2
C(16)	0.5524(18)	0.1896(19)	0.0913(10)	0.046(4)	1	2
C(17)	0.5899(19)	0.142(2)	0.1932(10)	0.053(4)	1	2
C(18)	0.3574(14)	0.3765(15)	-0.0668(9)	0.026(2)	1	2
C(19)	0.2085(19)	0.5196(19)	-0.1144(10)	0.047(4)	1	2
C(110)	0.1466(19)	0.5478(16)	-0.2124(10)	0.045(4)	1	2
C(111)	0.2357(15)	0.4350(15)	-0.2675(9)	0.028(3)	1	2
C(112)	0.3876(19)	0.299(2)	-0.2244(11)	0.060(5)	1	2
C(113)	0.448(2)	0.271(2)	-0.1244(11)	0.066(6)	1	2
C(114)	0.1538(14)	0.4531(13)	-0.3697(8)	0.020(2)	1	2
C(21)	-0.1038(14)	0.0449(15)	0.6316(9)	0.026(2)	1	2
C(22)	-0.0997(13)	0.0487(14)	0.7403(8)	0.025(2)	1	2
C(23)	-0.0315(16)	0.1612(14)	0.7691(9)	0.029(3)	1	2
C(24)	0.0027(15)	0.1442(15)	0.8698(8)	0.026(2)	1	2
C(25)	-0.0257(14)	0.0130(14)	0.9457(9)	0.026(2)	1	2
C(26)	-0.1100(15)	-0.0875(14)	0.9173(8)	0.024(2)	1	2
C(27)	-0.1465(14)	-0.0700(15)	0.8141(8)	0.025(2)	1	2

Structure **22**, $\text{Sc}(\text{O}_2\text{CC}_{12}\text{H}_8\text{CO}_2)_{1.5}(\text{H}_2\text{O})_{0.125}$, is a novel three dimensional scandium carboxylate material. The scandium to carboxylate linker ratio is similar to that of other scandium carboxylate structures reported in the literature.^{49, 52} Structure **22** consists of isolated ScO_6 octahedra which form layers, parallel to (100). These layers are linked together via two 4,4'-biphenyldicarboxylate linkers which can assume one of two orientations, figure 6.13.

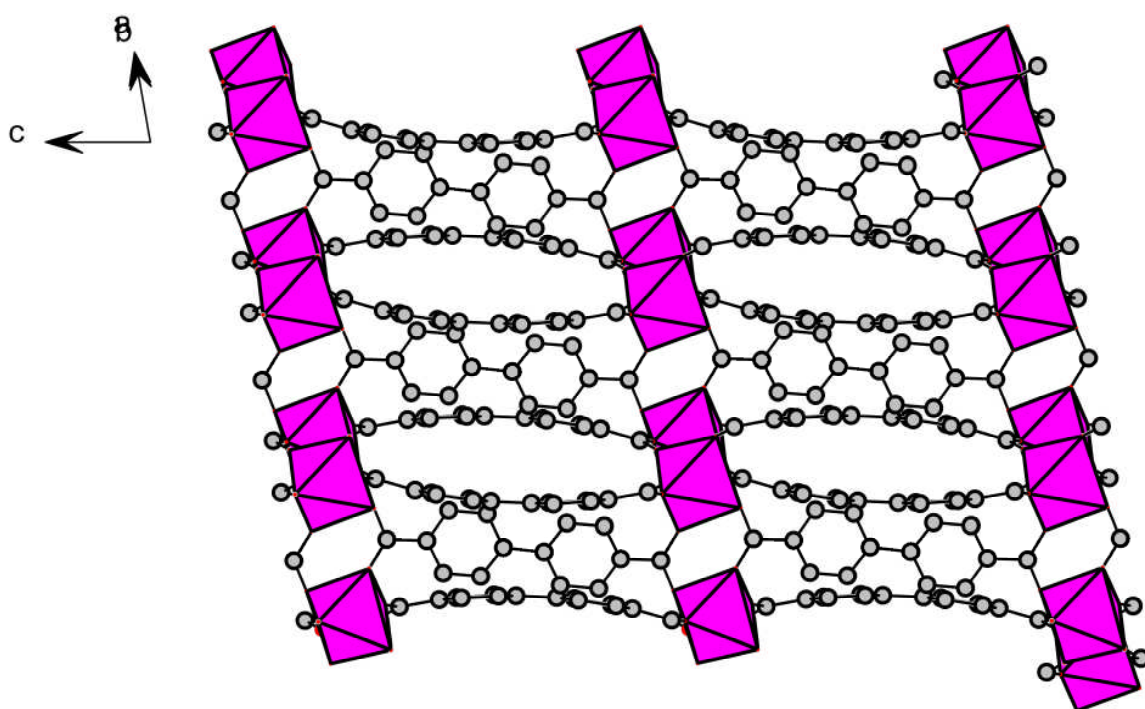


Figure 6.13: Representation of structure 22 showing isolated scandium octahedra, arranged in columns linked by the biphenyldicarboxylate

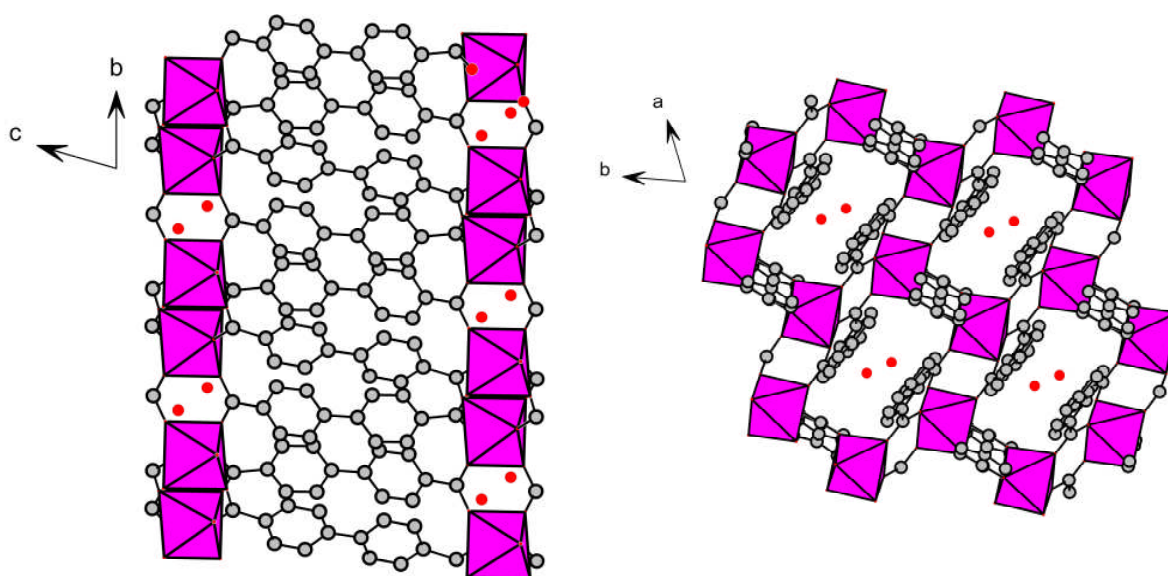


Figure 6.14: (Left) Projection down [100] of structure 22 showing rows of isolated scandium octahedra. (Right) Projection down [001] showing a single layer of isolated octahedra. Water molecules are shown situated within the pores.

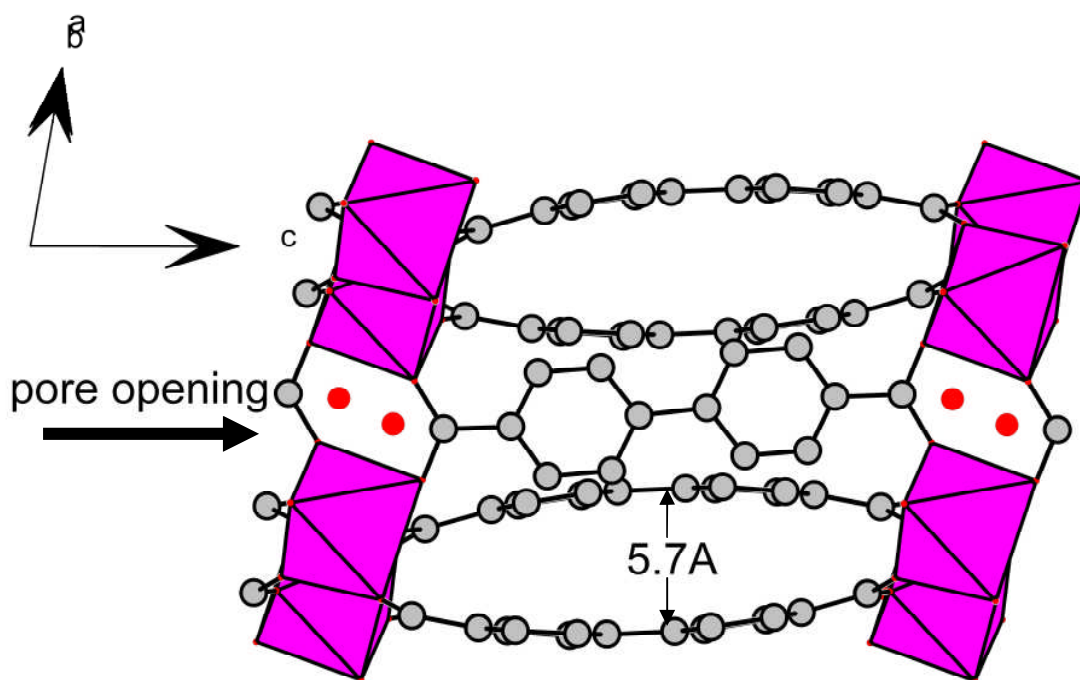


Figure 6.15: ScO_6 octahedra, showing the way in which the 4,4'-biphenyldicarboxylate linkers join the columns together. Hydrogen atoms have been omitted for clarity

There is a one-dimensional channel system running parallel to [001] with a pore window size of approximately 5.5\AA , giving an estimated free pore diameter of *ca.* 2\AA , at the pore centre, taking into account van der Waals radii of carbon and hydrogen atoms. The channel is made up of four biphenyl groups which are connected to six ScO_6 octahedra at the pore window of both ends of the channel. The pore size is reduced in the centre of the channel due to a 'bow-like' conformation of one of the carboxylate groups, shown in figure 6.16. Each pore is occupied by a water molecule, O(7), which assumes two distinct crystallographic sites within the pore and is situated at the widest point of the pore, in the same plane as the isolated scandium octahedra. The water molecule is 3.2\AA from its closest carbon atom, C(114). The crystallographic occupancy of O(7) is 0.125. This implies that there is one water molecule for every four pore windows. TGA shows a weight loss of 55.7% between 535 and 555°C but no evidence of water loss at lower temperatures is observed, so the solid does not reversibly adsorb and desorb water. The product after heating is amorphous.

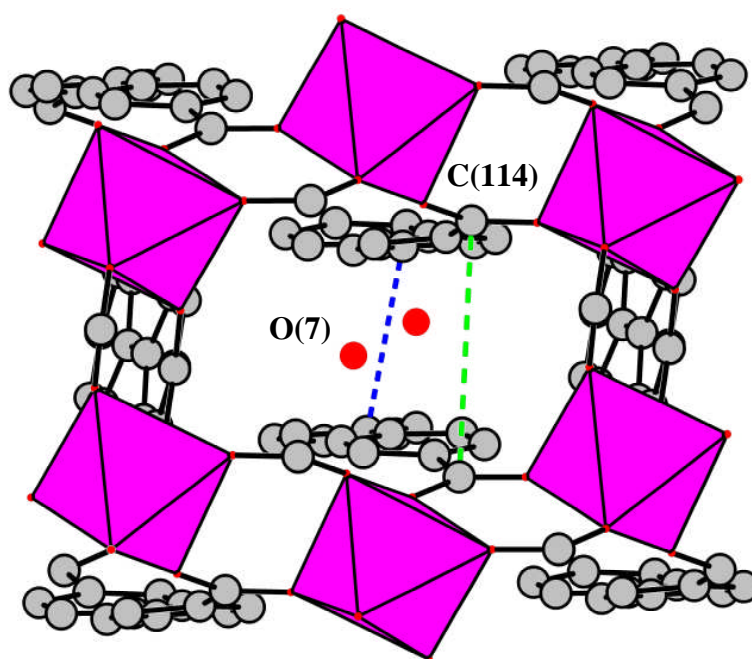


Figure 6.16: Representation of the pore system present in structure 22. The distance between the biphenyl rings at their centre is 3.51\AA (blue). The distance between the carboxylic groups of the biphenyl linker is 4.83\AA (green).

Solid state ^{45}Sc MAS NMR (figure 6.17) shows an intense signal at -30.6ppm with a quadrupolar lineshape that can be attributed to the single independent scandium site located by single crystal X-ray crystallography.

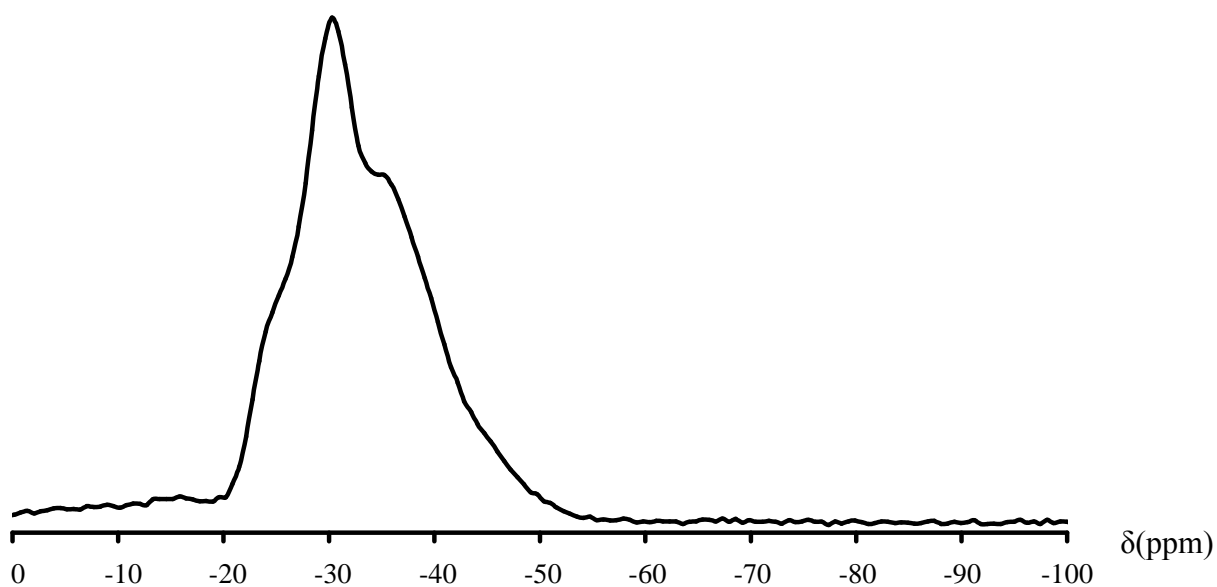


Figure 6.17: ^{45}Sc MAS NMR showing a maximum signal at -30.6ppm which can be attributed to the single independent scandium site located by single crystal X-ray crystallography.

Although there are examples in the literature of both transition metal and rare earth MOFs or co-ordination polymers prepared using biphenyldicarboxylic acid molecules as linkers^{181, 184-190}, there are none which include scandium.

6.5.2 Scandium isophthalate $\text{Sc}_2(\text{O}_2\text{CC}_6\text{H}_4\text{CO}_2)_3$ - Structure 23

Structure **23**, $\text{Sc}_2(\text{O}_2\text{CC}_6\text{H}_4\text{CO}_2)_3$, was solved from single crystal X-ray data by direct methods and Fourier syntheses, using the SHELXS program.⁸¹ The crystallographic information is outlined in table 6.2, with atomic co-ordinates listed below in table 6.9

Table 6.9: Atomic co-ordinates for structure 23

Atom	x	y	z	U _{iso}	Occ	Multiplicity
Sc(1)	0.83130(3)	0.66870(3)	0.33130(3)	0.0100(2)	1	4
Sc(2)	0.58317(3)	0.58317(3)	0.58317(3)	0.0103(2)	1	4
O(1)	0.67666(12)	0.65650(12)	0.32630(12)	0.0124(4)	1	12
O(2)	0.55769(12)	0.60366(13)	0.43024(12)	0.0130(4)	1	12
O(3)	0.64051(12)	0.32264(13)	-0.01320(12)	0.0122(4)	1	12
O(4)	0.76545(18)	0.39929(13)	0.06442(13)	0.0144(4)	1	12
C(1)	0.60398(19)	0.59928(19)	0.34823(18)	0.0127(5)	1	12
C(2)	0.56947(2)	0.52275(19)	0.27403(19)	0.0124(5)	1	12
C(3)	0.47340(19)	0.48230(2)	0.28140(2)	0.0162(6)	1	12
C(4)	0.63477(2)	0.48721(19)	0.20119(19)	0.0133(5)	1	12
C(5)	0.44250(2)	0.40730(2)	0.21650(2)	0.0192(6)	1	12
C(6)	0.50810(19)	0.37060(2)	0.14420(2)	0.0172(6)	1	12
C(7)	0.60411(19)	0.41034(19)	0.13690(19)	0.0137(5)	1	12
C(8)	0.67484(3)	0.37450(18)	0.05749(18)	0.0117(5)	1	12

Structure **23**, $\text{Sc}_2(\text{O}_2\text{CC}_6\text{H}_4\text{CO}_2)_3$, is a novel three dimensional scandium isophthalate material. There are 2 crystallographically unique scandium sites in the structure, each of which is coordinated to six oxygen atoms. The mean Sc – O bond length [2.080 (18) Å] is typical for this type of structure. Each ScO_6 octahedron is linked to 6 isophthalate groups, 2 of which bridge the scandium atoms in the asymmetric unit, 4 of the isophthalate groups act as linkers going to ScO_6 octahedra in different asymmetric units, and four bridging isophthalate groups are being received from independent asymmetric units.

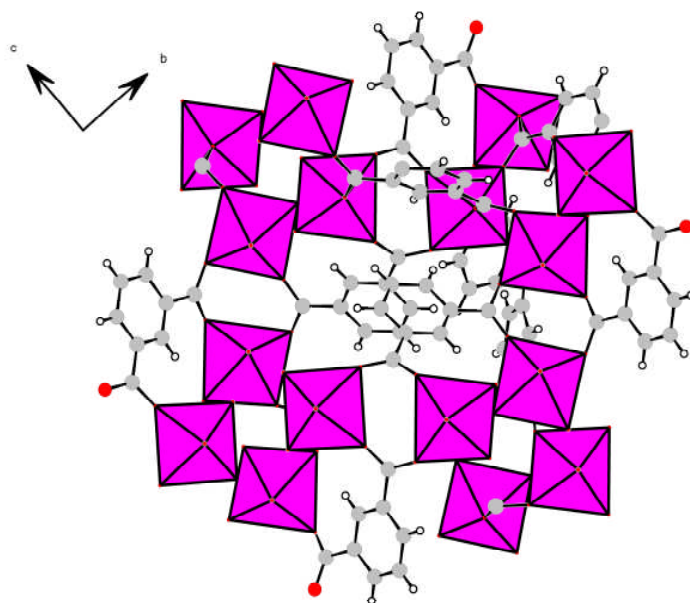


Figure 6.18: Projection onto [100] of structure 23 showing a complex three dimensional framework structure.

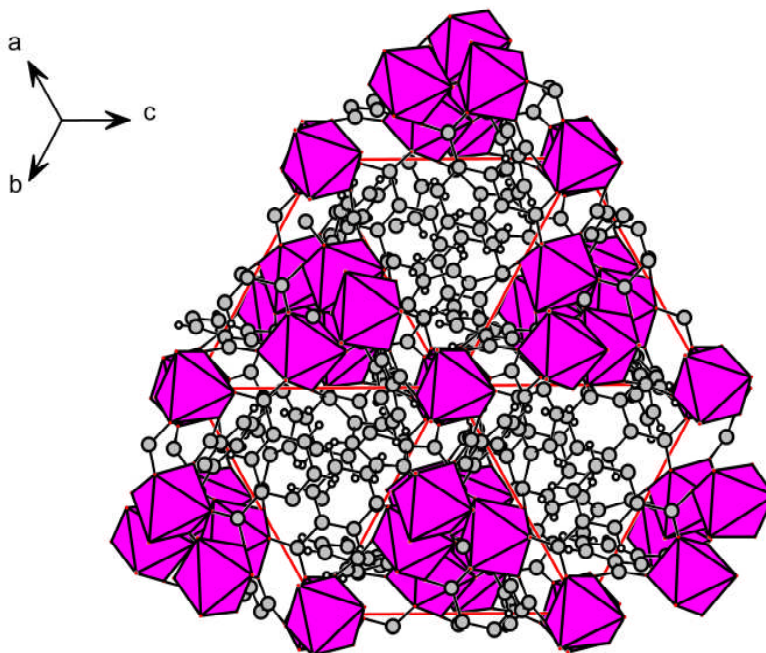


Figure 6.19: Projection down [111] of structure 23 showing groups of isolated scandium octahedral which are surrounded by isolated octahedra which are shown in rows.

The framework comprises of isolated ScO_6 octahedra which are fully connected to isophthalate linkers. Due to the symmetry of the framework, the structural motif is difficult to describe, but can be thought of as containing helical columns of ScO_6 octahedra. Each ScO_6 octahedron is joined to 3 other octahedra, by sharing two carboxylate carbons (C(1) or C(8)), from the same edge of the octahedral unit.

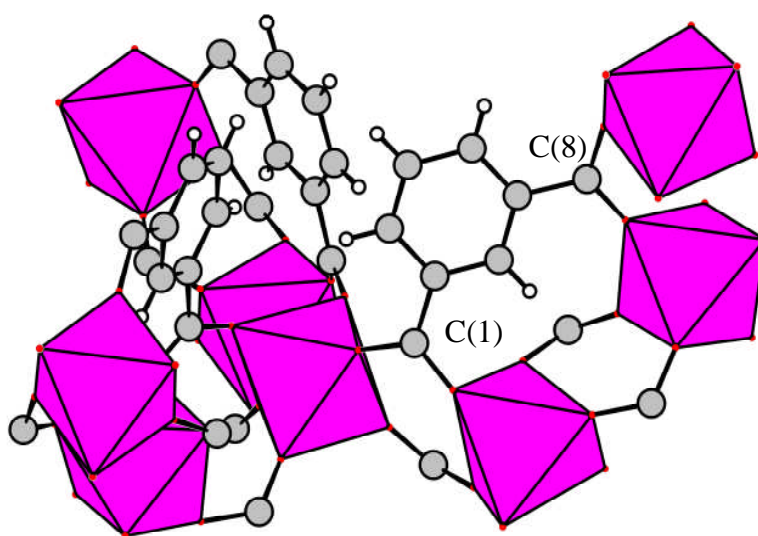


Figure 6.20: Representation of how the isophthalate bonds to the scandium octahedral units within structure 23

Although the framework of structure **23** is very complex with a large number of isophthalate linkers and scandium octahedra within the unit cell, cavities within the framework can be located. These ‘pear-shaped’ cavities have no pore opening, i.e. are inaccessible to gases or solvents and are not found to contain occluded water.

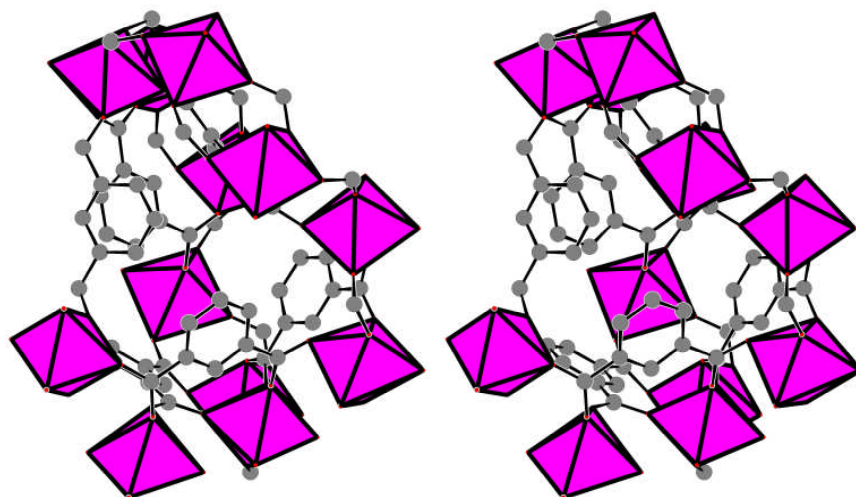


Figure 6.21: Stereo representation of the ‘pear-shaped’ cavities present within structure **23**

Solid state ^{45}Sc MAS NMR (figure 6.22) shows two independent scandium signals at 2.5 and -29.0ppm which can be attributed to the two independent scandium environments within structure **23**. Whereas one, ‘A’, has a very symmetric lineshape, the second, ‘B’, has a typical quadrupolar lineshape ($\eta = 0$). These will be discussed further in chapter 7.

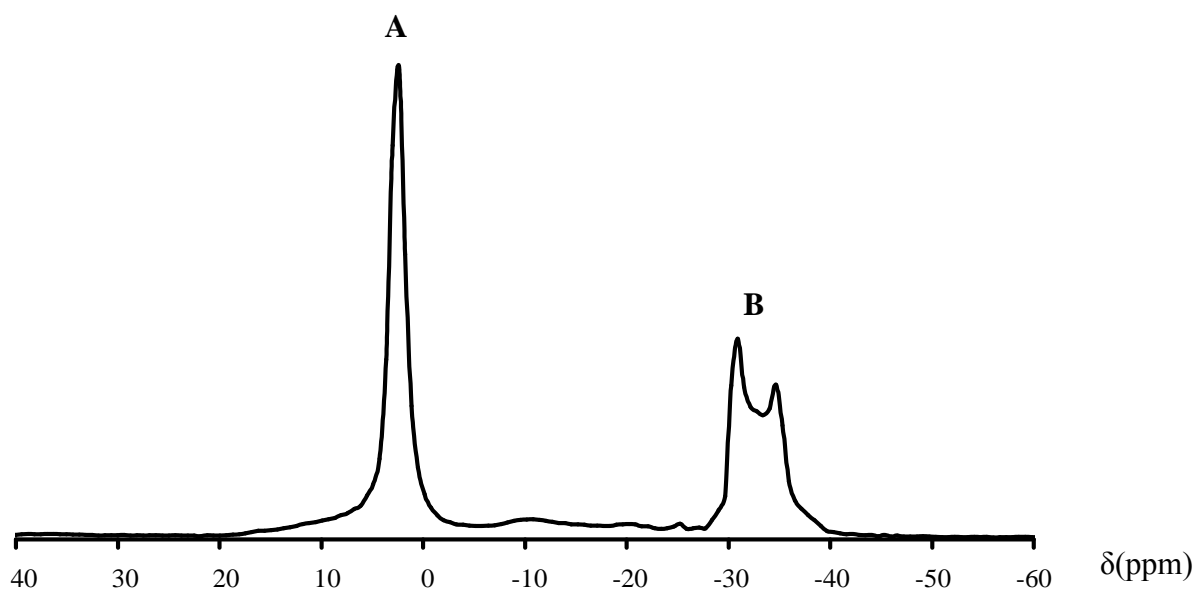


Figure 6.22: ^{45}Sc MAS NMR spectra for structure **23** showing two independent signals which correspond to the two unique scandium atoms within the framework.

Thermogravimetric analysis shows a significant weight loss of 53.2% occurring between 550 and 600 °C due to break down and loss of the isophthalic acid.

6.5.3 Scandium terephthalates

It was decided that a more in-depth examination of the scandium terephthalate system was appropriate, as initial experiments suggested that several phases could form. There are several different framework topologies which are described in the literature in which the metal ion is chemically similar to scandium, including MIL-53 which has attractive porous topologies and has been prepared using Al^{3+} , Cr^{3+} and In^{3+} , all of which have cationic radii similar to Sc^{3+} (page 14).

The reaction stoichiometries used to investigate the scandium terephthalate system are discussed below as ‘phase’ or ‘composition space’ diagrams. Initial investigations concentrated on hydrothermal syntheses with and without hydrofluoric acid as a possible mineralising agent, as observed for MIL-100 (Fe, Cr).^{161, 191} Preliminary experiments were also performed where solvents such as DMF and DEF were used in place of water, as these have been used successfully for materials such as MIL-53, MIL-88 and MIL-100.^{168, 172, 191, 192}

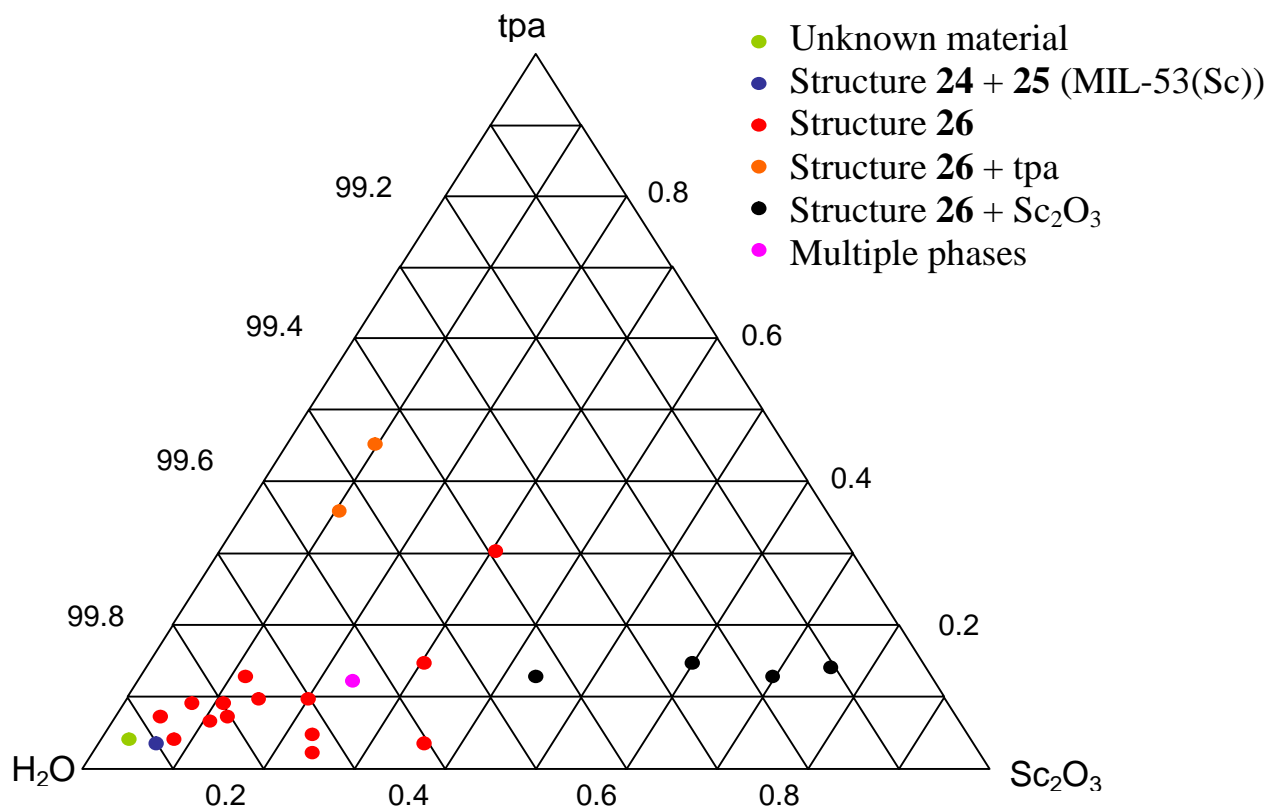


Figure 6.23: *Triangular plot showing different reaction stoichiometries of scandium terephthalate crystallizations performed (no HF). Reactions were performed for 48h at 220°C*

In the absence of hydrofluoric acid, the crystallisation of scandium terephthalate materials occurs at relatively low concentrations of scandium oxide and terephthalic acid in comparison to water. At high concentrations of water, i.e. > 99%, several different crystalline phases are observed. Structures **24** and **25** (discussed later in this chapter) have only been observed to form using these conditions and both contain Sc-OH-Sc chains.

The main phase formed in the absence of hydrofluoric acid is described later in this chapter as structure **26**. Changing the ratio of scandium oxide to terephthalic acid mainly results in the formation of structure **26** with excess scandium oxide or terephthalic acid. X-ray diffraction patterns of the different phases which have been observed to form in the absence of hydrofluoric acid are shown in figure 6.24.

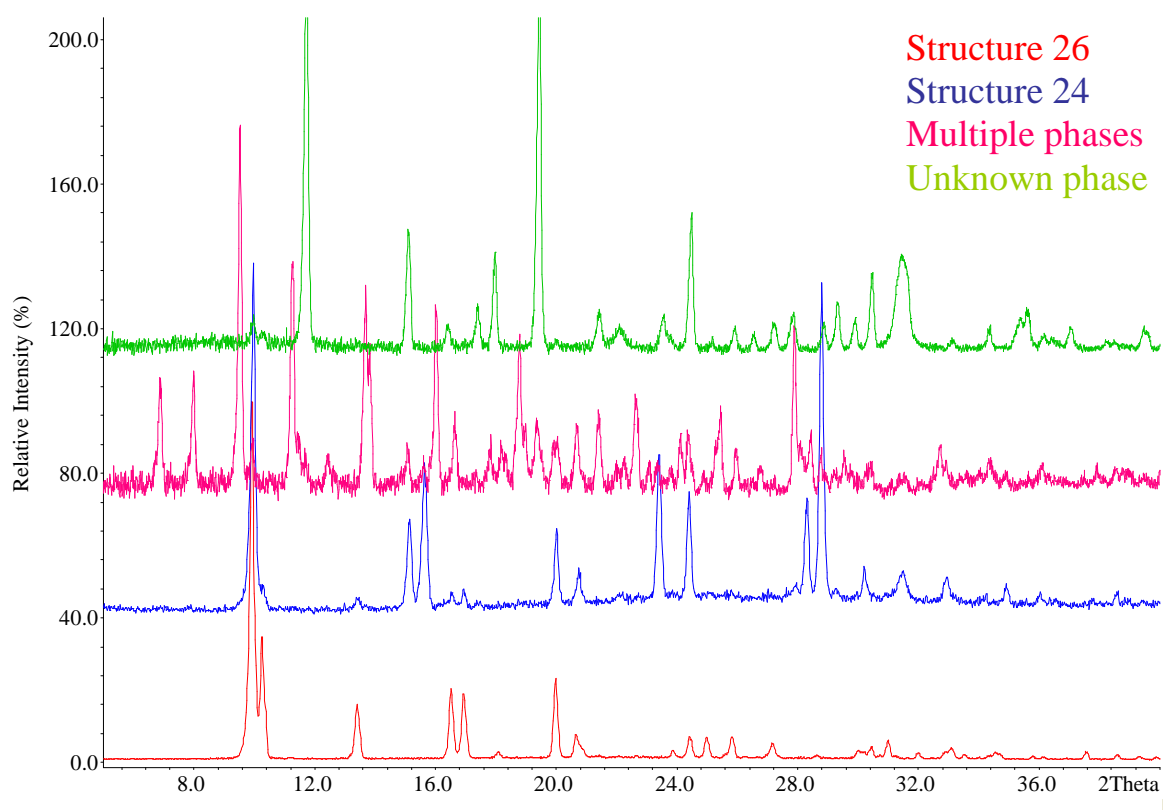


Figure 6.24: Powder XRD patterns for selected scandium terephthalate materials prepared in the absence of HF

The formation of products other than structure **26** appeared to be favoured by low scandium oxide and terephthalic acid concentrations. It was thought that the excess water could act as a mineralising agent and promote the formation of phases alternative to structure **26**. A series of experiments were also performed using hydrofluoric acid as a mineralising agent, in order to further investigate the possible structures which could be formed using scandium and terephthalic acid. Figure 6.25 shows a plot of the reaction stiochiometeries which were used in order to investigate this system.

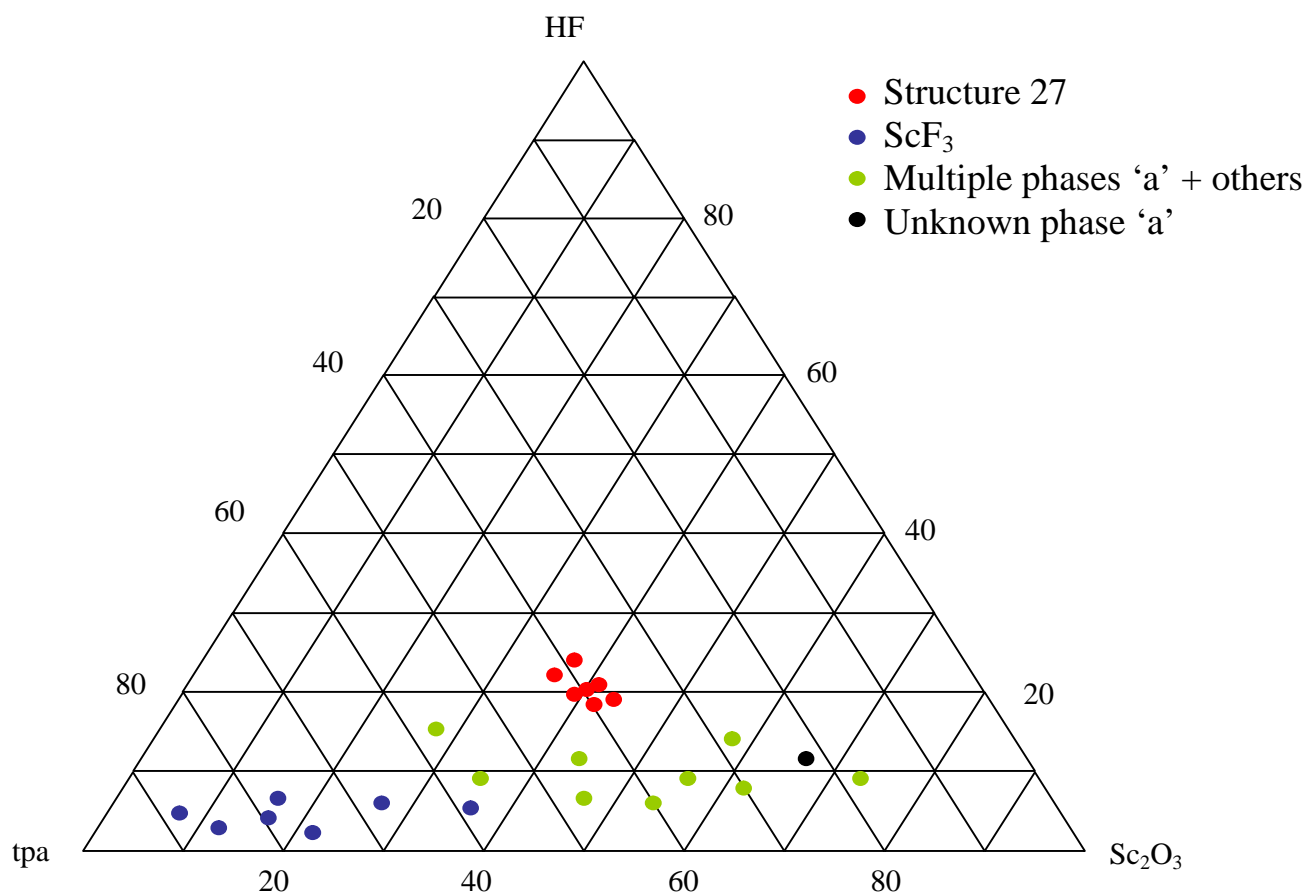


Figure 6.25: Triangular plot showing different reaction stoichiometries of scandium terephthalate reactions which were prepared in the presence of HF. (48h at 220°C).

6.5.4 Scandium terephthalate hydroxide (α) $\text{Sc}(\text{OH})[\text{O}_2\text{CC}_6\text{H}_4\text{CO}_2]$ – Structure 24

Structure **24**, $\text{Sc}(\text{OH})[\text{O}_2\text{CC}_6\text{H}_4\text{CO}_2]$, was solved from single crystal X-ray data collected on station 9.8 at the synchrotron radiation facility, Daresbury, by direct methods and Fourier syntheses, using the SHELXS program.⁸¹ The crystallographic information is outlined in table 6.2, with atomic co-ordinates listed below in table 6.10.

Table 6.10: Atomic co-ordinates for structure **24**

Atom	x	y	z	U _{iso}	Occ	Multiplicity
Sc(1)	0	0.5	0	0.0069(1)	1	4
O(1)	0.00554(16)	0.38998(5)	0.10459(14)	0.0111(2)	1	8
O(2)	-0.34217(18)	0.50315(5)	-0.12442(18)	0.0109(2)	1	8
O(3)	0	0.45201(7)	-0.25	0.0105(3)	1	4
C(1)	0	0.27237(9)	0.25	0.0087(3)	1	4
C(2)	0	0.35659(9)	0.25	0.0088(3)	1	4
C(3)	0.0224(2)	0.23305(7)	0.09918(19)	0.0108(2)	1	8
C(4)	0.0204(2)	0.15447(7)	0.09746(19)	0.0113(3)	1	8
C(5)	0	0.11566(9)	0.25	0.0093(3)	1	4
C(6)	-0.5	0.46930(9)	-0.25	0.0089(3)	1	4

Sc(OH)[O₂CC₆H₄CO₂], structure **24**, is a novel scandium terephthalate material in which the linker to metal ratio is 1:1, containing chains of ScO₅OH octahedra which run parallel to [001], figure 6.26. The chains of scandium octahedra, which are joined together by hydroxyl groups, run through the structure, parallel to the *c*-axis.

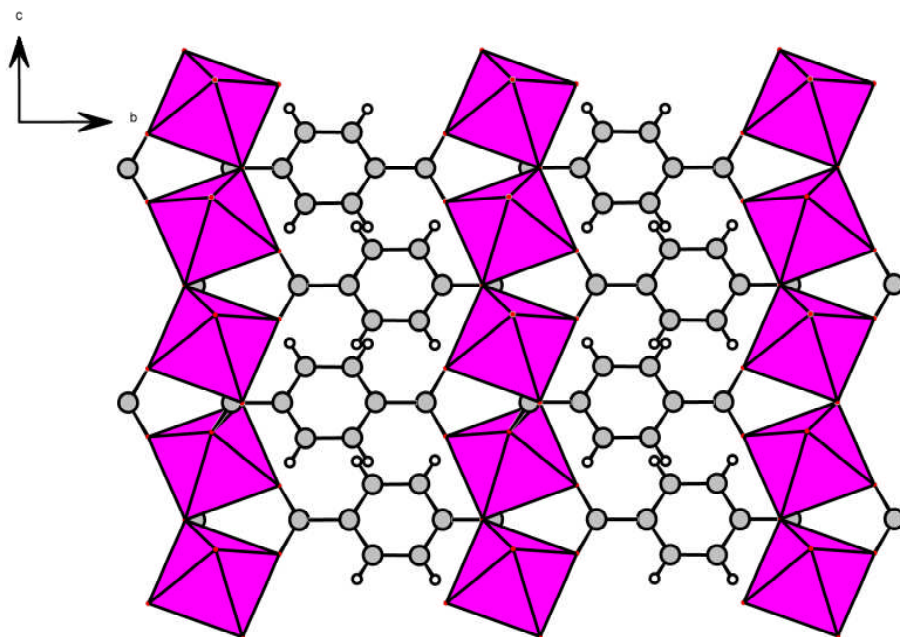


Figure 6.26: Projection down [100] of structure **24** showing chains of ScO₅OH octahedra, bonded together via a hydroxyl group.

The carboxylic groups of the terephthalic acid are situated in perpendicular planes to each other, allowing for a single terephthalate ligand to bridge two scandium octahedra within the same row, as well as acting as a bridge between different rows of scandium octahedra, as shown in figures 6.27 and 6.28.

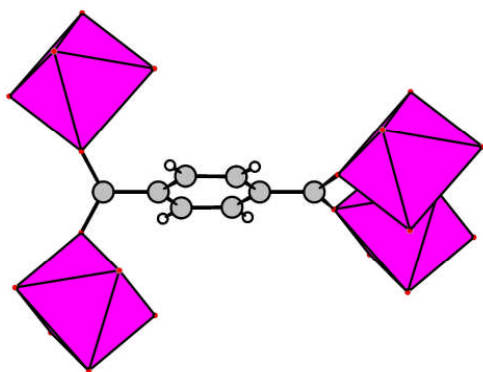


Figure 6.27: Representation of the coordination environment for the terephthalate ligand, showing the carboxylic linker at the top of the figure bonded to two different octahedral units within the same row, and the carboxylic acid group at the bottom of the figure bridging two scandium octahedral units from different rows

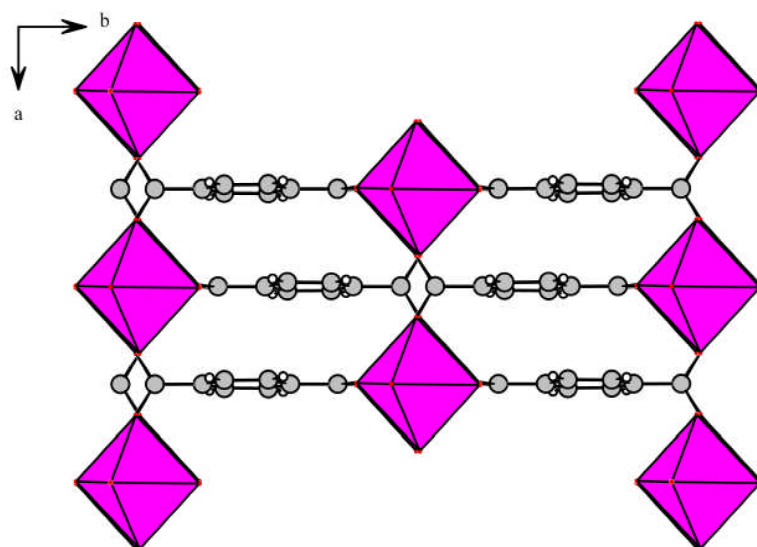


Figure 6.28: structure 24 viewed down the [001] axis, showing clearly how chains of ScO_5OH octahedra are linked to each other through the carboxylate groups of the terephthalate.

Thermogravimetric analysis shows a weight loss of 52.8% occurring between 575 and 605 °C due to removal of the terephthalic acid. The material is amorphous after heating. Quantities of structure 24 suitable for ^{45}Sc MAS NMR investigations have not yet been obtained.

6.5.5 Scandium terephthalate hydroxide (β) $\text{Sc}(\text{OH})[\text{O}_2\text{C}_6\text{H}_4\text{CO}_2]$ – Structure 25

Structure **25**, $\text{Sc}(\text{OH})[\text{O}_2\text{C}_6\text{H}_4\text{CO}_2]$, was solved from single crystal X-ray data by direct methods and Fourier syntheses, using the SHELXS program.⁸¹ The crystallographic information is outlined in table 6.3, with atomic co-ordinates listed below in table 6.11

Table 6.11: Atomic co-ordinates for structure 25

Atom	x	y	z	U_{iso}	Occ	Multiplicity
SC(1)	0.75	0.25	0.25	0.0299(16)	1	4
O(1)	0.6696(13)	0.3608(9)	0.1495(5)	0.030(4)	1	1
O(2)	0.75	0.1649(15)	0	0.045(3)	1	4
C(1)	0.5387(2)	0.4715(17)	0.1577(8)	0.049(6)	1	1
C(2)	0.6388(2)	0.3834(13)	0	0.062(7)	1	2
C(3)	0.5684(2)	0.4496(15)	0	0.073(6)	1	2

Although repeated efforts have been made to prepare **25** pure this has not yet been achieved. The crystal from which the data for this structure was obtained was extracted from a sample in which the majority phase present was that of structure **24**.

Structure **25**, $\text{Sc}(\text{O}_2\text{C}_6\text{H}_4\text{CO}_2)\text{OH}$, has the same chemical formula as structure **24**, and also includes Sc-OH-Sc chains, but has a remarkably different framework structure. It is isostructural to aluminium, chromium, iron and indium carboxylates. The most notable of these structures are the aluminium and chromium structures, synthesised and characterised by Férey *et al*, and given the name MIL-53.¹⁹²

Structure **25** is composed of chains of octahedral scandium units which are joined together via bridging hydroxyl groups, forming Sc-OH-Sc chains parallel to the *a*-axis. The oxygen atoms of the terephthalate groups occupy the equatorial positions of the scandium octahedral, allowing for the terephthalate linker to bridge the scandium chains, figure 6.29, allowing the formation of a three dimensional framework with relatively large pores running parallel to *a*, as shown in figure 6.30

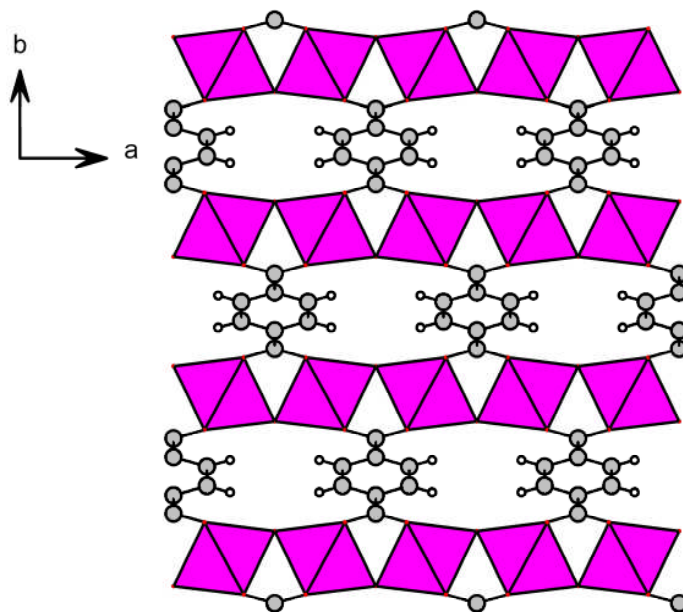


Figure 6.29: Projection down $[001]$ of structure **25** showing chains of scandium octahedra, joined by hydroxyl groups.

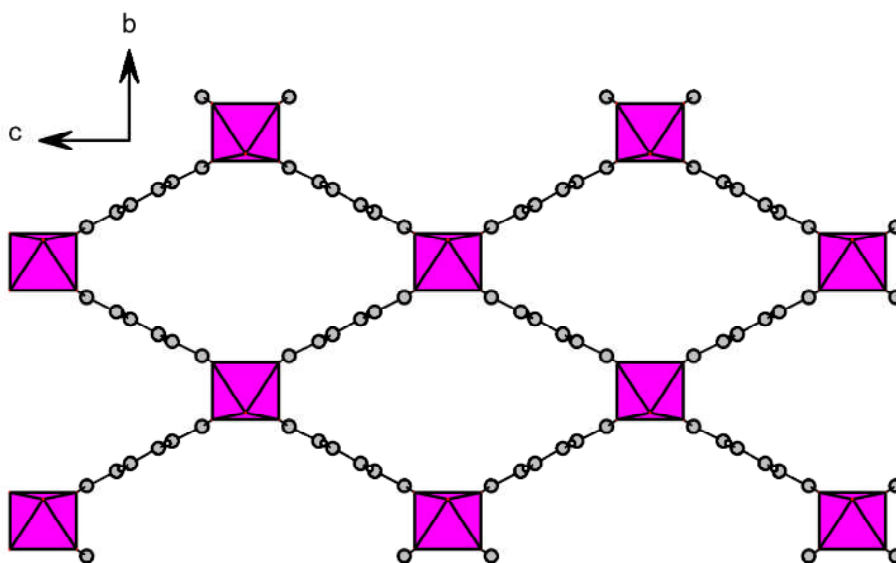


Figure 6.30: Projection down $[100]$ for structure **25** showing large diamond shape pores.

It is instructive to compare the crystallographic parameters of structure **25** with those of other MIL-53 type structures in order to understand the effects which the scandium cation has upon the system. Table 6.12 gives various cell parameters of different MIL-53 type structures, including structure **25**.

Table 6.12: Cell parameters comparing various forms of the MIL-53 structure type, with ‘as’ denoting the as-synthesised solid and ‘ht’ denoting the solid at high temperature.

Sample name	Crystal System / Space group	Unit Cell		
		a(Å)	b(Å)	c(Å)
MIL-53as(Cr) ¹⁹²	Orthorhombic / Pnam	17.340(1)	12.178(1)	6.822(1)
MIL-53ht(Cr) ¹⁹²	Orthorhombic / Imcm	16.733(1)	13.038(1)	6.812(1)
MIL-53as(Sc) 25	Orthorhombic / Imcm	18.11(1)	11.59(2)	7.22(4)

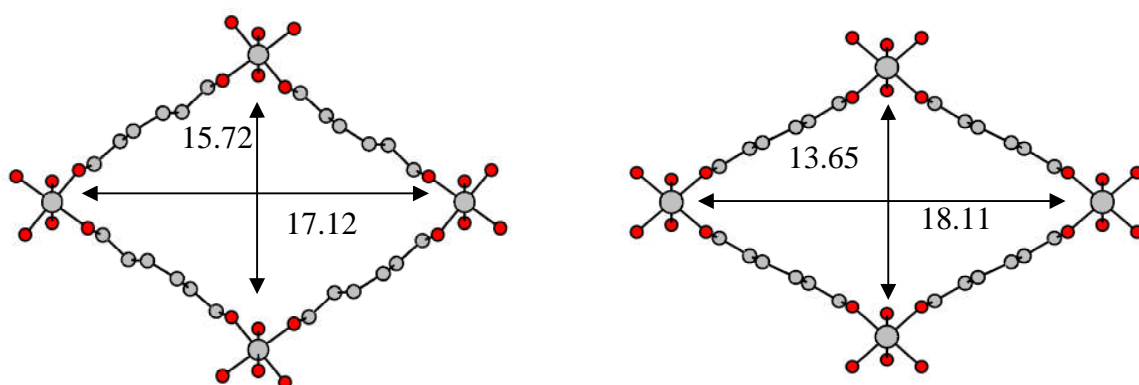


Figure 6.31: Schematic representations of a single pore of the chromium MIL-53as structure (left) and a single pore from structure **25**. Diameters have been shown, illustrating the breadth and depth of the pore, showing that the pore in structure **25** is 2Å shorter in height, and 1Å wider than its chromium analogue.

The cell parameters for the ‘as-synthesised’ materials, listed in table 6.12, show that the *b*-axis, and consequently the ‘width’ of the pore, is shorter for structure **25** (11.59Å) than that for the chromium version of the MIL-53 material (12.18Å). The *a*-axis and consequently the long dimension of the pore being slightly longer, is slightly longer for structure **25** (18.11Å) in comparison with that reported for the as-prepared chromium MIL-53 material (17.34Å). These differences are predominantly due to the flexibility of the lattice via scissoring motions, rather than differences in the cationic radii between the different trivalent metal cations.

During the original work on the chromium and aluminium versions of the MIL-53 type structure, no single crystals were obtained, and structure determination was performed by Rietveld refinements using the MIL-47 type structure as a starting model. Férey *et al* reported the presence of disordered terephthalic acid moieties situated within the pores of the as-prepared material.¹⁹² Thermal analysis of MIL-53as indicated the loss of a total of 0.75

terephthalic acid molecules upon heating, without interrupting the structure's integrity. When the structure was cooled, water was adsorbed into the free pore space, causing a hydrogen bonding network to be established between the guest water molecules and the hydroxyl groups bridging the metal cations and a contraction in the shorter pore dimension. This 'closed' structure was called the low temperature form of MIL-53, or MIL-53lt. The water molecules could be successfully removed upon heating, allowing the framework to 'relax' and open. This structure was called the high temperature form of MIL-53, or MIL-53ht. The manner in which the MIL-53 type solid behaves when heated has been discussed in detail, with the behaviour being described as 'breathing' upon heating and cooling, figure 6.32.¹⁷² It has not yet been possible to synthesise structure **25**, (MIL-53(Sc)), phase pure so it has not been possible to study its thermal behaviour.

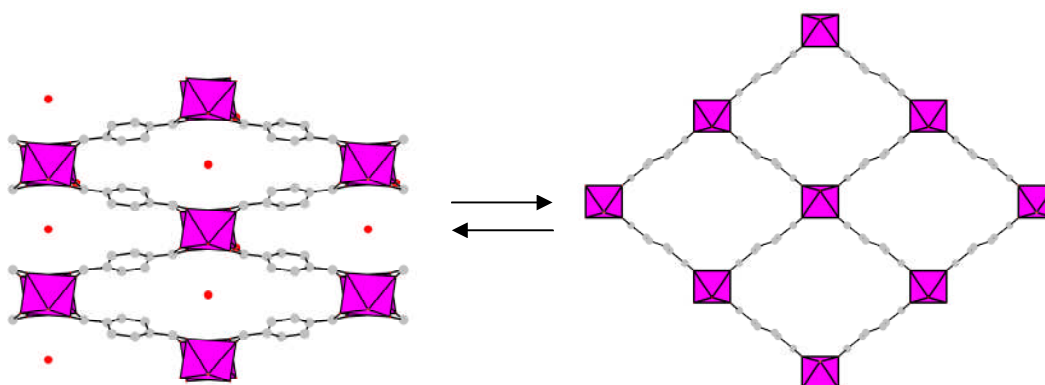


Figure 6.32: Projection down [010] of MIL-53. **Left:** low temperature framework of MIL-53 showing a distortion in the pore dimensions due to a hydrogen bonding network between the hydroxyl groups and water molecules occupying the pore. **Right:** high temperature framework of MIL-53, illustrating a larger free pore created as a consequence of the absence of the water molecule, removing the potential for hydrogen bonding

6.5.6 Scandium terephthalate $\text{Sc}_2(\text{O}_2\text{CC}_6\text{H}_4\text{CO}_2)_3$ – Structure **26**

$\text{Sc}_2(\text{O}_2\text{CC}_6\text{H}_4\text{CO}_2)_3$, structure **26**, is a novel scandium terephthalate material, metal to linker; 2:3, comprising of a remarkable three-dimensionally connected framework that is made up of chains of isolated ScO_6 octahedra running parallel to [100]. The crystallographic information relating to structure **26** is given in table 6.3, with atomic coordinates given below in table 6.13

Table 6.13: Atomic coordinates for structure 26

Atom	x	y	z	U _{iso}	Occ	Multiplicity
Sc(1)	0.375	0.375	0.11433(2)	0.00272(2)	1	16
O(1)	0.50513(3)	0.45837(3)	0.11472(3)	0.01351(5)	1	32
O(2)	0.24536(4)	0.41579(3)	0.15743(3)	0.01983(6)	1	32
O(3)	0.24147(4)	0.41664(7)	0.07046(4)	0.4586(1)	1	32
C(1)	0.48853(6)	0.59143(7)	0.12457(6)	0.00925(4)	1	32
C(2)	0.625	0.55825(4)	0.125	0.02259(3)	1	16
C(3)	0.625	0.48637(3)	0.125	0.00929(7)	1	16
C(4)	-0.10379(5)	0.48046(8)	0.02789(4)	0.00981(4)	1	32
C(5)	0.15381(7)	0.48582(3)	0.00464(8)	0.02202(4)	1	32
C(6)	0.04973(7)	0.46629(7)	0.03255(8)	0.01811(5)	1	32
C(7)	0.10237(5)	0.43031(6)	0.06763(9)	0.02152(5)	1	32

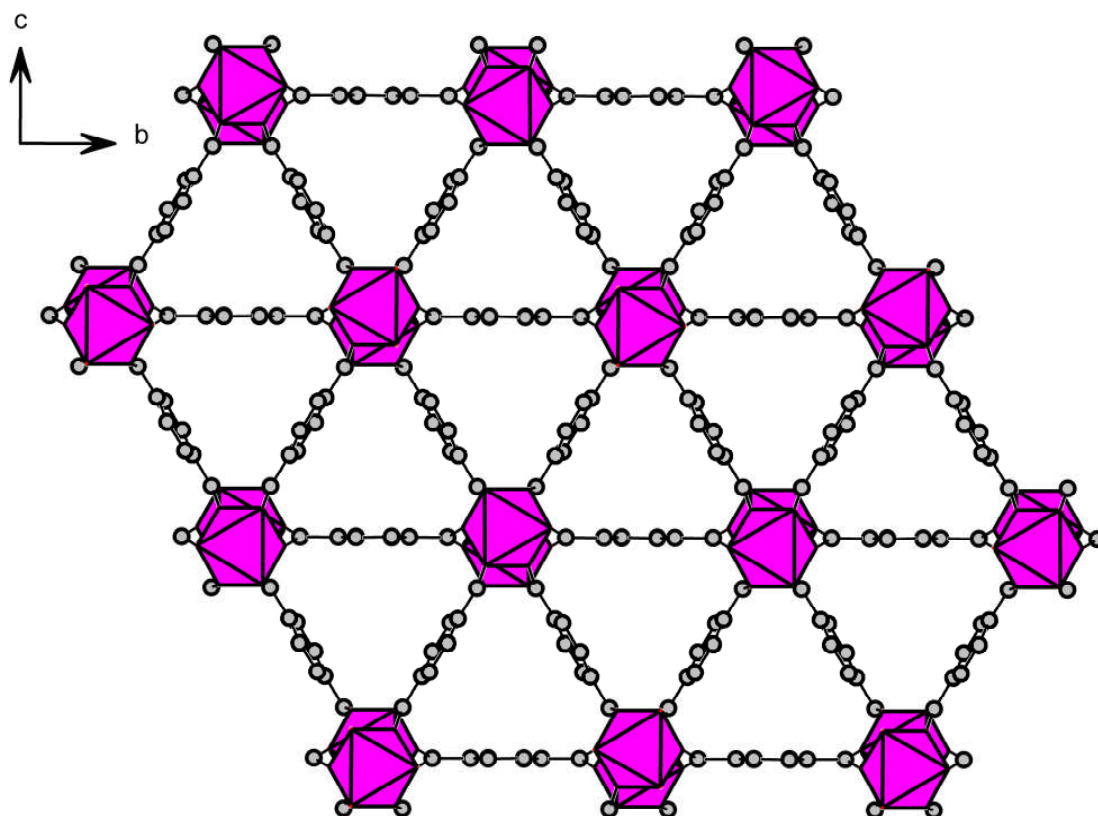


Figure 6.33: Projection down [100] of structure 26 showing triangular pores lined by terephthalate linkers, with the apex of each triangle being occupied by isolated ScO_6 octahedral units

Each ScO_6 octahedron in the chain is linked to those above and below by three carboxylate units, each of which is monodentate to two scandium ions along the a -axis, i.e. three terephthalate linkers bridge two phases of two octahedral units. Each chain is linked to six

adjacent chains through terephthalate units: two of the six sets of terephthalate linkers (parallel to the b -axis) connect to chains of ScO_6 octahedra at the same fractional coordinate along the a -axis, with the other four (parallel to planes of the form $\{001\}$) connected alternately to chains at higher and lower co-ordinates, figure 6.34.

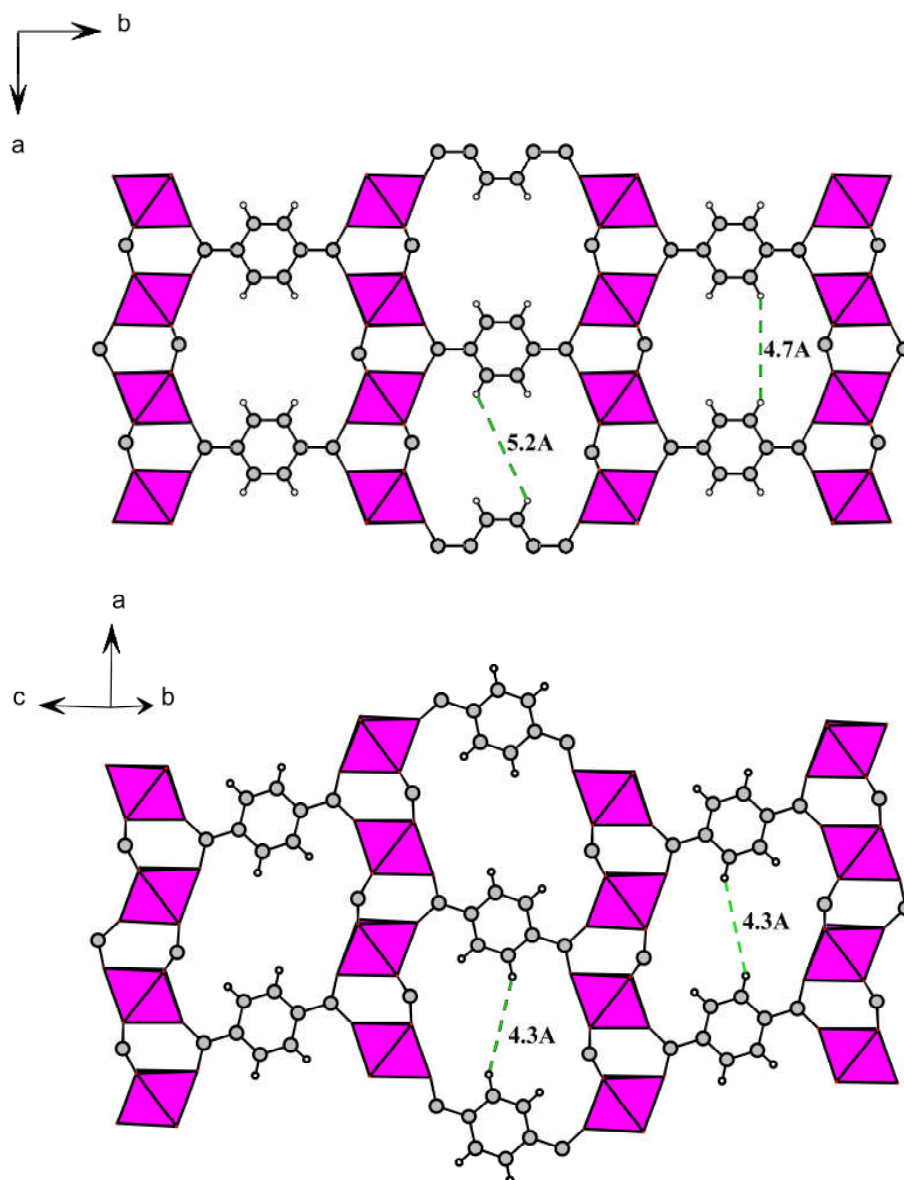


Figure 6.34: *Top:* Projection down $[001]$ showing the terephthalate linker bridging two scandium octahedral units within the same row and connecting to the equivalent two in another row. **Bottom:** Projection onto (110) showing the terephthalate linker connecting to scandium octahedral units within different rows, at different levels.

The framework includes small channels along the a -axis that have triangular cross sections: the triangle is made up of the projection (parallel to the plane) of terephthalate units linking

chains of ScO_6 octahedra. These channels are linked perpendicularly through small windows between adjacent aromatic rings. The channels have free diameters (taking van der Waals radii of C into account) of around 3\AA , although the staggered arrangement of the terephthalic linkers makes description difficult. The windows between aromatic rings stacked along a axis, between adjacent channels, calculated from the positions of the terephthalate groups determined by single crystal X-ray diffraction, are small (4.7 and 4.3\AA). Four of the six sets of terephthalate linkers from any one column of ScO_6 octahedra join to adjacent chains of octahedra at different levels, as described previously in figure 6.34, so that it is not possible for this structure to show 'isoreticulation'. That is, the terephthalate could not straightforwardly be replaced by longer linear dicarboxylic acids, such as 4,4-biphenyldicarboxylic acid, as has been demonstrated with other families of solids such as MOF-5 or MIL-88, which sometimes leads to the longer linkers yielding a larger pore size.

Negligible electron density in the pores was observed by the single crystal diffraction measurement, although TGA in an oxygen atmosphere, figure 6.35, showed an initial weight loss of 5%, attributed to loss of very weakly bound surface water. The TGA shows a further weight loss of around 5% up to $275\text{ }^\circ\text{C}$, due to the loss of free terephthalic acid. After this, the material shows low weight loss until a major weight loss (ca. 60%) occurs at around $500\text{ }^\circ\text{C}$ as the carboxylate decomposes. A sample heated at $275\text{ }^\circ\text{C}$ overnight to remove free acid and subsequently re-examined by TGA showing a single weight loss at around $475\text{ }^\circ\text{C}$ (expected weight loss to leave scandium oxide, 76 wt%; measured loss to $600\text{ }^\circ\text{C}$, 74%).

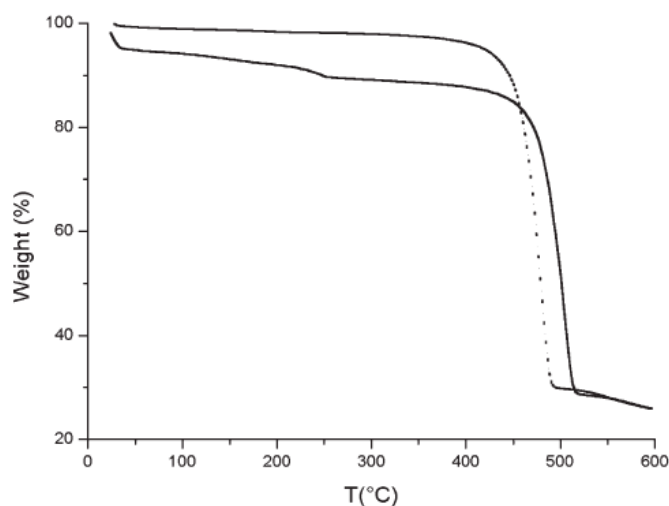


Figure 6.35: Thermogravimetric analysis of as-prepared $\text{Sc}_2(\text{O}_2\text{CC}_6\text{H}_4\text{CO}_2)_3$ and a sample previously heated at $275\text{ }^\circ\text{C}$ to remove free terephthalic acid.

Thermal analysis of structure 26 revealed that the solid has a high thermal stability for a porous terephthalate, with *in situ* X-ray thermodiffraction under air, figure 6.36 indicates that the solid remains crystalline up to 400 °C, at which temperature the structure begins to decompose. Thermal decomposition begins at a higher temperature (by *ca.* 100 °C) in nitrogen.

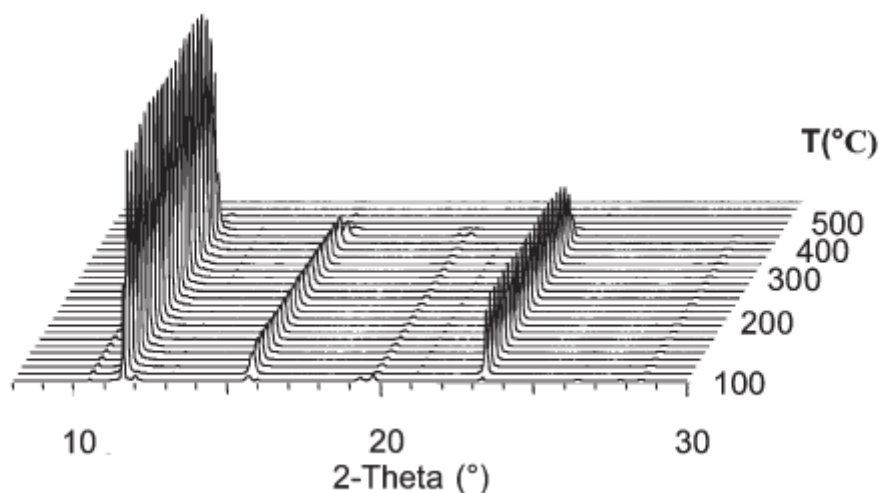


Figure 6.36: *In-situ* X-ray thermodiffraction ($\text{Co } K\alpha$, $\lambda = 1.790 \text{ \AA}$) indicates that the solid remains crystalline in air up to 400 °C.

As-prepared samples of the solid, heated under vacuum to remove any residual water, display Type I isotherms for N_2 adsorption at 77 K, with a maximum uptake of around 21wt%, as shown in figure 6.37. This corresponds to an uptake of $168 \text{ cm}^3(\text{stp}) \text{ g}^{-1}$, a pore volume of $0.26 \text{ cm}^3 \text{ g}^{-1}$. This corresponds to *ca.* 32 molecules of nitrogen per unit cell of the framework, or two per channel per unit cell repeat along the x axis. The apparent discrepancy between the apparent free diameter of the channels (*ca.* 3 \AA) and the ease with which the solid takes up N_2 , the kinetic diameter of which is normally estimated at 3.6 \AA , suggests that the kinetic diameter of N_2 is overestimated, as using a two-centre Lennard-Jones model to describe the molecular diameter for N_2 instead of the single centre Lennard-Jones model, gives a molecular diameter of 3.32 \AA instead of 3.64 \AA .¹⁹³ It may also be that the framework may be able to adjust to accommodate guests.

Interesting behaviour of that kind has recently been described for hydrogen in an organic–inorganic hybrid.¹⁹⁴ In an extreme case, if the aromatic rings of one set of terephthalate linkers along the *a* axis were to rotate by 90° , they would give rise to cavities that could hold spheres *ca.* 6 \AA in free diameter.

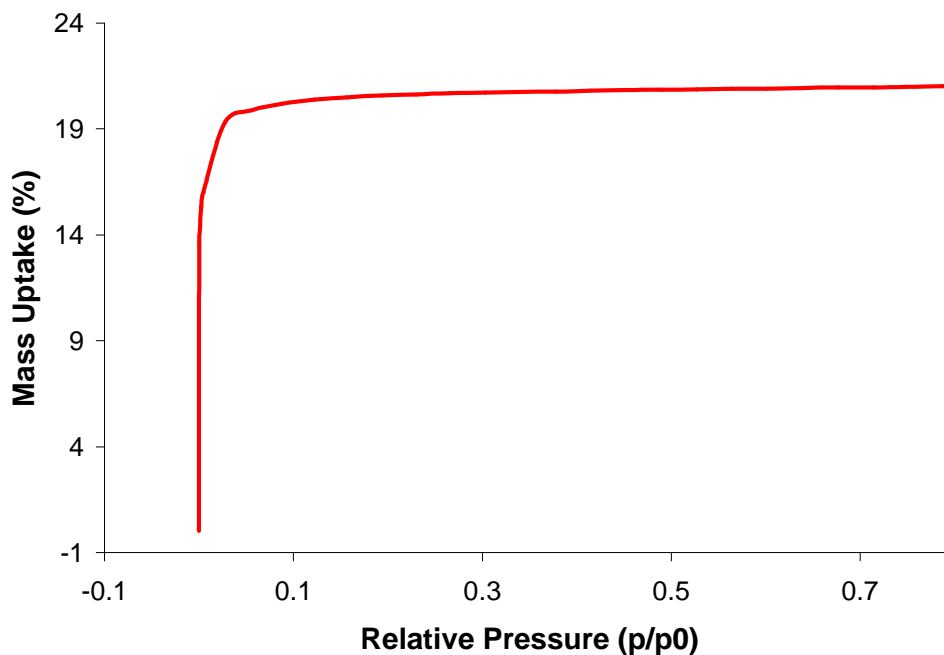


Figure 6.37: N_2 adsorption isotherm of structure **26** at 77 K showing a type I isotherm, with a maximum uptake of approximately 21wt%.

Solid state ^{45}Sc MAS NMR (figure 6.38) shows an intense signal with a typical quadrupolar lineshape, which is most intense at -0.5 and -6.9ppm. This is attributed to the single scandium site identified by X-ray crystallography.

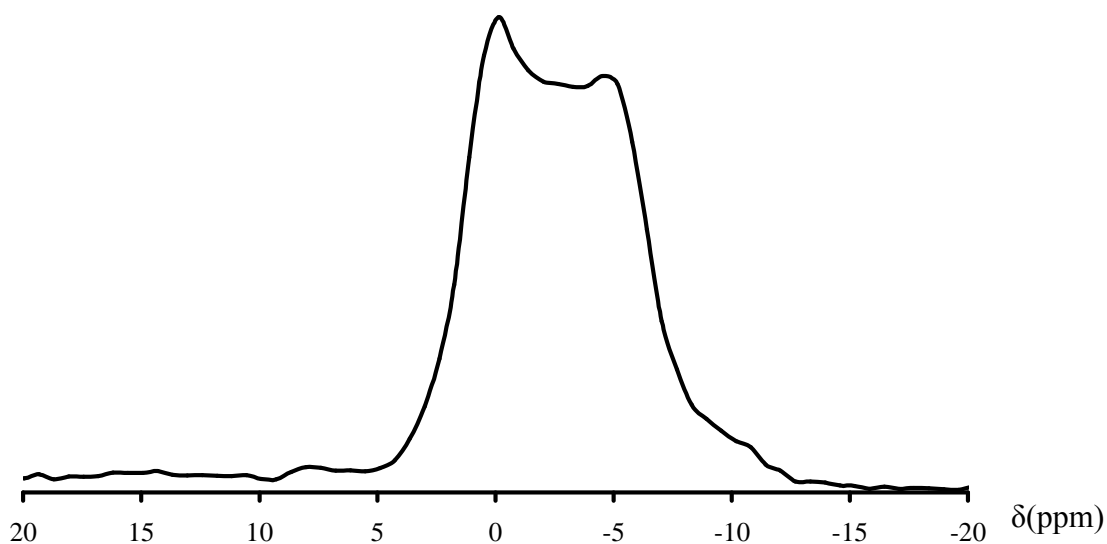


Figure 6.38: ^{45}Sc MAS NMR showing an intense signal with a typical quadrupolar lineshape, which is most intense at -0.5 and -6.9ppm

6.5.7 Scandium terephthalate fluoride $\text{ScF}[\text{O}_2\text{CC}_6\text{H}_4\text{CO}_2]$ – Structure 27

Structure 27, $\text{ScF}[\text{O}_2\text{CC}_6\text{H}_4\text{CO}_2]$, was solved from single crystal X-ray data by direct methods and Fourier syntheses, using the SHELXS program.⁸¹ The crystallographic information is outlined in table 6.3, with atomic co-ordinates listed below in table 6.14. It was prepared in the presence of F^- as a mineraliser, but this has become included in the framework of the material. The chains of ScO_4F_2 octahedra present within 27 are different from those reported in structures 24 and 25, in that the presence of fluorine within the framework gives a Sc-F-Sc bond angle of 180° . The presence of fluorine in the framework is confirmed by EDX analysis.

Table 6.14: Atomic co-ordinates for structure 27

Atom	x	y	z	U_{iso}	Occ	Multiplicity
Sc(1)	0	0.59992(6)	0.25	0.0137(10)	1	4
F(1)	0	0.1006(18)	0.25	0.0222(19)	1	4
O(1)	0.08622(3)	0.62415(16)	0.13955(7)	0.0138(17)	1	8
O(2)	-0.07(4)	0.5816(16)	0.07237(7)	0.0194(17)	1	8
C(1)	0.10666(5)	0.56787(3)	0.02709(11)	0.0093(2)	1	8
C(2)	0.18038(5)	0.66992(2)	0.01125(10)	0.0168(2)	1	8
C(3)	0.21941(5)	0.87505(2)	0.10735(11)	0.0222(2)	1	8
C(4)	0.21073(5)	0.54758(3)	-0.0961(11)	0.0201(2)	1	8

$\text{ScF}(\text{O}_2\text{CC}_6\text{H}_4\text{CO}_2)$, structure 27, is a novel scandium terephthalate material in which the linker to metal ratio is 1:1, containing chains for ScO_4F_2 octahedra which run parallel to [010]. The chains of ScO_4F_2 are arranged in columns along c which are bridged by the carboxylic acid group of the terephthalate linker.

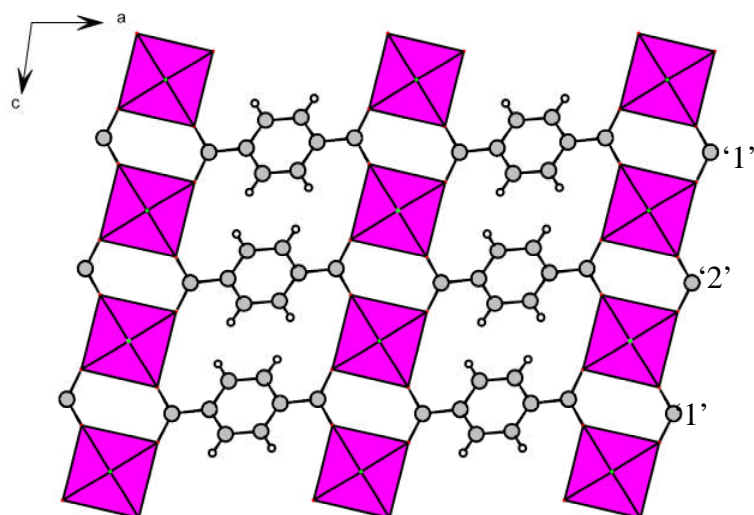


Figure 6.39: Projection down $[010]$ showing how the rows of ScO_4F_2 are linked to rows above and below via the carboxylic bridge. The rows are connected along the a -axis through the terephthalate linker.

There are two different orientations which are assumed by the terephthalate linker within structure **27**. The rows of terephthalate linkers labeled '1' and '2' in figure 6.39, above, are shown below as viewed down the a -axis. The linkers alternate between connecting to the ScO_4F_2 octahedra in front of its point of origin, in relation to the b -axis and behind its point of origin.

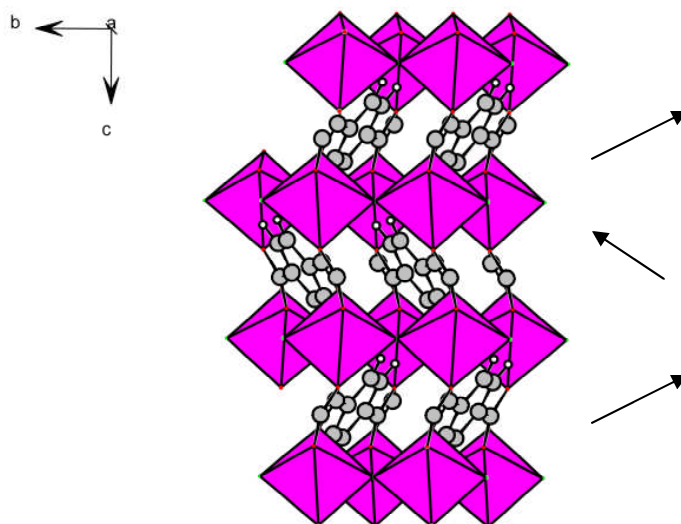


Figure 6.40: Projection down $[100]$ of structure **27** showing the different orientations assumed by the terephthalate linker

Thermogravimetric analysis shows a significant weight loss of 52.3% occurring between 547 and 595 °C due to combustion of the terephthalic acid. The material is amorphous after heating. Quantities of structure **27** suitable for ^{45}Sc MAS NMR investigations have not yet been obtained.

6.6 Conclusions

Within chapter 6, the hydrothermal chemistry of scandium carboxylate-based system has been explored. This has led to the synthesis and characterisation of nine scandium carboxylate materials, seven of which are novel.

Since the publication of the first scandium carboxylate-based material in 2003 by Perles *et al.*,⁵³ only three other scandium carboxylate-based materials have been reported, with one being a result of the work described in this chapter (**26**). Table 6.15 lists the scandium carboxylate based structures which can be found in the literature to date, as well as work discussed within this chapter which is yet to be published.

Table 6.15: Scandium carboxylate materials which have been published and which have yet to be published as a result of the work presented within this chapter.

structure	carboxylic acid	Ref
$\text{Sc}_3\text{O}(\text{H}_2\text{O})_3(\text{H}_2\text{dhtp})_3\text{X}\cdot(\text{DEF})_4$ (X = Cl, NO ₃)	2,5-dihydroxyterephthalic acid	51
Scandium oxalate	Oxalic acid	50
$\text{Sc}_2(\text{O}_2\text{CC}_2\text{H}_4\text{CO}_2)_3$	Succinic acid	(19)
$\text{Sc}_2(\text{O}_2\text{CC}_2\text{H}_4\text{CO}_2)_{2.5}(\text{OH})$	Succinic acid	⁵³ + (20)
$\text{Sc}_2(\text{O}_2\text{CC}_3\text{H}_6\text{CO}_2)_3$	Glutaric acid	(21)
$\text{Sc}(\text{O}_2\text{CC}_{12}\text{H}_8\text{CO}_2)_{1.5}\cdot(\text{H}_2\text{O})_{0.125}$	4,4'-biphenyldicarboxylic acid	(22)
$\text{Sc}_2(\text{O}_2\text{CC}_6\text{H}_4\text{CO}_2)_3$	Isophthalic acid	(23)
$\text{ScOH}(\text{O}_2\text{CC}_6\text{H}_4\text{CO}_2)_3$	Terephthalic acid	(24)
$\text{ScOH}(\text{O}_2\text{CC}_6\text{H}_4\text{CO}_2)$	Terephthalic acid	(25)
$\text{Sc}_2(\text{O}_2\text{CC}_6\text{H}_4\text{CO}_2)_3$	Terephthalic acid	(26) ^{49, 52}
$\text{ScF}(\text{O}_2\text{CC}_6\text{H}_4\text{CO}_2)$	Terephthalic acid	(27)

Within both the aliphatic and aromatic carboxylate systems, the stoichiometry of the gel has proven pivotal to the outcome of the reaction, which is demonstrated by structures **19** and **20**, both synthesised using succinic acid, and also by the numerous solids which have been synthesised during the examination of scandium terephthalate materials.

Within the structures reported in this chapter, scandium has been observed in different environments, such as isolated octahedra, $-\text{ScO}_4\text{F}_2-$ chains and $-\text{ScO}_4(\text{OH})_2-$ chains. Such geometries, or combinations of them, can be connected by different numbers of carboxylate linkers. The solid state NMR of scandium for these samples show a range of typical quadrupolar peak shapes, and is discussed in more detail in chapter 7.

Structure **26** is a small pore scandium terephthalate material which shows considerable gas adsorption potential. The pore aperture is estimated to be around 3\AA , taking into consideration van der Waals radii. The work reported later in this chapter has describes how adsorption experiments were performed on this material using a variety of adsorbates (CO_2 , C_3H_8 , C_2H_6 , CH_4 , O_2 , CO , N_2 , He and H_2), some of which have been located via single crystal experiments performed at the ESRF, Grenoble.

6.7 Further Examination of Adsorption Properties of Scandium Terephthalates

As previously stated, the main driving force into the research and development of porous materials is that such materials can be suitable candidates for applications such as gas adsorption and separation. Structure **26** is a small pore MOF which has several advantages in terms of gas adsorption compared with other MOF materials in the literature. Structure **26** is a rigid framework material, i.e. shows no 'breathing' when heated or cooled which could be important when preparing solids for applications. Owing to the hydrophobicity and architecture of the pore type within **26** there are no residual water or terephthalic acid molecules located within the pores, so that the material does not have to be activated prior to gas adsorption, (as is the case for MIL-53, for example).

Whilst investigating the scandium terephthalate system, large single crystals ($\approx 150\mu\text{m}$) were obtained via solvothermal methods. In a typical solvothermal preparation, $\text{Sc}(\text{NO}_3)_3 \cdot 6\text{H}_2\text{O}$ (Alfa, 0.34 g, 1 mmol), H_2BDC (Aldrich, 0.170 g, 1 mmol), H_2O_2 (Aldrich, 0.25 ml), pyridine (Aldrich, 0.5 ml) and DMF (Aldrich, 10 ml) were sealed in a Parr autoclave with a 23 ml Teflon liner. The mixture was subsequently heated to 220°C and allowed to react for 2 days. The autoclave was then cooled and the final product was filtered and washed with DMF.

Large single crystals of **26** were obtained as the only product. Characterisation was completed with single crystal and powder X-ray diffraction analysis, thermal analysis and nitrogen adsorption (showing an uptake of $\approx 6.5 \text{ mmol g}^{-1}$, i.e. $\approx 18\%$), which confirmed the structure and purity of the material. The powder X-ray diffraction pattern, thermal analysis and nitrogen isotherm are shown below in figure 6.41 and 6.42.

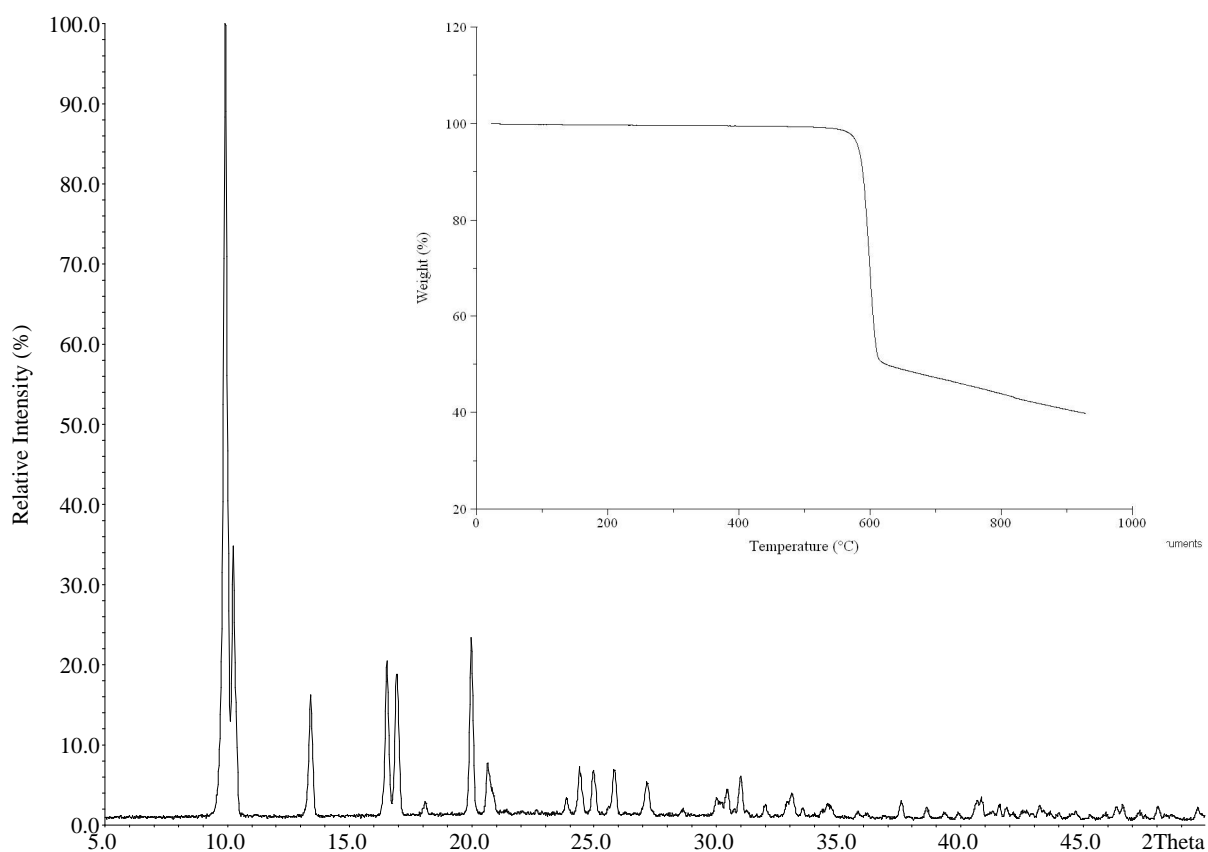


Figure 6.41: Powder X-ray diffraction pattern of solvothermally prepared **26**, with the thermal plot shown as an inset.

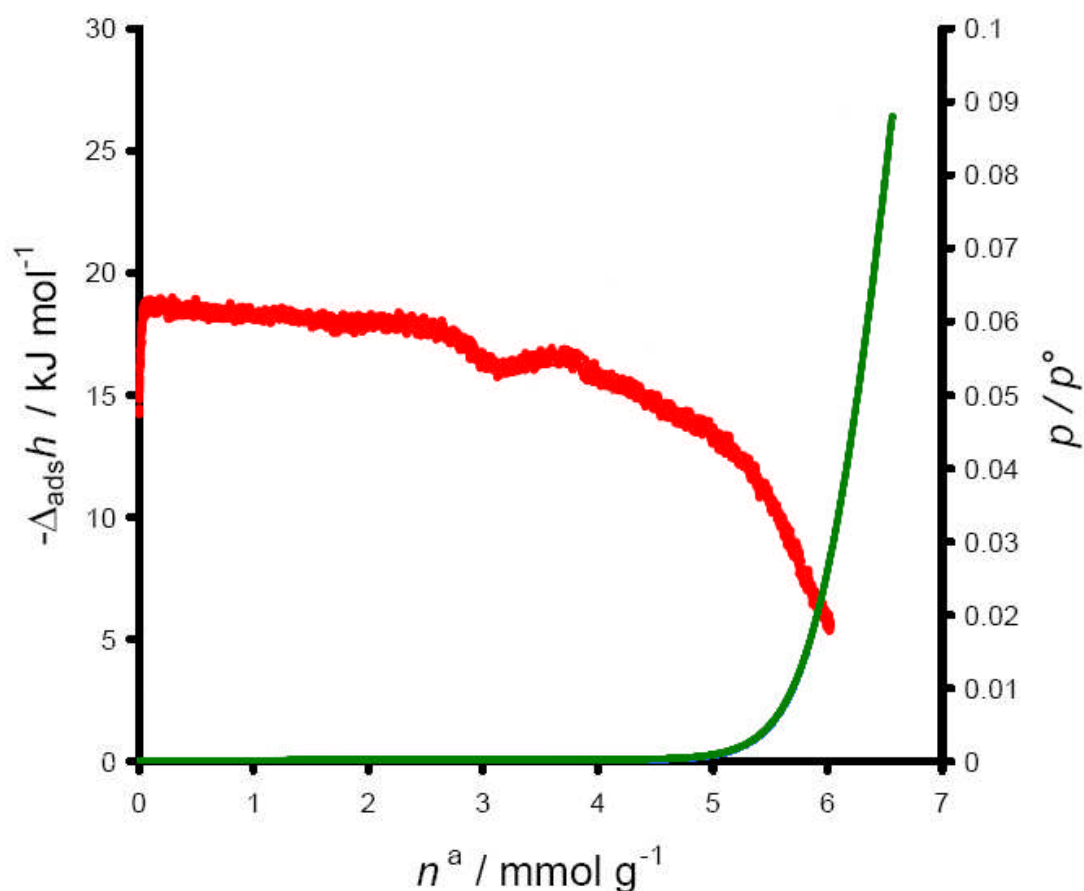


Figure 6.42: N_2 adsorption isotherm for solvothermal preparation of structure **26**.

In order to analyse the behaviour of the structure of **26**, single crystal data was collected, for a crystal prepared solvothermally, at room temperature (298K) and at 93K. Comparison of the structures collected at different temperatures shows no significant change in cell parameters or orientation of the terephthate groups within the material, with both structures being solved in the same spacegroup (Fddd). The unit cell parameters for structure **26** collected at both temperatures are given below, table 6.16.

Table 6.16: Unit cell parameters of structure **26** collected at two different temperatures

	a (Å)	b (Å)	c (Å)
Structure 26 (298K)	8.750(1)	20.754(3)	34.366(4)
Structure 26 (93K)	8.766(5)	20.795 (13)	34.414(23)

As discussed in section 6.5.5, structure **26** possesses small ‘triangular’ rigid pores. The channels have free diameters of around 3Å, with small ‘gaps’ between the channels of around 2-2.5Å, (taking van derWaals radii of C and H into account).

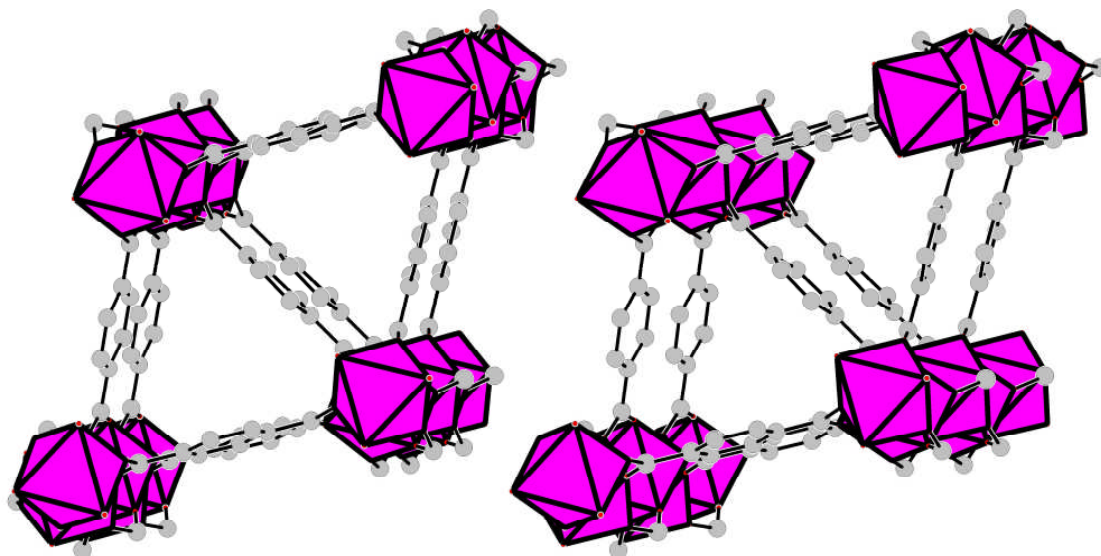


*Figure 6.43: Stereo representation of two channels within structure **26**, showing how the channels are connected. Hydrogen atoms have been omitted for clarity.*

Further investigation of the adsorption properties of structure **26** was performed using a series of small diatomic molecules and short chained hydrocarbons. These experiments were performed using a manometric device at the **MA**tériaux **DI**visés, **Rev**êtements, **EL**ectrocéramiques, **MADIREL**, in Marseille. The experiments were performed in conjunction with Drs P. Llewellyn and S. Bourelly, and Miss L. Gaberova. A table of the gases used during this investigation is given below (table 6.17) which lists the molecular radii of each species.

Table 6.17: Gas molecules and their molecular radii used whilst investigating the adsorption properties of structure **26**.^{193, 195-197}

Gas molecule	σ (LJ sphere)	2CLJQ model	
		σ	L
H ₂	2.89Å		
He	2.60Å		
N ₂	3.64Å	3.32Å	1.05Å
CO	3.76Å	3.30Å	1.14Å
CO ₂	3.30Å	2.98Å	2.42Å
O ₂	3.46Å	3.11Å	0.97Å
CH ₄	3.8Å		
C ₂ H ₄		3.76Å	1.27Å
C ₂ H ₆		3.49Å	2.38Å

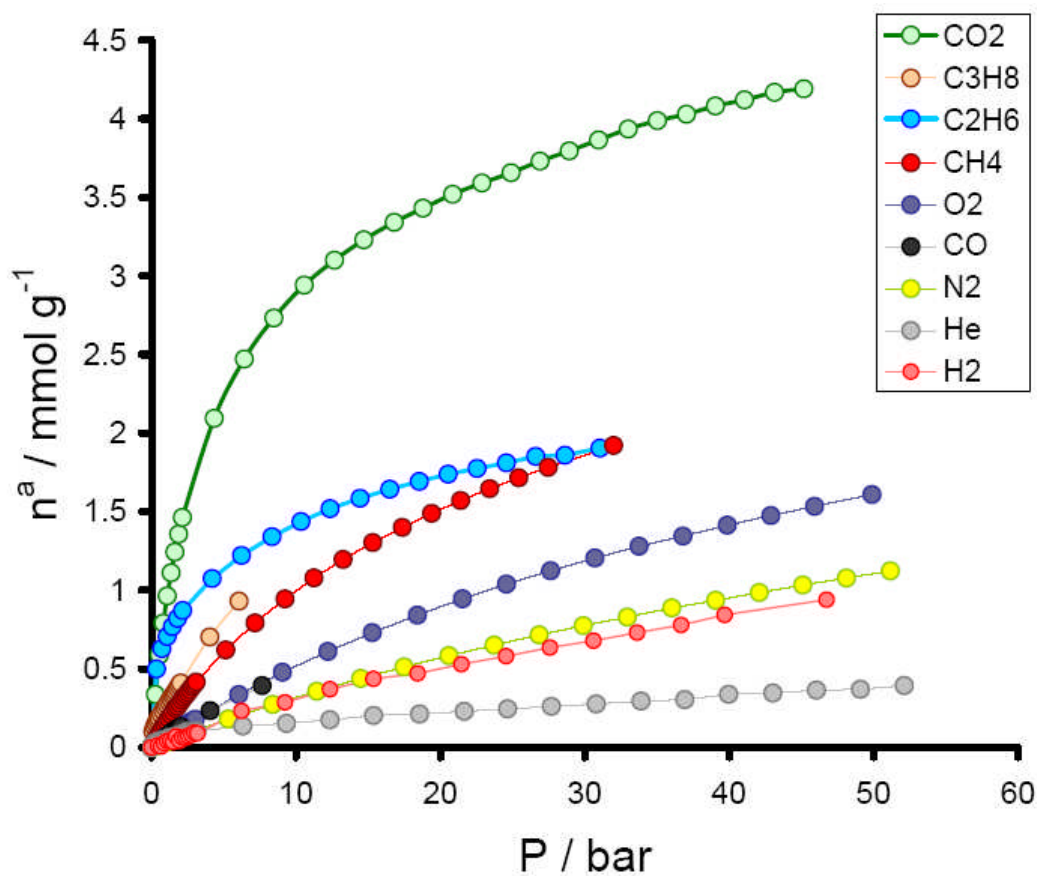


Figure 6.44: Adsorption isotherms for different gases on structure **26**. The isotherms were recorded at 303 K.

The crystals were used in *in situ* adsorption experiments carried out in BM01 at the ESRF in Grenoble, in collaboration with C. Serre, T. Devic, P Llewellyn and Y. Filinchuk, in order to provide information on the structure of the sorbent-sorbate systems and permit a more detailed understanding of the mechanisms of adsorption within this solid.

A single crystal of **26** was mounted on a glass fibre, which was then carefully introduced in a 0.3 mm quartz capillary and glued to it. The capillary was then connected to a home-made vacuum/gas pressure controller and put on a goniometer head (figure 6.45).

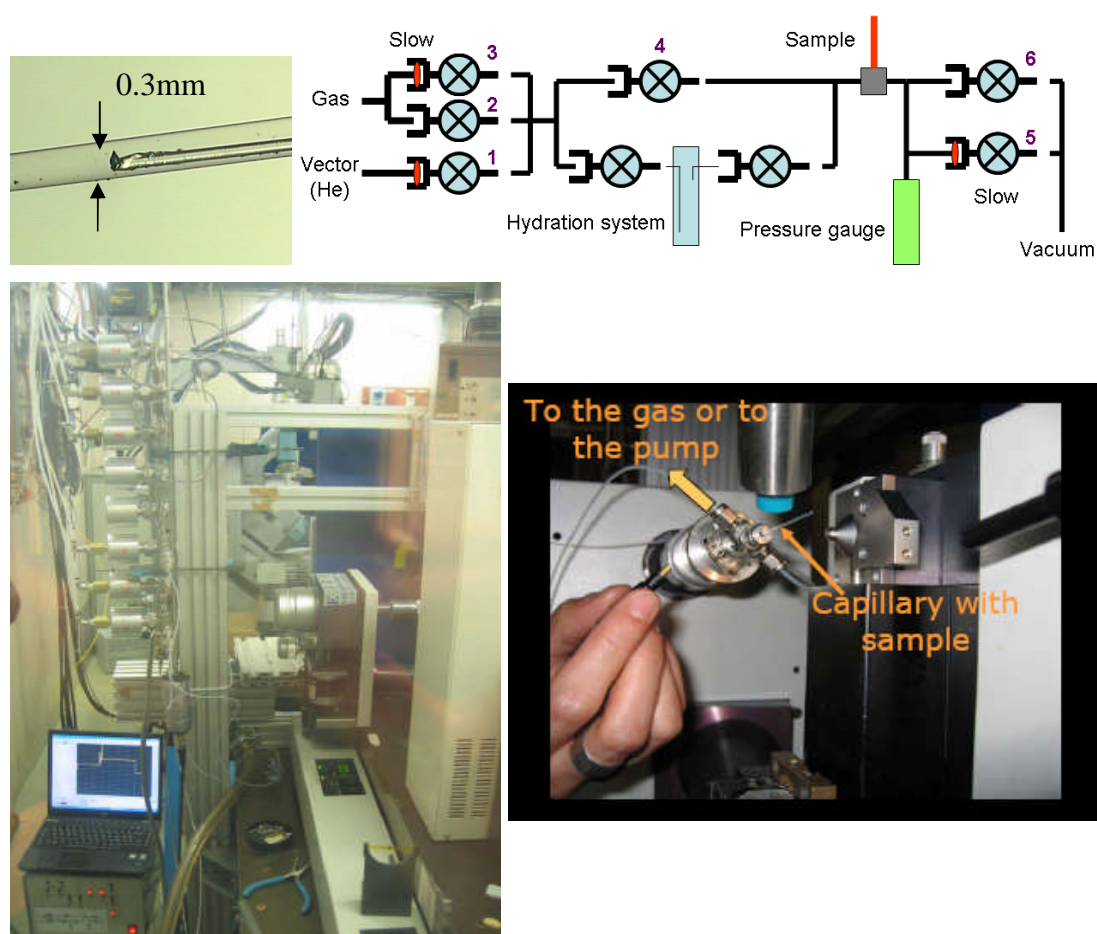


Figure 6.45: (top left) Single crystal of **26** mounted on a glass fibre within a 0.3mm quartz capillary; (top right) Schematic representation of adsorption apparatus used during experiment. (bottom left) Photograph of the experimental set-up on BM01 at the ESRF, Grenoble; (bottom right) Quartz capillary filled with sample and attached to adsorption apparatus

The quality of the crystals was checked under vacuum, recording 20 frames at room temperature. When a good crystal was found, a small amount of ethane was introduced ($P = 5$

bar) and the capillary was cooled down to 230 K. 175 frames were then collected at $\lambda \approx 0.81 \text{ \AA}$ using the MAR-345 image plate detector. The same procedure was applied for other gases in related studies (CH_4 : P = 9 bar, T = 230 K, CO_2 : P = 1 bar, T = 230 K) by T. Devic, C. Serre, P. Llewellyn and Y. Filinchuk.

In each case, good datasets were obtained. Data were processed using the CrysAlis software.¹⁹⁸ Cell parameters of the precursor and the gas-loaded compounds are summarized in table 6.18.

Table 6.18: Crystallographic information for structure **26** with different gases adsorbed.

*Structure **26** is denoted by $\text{Sc}_2(\text{BDC})_3$

	<i>As-prepared</i>	C_2H_4	CH_4	CO_2
<i>formula</i>	$\text{Sc}_2(\text{BDC})_3$	$\text{Sc}_2(\text{BDC})_3 \cdot (\text{C}_2\text{H}_8)_2$	$\text{Sc}_2(\text{BDC})_3 \cdot (\text{CH}_4)_3$	$\text{Sc}_2(\text{BDC})_3 \cdot (\text{CO}_2)$
<i>T</i>	293 K	230 K	230 K	235 K
<i>unit cell</i> (\AA)	orthorhombic	orthorhombic	orthorhombic	monoclinic
	a = 8.766(5)	a = 8.8650(8)	a = 8.7550(31)	a = 8.747(2)
	b = 20.795(13)	b = 20.7001(19)	b = 20.7786(16)	b = 34.464(8)
	c = 34.414(23)	c = 34.3750(20)	c = 34.4075(48)	c = 11.092(2)
				$\beta = 110.95^\circ$ (3)
	V = 6259 \AA^3	V = 6308 \AA^3	V = 6294 \AA^3	V = 3122 \AA^3
<i>space group</i>	Fddd	Fddd	Fddd	C2/c
<i>Z</i>	32	32	32	8
<i>Pressure</i>	-	5 bar	9 bar	1 bar

The experimental temperatures (230/235K) of the data sets of the single crystal measurements on structure **26** with adsorbed species are lower than those of the isotherms shown in figure 6.46 so this data can not be directly compared. At this stage, however, it is informative to examine the sites adopted by the adsorbed molecules.

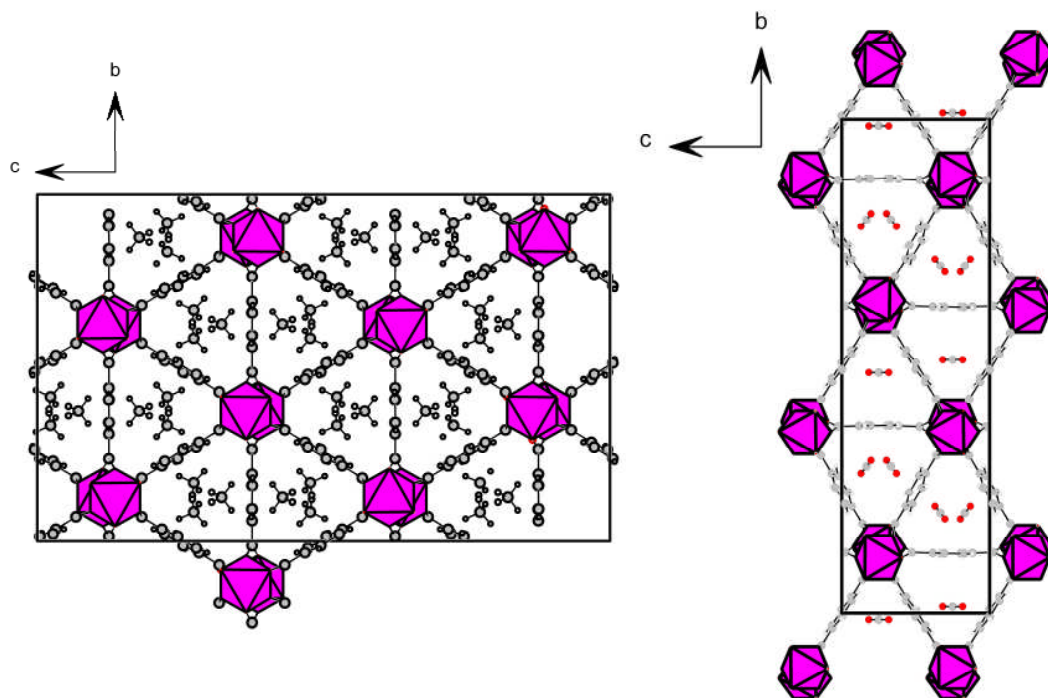


Figure 6.46: (left) Structure **26** with CH_4 adsorbed into the pores. (right) Structure **26** with CO_2 adsorbed into the pores. Both structures were solved from single crystal data.

Single crystal studies on the adsorption of ethane within structure **26** shows that there are several possible positions for the ethane molecule to assume. Similar to the CO_2 and CH_4 adsorption, one of the sites of adsorption is within the central pore of the structure. Ethane can assume two positions within the triangular pore, which is shown schematically figure 6.47.

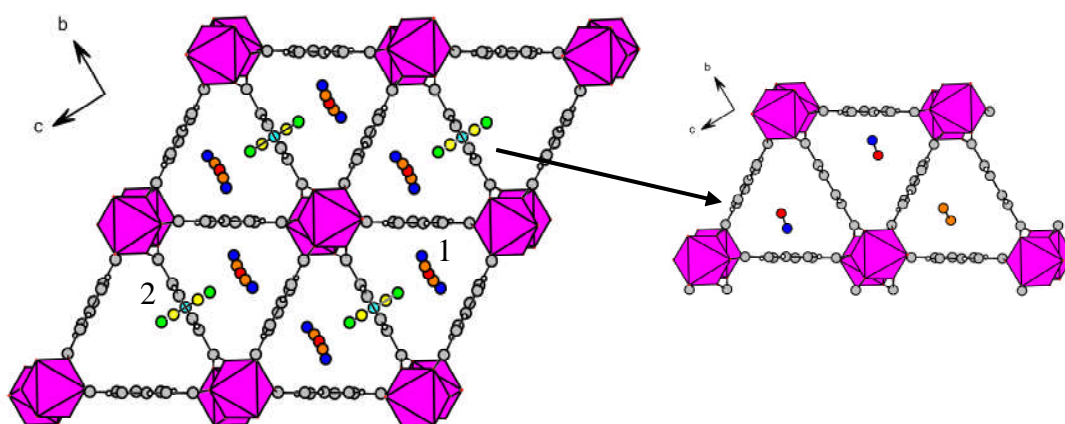


Figure 6.47: (Right) Projection down $[100]$ of structure **26** showing disordered ethane positions. (Left) Projection down $[100]$ showing only three pores of structure **26** with a representation of adsorbed ethane molecules without any disorder.

The alternative site for ethane adsorption, designated '2' in figure 6.48 and shown by the green, yellow and cyan atoms. This site of adsorption has not been observed for CO₂ or CH₄ adsorption studies.

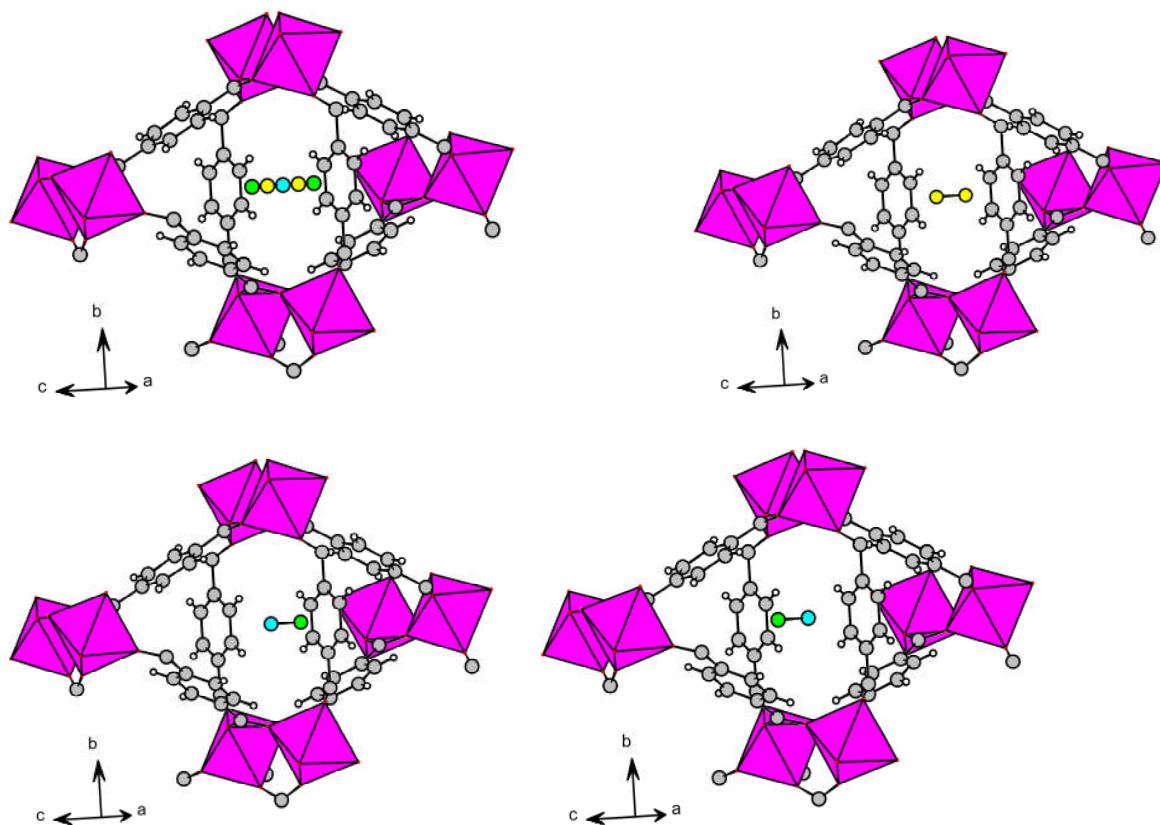


Figure 6.48: Schematic representation of positions assumed by ethane within **26**.

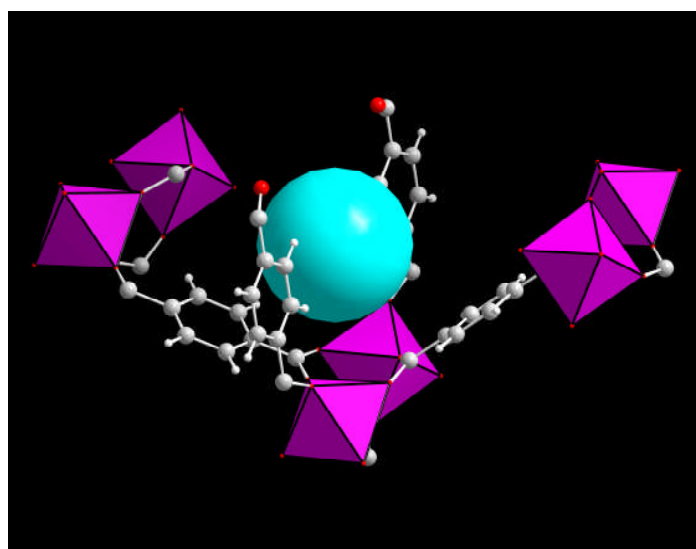


Figure 6.49: Representation of adsorption site '2' using a spacefilling sphere in order to illustrate the space available between the aromatic rings

The difference between the sites occupied by the different species indicate how the shape of the pore, combined with the different dimensions and charge distributions of the adsorbed molecules critically effect their locations.

Chapter 7:
A note on the ^{45}Sc MAS
NMR of Scandium-bearing
Open Framework Solids

7.1 A note on the ^{45}Sc MAS NMR of scandium-bearing open framework solids

Prior to the studies presented within this thesis, there was relatively little ^{45}Sc MAS NMR for microporous materials containing scandium. This is due to the paucity of scandium-based microporous materials within the literature and also because of the quadrupolar nature of the ^{45}Sc nucleus. One example of ^{45}Sc MAS NMR data within the literature is the scandium phosphate-based framework reported by Park *et al.*⁴² A combination of MQMAS and line shape calculations, deriving the asymmetry parameter (η_Q), is used in order to assign the independent scandium environments to the isotropic chemical shift values

As described in chapter 1 of this thesis, ^{45}Sc is the only isotope of scandium, and is therefore 100% abundant; it is also a quadrupolar nucleus, with a spin of $7/2$. Quadrupolar nuclei have a non-spherical charge distribution and consequently a non-zero nuclear electric quadrupolar moment, eQ . The interaction of quadrupolar moments with an electric field gradient, which is known as quadrupolar interaction, strongly influences line widths and shapes. The line widths and shapes which are obtained from quadrupolar nuclei are influenced by two parameters, η_Q (the asymmetry parameter) and C_Q (the quadrupolar coupling constant), which can be calculated by spectral fitting.

The local environments of scandium within the structures reported within this thesis are compared to the ^{45}Sc NMR spectra collected, noting C_Q , η_Q and isotropic chemical shift for each solid. Scandium has been observed in a variety of environments, including $\text{Sc}_3(\text{OH})_2\text{O}_{14}$ trimers, ScO_4F_2 chains, $\text{Sc}_4\text{F}_4\text{O}_{16}$ tetramers and as isolated octahedra, which have been identified within different structural systems, ranging from phosphates to carboxylates.

The ^{45}Sc MAS NMR spectra for each material discussed in this thesis are reported and discussed within the relevant chapters. In order to demonstrate the variety of ^{45}Sc lineshapes and shifts obtained within this work it is helpful to show ^{45}Sc spectra plotted in the same figure and with the same chemical shift scale (figure 7.1 – 7.4).

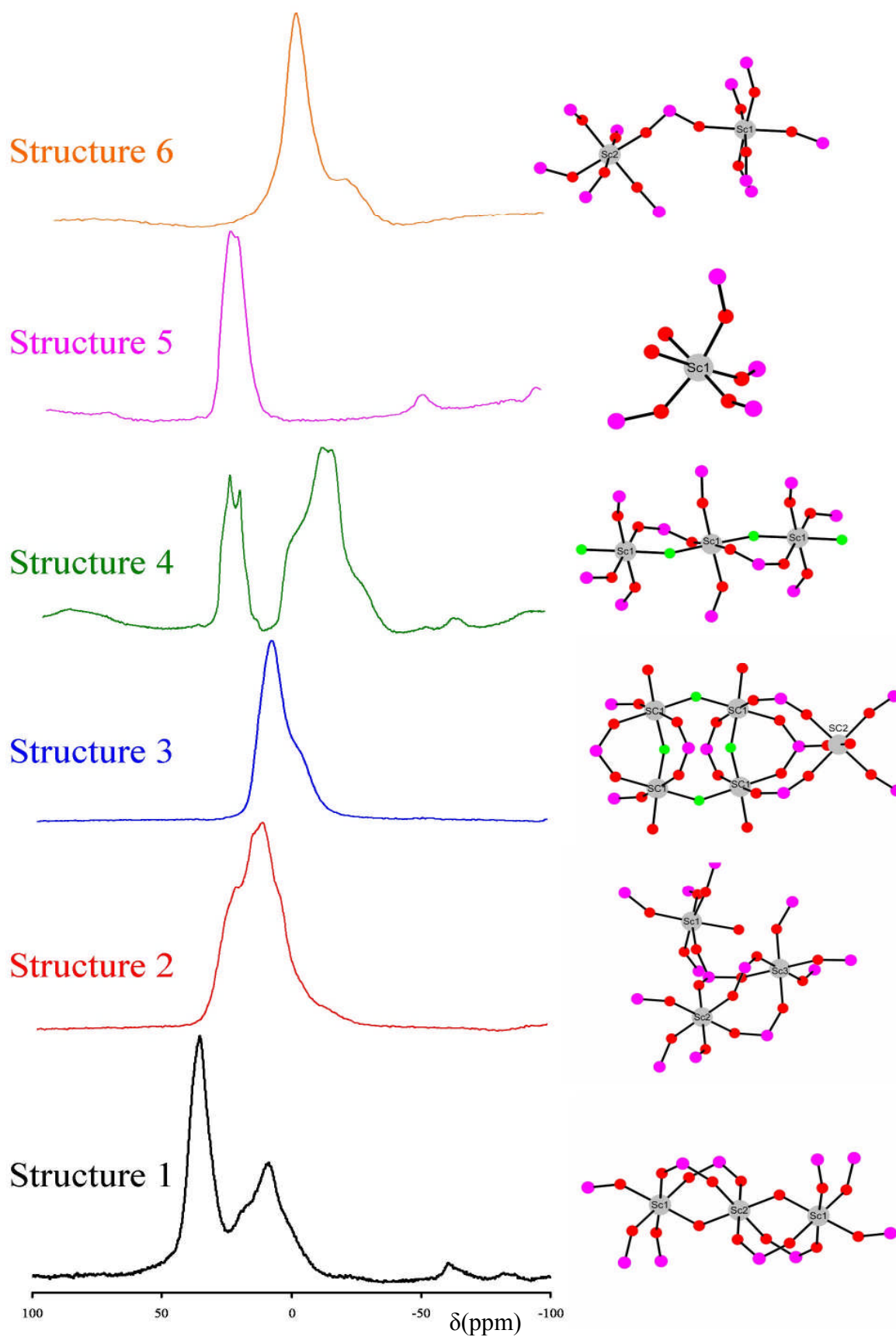


Figure 7.1: ^{45}Sc MAS NMR spectra for structures 1 – 6. (Scandium phosphates)

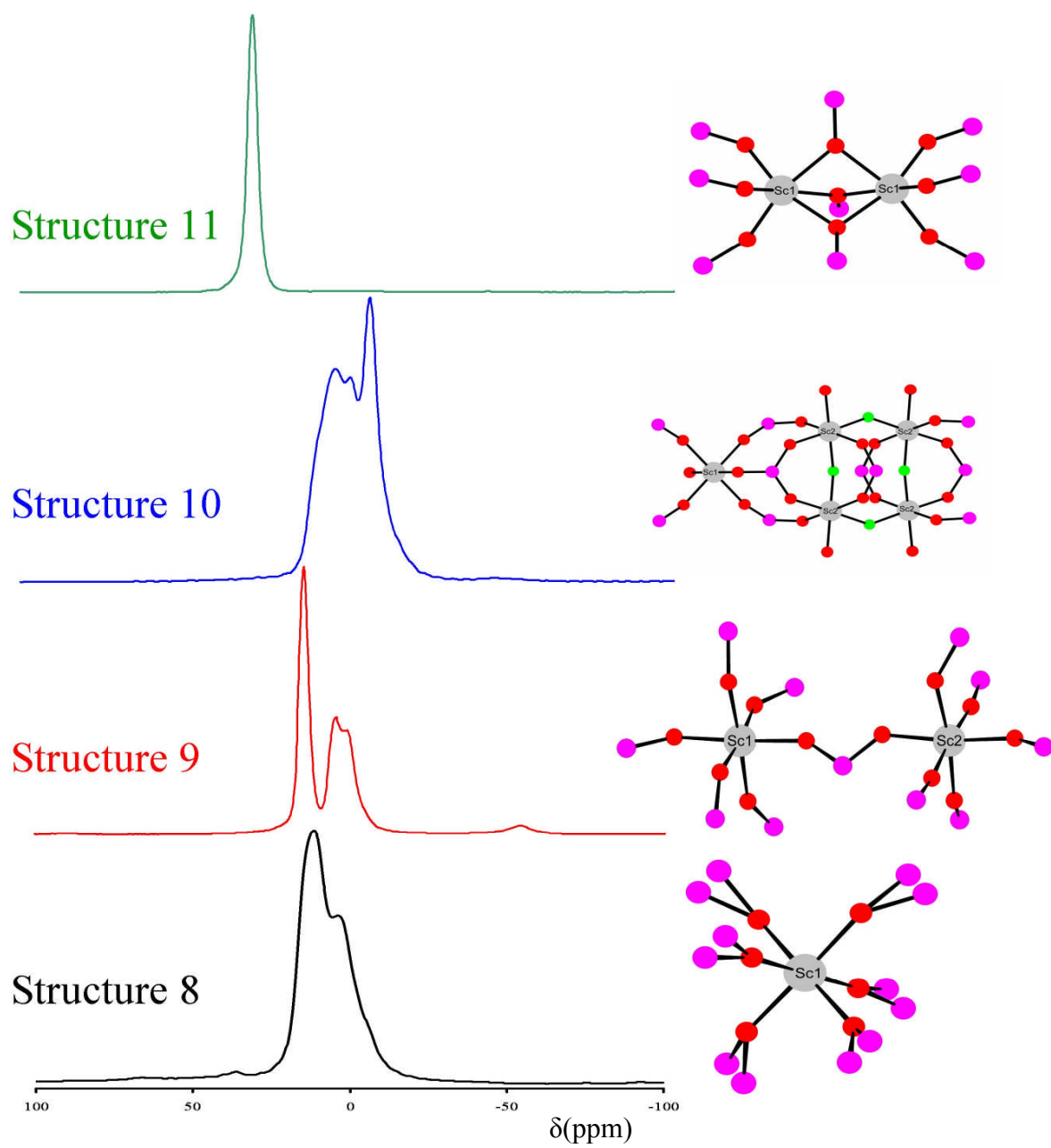


Figure 7.2: ^{45}Sc MAS NMR spectra for structures 8 – 11. (Scandium phosphites)

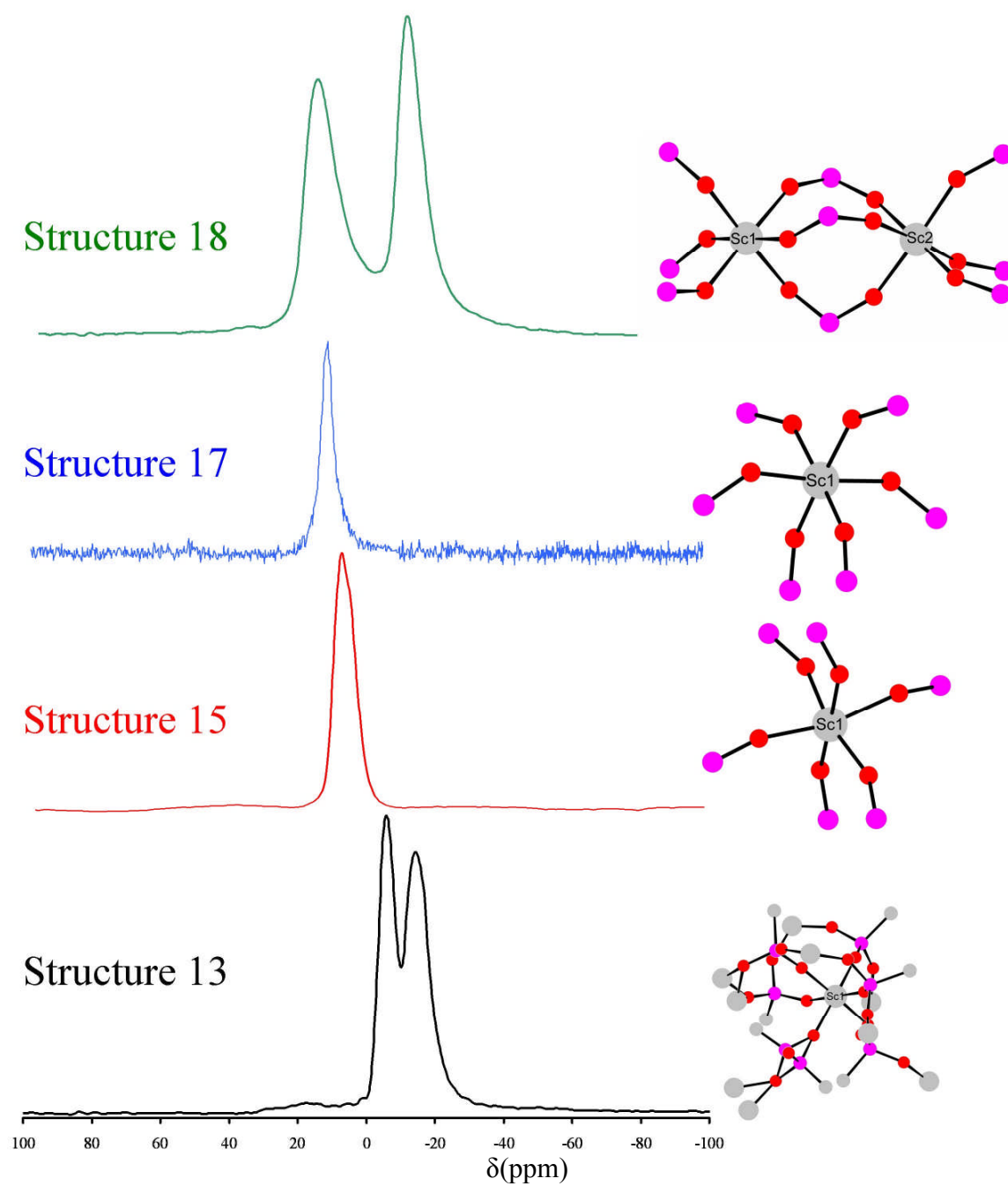


Figure 7.3: ^{45}Sc MAS NMR spectra for 13, 15, 17 and 18. (Scandium phosphonates)

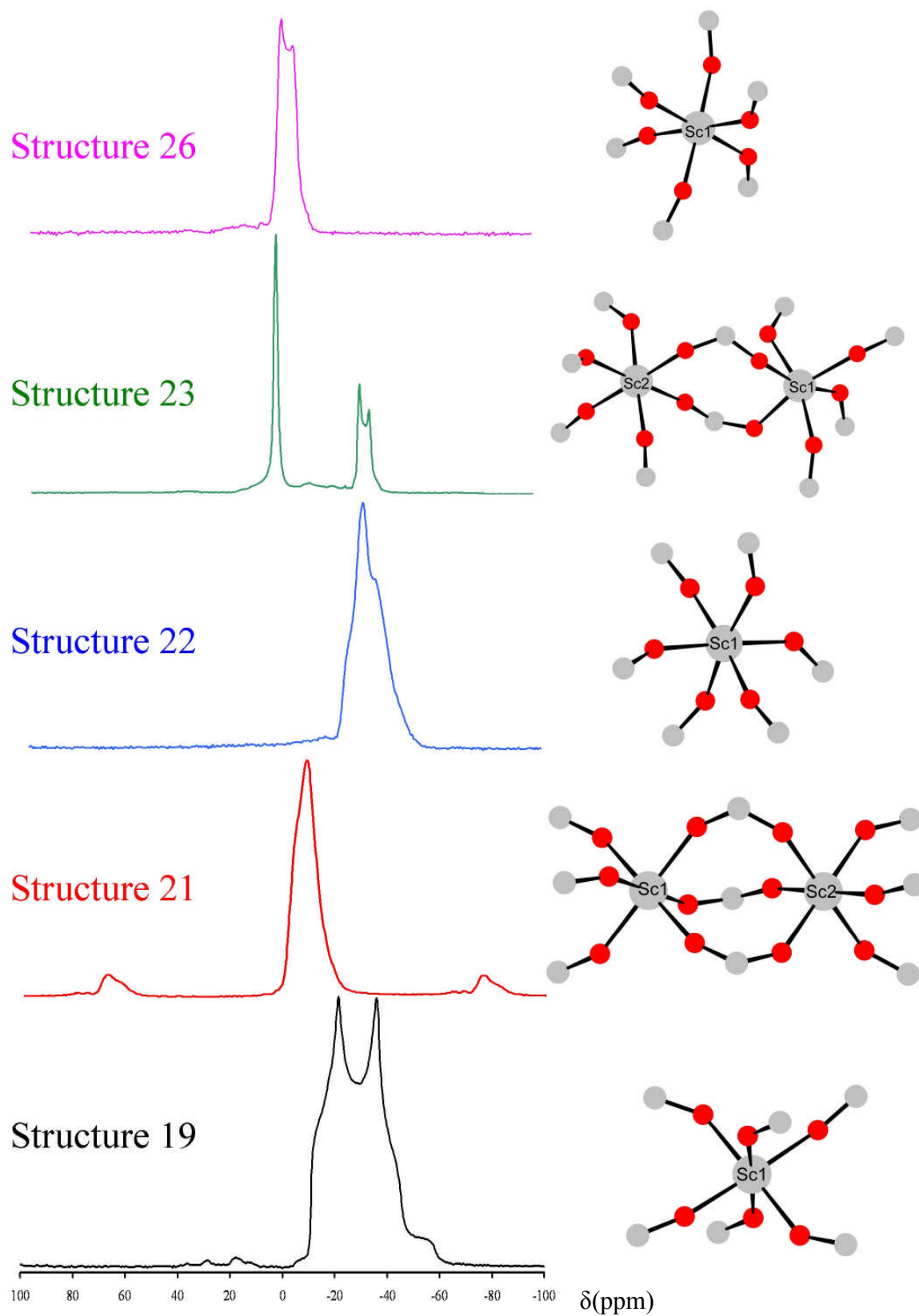


Figure 7.2: ^{45}Sc MAS NMR spectra for **19**, **21** – **23** and **26**. (Scandium carboxylates)

Although the experimental parameters for each spectrum were individually optimised and therefore differ from each other, these figures show how the local environment of the scandium atoms within each structure affect the lineshape and position of the peaks. The ‘true’ chemical shift value for each spectra is not attributed to the most intense point of the signal and therefore must be obtained by ‘fitting’ the lineshape of the spectra, allowing for quadrupolar effects. In order to provide analysis of the ^{45}Sc spectra the fitting program DMFIT¹⁸⁰ has been used to fit each spectra to the number of scandium sites suggested by single crystal analysis. DMFIT enables fitting of the spectra by allowing varying numbers of independent sites to be refined in respect to their lineshape, width, asymmetry and amplitude. Table 7.1 gives the true chemical shift value, the quadrupolar coupling constant (C_Q) and the asymmetry parameter (η_Q). In some cases the broadness of lines and the overlap of resonances result in fitting ‘solutions’ that are unlikely to be unique. These cases are asterisked in table 7.1.

Table 7.1: Analysis of ^{45}Sc lineshapes (* ambiguity due to severe peak overlap)

Structure	Gaus / Lor			Qmas 1/2		
	δ_{iso} (ppm)	Width (ppm)	xG/(1-x)L Gaussian/Lorentzian	Em au	C_Q MHz	η_Q
1 site (1)	38.9	-	-	477.88	5.1(1)	0.63
1 site (2)	29.1	-	-	182.68	8.9(1)	0.54
2 site (1)*	34.8	-	-	271.91	13.2(1)	0.32
2 site (2)*	28.3	-	-	654.17	8.6(1)	0.30
2 site (3)*	16.2	-	-	429.71	7.5(1)	0.46
3 site (1)*	13.8	-	-	469.09	6.0(1)	0.60
3 site (2)*	4.1	-	-	342.39	6.5(1)	0.63
4 site (1)	2.48	-	-	169.35	9.3(1)	0.70
5 site (1)	28.3	-	-	384.56	6.0(1)	0.44
6 site (1)	-2.6	9.96	0.10	-	-	-
6 site (2)	4.2	-	-	159.65	11.0(1)	0.28
8 site (1)	19.1	-	-	506.55	6.5(1)	0.14
9 site (1)	14.4	3.62	0.68	-	-	-
9 site (2)	7.8	-	-	514.17	4.5(1)	0.19
10 site (1)	12.2	-	-	425.41	5.1(1)	0.58
10 site (2)	1.2	-	-	284.97	4.8(1)	0.89
11 site (1)	28.8	3.68	0.52	-	-	-
13 site (1)	-5.8	4.84	0.92	-	-	-
13 site (2)	-14.6	8.64	0.19	-	-	-
15 site (1)	9.3	-	-	416.31	5.0(1)	0.00
18 site (1)	13.5	12.10	0.91	-	-	-
18 site (2)	-13.5	8.99	0.055	-	-	-
19 site (1)	-8.2	-	-	67.74	8.5(1)	0.00
21 site (1)*	-3.3	-	-	622.93	4.5(1)	0.68
21 site (2)*	-0.5	-	-	603.69	4.4(1)	0.00
22 site (1)	-22.58	-	-	361.47	5.9(1)	0.05
23 site (1) 'A' in fig 6.22	2.5	1.77	0.15	-	-	-
23 site (2) 'B' in fig 6.22	-29.0	-	-	309.93	3.8(1)	0.00
26 site (1)	2.8	-	-	337.14	5.5(1)	0.20

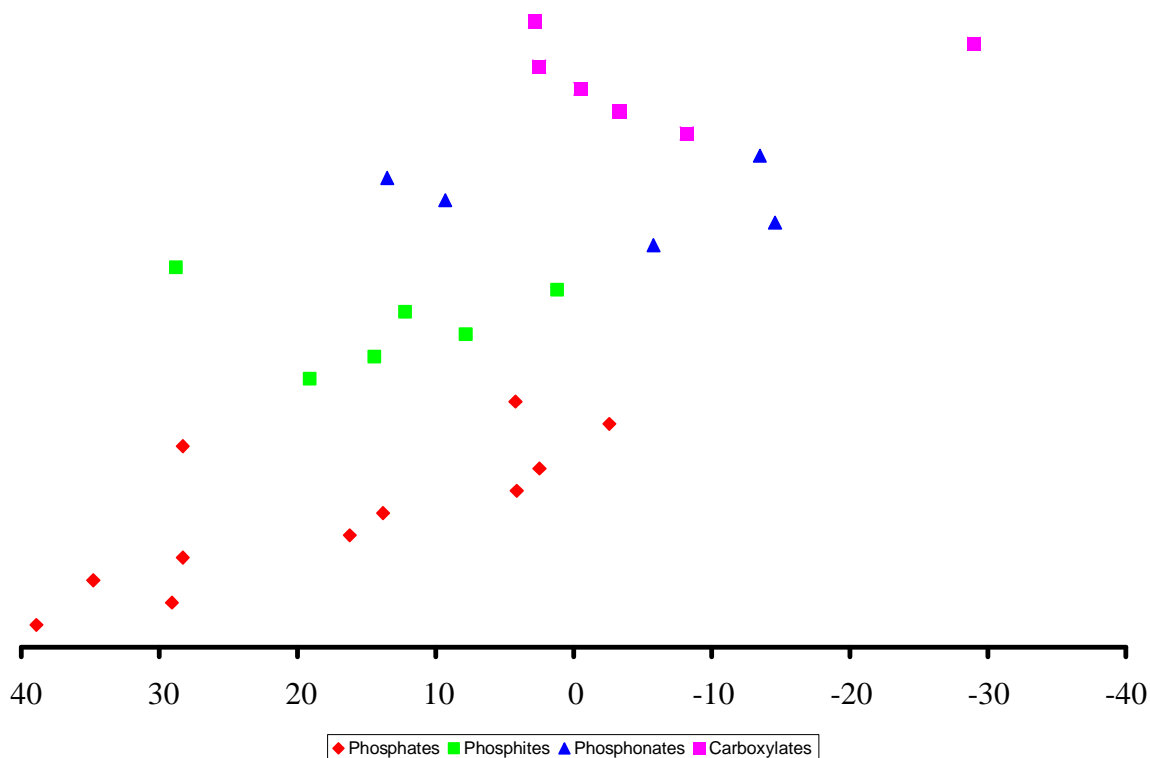


Figure 7.5: Plot showing the chemical shift values for the different systems examined in this work. These values are listed in table 7.1

No simple trends emerge from this data between the isotropic chemical shifts, the quadrupolar coupling constant or the asymmetry parameter and measures of the deviation of the ScO_6 (or $\text{ScO}_{6-x}\text{F}_x$) octahedra from a regular octahedron as measured by standard deviations of Sc-O bond lengths or O-Sc-O angles. This indicates that the overall crystal environment in what are chemically quite different solids is more important. Some comments can be made where there are two well resolved and fitted quadrupolar lineshapes from ^{45}Sc nuclei within the same sample, e.g. structure **23**.

A comparison of the ‘ligand’ style or chemical matrix in which the ^{45}Sc nuclei are situated reveals a trend, suggesting that the surrounding framework chemistry effects the shift, with higher δ values being observed for phosphates > phosphites > phosphonates > carboxylates. This is shown in figure 7.6.

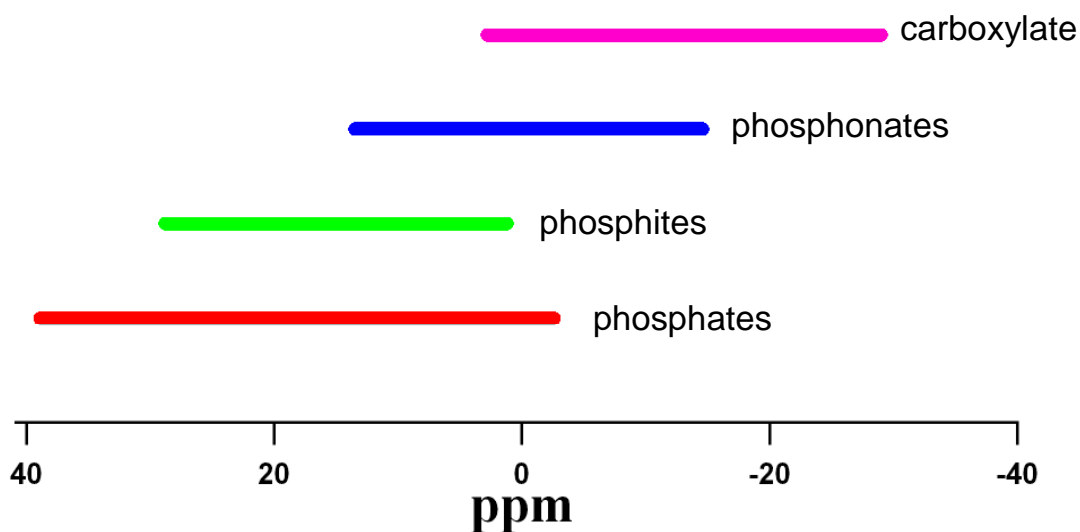


Figure 7.6: Representation of the chemical shift range which ^{45}Sc nuclei are observed within different framework materials.

Further examination of Structure **23** enables the different signals in the ^{45}Sc MAS NMR spectra to be unambiguously attributed to the crystallographically independent scandium sites observed in the crystallography. Large deviations in bond angles and lengths in an octahedral unit can result in typical quadrupolar lineshapes, i.e. as observed for site 'B' in figure 6.22. A comparison of the bond lengths and angles for Sc(1) and Sc(2) shows that Sc(1) has the higher degree of asymmetry and can therefore probably be attributed to site 'B' on figure 6.22.

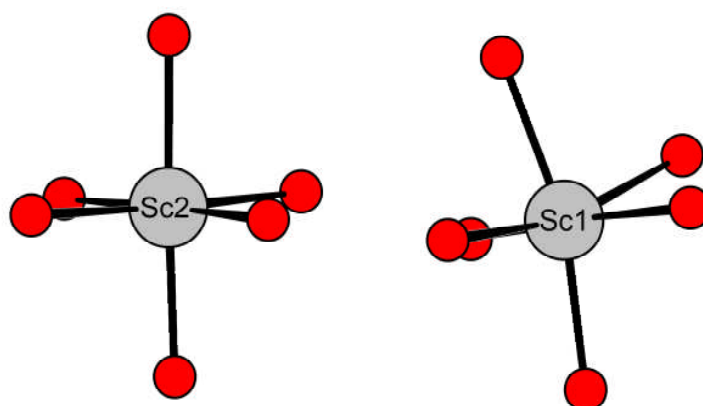


Figure 7.7: Representation of the local environments of Sc(1) and Sc(2) within structure **23**, showing a larger deviation from a 'perfect' octahedral unit for Sc(1)

It is clear from the data presented in this chapter that further analysis of the ^{45}Sc MAS NMR is required in order to gain a better understanding of the NMR properties of scandium within open framework materials. Where there is ambiguity caused by peak overlap or broadening due to disorder, the samples should be examined at different field strengths, because for resonances with very different quadrupolar coupling constants the centres of gravity of the peaks will change differently with changing field strengths, leading to enhanced resolution. Furthermore, multiple quantum NMR would be essential to derive accurately spectral parameters for resonances where more than one scandium site is present within the 1D MAS NMR signal. It would also be informative to calculate the ^{45}Sc MAS NMR lineshapes using the CASTEP program, and to compare them to the results presented here.

Chapter 8: General Summary, Conclusions and Further Work

8.1 General Conclusions

The main aim of this thesis was to explore the hydrothermal chemistry of scandium to yield microporous materials. Experiments were therefore carried out investigating scandium within four chemically different framework types.

An investigation into scandium phosphate-based materials was chosen as a starting point, as similar materials had been published prior to this work.⁴¹⁻⁴⁶ The work presented within this thesis on scandium phosphate systems showed that structure direction could be achieved using mono and di- primary amine molecules, but the use of secondary or tertiary amines or alkyl ammonium salts resulted in the formation of dense phase scandium phosphates (kolbeckite ($\text{Sc}(\text{PO}_4)\cdot 2\text{H}_2\text{O}$) or langbeinite ($(\text{NH}_4)_2\text{Sc}_2(\text{HPO}_4)(\text{PO}_4)_2$). The use of aliphatic diamines and cyclohexylamine resulted in the formation of chain, layer and framework phosphates, but the frameworks did not remain intact upon removal of the template, due largely to the disruption of hydrogen bonding interactions between the amine and P-OH groups within the materials.

Subsequently, scandium phosphite-based materials were synthesised in order to reduce the number of terminal P-O groups within the materials, and hence the likelihood for hydrogen bonding networks. The use of aliphatic diamines as templating agents resulted in a scandium phosphite ($[(\text{H}_3\text{N}(\text{CH}_2)_2\text{NH}_3)_2][\text{Sc}_4(\text{HPO}_3)_8]$) and scandium phosphite / phosphate material, ($[(\text{H}_3\text{N}(\text{CH}_2)_4\text{NH}_3)_2][\text{Sc}_5\text{F}_4(\text{HPO}_3)_7(\text{HPO}_4)]$) which were isomorphous to scandium phosphates already reported, either in the previous chapter, or in the literature.⁴⁵ This suggests that the framework topologies of scandium phosphite materials, within which the phosphite tetrahedra are not fully connected, can be closely related to the topologies of scandium phosphate materials. Thermal analysis of the templated scandium phosphites and phosphite / phosphates revealed the the organic template could not be removed without affecting the structural integrity of the material. The use of lithium hydroxide as a structure directing agent within scandium phosphites resulted in the formation of a phase (structure **8**) isostructural to the ethylenediamine-templated scandium phosphite (structure **9**). Larger structure directing agents and alkyl ammonium salts resulted in the formation of a small pore scandium phosphite material, within which scandium assumes a face-sharing environment (Structure **11**).

Chapter 5 investigated the structural chemistry of scandium phosphonate-based materials, as the use of phosphonic acids allowed the structure directing effects of an organic moiety, without it having to be removed from the final product. The initial approach for this work

examined the substitution of scandium into aluminium methylphosphonate materials which have been fully characterised within the literature.^{140, 148, 149} It was established that the source of scandium cations influenced the product within the AlMePO systems, with Sc₂O₃ yielding a mixed α - and β - AlMePO material, and Sc(NO₃)₃ yielding a novel layered ScAlMePO (Structure **13**). Initial attempts to synthesise novel scandium methylphosphonates proved successful, but the crystalline material which was synthesised could not be characterised. Altering the pH of the synthesis using HF and alkali hydroxides resulted in the synthesis and characterisation of three novel scandium phosphonate materials (Structures **14** – **16**). The addition of fluorine to the synthesis resulted in a novel scandium phosphonate material consisting of -Sc-F-Sc- chains (Structure **14**). Altering the pH of the solution using sodium hydroxide result in a novel small pore sodium scandium phosphonate material (Structure **15**) which shows reversible adsorption of water, whereas altering the pH of the starting solution using lithium hydroxide resulted in the crystallisation of a novel scandium methylphosphonate (Structure **16**) however there is no evidence of lithium cations being included within the material.

The crystallisation of scandium bisphosphonates was investigated, aspiring towards porous scandium phosphonate frameworks. The use of ethylenebisphosphonic acid resulted in the formation of a material, isostructural to a vanadium bisphosphonate reported by Zubieta *et al.*,¹⁵⁷ consisting of inorganic layers which are separated by the organic (Structure **17**). More complex bisphosphonic acids were also investigated. Recent studies into the reactions of N,N'-piperazinebismethylenephosphonic acid and 2-methyl-N,N'-piperazinebismethylene-phosphonic acid with transition metals have led to the isolation and characterisation of several porous framework materials, which show great potential for adsorption.^{60, 67-69} Including these ligands into scandium phosphonate systems resulted in the formation of three different microcrystalline materials. The structure of the scandium 2-methylpiperazinemismethylene phosphonate (Structure **18**) was solved from powder data by a combination of techniques, revealing a small pore framework material which has reversible water adsorption.

An investigation into scandium carboxylate-based materials is described in chapter 6. Prior to this work, only one scandium carboxylate was described in the literature, the reaction conditions of which were used as a starting point for this investigation.⁵³ Initial work within the scandium carboxylate system focused on the use of aliphatic carboxylates with different chain lengths. This resulted in the formation of five different scandium carboxylates, three of which were solved by single crystal diffraction (Structures **19** – **21**).

Using aromatic carboxylic acids, such as 4,4'-biphenyldicarboxylic and isophthalic acid resulted in the crystallisation of a framework carboxylates with either small channels created by the arrangement of the biphenyl linkers (Structure **22**) or 'pear-like' cavities (Structure **23**).

Investigating scandium terephthalates proved fruitful, with the crystallisation of several phases. At least five different phases were found to crystallise in the absence of hydrofluoric acid, three of which were fully characterised (Structure **24** – **26**). Using a very high level of water in relation to scandium and terephthalic acid yielded a close packed scandium terephthalate consisting of corner-sharing $\text{ScO}_4(\text{OH})_2$ octahedra (Structure **24**) and also a framework scandium terephthalate with a one dimensional pore system (Structure **25**), isostructural to MIL-53,¹⁹² collected as a by-product.

The main phase formed whilst investigating the scandium terephthalate system in the absence of hydrofluoric acid was a novel framework material (Structure **26**), which contained small pores (3-4Å). The use of hydrofluoric acid within the reactions resulted in the formation of a scandium terephthalate with –Sc-F-Sc- chains within which the Sc-F-Sc bond angle is 180°.

Adsorption studies conducted on Structure **26** shows that the framework can accommodate several different diatomic gases (H_2 , N_2 , O_2 , He, CO_2 and CO) and small hydrocarbons (CH_4 , C_2H_4 , C_2H_6 and C_3H_8). In the cases of methane, carbon dioxide and ethane, experiments were performed at the ESRF in order to locate the preferred sites of adsorption.

Throughout this work each structure has been characterised by X-ray diffraction, thermal analysis and, where possible, by solid state NMR. The ^{45}Sc MAS NMR was collected for nineteen of the materials discussed throughout this thesis. From the nineteen spectra collected, eighteen were fitted computationally, using DMFIT, in order to collate the chemical shift and quadrupolar coupling constant and determine what effect the local environment of the Sc^{3+} cation had on the spectrum. It was concluded that the framework type, i.e. phosphate, phosphite, phosphonate or carboxylate had a greater effect on the chemical shift than the direct local environment, i.e. ScO_6 or ScO_4F_2 .

8.2 Further Work

The work presented within this thesis demonstrates that scandium can be included in the crystallisation of different framework types, producing novel structures and structures which are isostructural to those already reported, but with different chemical compositions.

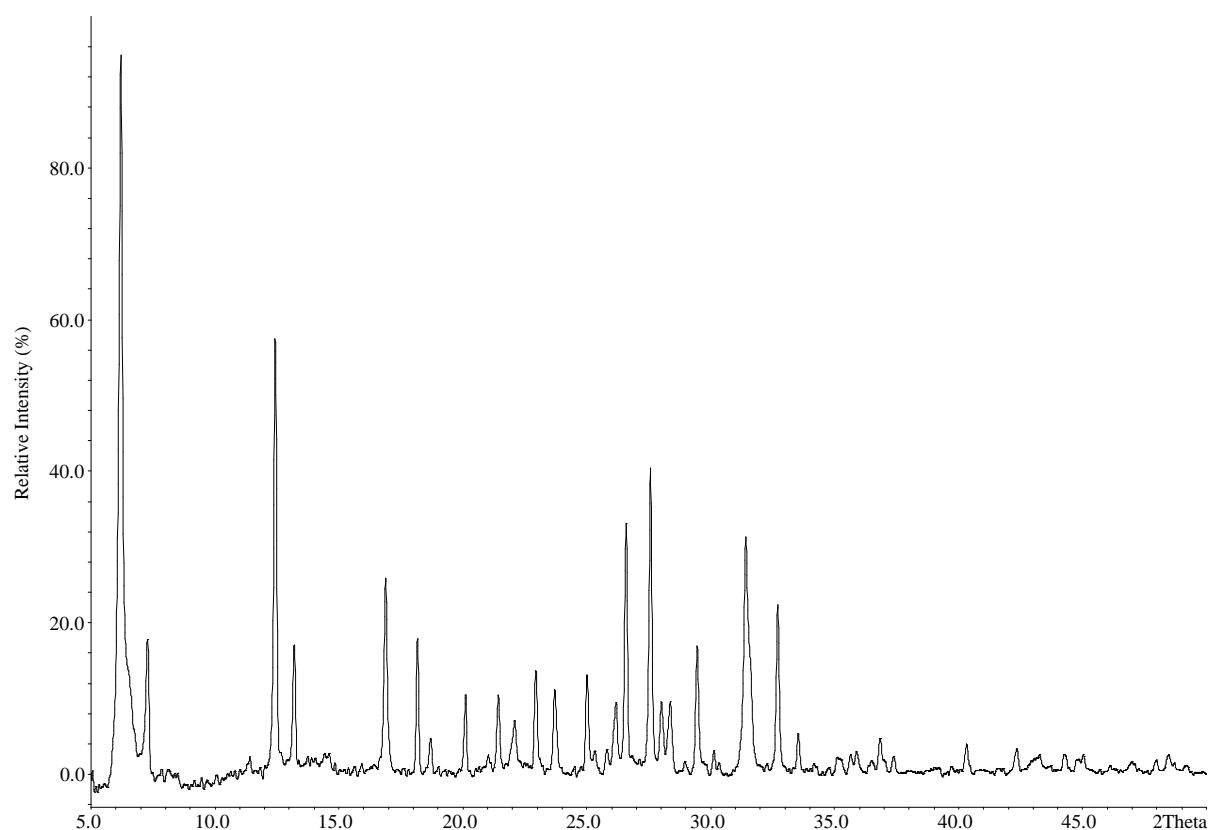
Some of the materials reported within this work have not been synthesised pure and some pure phases which have been synthesised as powders have not yet been fully characterised.

Conduction studies should be performed on structures **6**, **7** and **8** in order to check for their potential as proton or lithium conductors.

Structure **25**, MIL-53(Sc), was determined from a single crystal obtained from a different phase (Structure **24**). Synthesising this material as a single phase would be interesting in order to compare its thermal and adsorption behaviour to that of its chromium and aluminium analogues. Furthermore among the carboxylates, work carried out by Dietzel *et al*⁵¹ demonstrated that three scandium atoms can share a single oxygen atom (μ_3) suggesting that the crystallisation of scandium versions of MIL-100 and MIL-101 is attainable.

Further adsorption studies on structure **26** is in progress, collecting isotherms at the same temperature at which single crystal data has been collected the ESRF, to enable direct comparison. It would also be interesting to collect single crystal data during different pressures of CO₂ adsorption to investigate the pressure at which the crystal system changes from orthorhombic to monoclinic.

Although no scandium silicate materials were presented within this work, preliminary work indicates that the formation of such materials is possible. A series of experiments were performed investigating different stoichiometries of scandium silicate preparations, using different cations and silica sources. Two synthetic preparations yielded promising powder X-ray diffraction patterns, shown in figure 8.1.



A combination of X-ray analysis and SAED of the sodium scandium silicate material suggests an orthorhombic unit cell (Pban) where $a = 14.18\text{\AA}$, $b = 14.55\text{\AA}$ and $c = 28.0\text{\AA}$. The full characterisation of this material would further demonstrate the potential of the Sc^{3+} cation.

Further analysis of the ^{45}Sc MAS NMR data is required in order to gain a better understanding of the NMR properties of scandium within open framework materials. Some of the materials presented show peak overlap or broadening due to disorder, causing ambiguity when assigning the peaks, so these samples should be examined at different field strengths in order to enhance resolution. Furthermore, multiple quantum NMR is essential to derive accurately spectral parameters for resonances where more than one scandium site overlap within the 1D MAS NMR signal. It would also be informative to calculate the ^{45}Sc MAS NMR lineshapes using the CASTEP program, and to compare them to the results presented here.

Chapter 9: References

- 1 K. Barthelet, J. Marrot, G. Férey, and D. Riou, *J. Chem. Soc., Chem. Commun.*, 2004,
520.
- 2 A. F. Cronstedt, *Kongl. Svenska Vetenskaps Akademiens*, 1756, **17**, 20.
- 3 C. R. Hebd and H. d. S. C. Deville, *Seances Acad. Sci.*, 1862, **54**, 324.
- 4 J. W. McBain, *Rutledge, London*, 1932, **ch. 5**.
- 5 www.dow.com/ucc/index.htm.
- 6 R. M. Barrer, *J. Chem. Soc.*, 1948, 2158
- 7 D. W. Breck, W. G. Eversole, R. M. Milton, T. B. Reed, and T. L. Thomas, *J. Am.
Chem. Soc.*, 1956, **23**, 5963.
- 8 S. T. Wilson, B. M. Lok, C. A. Messina, T. R. Cannan, and E. M. Flanigen, *J. Am.
Chem. Soc.*, 1982, **104**, 1146.
- 9 A. K. Cheetham, G. Férey, and T. Loiseau, *Angew. Chem. Int. Ed.*, 1999, **38**, 3268.
- 10 S. H. Lee, D. K. Lee, C. H. Shin, Y. K. Park, P. A. Wright, W. M. Lee, and S. B.
Hong, *J. Cat*, 2003, **1**, 151.
- 11 J. B. Parise, *J. Chem. Soc., Chem. Commun.*, 1985, 606.
- 12 T. Kopac, E. Kaymakci, and M. Kopac, *Chem. Eng. Commun.*, 1998, **164**, 99.
- 13 M. Katoh, T. Yoshikawa, T. Tomonari, K. Katayama, and T. Tomida, *J. Colloid
Interface Sci.*, 2000, **226**, 145.
- 14 www.iza-online.org.
- 15 C. Baerlocher, W. M. Meier, and D. H. Olson, *Atlas of Zeolite Framework Types*,
Elsevier, Amsterdam, 2001, **5th Edition**.
- 16 R. M. Barrer, L. Hinds, and E. A. White, *J. Chem. Soc.*, 1953, 1466.
- 17 S. L. Burkett and M. E. Davis, *Chem. Mater.*, 1995, **7**, 1453.
- 18 M. E. Davis and R. F. Lobo, *Chem. Mater.*, 1992, **4**, 756.
- 19 R. Szostak, 1989.
- 20 R. J. Francis and D. O'Hare, *J. Chem. Soc., Dalton Trans.*, 1998, 3133.

- 21 G. T. Kerr, *J. Phys. Chem*, 1966, **70**, 1047.
- 22 F. Testa, R. Szostak, R. Chappetta, R. Aiollo, A. Fonseca, and J. B. Nagy, *Zeolites*, 1997, **18**, 106.
- 23 L. Pauling, *J. Am. Chem. Soc.*, 1929, **51**, 1010.
- 24 W. Loewentstein, *Am. Mineral.*, 1954, **39**, 92.
- 25 T. F. W. Barth, *J. Chem. Phys.*, 1935, **3**, 323.
- 26 A. Huang and S. J. Hwu, *Chem. Mater.*, 2001, **13**, 1794.
- 27 W. Depmeier, *Acta Cryst. C*, 1984, **40**, 226.
- 28 R. M. d. Vos and H. Verweij, *Science*, 1998, **279**, 1710.
- 29 G. Ferey, M. Latroche, C. Serre, F. Millange, T. Loiseau, and A. Percheron-Guegan, *J. Chem. Soc., Chem. Commun.*, 2003, 2976.
- 30 N. L. Rosi, J. Eckert, M. Eddaoudi, D. T. Vodak, J. Kim, M. O'Keefe, and O. M. Yaghi, *Science*, 2003, **300**, 1127.
- 31 J. L. Attwood, L. J. Barbour, and A. Jerga, *Angew. Chem. Int. Ed.*, 2004, **43**, 2948.
- 32 G. Ferey, C. Serre, C. Mellot-Draznieks, F. Millange, S. Surble, J. Dutour, and I. Margiolaki, *Angew. Chem. Int. Ed.*, 2004, **43**, 6296.
- 33 G. Ferey, C. Mellot-Draznieks, C. Serre, F. Millange, J. Dutour, S. Surble, and I. Margiolaki, *Science*, 2005, **309**, 2040.
- 34 E. Biemmi, T. Bein, and N. Stock, *Solid State Sciences*, 2006, **8**, 363.
- 35 www.webelements.com/webelements/scholar/elements/scandium/history.html.
- 36 <http://pearl1.lanl.gov/periodic/elements/21.html>.
- 37 S. Narita, K. Yokoyama, T. Morikawa, and T. Shibuya, *J. Mol. Struct.*, 2002, 49.
- 38 <http://periodic.lanl.gov/elements/21.html>.
- 39 B. Ewald, Y. Prots, C. Kudla, D. Gruner, R. Cardoso-Gil, and R. Kniep, *Chem. Mater.*, 2006, **18**, 673.
- 40 S. R. Miller, A. M. Z. Slawin, P. Wormald, and P. A. Wright, *J. Solid State Chem.*, 2005, **178**, 1738.
- 41 B. Ewald, Y. Prots, H. Zhang, and R. Kniep, *Z. Kristallogr.*, 2004, **219**, 343.
- 42 H. Park, I. Bull, L. Peng, V. G. Y. Jr., C. P. Grey, and J. B. Parise, *Chem. Mater.*, 2004, **16**, 5350.
- 43 B. Ewald, S. Natarajan, Y. Prots, and R. Kniep, *Z. Kristallogr.*, 2004, **219**, 335.
- 44 I. Bull, V. Young, S. J. Teat, L. Peng, C. P. Grey, and J. B. Parise, *J. Chem. Soc., Chem. Commun*, 2003, **15**, 3818.
- 45 D. Riou, F. Fayon, and D. Massiot, *Chem. Mater.*, 2002, **14**, 2416.

- 46 I. Bull, P. S. Wheatly, P. Lightfoot, R. E. Morris, E. Sastre, and P. A. Wright, *J. Chem. Soc., Chem. Commun.*, 2002, 1180.
- 47 S. R. Miller, E. Lear, J. Gonzalez, A. M. Z. Slawin, P. A. Wright, N. Guillou, and G. Ferey, *J. Chem. Soc., Dalton Trans.*, 2005, 3319.
- 48 J. J. Lu, J. A. Schlueter, and U. Geiser, *J. Solid State Chem.*, 2006, **179**, 1559.
- 49 S. R. Miller, P. A. Wright, C. Serre, T. Loiseau, J. Marrot, and G. Ferey, *J. Chem. Soc., Chem. Commun.*, 2005, 3850.
- 50 N. Mahe and N. Audebrand, *Solid State Sciences*, 2006, **8**, 988.
- 51 P. D. C. Dietzel, R. Blom, and H. Fjellvag, *J. Chem. Soc., Dalton Trans.*, 2006, 2055.
- 52 J. Perles, M. Iglesias, M. Martin-Luengo, M. A. Monge, C. Ruiz-Valero, and N. Snejko, *Chem. Mater.*, 2005, **17**, 5837.
- 53 J. Perles, M. Iglesias, C. Ruiz-Valero, and N. Snejko, *J. Chem. Soc., Chem. Commun.*, 2003, 346.
- 54 N. F. Stephens and P. Lightfoot, *Acta. Cryst. C*, 2006, **62**, I103.
- 55 N. F. Stephens and P. Lightfoot, *Solid State Sciences*, 2006, **8**, 197.
- 56 N. F. Stephens, A. M. Z. Slawin, and P. Lightfoot, *J. Chem. Soc., Chem. Commun.*, 2004, 614.
- 57 C. Gaicovazzo, *Oxford University Press*, 1992.
- 58 M. C. Burla, M. Camalli, B. Carrozzini, G. L. Cascarano, C. Gaicovazzo, G. Polidori, and R. Spagna, *J. Appl Cryst*, 2003, **36**, 1103.
- 59 WINXPOW.
- 60 J. A. Groves, S. R. Miller, S. J. Warrender, C. Mellot-Draznieks, P. Lightfoot, and P. A. Wright, *J. Chem. Soc., Chem. Commun*, 2006, 3305
- 61 A. Boultif and D. Louer, *J. Appl. Crystallogr.*, 2004, **37**, 724.
- 62 A. L. Spek, *J. Appl. Cryst.*, 2003, **36**, 7.
- 63 A. Altomare, R. Caliendo, M. Camalli, C. Cuocci, C. Giacovazzo, A. Grazia, G. Moliterni, and R. Rizzi, *J. Appl. Cryst.*, 2004, **37**, 1025.
- 64 G. C. A. Altomare, C. Giacovazzo and A. Guagliardi, *J. Appl. Cryst.*, 1993, **23**, 343.
- 65 M. C. B. A. Altomare, G. L. Cascarano, C. Giacovazzo, A. Guagliardi, G. Moliterni and G. Polidori, *J. Appl Cryst*, 1995, **28**, 842.
- 66 H. D. a. J. L. F. A. Le Bail, *Mat. Res. Bull.*, 1988, **23**, 447.
- 67 C. Serre, J. A. Groves, P. Lightfoot, A. M. Z. Slawin, P. A. Wright, N. Stock, T. Bein, M. Haouas, F. Taulelle, and G. Ferey, *Chem. Mater.*, 2006, **18**, 1451.
- 68 J. A. Groves, P. A. Wright, and P. Lightfoot, *Inorg. Chem.*, 2005, **44**, 1736.

- 69 C. Serre, J. A. Groves, P. Lightfoot, A. M. Z. Slawin, P. A. Wright, N. Stock, T. Bein, M. Haouas, F. Taulelle, and G. Ferey, *Chem. Mater.*, 2006, **18**, 1451.
- 70 A. K. Rappe, C. J. Casewit, K. S. Colwell, W. A. G. III, and W. M. Skiff, *J. Am. Chem. Soc.*, 1992, **114**, 10024.
- 71 L. Vega, E. de Miguel, L. F. Rull, G. Jackson, and I. A. McLure, *J. Chem. Phys.*, 1992, **96**, 2296.
- 72 R. C. V. Favre-Nicolin, *Materials Science Forum*, 2004, **443-444**, 35.
- 73 H. M. Rietveld, *Acta. Cryst.*, 1966, **21**, A228.
- 74 M. C. B. A. Altomare, M. Camalli, B. Carrozzini, G. L. Casciarano, C. Giacovazzo, A. Guagliardi, A. G. G. Moliterni, G. Polidori and R. Rizzi, *J. Appl Cryst*, 1999, **32**, 339.
- 75 A. C. Larson and R. B. v. Dreele, *Generalized Crystal Structure Analysis System, Los Alamos National Laboratory, USA*, 1988.
- 76 M. H. Levitt, 'Spin Dynamics, Baics of Nuclear Magnetic Resonance', Wiley, 2001.
- 77 S. E. Ashbrook and S. Wimperis, *Mol. Phys.*, 2000, **98**, 1.
- 78 J. B. Parise, *Inorg. Chem.*, 1985, **24**, 4312.
- 79 A. Choudhury and S. Natarajan, *Int. J. Inorg. Mater.*, 2000, **2**, 217.
- 80 S. S. Dhingra and R. C. Haushalter, *J. Chem. Soc., Chem. Commun*, 1993, 1665.
- 81 G. M. Sheldrick, *SHELXL97*, 1997.
- 82 A. S. Wills and I. D. Brown, *CEA, France*, 1999.
- 83 J. L. Kissick, A. R. Cowley, and A. M. Chippendale, *J. Solid State Chem.*, 2002, **167**, 17.
- 84 C. Chen, Z. Yi, M. Bi., Y. Liu, C. Wang, L. Liu, Z. Zhao, and W. Pang, *J. Solid State Chem.*, 2006, **179**, 1478.
- 85 K. Maeda, A. Tuel, S. Caldarelli, and C. Baerlocher, *Microporous and Mesoporous Mater.*, 2000, **39**, 465.
- 86 A. M. Chippendale and A. D. Law, *Journal of Solid State Chemistry*, 1999, **142**, 236.
- 87 M. P. Attfield, A. K. Cheetham, and S. Natarajan, *Mater. Res. Bull.*, 2000, **37**, 1007.
- 88 A. M. Chippendale and S. J. Brech, *J. Chem. Soc., Chem. Commun.*, 1996, **24**, 2781.
- 89 K. H. Lii and Y. F. Huang, *J. Chem. Soc., Dalton Trans.*, 1997, **13**, 2221.
- 90 M. B. Korzenski, G. L. Schimek, and J. W. Kolis, *Eur. J. Solid State Inorg.*, 1998, **2**, 143.160.
- 91 R. D. Shannon, *Acta Cryst. A*, 1976, **32**, 751.
- 92 M. H. Hey, C. Milton, and E. J. Dwornik, *Miner. Mag.*, 1982, **46**, 493.
- 93 M. E. Mrose and B. Wapner, *Geol. Soc. Am. Bull.*, 1959, **70**, 1648.

- 94 K. Sugiyama, *Acta Cryst. C.*, 1999, **55**, 279.
- 95 A. Zemann and J. Zemann, *Acta Cryst.*, 1957, **10**.
- 96 B. Grossner and I. Koch, *Z. Kristallogr.*, 1931, **80**, 455.
- 97 I. V. Zatonvskii, N. S. Slobodyanik, T. I. Ushchapivskaya, I. V. Ogoronik, and A. A. Babarik, *Russ. J. Appl. Chem.*, 2006, **79**, 10.
- 98 T. Dross and R. Glaum, *Acta Cryst. E*, 2004, i58.
- 99 Z. H. a. S. N. X. Zhang, *Acta Cryst. E*, 2005, i82.
- 100 B. Lajmi, M. Hidouri, A. Wattiaux, L. Fournes, J. Darriet, and M. B. Amara, *J. Alloys Comd.*, 2003, **361**, 77.
- 101 R. V. Shpanchenko, O. A. Lapshina, E. V. Antipov, J. Hadermann, E. E. Kaul, and C. Geibel, *Mater. Res. Bull.*, 2005, **40**, 1569.
- 102 A. I. Orlova, I. G. Trubach, V. S. Kurazhkovskaya, P. Pertierra, M. A. Salvado, S. Garcia-Granda, S. A. Khainakov, and J. R. Garcia, *J. Solid State Chem.*, 2003, **173**, 314.
- 103 K. K. Rangan and J. Gopalakrishnan, *J. Solid State Chem.*, 1994, **109**, 116.
- 104 S. T. Norberg, *Acta Cryst. B*, 2002, **B58**, 743.
- 105 Y. Fu, Z. Xu, J. Ren, and S. W. Ng, *Acta Cryst. E*, 2005, **E61**, i158.
- 106 J. C. M. Gustafsson, S. T. Norberg, and G. Svensson, *Acta Cryst. E*, 2006, **E62**, i160.
- 107 A. Clearfield, M. A. Subramanian, W. Wang, and P. Jerus, *Solid State Ionics*, 1983, **9-10**, 895.
- 108 F. Genet and M. Barj, *Solid State Ionics*, 1983, **9-10**, 891.
- 109 K. Byrappa and G. S. Gopalakrishna, *Prog. Cryst. Growth Charact. Mater.*, 1985, **11**, 89.
- 110 G. D. Ilyushin, *Kristallografiya*, 1989, **34**, 839.
- 111 R. Shimanouchi-Futagami, M. Nishimori, and H. Nishizawa, *J. Mater. Sci. Let*, 2000, **19**, 405.
- 112 S. Tamura, N. Imanaka, and G. Adachi, *Solid State Ionics*, 2000, **136**, 423.
- 113 G. X. Wang, D. H. Bradhurst, S. X. Dou, and H. K. Liu, *J. Powder Sources*, 2003, **124**, 231.
- 114 I. A. Stenina, Y. A. Velikodnyi, V. A. Ketsko, and A. B. Yaroslavtsev, *Inorg. Mater.*, 2004, **40**, 967.
- 115 A. Aatiq, R. Hassine, M. R. Tigha, and I. Saadoune, *Powder Diffraction*, 2005, **20**, 33.

- 116 G. S. Gopalakrishna, B. H. Doreswamy, M. J. Mahesh, M. Mahendra, M. A. Sridhar, J. S. Prasad, and K. G. Ashamanjari, *Bull. Mat. Sci.*, 2005, **28**, 1.
- 117 A. Ignaszak, P. Pasierb, R. Gajerski, and S. Komornicki, *Thermochimica Acta.*, 2005, **426**, 7.
- 118 M. P. Crosnier-Lopez, M. Barre, F. Le Berre, and J. L. Fourquet, *J. Solid State Chem.*, 2006, **179**, 2714.
- 119 T. Masui, K. Koyabu, S. Tamura, and N. Imanaka, *J. Alloys Comd.*, 2006, **418**, 73.
- 120 M. Shieh, K. J. Martin, P. J. Squattrito, and A. Clearfield, *Inorg. Chem.*, 1990, **29**, 958.
- 121 C. Y. Ortiz-Avila, P. J. Squattrino, M. Shieh, and A. Clearfield, *Inorg. Chem.*, 1989, **28**, 2608
- 122 J. Durand, M. Loukili, N. Tijani, M. Rafiq, and L. Cot, *Solid State Inorg. Chem.*, 1988, **25**, 297
- 123 J. X. Pan, S. T. Zheng, and G. Y. Yang, *Crystal Growth and Design*, 2005, **5**.
- 124 J. Ling, J. Li, J. Yu, Q. Pan, Q. Fang, and R. Xu, *Journal of Solid State Chemistry*, 2005, **178**, 2673
- 125 U. C. Chung, J. L. Mesa, V. Jubera, L. Lezama, M. I. Arriortua, and T. Rojo, *Journal of Solid State Chemistry*, 2005, **178**, 2913.
- 126 A. Kirkpatrick and W. T. A. Harrison, *Solid State Sciences*, 2004, **6**, 593.
- 127 Y. J. Zhong, Y. M. Chen, Y. Q. Sun, and G. Y. Yang, *Journal of Solid State Chemistry*, 2005, **178**, 2613.
- 128 N. Li and S. Xiang, *J. Mater. Chem.*, 2002, **12**, 1397.
- 129 S. Fernandez, J. L. Mesa, J. L. Pizarro, L. Lezema, M. I. Arriortua, and T. Rojo, *Chem. Mater.*, 2002, **14**, 2300
- 130 M. Sghyar, J. Durand, L. Cot, and M. Rafiq, *Acta Cryst.*, 1991, **C47**, 2515
- 131 R. E. Morris, M. P. Attfield, and A. K. Cheetham, *Acta Cryst.*, 1994, **C50**, 473.
- 132 B. Ewald, Y. Prots, and R. Kniep, *Z. Kristallogr.*, 2003, **218**, 377.
- 133 P. B. Moore, T. Araki, I. M. Steele, G. H. Swihart, and A. R. Kampf, *American Mineralogist*, 1983, **68**, 1022.
- 134 A. S. Willis and I. D. Brown, *CEA, France*, 1999.
- 135 X. Chen, Y. Wang, J. Yu, Y. Zou, and R. Xu, *Journal of Solid State Chemistry*, 2004, **177**, 2518.
- 136 Y. Wang, J. Yu, Y. Du, Z. Shi, Y. Zou, and R. Xu, *J. Chem. Soc. Dalton Trans.*, 2002.

- 137 S. Mandal, S. Pati, M. A. Green, and S. Natarajan, *Chem. Mater.*, 2005, **17**, 638.
- 138 S. Fernandez-Armas, J. L. Mesa, J. L. Pizarro, J. S. Garitaonandia, M. I. Arriortua, and T. Rojo, *Angew. Chem. Int.*, 2004, **43**, 977.
- 139 K. Maeda, J. Akimoto, Y. Kiyozumi, and F. Mizukami, *Angew. Chem. Int.*, 1995, **34**, 1199.
- 140 K. Maeda, J. Akimoto, Y. Kiyozumi, and F. Mizukami, *Angew. Chem. Int. Ed.*, 1995, **34**, 1199.
- 141 k. Maeda, Y. Kiyozumi, and F. Mizukami, *J. Phys. Chem. B*, 1997, **101**, 4402.
- 142 V. J. Carter, P. A. Wright, J. D. Gale, R. E. Morris, E. Sastre, and J. Perez-Pariente, *J. Mater. Chem.*, 1997, **7**, 2287.
- 143 V. J. Carter, J. Kujanpaa, F. G. Riddell, P. A. Wright, J. F. C. Turner, C. R. A. Catlow, and K. S. Knight, *Chem. Phys. Lett.*, 1999, **313**, 505.
- 144 M. Edgar, V. J. Carter, D. P. Tunstall, P. Grewal, V. Favre-Nicolin, P. A. Cox, P. Lightfoot, and P. A. Wright, *Chem. Commun.*, 2002.
- 145 M. Edgar, V. J. Carter, P. Grewal, L. J. Sawers, E. Sastre, D. P. Tunstall, P. A. Cox, P. Lightfoot, and P. A. Wright, *Chem. Mater.*, 2002, **14**, 3432.
- 146 C. Shumacher, J. Gonzalez, P. A. Wright, and N. A. Seaton, *Phys. Chem. Chem. Phys.*, 2005, **7**, 2351.
- 147 C. Paulet, C. Serre, T. Loiseau, D. Riou, and G. Ferey, *C. R. Acad. Sci. Paris, Ser. IIC*, 1999, **2**, 631.
- 148 K. Maeda, Y. Kiyozumi, and F. Mizukami, *J. Phys. Chem. B*, 1997, **101**, 4402.
- 149 K. Maeda, J. Akimoto, Y. Kiyozumi, and F. Mizukami, *J. Chem. Soc., Chem. Commun.*, 1995, 1033.
- 150 V. J. Carter, J. P. Kujanpaa, F. G. Riddell, P. A. Wright, J. F. C. Turner, C. R. A. Catlow, and K. S. Knight, *Chem. Phys. Let.*, 1999, **313**, 505.
- 151 K. Moedritzer and R. R. Irani, *J. Org. Chem.*, 1966, **31**, 1603.
- 152 J. Gonzalez, 'Adsorption proerties of organically functionalised mesoporous solids and dynamics of absrobed molecules in microporous organic-inorganic hybrid solids', University of St. Andrews, 2005.
- 153 L. J. Sawers, V. J. Carter, A. R. Armstrong, P. G. Bruce, P. A. Wright, and B. E. Gore, *J. Chem. Soc., Dalton Trans.*, 1996, 3159.
- 154 A. Fitch, *J. Res. Natl. Inst. Stand. Technol.*, 2004, **109**, 133.

- 155 A. Altomare, M. C. Burla, M. Camalli, B. Carrozzini, G. L. Cascarano, C. Giacobazzo, A. Guagliardi, A. G. G. Moliterni, G. Polidori, and R. Rizzi, *J. Appl Cryst*, 1999, **32**, 339.
- 156 V. Soghomonian, R. C. Haushalter, and J. Zubieta, *Chem. Mater.*, 1995, **7**, 1648.
- 157 V. Soghomonian, R. C. Haushalter, and J. Zubieta, *Chem. Mater.*, 1995, **7**, 1648.
- 158 J. A. Groves, N. F. Stephens, P. A. Wright, and P. Lightfoot, *Solid State Sciences*, 2006, **8**, 397.
- 159 J. A. Groves, P. A. Wright, and P. Lightfoot, *J. Chem. Soc., Dalton Trans.*, 2005, 2007.
- 160 J. A. Groves, P. A. Wright, and P. Lightfoot, *Inorg. Chem.*, 2005, **44**, 1736.
- 161 P. Horcajada, S. Surble, C. Serre, D. Y. Hong, Y. K. Seo, J. S. Chang, J. M. Greneche, I. Margiolaki, and G. Ferey, *J. Chem. Soc., Chem. Commun.*, 2007, 2820.
- 162 N. A. Ramsahye, G. Maurin, S. Bourrelly, P. Llewellyn, T. Loiseau, and G. Ferey, *Phys. Chem. Chem. Phys.*, 2007, **9**, 1059.
- 163 S. H. Jung, J. H. Lee, J. W. Yoon, C. Serre, G. Ferey, and J. S. Chang, *Adv. Mater.*, 2007, **19**, 121.
- 164 S. Surble, F. Millange, C. Serre, T. Duren, M. Latroche, S. Bourrelly, P. L. Llewellyn, and G. Ferey, *JACS*, 2006, **128**, 14889.
- 165 C. Serre, F. Millange, T. Devic, N. Audebrand, and W. Van Beek, *Mater. Res. Bull.*, 2006, **41**, 1550.
- 166 C. Volkringer and T. Loiseau, *Mater. Res. Bull.*, 2006, **41**, 948.
- 167 S. Surble, C. Serre, F. Millange, and G. Ferey, *Solid State Sciences*, 2006, **8**, 413.
- 168 S. Surble, C. Serre, C. Mellot-Draznieks, F. Millange, and G. Ferey, *J. Chem. Soc., Chem. Commun.*, 2006, 284.
- 169 T. Devic, C. Serre, N. Audebrand, J. Marrot, and G. Ferey, *JACS*, 2005, **127**, 12788.
- 170 C. Serre, J. Marrot, and G. Ferey, *Inorg. Chem.*, 2005, **44**, 654.
- 171 C. Serre, F. Millange, S. Surble, J. M. Greneche, and G. Ferey, *Chem. Mater.*, 2004, **16**, 2706.
- 172 T. Loiseau, C. Serre, C. Huguenard, G. Fink, F. Taulelle, M. Henry, T. Bataille, and G. Ferey, *Chem. Eur. J.*, 2004, **10**, 1373.
- 173 N. L. Rosi, J. Eckert, M. Eddaoudi, D. T. Vodak, J. Kim, M. O'Keeffe, and O. M. Yaghi, *Science*, 2003, **300**, 1127.
- 174 C. Mellot-Draznieks, J. Dutour, and G. Ferey, *Angew. Chem. Int. Ed.*, 2004, **43**, 6290.

- 175 C. Mellot-Draznieks, J. M. Newsam, A. M. Gorman, C. M. Freeman, and G. Ferey, *Angew. Chem. Int. Ed.*, 2000, **39**, 2270.
- 176 C. Mellot-Draznieks, G. Ferey, C. Schon, Z. Cancarevic, and M. Jansen, *Chem. Eur. J.*, 2002, **18**, 4102.
- 177 C. Mellot-Draznieks, S. Girard, and G. Ferey, *J. Am. Chem. Soc.*, 2002, **124**, 15326.
- 178 J. Perles, M. Iglesias, C. Ruiz-Valero, and N. Snejko, *J. Mater. Chem.*, 2004, **14**, 2683.
- 179 M. Latroche, S. Surble, C. Serre, C. Mellot-Draznieks, P. L. Llewellyn, J. H. Lee, J. S. Chang, S. H. Jhung, and G. Ferey, *Angew. Chem. Int. Ed.*, 2006, **45**, 8227.
- 180 D. Massiot, F. Fayon, M. Capron, I. King, S. Le Calve, B. Alonso, J.-O. Durand, B. Bujoli, Z. Gan, and G. Hoatson, *Mag. Res. Chem.*, 2002, **40**, 70.
- 181 T. Loiseau, H. Muguerra, G. Ferey, M. Haouas, and F. Taulelle, *J. Solid State Chem.*, 2005, **178**, 621.
- 182 A. Carton, S. Abdelouhab, G. Renaudin, P. Rabu, and M. Francois, *Solid State Sciences*, 2006, **8**, 958.
- 183 M. Eddaoudi, H. L. Li, and O. M. Yaghi, *JACS*, 2000, **122**, 1391.
- 184 J. Tao, X. Yin, R. B. Huang, L. S. Zheng, and S. W. Ng, *Inorg. Chem. Commun.*, 2002, **5**, 975.
- 185 L. Long, T. Ren, L. Ma, Y. Jiang, R. Huang, and L. Zheng, *Inorg. Chem. Commun.*, 2003, **6**, 690.
- 186 F. A. A. Paz and J. Klinowski, *J. Chem. Soc., Chem. Commun.*, 2003, 1484.
- 187 S. Surble, C. Serre, C. Mellot-Draznieks, F. Millange, and G. Ferey, *J. Chem. Soc., Chem. Commun.*, 2006, 284.
- 188 T. Yuen, C. L. Lin, J. A. Zan, L. Pan, and J. Li, *J. Appl. Phys.*, 2005, **97**.
- 189 L. S. Long, Y. P. Ren, L. H. Ma, Y. B. Jiang, R. B. Huang, and L. S. Zheng, *Inorg. Chem. Commun.*, 2003, **6**, 690.
- 190 W. Yuan and L. S. Long, *Appl. Organomet. Chem.*, 2003, **17**, 257.
- 191 G. Ferey, C. Mellot-Draznieks, C. Serre, F. Millange, J. Dutour, S. Surble, and I. Margiolaki, *Science*, 2005, **309**, 2040.
- 192 C. Serre, F. Millange, C. Thouvenot, M. Nogues, G. Marsolier, D. Louer, and G. Ferey, *J. Am. Chem. Soc.*, 2002, **124**, 13519.
- 193 D. W. Breck, 'Zeolite Molecular Sieves', Wiley, 1974.
- 194 B. Zhao, B. Xiao, A. J. Fletcher, K. M. Thomas, D. Bradshaw, and M. J. Rosseinsky, *Science*, 2004, **306**, 1012.

- 195 P. A. Wright, 'Microporous Framework Solids', ed. R. M. Monographs, Royal Society of Chemistry, 2008.
- 196 G. Onyestyak, J. Valyon, and L. V. C. Rees, *Solid State Ionics*, 2001, **141**, 93.
- 197 W. H. Lin and T. S. Chung, *J. Membr. Sci.*, 2001, **186**, 183.
- 198 http://www.oxford-diffraction.com/new_2006_01_19.asp.